REPORT NO.
EERC 76-22
OCTOBER 1976

EARTHQUAKE ENGINEERING RESEARCH CENTER

RESPONSE OF THE OLIVE VIEW HOSPITAL MAIN BUILDING DURING THE SAN FERNANDO EARTHQUAKE

by
STEPHEN A. MAHIN
VITELMO V. BERTERO
ANIL K. CHOPRA
ROBERT G. COLLINS

Report to Sponsor:
National Science Foundation

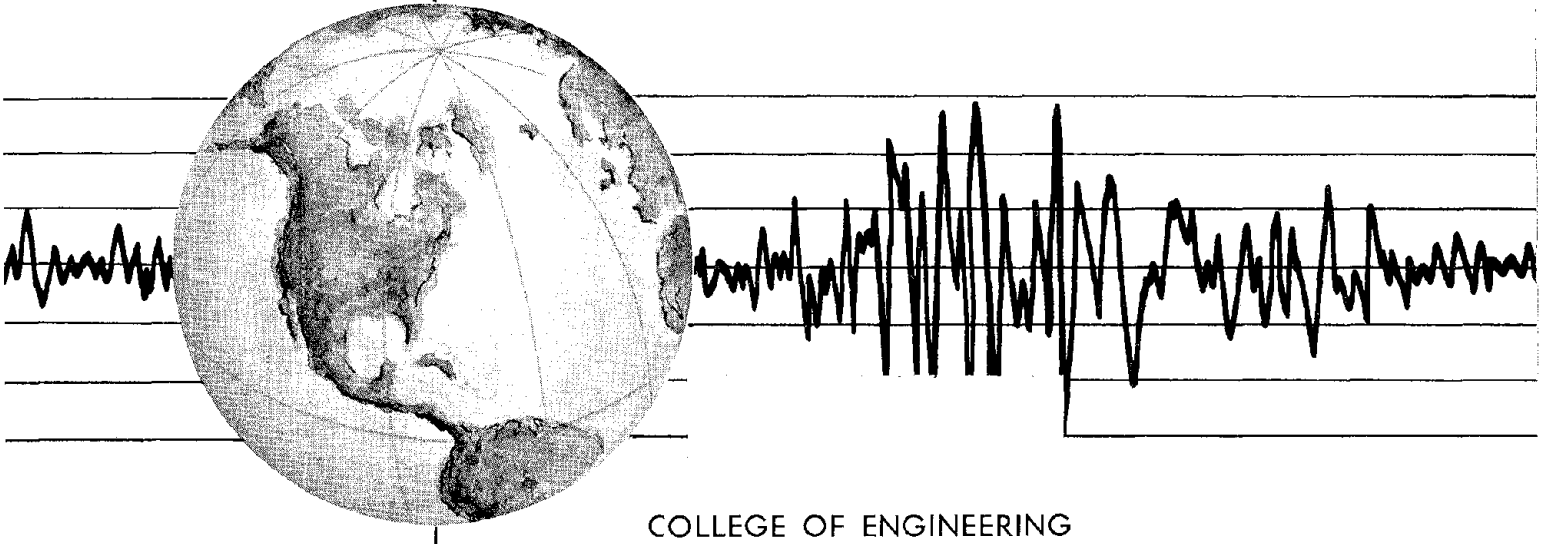

COLLEGE OF ENGINEERING

UNIVERSITY OF CALIFORNIA · Berkeley, California

BIBLIOGRAPHIC DATA SHEET	1. Report No. EERC 76-22	2.	3. Recipient's Accession No.
4. Title and Subtitle Response of the Olive View Hospital Main Building during the San Fernando Earthquake			5. Report Date October 1976 6.
7. Author(s) S.A. Mahin, V.V. Bertero, A.K. Chopra and R.G. Collins			8. Performing Organization Rept. No. 76-22
9. Performing Organization Name and Address Earthquake Engineering Research Center University of California, Berkeley 1301 South 46th Street Richmond, California 94804			10. Project/Task/Work Unit No. 11. Contract/Grant No. GI-29933 AEN-307732A02
12. Sponsoring Organization Name and Address National Science Foundation 1800 G Street, N.W. Washington, D.C. 20550			13. Type of Report & Period Covered 14.
15. Supplementary Notes			

16. Abstracts This report presents the results of an extensive field and analytical investigation of the structural performance of the main building of the Olive View Hospital Medical Treatment and Care Facility during the 1971 San Fernando earthquake. This modern, six-story, cast-in-place, reinforced concrete building suffered such severe structural and nonstructural damages that it had to be demolished after the earthquake. The observed structural damages are compared with those predicted in a series of quantitative elastic and nonlinear dynamic analysis of the building in order to: (1) reassess current seismic-resistant design practices; (2) identify the principal parameters that controlled the response of the building; and (3) evaluate the ability of currently available analytical methods to predict seismic behavior.

The relatively irregular and complex structural system employed in the building is described in detail in this report along with the original design criteria. The building had four wings located around a central courtyard. Numerous structural (shear) walls were located in the upper four stories, but these did not continue down through the bottom two stories to the foundations.

Damages to the building were particularly severe in the bottom two stories, including story drifts exceeding 30 in. at some locations, substantial inelastic deformations in slabs and columns, and the failure of numerous tied columns which resulted in the collapse of some parts of the building. The main features of the damages appear to be a consequence of ground shaking and not of faulty materials or poor workmanship.

Since no ground motion records were obtained near the building site, several accelerograms were numerically simulated or taken from recordings obtained at other sites in order to perform the desired seismic response analysis. Ground motions obtained near the fault rupture are shown to contain relatively high amplitude, long-duration acceleration pulses, which could partially account for the type of damage observed.

A complete three-dimensional mathematical model of the building is analyzed for biaxial horizontal ground accelerations to assess the structure's overall dynamic characteristics and to identify the initial member failures. This analysis, in conjunction with member capacity studies, identifies the concentration of deformations in the bottom two stories and the brittle type of failure observed in the tied columns. The elastic results were, however, unable to predict the severity and distribution of the inelastic deformations and the large lateral displacements that were observed in the building.

Since the elastic results indicate that the horizontal, translational degrees-of-freedom of the building are essentially uncoupled and that torsion did not have a (cont.)

18. Availability Statement	19. Security Class (This Report)	21. No. of Pages
Release unlimited	UNCLASSIFIED	320
	20. Security Class (This Page) UNCLASSIFIED	22. Price A14 - A01

BIBLIOGRAPHIC DATA SHEET	1. Report No. EERC 76-22	2.	3. Recipient's Accession No.
4. Title and Subtitle Page 2, Continued from page 1.			5. Report Date 6.
7. Author(s)			8. Performing Organization Rept. No.
9. Performing Organization Name and Address			10. Project/Task/Work Unit No. 11. Contract/Grant No.
12. Sponsoring Organization Name and Address			13. Type of Report & Period Covered 14.
15. Supplementary Notes			

16. Abstracts

(continued from page 1) significant effect on the overall response, a two-dimensional nonlinear model of a part of the building is developed to obtain guidelines regarding the effect of inelastic action on the response of the building. In the first series of nonlinear analyses, the possibility of member failure is disregarded. But in the second series such features as member spalling or failure and hammering of the building against adjacent structures is explicitly considered.

The inelastic analyses reveal that the building was designed to be very strong in comparison with building code specifications, but that for some members (notably the tied columns and flat slabs in the bottom two stories) the required inelastic deformations are larger than they could develop according to their detailing. The inelastic analyses also indicate that the relatively small strength and stiffness of the bottom two stories resulted in a partial sidesway collapse mechanism which concentrated drifts and inelastic deformations in these two stories. The displacements predicted by the inelastic analyses, although generally larger than those predicted by the elastic analyses, were smaller than the permanent displacements observed in the building. While this may be partially due to the simplifications introduced in the inelastic analyses, the results indicate that the response is only moderately affected by changes in the modeling parameters. On the other hand, the inelastic response is found to be very sensitive to the ground motion record used. In particular, records that contain severe, long-duration acceleration pulses like those obtained near the fault rupture result in very large lateral displacements when a collapse mechanism forms.

It is believed that the overall poor performance of this building was due to the combination of an inadequate structural system, the poor detailing of some members and the severe ground motions experienced at the site. Additional conclusions regarding the adequacy of the structural system, the adequacy and reliability of analytical methods for predicting seismic behavior, and the effect of detailing and workmanship on seismic performance are offered in the report along with a number of recommendations for improving seismic resistant design practices.

17c. COSATI Field/Group

18. Availability Statement	19. Security Class (This Report) UNCLASSIFIED	21. No. of Pages
ia	20. Security Class (This Page) UNCLASSIFIED	22. Price

RESPONSE OF THE OLIVE VIEW HOSPITAL MAIN BUILDING DURING THE SAN FERNANDO EARTHQUAKE

by

Stephen A. Mahin

Vitelmo V. Bertero

Anil K. Chopra

Robert G. Collins

A Report on Research Sponsored by
the National Science Foundation

Report No. EERC 76-22

Earthquake Engineering Research Center
College of Engineering
University of California
Berkeley, California

October 1976

ABSTRACT

This report presents the results of an extensive field and analytical investigation of the structural performance of the main building of the Olive View Hospital Medical Treatment and Care Facility during the 1971 San Fernando earthquake. This modern, six-story, cast-in-place, reinforced concrete building suffered such severe structural and nonstructural damages that it had to be demolished after the earthquake. The observed structural damages are compared with those predicted in a series of quantitative elastic and nonlinear dynamic analysis of the building in order to: (1) reassess current seismic-resistant design practices; (2) identify the principal parameters that controlled the response of the building; and (3) evaluate the ability of currently available analytical methods to predict seismic behavior.

The relatively irregular and complex structural system employed in the building is described in detail in this report along with the original design criteria. The building had four wings located around a central courtyard. Numerous structural (shear) walls were located in the upper four stories, but these did not continue down through the bottom two stories to the foundations.

Damages to the building were particularly severe in the bottom two stories, including story drifts exceeding 30 in. at some locations, substantial inelastic deformations in slabs and columns, and the failure of numerous tied columns which resulted in the collapse of some parts of the building. The main features of the damages appear to be a consequence of ground shaking and not of faulty materials or poor workmanship.

Since no ground motion records were obtained near the building site, several accelerograms were numerically simulated or taken from recordings obtained at other sites in order to perform the desired seismic response analysis. Ground motions obtained near the fault rupture are shown to contain relatively high amplitude, long-duration acceleration pulses, which could partially account for the type of damage observed.

A complete three-dimensional mathematical model of the building is analyzed for biaxial horizontal ground accelerations to assess the structure's overall dynamic characteristics and to identify the initial member failures. This analysis, in conjunction with member capacity studies, identifies the concentration of deformations in the bottom two stories and the brittle type of failure observed in the tied columns. The elastic results were, however, unable to predict the severity and distribution of the inelastic deformations and the large lateral displacements that were observed in the building.

Since the elastic results indicate that the horizontal, translational degrees-of-freedom of the building are essentially uncoupled and that torsion did not have a significant effect on the overall response, a two-dimensional nonlinear model of a part of the building is developed to obtain guidelines regarding the effect of inelastic action on the response of the building. In the first series of nonlinear analyses, the possibility of member failure is disregarded. But in the second series such features as member spalling or failure and hammering of the building against adjacent structures is explicitly considered.

The inelastic analyses reveal that the building was designed to be very strong in comparison with building code specifications, but that for some members (notably the tied columns and flat slabs in the bottom two stories) the required inelastic deformations are larger than they could develop according to their detailing. The inelastic analyses also indicate that the relatively small strength and stiffness of the bottom two stories resulted in a partial sidesway collapse mechanism which concentrated drifts and inelastic deformations in these two stories. The displacements predicted by the inelastic analyses, although generally larger than those predicted by the elastic analyses, were smaller than the permanent displacements observed in the building. While this may be partially due to the simplifications introduced in the inelastic analyses, the results indicate that the response is only moderately affected by changes in the modeling parameters. On the other hand, the inelastic response is found to be very sensitive to the ground motion record used. In particular, records that contain severe, long-duration acceleration pulses like those obtained near the fault rupture result in very large lateral displacements when a collapse mechanism forms.

It is believed that the overall poor performance of this building was due to the combination of an inadequate structural system, the poor detailing of some members and the severe ground motions experienced at the site. Additional conclusions regarding the adequacy of the structural system, the adequacy and reliability of analytical methods for predicting seismic behavior, and the effect of detailing and workmanship on seismic performance are offered in the report along with a number of recommendations for improving seismic resistant design practices.

ACKNOWLEDGEMENTS

This investigation was undertaken as part of an in-depth study of the performance of the Olive View Medical Center buildings during the 1971 San Fernando earthquake. Financial support for this study was provided by the National Science Foundation under Grant Nos. GI-29933 and AEN307732A02. The efforts of Dr. C. Thiel of NSF-RANN in supporting the overall studies of the San Fernando earthquake are gratefully acknowledged.

The authors would like to express their appreciation to T. M. Hsueh, L. Edgar and M. Quint for their assistance with portions of this investigation. Discussions with Professors B. Bresler and L. Selna were of great assistance. The cooperation provided by the Los Angeles County Engineers is also greatly appreciated.

The editorial guidance of L. Tsai and secretarial assistance of K. Pilcher and M. Ward is gratefully acknowledged. The technical illustrations by L. Hashizume and E. Loh are appreciated.

TABLE OF CONTENTS

I. INTRODUCTION

1.1 GENERAL

The February 9, 1971 San Fernando earthquake was the largest and most destructive earthquake to occur in the metropolitan Los Angeles area during the last fifty years. The main shock of the earthquake was centered north of the city, in the San Gabriel mountains (Fig. 1.1). It has been assigned a magnitude of 6.6 on the Richter scale. Although this was an earthquake of only moderate magnitude, a 400-square-mile area inhabited by more than 400,000 people was subjected to very intense ground shaking.

Heaviest damage occurred in the Sylmar-San Fernando area, where the breaking along the fault plane reached the ground surface. Some buildings in two hospital complexes collapsed completely or suffered heavy damages. Several schools were severely damaged, and hundreds of homes were destroyed or seriously damaged. Ten highway overpasses collapsed. Public utilities sustained major damages; many sewer, gas and water lines were torn up, and several large water and electric facilities were rendered inoperable by the earthquake. Much of the earthen embankment of the Lower Van Norman Reservoir also collapsed, and the possibility of the complete failure of this dam necessitated the evacuation of 80,000 residents from the Mission Hills area of the San Fernando Valley [1.1].

In all, sixty-four persons were killed as a result of the earthquake, and property damages totaling nearly $500 million have been reported. The earthquake occurred at 6 a.m. Had it occurred during working hours, when public buildings, businesses and highways were crowded, the number of fatalities and serious injuries would probably have been much greater.

It is important that selected structures damaged during earthquakes be investigated in order to provide the quantitative information necessary to evaluate, and, where necessary, improve the design criteria and construction techniques used for earthquake-resistant buildings. Such studies have proven invaluable in the past.

Following a preliminary survey of the general features of damaged structures, the buildings at the Los Angeles County Olive View Hospital Medical Treatment and Care Facility were selected for a program of study to be conducted at the Berkeley and Los Angeles campuses of the University of California. The Medical Center, located in the area of northern Sylmar (Fig. 1.1) in the region of greatest damage, consisted of eight structures which can be seen in Figs. 1.2 to 1.4. These buildings employed a variety of different structural systems and materials and sustained varying degrees of damage, including partial and complete collapse. The structural design of the $27.5 million Medical Center was begun in 1965, and construction was completed in October 1970, just four months before the earthquake. Since the buildings were designed according to modern codes and constructed with modern techniques, reconciliation of their structural damages with a quantitative analytical evaluation of their dynamic behavior would provide a valuable reassessment of current engineering practices for earthquake-resistant design.

This report examines an analytical investigation of the seismic behavior of the Main Hospital building. This six-story, cast-in-place, reinforced concrete building was the largest in the medical complex (Figs. 1.2 and 1.3). During the earthquake it sustained such extensive damage, as can be seen in Fig. 1.4, that it had to be demolished. While the building's stairtowers, Figs. 1.3 through 1.5, were part of the main building, the collapse of these appendages was significant enough to warrant a separate investigation [1.2]; therefore, only those features of their design and response essential to the evaluation of the remainder of the main building will be discussed. Preliminary results of this investigation on the main building have been reported [1.3], and several other investigators have studied the building [1.4-1.6]. An experimental study of spiral columns like those found in the building has been conducted [1.7]. In addition, several other buildings of the Medical Center have been studied, including the ambulance canopy [1.8], warehouse [1.9], psychiatric unit [1.10], and exhaust pavilion [1.11], and the principal results of these studies have been summarized [1.12, 1.13].

1.2 OBJECTIVES

The main objectives of the analytical investigation of the Olive View Main Hospital building were to:

1. quantitatively reassess current design practices and code provisions for earthquake-resistant buildings;
2. identify the principal factors which controlled the seismic behavior of the main building and, where possible, determine whether alternative structural systems or design philosophies would have significantly mitigated the structural distress; and
3. evaluate the capability of currently available analytical methods to predict seismic behavior.

1.3 SCOPE AND ORGANIZATION OF RESEARCH

The investigation of the main building of the Olive View Hospital has been organized for convenience into three parts: (1) description of the structure and its damages, (2) estimation of the ground motion, and (3) analysis and evaluation of the response of the building.

The general features of the structural system, design methods, material quality and construction methods are examined in Chapter 2. An extensive field study has been conducted to document thoroughly the damage to the building. The features of this damage essential to the objectives of this report are presented in Chapter 3.

To perform the desired structural dynamic analyses, appropriate ground motion records had to be simulated since there were no accelerograms recorded in the immediate vicinity of the building site. Chapter 4 discusses the methods used to develop these records.

Two types of structural analyses were conducted. In Chapter 5 the results of extensive three-dimensional analyses of the entire building based on linear-elastic behavior are examined to ascertain the dynamic characteristics and initial behavior of the building. Since these results indicated that many elements would be stressed well beyond the elastic range, a representative model of the building suitable for further nonlinear analysis was identified using these

elastic results. The results of various nonlinear analyses of a discrete element model of a wing of the building are presented in the sixth chapter. Recommendations for improvements in design procedures, code provisions, and analytical methods are presented in Chapter 7.

II. BUILDING DESCRIPTION

2.1 INTRODUCTION

A general physical description of the Olive View Medical Center's Medical Treatment and Care Facility (the main building) is presented in this chapter. The structural features of the building are emphasized, and the criteria and methods used in the design of the building are outlined. The modeling for the original seismic design of the hospital is also examined in detail. These design assumptions are assessed, and possible alternatives are discussed. This chapter also compares the design material specifications with the results of field and mill tests performed during construction, and of laboratory tests. In the last part of the chapter, the quality of the actual construction, including the design details and construction workmanship, is assessed.

The design calculations and structural drawings, provided by the county of Los Angeles, were extensively used in the preparation of this report. In addition, numerous field inspections were made after the earthquake to study and photograph systematically the structural system and damages. Many photographs taken during construction were also examined.

2.2 PHYSICAL DESCRIPTION OF BUILDING

The Medical Treatment and Care Facility was the largest building of the Olive View Medical Center with over 500,000 square feet of floor space. The relationship of the main building to the rest of the medical center is illustrated in the aerial photographs of Figs. 1.2 and 1.3 and the schematic site plan of Fig. 1.5. The main building was a relatively massive, six-story reinforced concrete structure. As shown in Figs. 2.1 and 2.2, the building's ground story was considerably larger in plan than the upper five stories; approximately one-third of the building's total weight was concentrated at the first floor. The upper portion of the building consisted of four rectangular structures (Wings A, B, C, and D) connected to each other at right angles and enclosing an open courtyard. Typical plans of an upper floor are shown in Figs. 2.3 through 2.5. The point symmetry of the upper portion of

the building about the center of the courtyard is illustrated by Fig. 2.3. A stairtower appendage was located at the end of each wing (Figs. 2.1, 2.3 and 2.6). These were completely separated from the rest of the building except at the first floor level. A more complete discussion of these stairtowers is presented in Reference 1.2. Six small penthouses, located on the roof, were used to house mechanical equipment, as shown in Fig. 2.7.

The primary vertical load-carrying system used in the building consisted of columns and flat slabs with drop panels. Two different types of lateral load-resisting structural systems were used. In the upper four stories, numerous shear walls were provided to resist lateral loads. These walls, however, did not extend through the first and ground stories, so that the slabs and columns of these lower two stories formed a relatively more flexible, moment-resisting space frame.

The complexity of the structural system and the many special details used in the facility precludes a complete physical description. Consequently, only the essential features of the structure necessary for an understanding of the scope of this investigation will be presented here. In this presentation, particular emphasis will be placed on one-quarter of the building, Wing D.

2.2.1 Details of Seismic Joint and Foundation

Because of sloping terrain at the site, the ground story was above grade on the south and east sides of the building; but on the north and west sides, the ground story was separated from a retaining wall by a 2- to 4-in. wide, waterproofed seismic joint. This joint was intended to allow the main building to vibrate as a six-story structure without any external restraint at the first floor level. The extent in plan of the seismic joint is shown in Fig. 2.1; its outline indicates the portions of the ground story which were below grade. While the joint separation was 4 in. wide, Fig. 2.8 shows that the actual design allowed only about 2 in. of unrestrained horizontal displacement of the first floor before contact with the retaining wall actually occurred.

The foundation system consisted of spread footings under each column, as shown in Fig. 2.9. Most of the ground floor slab was poured directly on grade after the site had been excavated and leveled. However, an 8-ft. deep crawl space was located beneath this slab under the northern halves of Wings B and C so that the ground floor slab was designed as a flat slab with drop panels at these locations (Fig. 2.9).

2.2.2 Details of Ground and First Stories

The roof of the one-story portion of the ground story (i.e., the terrace canopy and courtyard) was located 1'-9" below the level of the interior first floor slab to allow for extensive landscaping in this area (Figs. 2.1 and 2.9). This section was framed with flat slabs having drop panels or beams and one-way slabs (Fig. 2.2) supported by rectangular tied columns. A 45.5-in. deep parapet was located along the perimeter of this slab (Fig. 2.10). The central courtyard also had flat slabs with drop panels at this level in conjunction with tied columns. These extended portions of the ground story contributed to the largest part of the mass at this level, not only because of their large tributary floor areas, but because the landscaping loads on them were extensive. The slab was generally 12 in. thick in the one-story section of the building. On top of this were a waterproofing membrane, a 4-in. layer of lightweight concrete fill, and 17 in. of earth fill. The resulting mass amounted to about 27 percent of the total dead load mass of the building.

The first floor slab within the multistory section of the building consisted of flat slabs with drop panels (Fig. 2.2) supported by spiral columns. Continuous deep beams were located along the boundary between the multistory and single story sections of the building to connect the two different first floor elevations (Fig. 2.10).

Three of the stairtowers (A, B, and D) were structurally attached (Fig. 2.6) to the main building at this floor level. The first floor slab of the fourth tower (C) rested directly on earth fill, and this tower was supported by six spread footings (Fig. 2.6). In the ground story, the three other towers were supported by six tied columns.

Above the first floor all four towers were similar, rigid box-like structures and were structurally separated from the rest of the building by 4-in. wide seismic joints (Fig. 2.6). The design of the towers, discussed in detail in Reference 1.2, assumed that they acted independently of the rest of the main building.

Column Details.- In the bottom two stories of the building, two different general types of transverse reinforcement were provided for the longitudinal column reinforcement--ties and spirals. This differentiation is important in view of the dramatically different behavior observed for each of these types of columns, as will be discussed in the next chapter. Details of many of the columns used in the building can be seen in Figs. 2.10 through 2.14. Tied columns were typically used in the one-story portion of the building as well as to support the stairtowers. Spirally reinforced columns were generally used in the bottom two stories of the multistory section. Thus in the ground story, more than half (i.e. 170) of the columns were tied; 142 of these were used to support the roof of the one-story section of the building, 18 were used to support the three stairtowers which were attached to the first floor slab, and 10 others were used in the remainder of the story. In the ground story, vertical support for the multistory section of the building was provided primarily by 163 spiral columns.

As in the ground story of the multistory section of the building, the first story contained primarily spiral columns (i.e. 148 out of a total of 164). These first story columns were generally continuous with the ground story columns but had slightly smaller cross-sections and lower amounts of longitudinal reinforcement. Twelve of the 16 tied columns used in the first story were located at the three exterior corners of each wing. These columns, shown in Fig. 2.13, were L-shaped for architectural reasons and, consequently, were not spirally reinforced. These tied columns were connected to shear walls above and spiral columns below.

The tied columns generally had rectilinear cross-sections and rectilinear longitudinal reinforcement patterns (both usually square). Their transverse reinforcement consisted of sparsely spaced ties

(usually #3 bars at 18-in. centers). A typical tied column in the ground story was 20-in. square and had four #11 bars for longitudinal reinforcement and #3 ties spaced at 18-in. for transverse reinforcement. The spiral columns generally had rectangular sections (usually square) with longitudinal reinforcement arranged in circular patterns. Their lateral reinforcement consisted of closelyspaced spirals which typically provided ratios of spiral reinforcement of about 2.3 percent. A typical spiral column had 5/8-in. diameter spirals spaced at 2.25 in. confining a circular concrete core and laterally restraining eight longitudinal bars equally spaced around the perimeter of the spirals. The longitudinal reinforcement ratios of the spiral columns ranged from 2.3 to 7.1 percent. The most heavily reinforced columns had longitudinal steel consisting of twelve #18 bars. Each of the columns with twelve bars had four bars outside the circular core which were laterally restrained with #3 ties at 18-in. centers (Fig. 2.12). Mechanical clamping devices were used to splice the reinforcement in the lower two stories, except for columns under shear walls where splices were typically butt welded.

Floor Slab Details. - The slabs at the first and second floors were typically 8-in. slabs with 5-in. drop panels at the supports or 10-in. slabs with 6-in. drop panels (see Figs. 2.2 and 2.3). As mentioned previously, deep beams framed into the columns around the perimeter of the multistory sections at the first floor level due to the difference in first floor elevation between the single and multistory portions of the building. Details of the reinforcing scheme used in a typical first floor slab is shown in Fig. 2.15. The depression indicated in the floor slab around the perimeter was typical and was required for architectural reasons. This depressed area was exposed to the weather. The details of the reinforcement in this area (Fig. 2.15) are of special concern, as are the details used in the second floor (Fig. 2.16) around the interior columns where depressions were usually required to install shower tubs.

2.2.3 Details of Second through Fifth Stories

The floor plans of the building's second, third, fourth, and

fifth stories were practically identical; a typical upper floor plan is shown in Fig. 2.3. At each of these levels, the floor plan of Wing A was the same as that for Wing C, and the plan for Wing B was the same as that for Wing D; detailed plans of these wings are shown in Figs. 2.4 and 2.5. With the exception of the shear walls, the typical upper floor plan was similar to that of the first story.

Shear Wall Details.- There were numerous shear walls in the upper stories of the building, as seen in Fig. 2.3. All of these shear walls were continuous between the second floor and the roof (Figs. 2.11 and 2.13). The shear walls at the elevator and stair shafts adjacent to the central courtyard (Figs. 2.3 and 2.4) continued down through the first story. These walls were not structurally connected to the first floor slab, however, and, thus, were ineffective in distributing shear forces to the first floor. Most of the shear walls in the second story had a thickness of 12-in.; this thickness decreased in the higher stories (see Figs. 2.4 and 2.5 for details). The walls which enclosed the elevator and stair shafts had a constant thickness throughout their height. The shear walls were asssumed to be nonbearing and were therefore detailed with a system of integral columns and floor girders to carry vertical loads.

Column Details.- As can be seen in the cross sections shown in Figs. 2.9 through 2.14, the first story columns continued through the upper stories of the building. The main exterior columns in the upper stories which were not part of the shear walls were channel-shaped, as shown in Figs. 2.4 and 2.10, and were provided with multiple ties for transverse reinforcement. In the bottom two stories, the corresponding columns were spirally reinforced. Because of the large beam depth in the exterior frames, the clear height of these channel columns was significantly less than that for the interior columns at these levels. At locations where the upper story columns acted as edge members of the shear walls, the columns were cast integrally with the walls.

The rest of the columns in the upper stories were generally smaller and had less longitudinal reinforcement than the corresponding

columns in the first story. Moreover, most of the upper story columns had transverse reinforcement which consisted of sparsely spaced ties (usually #3 ties spaced at 18 in.). Some of the second story columns had reinforcement which consisted of two adjacent spiral cages tied together by sparse ties (see Fig. 2.10). Splices in the longitudinal column reinforcement in stories two through five were made by lapping the reinforcement at 24 bar diameters.

Floor Slab Details.- Flat slab construction (Fig. 2.16) similar to that of the interior first floor was used throughout the upper floors. However, the reinforcement provided in the slabs at floor levels with shear walls was much less than that provided in the bottom two floor levels. This can be seen by comparing Figs. 2.15 and 2.16. There are two construction details at these levels (Fig. 2.16) which should be noted. One is the depression located at the drop panels, as discussed for the second floor, and the other is the absence of continuity or anchorage provided for the positive moment reinforcement at support lines.

The only beam elements located in the upper floors, other than those located in or between shear walls, were located around the perimeter of the building. These beams in the upper four floors were cast monolithically with deep sun shades which, as can be seen in Fig. 2.12, resulted in 5'-7" deep beams. The second floor slab also had deep beams at these locations, without the sun shade.

2.2.4 Penthouse Details

The four large penthouses housing mechanical equipment on the roof of the main building were quite similar (Figs. 2.1 and 2.7). The cross sections of Figs. 2.9 through 2.11 show elevations of Penthouse D. These penthouses were very rigid shear wall appendages. Two smaller penthouses were located on the roofs of Wings A and C (Fig. 2.7) at the top of the elevator and stair shafts. The plans of these two penthouses were identical and, like the other penthouses, were very rigid shear wall structures.

2.3 DESIGN CRITERIA

The Olive View Medical Center was designed during 1964-66 according to the provisions of the 1965 edition of the Los Angeles County Building Laws (LACBL) [2.1]. Many of the provisions of the 1964 Uniform Building Code (UBC) [2.2] and the 1956 American Concrete Institute Building Code (ACI) [2.3] were incorporated into these laws. The main building was designed using standard working stress methods in conjunction with the allowable stresses specified in the 1956 ACI Code. As required by the 1964 UBC, members were designed for both gravity loading (dead loads plus live loads), and combined seismic and gravity loading.

2.3.1 Gravity Loads

In determining the dead loads in the structure, structural concrete was assumed to have a unit weight of 150 lb/ft^3, and earth and concrete fill were assumed to have unit weights of 110 lb/ft^3. The contributions of partitions, ceilings, roofing, insulation, machinery, and so on, were also included in calculating the dead loads.

The live loads were determined using the recommendations of Sections 2304 and 2305 of the 1964 UBC. These live loads were reduced as permitted by Section 2306 of that Code.

In determining the internal forces due to gravity loading in the building's slabs and beams, moment distribution was carried out on the individual bents of the building. The forces in the columns were determined using the simplified loading specified in Section 1004 of the 1956 ACI Code.

2.3.2 Seismic Loads

The seismic design forces were determined for and distributed throughout the building in accordance with the earthquake regulations (Section 2314) of the 1965 LACBL and are presented in Fig. 2.17. This code uses the following formula to determine the design base shear:

$$V = ZKCW \qquad (2.1)$$

in which the terms are as defined in Appendix A.

Interpretation of code provisions is not straightforward for

structural systems as complex as the one selected for the main building. Consequently, the equivalent static lateral forces used in the design and their distribution could have been appreciably different depending on how the building had been idealized.

The modeling of the building used for its seismic design is shown in Fig. 2.17 along with the design calculations corresponding to this idealization. The relatively rigid upper four stories of the building were considered to be a setback (due to the change in lateral stiffness at the second floor level), and thus, the setback provisions of Section 2314(i) of the design code were applied. Under these provisions, the upper four stories of the building were treated as a separate structure, and the resulting base shear was then applied at the top of the lower part of the building which was otherwise considered separately for its own height. Commentaries to the SEAOC design recommendations, e.g. see [2.4], have consistently stated that the period used to calculate the lateral forces for both parts of such buildings can be based on an idealized structure with the mean height of the real structure. This interpretation would have significantly increased the height used to estimate the period of the structure, resulting in an increase in period and a corresponding decrease in the design lateral forces.

The upper portion of the building was designed to have a dual bracing system (K = 0.80 was used). This system consisted of shear walls capable of resisting all of the design lateral forces and a moment-resisting space frame capable of independently resisting 25 percent of the total lateral forces. However, there was no requirement that the behavior of the combined system be investigated as specified in current code requirements.

The bottom two stories of the building were designed as moment-resisting space frames. A K factor of 0.67 was used.

It is not clear from the design code whether different K factors could be combined in this manner within a single frame. While the Commentary to the SEAOC recommendations prior to 1967 suggests that in some cases different K values can be used for each principle direction of a building, no mention is made of combining K factors

for the same direction. Since 1967, the Commentary has considered this possibility in certain cases; however, it stipulates that the K factor must not decrease toward the bottom of the building as done in the design of the main building. Since the structural system does not fall within any of the main catagories in the SEAOC recommendations, a K factor of unity might have been more appropriate.

In accordance with the setback and K values assumed by the design engineers, the shear determined for the base of the upper portion of the building was 0.0774 W" (where W" is the total weight of the upper four stories); the base shear determined for the lower portion of the building was 0.08 W' (where W' is the total weight of the lower two stories) plus the concentrated loads for the upper four stories and the three stairtowers.

The contribution of the three relatively rigid stairtowers attached to the building at the first floor to the lateral design forces is difficult to assess without rational analysis [1.2]. The value used in the design, 170 kips, corresponds to 4.1 percent of their weight above this floor level and was calculated assumming that the portions of the stairtowers above the first floor level were setbacks. As such, they were treated as separate structures (K = 1.0 was assumed), and their computed base shear was applied to the main building at the first floor level.

The total design base shear was 10,340 kips; about 7.86 percent of the building's dead load weight. The designers calculated a total dead weight of 67,356 kips for the upper four stories; this weight was close to the value of 69,170 kips calculated during this study. The design weight of the bottom two stories was 61,989 kips; this value was calculated by the authors to be 63,498 kips. The distribution of weights, lateral forces, overturning moments, and horizontal torsional moments assumed in the seismic design of the building is shown in Tables 2.1 and 2.2.

While the lateral forces acting on the upper stories were included in calculating the seismic design shears in the bottom two stories, their contribution to the overturning moments in the lower stories was apparently neglected (see Table 2.2). If the overturning moment

from the upper stories had been included, the design overturning moment in the ground story would have been 474,000 k-ft instead of 270,000 k-ft (a 75 percent increase). The J factor for the design overturning moments (Fig. 2.17) was taken to be unity, as currently required.

The horizontal torsional moments applied to each floor level were assumed to be equivalent to the story shear acting at an eccentricity of five percent of the maximum building dimension at that level [as required in code Section 2314(g)]. Apparently, no special precautions were taken to account for the asymmetry of the ground story.

In the rigid upper portion of the building, the total horizontal shear at each floor level was distributed to the shear walls in proportion to their rigidities. Since these walls were not designed to be load bearing [see Code Section 2622(j)2], a moment-resisting frame was designed integrally with the walls to carry the gravity and overturning forces. To implement the dual bracing system assummed for these upper story levels, 25 percent of the total shear at each level was also distributed to the bents of the moment-resisting frames (excluding the shear walls) in proportion to their rigidities. In the bottom two stories of the building, the total seismic shear at each level was distributed to the individual bents in proportion to their rigidities. At each story, the shear forces due to the horizontal torsional moment were distributed to the various bents in proportion to their torsional rigidity about the center of rigidity of that level. Shear forces resulting from the torsional moment were disregarded when they would reduce the magnitude of the bent shears resulting from the direct lateral forces.

The seismic design forces in the members of the upper story frames were calculated using the portal method of analysis. The member forces in the bottom two stories were calculated using moment-distribution. Design forces were generally based on center-to-center dimensions and the foundation footings were assumed fixed. As mentioned previously, overturning forces were calculated in a simplistic manner, and in the case of the lower floors, these effects were generally underestimated.

2.3.3 Combined Gravity and Seismic Loading

The seismic and gravity design forces calculated for each member were combined to obtain the design forces. The design engineers took advantage of Section 2303 of the UBC (and LACBL) which stated that allowable stresses permitted for working stress design may be increased by one-third when considering earthquake forces combined with vertical gravity loads. As a result, the combined gravity and seismic design forces were effectively reduced by 25 percent; therefore, the critical design forces for many members were due to the gravity loads acting alone.

2.3.4 Compliance of Seismic Design With 1964 UBC

In a preliminary aseismic design and analysis of the main building, careful interpretation of the applicable code provisions was required to idealize realistically the setbacks and stairtowers, to establish appropriate values for the natural period, and to assign proper K factors. The basic seismic-resistant design procedure used for this building was in essential agreement with most provisions of the 1964 UBC. In fact, as will be discussed in later chapters, the design base shear could have been reduced appreciably by making different interpretations of certain code provisions and by computing the fundamental period using rational analytical methods. Moreover, individual members were generally designed to be stronger than the minimum values required by the code. However, ambiguities in several provisions of the design code (e.g., mixed K factors, treatment of setbacks, and computations of overturning moments for setbacks) could have resulted in interpretations significantly different than those made by the design engineers. The effect that alternative interpretations of code provisions regarding the computation of design lateral forces might have had on the structural behavior during the earthquake is briefly discussed in Chapter 6.

Codes promulgated since the design of the facility have clarified an ambiguous, yet important, requirement in the 1964 UBC regarding detailing of columns that proved to have serious consequences during the earthquake. Since the 1964 code provisions related to combined flexural and axial load conditions did not explicitly consider the effects of shearing forces, many engineers, including apparently the

designer of this building, did not design columns to resist shear. Consequently, only minimum ties spaced at maximum allowable intervals were installed in the columns. The design code [Section 2619(a) of the LACBL and 1964 UBC] actually required that two-thirds of the shear carried by members of frames not bounded by slabs (columns would meet this definition) be resisted by appropriately designed web reinforcement. In many cases, the shears developed in columns under the code working stress lateral forces were not high enough to require significant increases in the quantity of transverse reinforcement; i.e., the minimum requirements for size and spacing of shear reinforcement contained in code Section 2619(f) would have satisfied this shear requirement.

The code requirement that every longitudinal bar in tied columns be restrained by the equivalent of a 90 degree corner tie was generally met. However, the hoop spacing used in the tied columns was generally too large to provide the necessary confinement, shear strength and restraint against buckling of the longitudinal reinforcement to permit ductile behavior. The mechanical characteristics of the tied and spiral columns used in the main building are examined in greater detail in Appendix B.

2.3.5 Compliance of Seismic Design with 1973 UBC

Several major changes have been incorporated into the 1973 edition of the UBC [2.5] that would have had a substantial effect on the building's design. In fact, a few of these had been discussed and adopted by various engineering organizations before construction of the main building advanced beyond the preliminary stages. For example, requirements for ductile moment-resisting space frames in buildings with K factors equal to 0.67 or 0.80 had been adopted by the SEAOC in the years prior to 1966, and were published in the Recommended Lateral Force Requirements [2.6] during 1967. The Los Angeles County Building Laws were also amended in November, 1966, significantly altering design requirements, especially those regarding columns. Although construction of the building did not start until June 1966, and the first batch of concrete was not poured until September of that year, the design engineers did not modify their design to account for these considerations.

Since the construction of the building, several other changes have been incorporated into the UBC [2.5]. Ultimate strength design philosophies for reinforced concrete structures have replaced working stress procedures as the preferable design method. Reinforced concrete space frames in Seismic Zones 2 and 3 generally must be designed and detailed to be ductile moment-resisting, if they are part of the lateral force-resisting system or located on the perimeter of the structure. Additionally, unusual structures, such as this building, must now be evaluated considering the dynamic characteristics of the actual structural system. These and other new code provisions would have had a significant effect on the design of the main building. Furthermore, the State of California has enacted even more restrictive requirements for the design of hospitals [2.8] partially as a result of the severe damage suffered by this and other emergency facilities during the San Fernando earthquake. The impact of some of these newer provisions on the probable seismic behavior of the building will be briefly discussed in subsequent chapters.

2.4 MATERIAL PROPERTIES

The quality of construction materials and their conformance to design specifications are important considerations in evaluating the performance of buildings. In addition to reviewing the field concrete control tests and the mill test data for the reinforcement, an extensive experimental investigation of actual specimens removed from the facility has been conducted. The results of these material studies are covered in a separate report [2.9] and will only be briefly reviewed in this section.

2.4.1 Design Specifications

In the design and construction of the main building, the structural materials were assumed to have the following properties:

All cement was to be a standard brand of Portland cement conforming to ASTM C-150 type II.

All concrete was to be stone concrete that could develop a compressive strength of 3000 psi at 28 days except as follows:

1. The ground and first story columns were to have stone concrete that could develop a compressive strength of 5000 psi at 28 days.

2. Slabs on grade were to be stone concrete that could develop a compressive strength of 2500 psi at 28 days.

3. The concrete fill on the roof of the one-story section of the building was to be lightweight concrete that could develop a compressive strength of 3000 psi at 28 days and would not weigh more than 110 lb/ft^3 when oven dry.

All reinforcing steel, except vertical column reinforcement, was to be new, deformed intermediate grade billet steel bars conforming to ASTM specification A-15 or A-408 (f_y = 40 ksi). Bar deformations were to conform to ASTM A-305. All vertical column reinforcing was to conform to ASTM A-432 (f_y = 60 ksi).

2.4.2 Quality Control Tests

Concrete.- During construction, field control tests were performed to determine the 28-day compressive strength of the two types of structural concrete used in the facility. In reviewing these results [2.9], it was found that the quality control for the nominal 3000 psi concrete was very good, obtaining an average strength of 4,072 psi and a standard deviation of 416 psi. The average compressive strength for the concrete with a specified design strength of 5000 psi was 5,534 psi with a standard deviation of 580 psi. For a normal distribution, only 0.75 percent of the 3,000 psi concrete would have been expected to fail below the specified design strength, while nearly 17.5 percent of the 5,000 psi strength concrete would have. This information is summarized in Table 2.3.

Reinforcing Steel.- Mill test reports for the bars used in the main building were reviewed [2.9] with regard to the grade and size of the bar. However, no information was available for the specific distribution of each mill run within the building. Table 2.4 summarizes some of the data available from these tests. With the exception of the maximum elongation of the A-15 grade reinforcement, nearly all of the mill test results exceeded the minimum ASTM specifications.

The average yield strength was 52.6 ksi for the A-15 grade reinforcement; this was more than 30 percent higher than the specified minimum. If a normal distribution is assumed for the tests, nearly 98 percent of the steel yield strengths would fall between the limits of 44.6 ksi and 60.7 ksi. The ultimate tensile strength of this steel averaged 79.5 ksi with a standard deviation of about 3.3 ksi, which is well within the ASTM specified bounds of 70-90 ksi for this grade.

The A-432 grade reinforcing steel had an average yield strength of 71.1 ksi, 18 percent over the minimum specification, with a standard deviation of 6.7 ksi. The average ultimate tensile strength was 112.5 ksi, well above the specified minimum of 90 ksi.

It is interesting to compare these results with the current requirements for reinforcement for buildings in Seismic Zone 3. According to Section 2626(d)2 of the 1973 UBC [2.5], the yield stress must not exceed the specified minimum by more than 18 ksi; the ultimate tensile strength must exceed the yield stress determined by mill tests by at least 33 percent. In this case, it is apparent that much of the steel used in the building was substantially stronger than allowed by current practice. Assuming a normal distribution, seven percent of the A-15 grade reinforcement would be expected to yield at a stress greater than 58 ksi and fifteen percent of the A-432 grade reinforcement would yield above 78 ksi. The average ultimate tensile stresses are greater than 1.33 times the average yield stresses.

2.4.3 Laboratory Tests

Concrete.- A number of specimens of the concrete used in the building were collected after the earthquake by coring in the field or by removing several fairly large pieces of concrete rubble. These specimens were taken from locations where a compressive strength of 5000 psi was specified in the design. Laboratory tests on 3-in. x 6-in., 3-in. x 8-in., and 6-in. x 12-in. cylinders made from these specimens are described in detail in Reference 2.9. After adjusting for specimen size, the compressive strength of these cylinders, which were approximately one to two years old at the time of the tests, averaged 6,300 psi for locations in the multistory

section of the building and 7,000 psi for specimens taken from the stairtower columns. These values are stronger than the corresponding 28-day field control test average by fourteen and 21 percent, respectively. This increase in strength with age partially mitigates the risk of understrength concrete detected from the field control tests on the 5,000 psi strength concrete.

The modulus of elasticity of the specimens was also evaluated. The value obtained for both groupings of nominal 5000 psi concrete was 3.54 ksi, which is about thirteen percent below the value calculated from the ACI formula, $E = w^{1.5}33\sqrt{f'_c}$, based on the concrete design strength. If the actual test strength values are used, the modulus is 30 percent lower than the calculated value. This equation, however, is more representative than values suggested in the LACBL which gave $E = 1{,}000\ f'_c$.

Reinforcing Steel.- Twelve specimens of A-15 intermediate grade reinforcing steel and 16 specimens of A-432 steel bars were removed from the hospital buildings for testing. The specimens were taken from relatively unrestrained end portions of reinforcement protruding from the damaged structure. Results of these tests are shown in Table 2.5. The average yield stress for the A-15 intermediate grade bars was 50.4 ksi, about six percent lower than the value determined from the mill tests. This discrepancy might partially be explained by the different loading rates used in the two types of tests. The ultimate tensile stress came within two to three percent of the values determined from the mill tests.

Similar results for the A-432 grade steel are presented in Table 2.6. The average experimental yield stress for bars removed from the main building was 66.3 ksi, about eight percent smaller than the average of the mill tests. The ultimate tensile stress of this limited sample was about three percent lower than the mill test values.

In all but one case, a specimen removed from one column of the ambulance canopy, the grade of the specimens of steel removed from the various buildings at Olive View conformed to those specified in the design.

2.5 QUALITY OF CONSTRUCTION

The seismic response of a building depends on its actual construction rather than on its idealized design. Consequently, it is important to examine the detailing and workmanship used in the building. Figure 2.18 shows the main building under construction.

2.5.1 Structural Drawings

There were only a few minor differences between the structural system shown in the design calculations and the one represented in the structural blueprints. The structural drawings were not particularly easy to interpret, however. Most of the information required for construction was contained in the drawings, yet in many instances the information was difficult to find. In a number of cases, the contractor was required to extrapolate particular details from general details given in the drawings for other locations.

Besides the overall problems related to the type of structural system and the complexity of the structural configuration, there were some instances of poor esthetic planning resulting in increased lateral forces and poor design detailing that became apparent after the earthquake and which will be examined in Chapter 3. These included unnecessary masses in the structural and nonstructural elements, and types of columns (Fig. 2.19). Column dowels were not properly laterally reinforced. Column ties were terminated by 90 degree hooks rather than the preferable 135 degree hooks. Also, the detailing of reinforcement splices and of joint connections between columns and slabs was generally inadequate.

2.5.2 Construction Workmanship

The building was generally constructed according to the design drawings. The overall workmanship could be rated as good since there were no major discrepancies between the specifications and actual construction with regards to materials used, amounts of steel reinforcement, and dimensioning. However, there were a few instances of poor workmanship. For example, in several cases, the placement of the reinforcing bars was not carefully performed, and the cover of the concrete varied considerably from that specified,

thus affecting the strengths of the members.

In a number of cases, the spirals at the tops of the ground and first story columns did not continue into the joints, but were terminated below the joint. This reduced the shear strengths of these columns considerably and resulted in their failure as discussed in Chapter 3 (Fig. 3.14). In the structural drawings, a general detail indicated that the spirals were to extend up through the drop panel to the bottom main slab reinforcement above each column; each spiral was to be terminated by one-and-one-half extra turns at its end. There were, however, no details showing what was to be done in the case of columns framing into beams instead of slabs. It was generally in these cases that the spirals were terminated below the joints. As discussed in Chapter 3, several failures were observed in these regions.

2.5.3 Detailing of Nonstructural Elements

There were many nonstructural elements in the building that affected the seismic response and were not considered in the seismic design. For example, the plaster partition walls probably increased the initial stiffness and strength of the building. The most outstanding example of the unforeseen effects of nonstructural elements occurred in the ground story. In this story there were concrete block masonry walls in Wing C which were not intended to interact with the structure in the case of lateral movement. However, while a continuous horizontal gap between these walls and the first floor slabs was provided to allow lateral movement, the edges of beams which extended below the bottom of the slab were not separated from these walls by vertical gaps. Consequently, relative lateral movement between the beams and the walls was prevented and the building interacted with these walls.

2.6 CONCLUDING REMARKS

The main building had a complex structural system incorporating a wide variety of structural elements. The design generally followed the recommendations of the governing codes; however, the complexity of the building makes a clear interpretation of many code provisions difficult. Changes in the design codes since the building was designed

could have modified the design appreciably. The materials used in the building generally met or exceeded the properties specified in the design. The quality of workmanship was, on the whole, good, but a number of poor details and misplaced reinforcement resulted in some significant damage which will be reviewed in the next chapter.

III. STRUCTURAL DAMAGE

3.1 INTRODUCTION

This chapter briefly reviews some of the general features of the structural damage to the Olive View Medical Center resulting from the San Fernando earthquake. Some of the more important aspects of the damage observed throughout the main building are discussed, and a thorough survey of the damage in Wing D is presented. Wing D was selected for this presentation because its damage was believed to be representative of the damage that occurred throughout the structure, and because it serves as the basis of detailed analytical studies described later in this report.

The survey of damages described in this chapter is based on observations made by the authors during numerous field trips to the site following the earthquake. Space limitations preclude a thorough presentation of these observations in this report. Further information regarding the damage to the facility may be found in Reference 3.1.

3.2 GENERAL FEATURES OF DAMAGE IN VICINITY OF MAIN BUILDING

No active faults were detected in the immediate vicinity of the Olive View Medical Center. While some surface rupturing due to soil subsidence was observed, none of the structural damage could be attributed to this cause. Thus, all of the damage appeared to be the result of ground shaking.

All major structures of the Medical Center (Fig. 1.5) sustained heavy structural and nonstructural damage, as shown in Fig. 1.3. In fact, the severity of the damage prompted the County of Los Angeles to order demolition of all the structures, except for the power plant which was deemed repairable.

The one-story, masonry and reinforced concrete warehouse [1.9], which was separated from the main building by a 4-in. seismic joint, suffered considerable structural damage as a result of the impact of the main building. The reinforced concrete ambulance canopy [1.8] collapsed, as seen in Fig. 3.1, due to shear failures of its tied columns. The bottom story of the two-story, reinforced concrete

psychiatric unit [1.10] also collapsed due to the shear failure of its tied columns. The one-story, reinforced concrete assembly building sustained large horizontal deformations due to yielding in its columns, but it did not collapse entirely. The exhaust pavilion [1.11] suffered little damage; however, the surrounding architectural canopy, which was separated from the pavilion, suffered severe structural damage due to reinforcement anchorage failures.

3.3 DAMAGE TO MAIN BUILDING

The main building suffered extensive structural and nonstructural damage in its bottom two stories (see Figs. 1.4 and 3.1). There were lesser amounts of structural damage, but still a great deal of cracking and nonstructural damage, in the top four stories that contained numerous shear walls. The tied columns in the bottom two stories generally failed in shear, resulting in the collapse of three of the stairtowers (Towers A, B, and D) and much of the single-story portion of the ground story (the terrace canopy and courtyard).

Very large, permanent deformations were observed in the bottom two stories. The residual displacements consisted primarily of translations toward the northeast, as can be seen in Figs. 3.2 through 3.4. The largest story drifts occurred in the first story which sustained an average northward drift of about 20 in., an average eastward drift of about 7.5 in., and an average angular rotation of about 0.15 degrees about a vertical axis. Drifts exceeding 30 in. were observed at some locations in this story. The average drift of the ground story was about 5.5 in. northward and 3 in. eastward. Northward drifts of about 1-in. were observed in the crawl space located under the ground floor slab in the northern part of the building (see Figs. 2.9 and 3.4). The interstory drifts in the upper four stories were small due to the presence of shear walls in these stories.

Deformations in the ground story were restrained in the N-E direction by the retaining wall and warehouse. The floors above this level were partially restrained against northward deflection by Stairtower C which was completely separated from the main building

by a 4-in. seismic joint for its full height. Although this stair-tower did not collapse, the impact of the main building caused it to tilt considerably towards the north (Fig. 3.5). The presence of this tower may have been responsible for the permanent torsional rotation observed in the complete first story.

3.3.1 Seismic Joint and Foundation

The drifts in the ground story were sufficient to cause impact of the first floor with the north retaining wall and the west and south sides of the warehouse. These were initially separated from the first floor by a 4-in. wide seismic joint, as shown in Fig. 2.8. In many places, this joint could provide only 2 in. of unrestrained horizontal movement prior to contact. Extensive damage and permanent displacement of the retaining walls (Fig. 3.6) and warehouse (Fig. 3.7) resulted from the impact. The damage to column FF-26, shown in Fig. 3.6(b), indicates that no significant reversals of deformation occurred at this location.

It is believed that the impact of the main building with adjacent structures at the first floor level had a significant effect on the subsequent seismic response as well as on the distribution of damage. The main building would behave essentially like a six-story structure with two soft stories when vibrating towards the south or before contacting the adjacent structures on the north. When the seismic joints at the first floor level were closed, however, the building would behave essentially like a five-story structure with only a single soft story. The ramifications of this behavior will be discussed in subsequent chapters.

For the most part, the foundation system performed well, and little of the structural damage could be directly attributed to failure of the spread footing or the supporting soil. Regions of inelastic deformation (plastic hinging) were noted in many of the ground story spiral columns [Fig. 3.8(a)], especially at a level just above the ground slab, indicating the effectiveness of the foundation system [Fig. 3.8(b)]. There was little evidence of yielding in some of the other columns at the ground level; however, significant base

rotations were observed nonetheless [Fig. 3.8(c)]. It is not clear whether these rotations were caused by rotation of the supporting spread footing or by unobserved yielding in the portions of the column that were below grade (Fig. 2.9). As a consequence of these rotations, the grade slabs translated horizontally in many locations, opening large gaps at expansion/construction joints [Fig. 3.8(c)].

Many shear failures (Fig. 3.9) were observed in the short, tied columns used in the crawl space (Fig. 2.9) located below the ground level slab in the northern part of the main building. These failures resulted in substantial subsidence in the terrace canopy along column line CC of the ground story (see Fig. 3.10).

3.3.2 Ground and First Stories

There was extensive damage throughout the ground story of the main building. Most of the tied columns, including those supporting the stairtowers, failed in shear. These failures led to the collapse of substantial portions of the terrace canopy (Fig. 3.11) and courtyard, and the overturning of three of the stairtowers. The impact of these stairtowers on the adjacent terrace canopy resulted in significant additional damages to the canopy (Fig. 3.1).

The damage in the first story was also extensive. The permanent drifts in this story were the largest observed in the main building. Unlike the ground story, no major portions of the first story were supported exclusively by tied columns. The tied columns in the first story failed (Fig. 3.10). Fortunately, the load was successfully redistributed by the walls acting as cantilevers to adjacent spiral columns in this story, and there was no major collapse in this story.

Columns. - All of the tied columns in these two stories failed, generally in shear. Many of the spiral columns in the ground story spalled major parts of their concrete covers and sustained yielding at both the top and bottom (Fig. 3.8). As discussed, there was generally less damage in those columns where subgrade rotation was observed.

The spiral columns in the first story underwent relatively larger inelastic deformations than those in the ground story. Most of these columns spalled their concrete covers outside the spirals, but retained their ability to support the superstructure. The damage in the tied and spiral columns of the first story is compared in Fig. 3.12.

Two major examples of poor detailing and workmanship were noted from the damage to the spiral columns. Shear failures were noted at the tops of several spiral columns (see Figs. 3.13 and 3.14) where the spiral reinforcement was improperly placed, or terminated below the lowest member framing into the column, i.e., the spirals did not continue into the beam-column joint. Such failures in the joints or at the tops of columns could be eliminated by careful detailing, workmanship, and thorough inspection during construction. Another deficiency was the improper detailing of dowels extending into the first story columns from below (e.g., see Fig. 3.12). The absence or inadequacy of transverse reinforcement confining the concrete around the dowels resulted in premature concrete splitting and spalling, and, thereby, a reduction in the load carrying capacity of the column. Although these errors were the cause of much of the visible local damage, they were not the primary reasons for the severe overall damage observed in the building.

The overall performance of the spiral columns was good, indicating that confined reinforced concrete can be designed and detailed to behave in a ductile manner under severe earthquake excitations. However, the large lateral displacements resulting from the insufficient overall lateral stiffness of the first two stories, and the early failures of the inadequately confined tied columns and the poorly detailed and constructed spiral columns in the first and ground stories indicate that: (1) ductile behavior can only be achieved with careful attention to design, detailing, and construction workmanship; and (2) ductility by itself is not sufficient to control overall damage; it is also necessary to provide a structure with sufficient stiffness.

Floor Slabs. - Much of the ground story's terrace canopy and courtyard collapsed or subsided significantly due to the failure of the unconfined tied columns used for their support. Elsewhere, substantial

punching shear failures were observed in the first floor slab and drop panels near the spiral columns. Punching shear failures were the cause of significant upheaving and subsidence of the slab at many locations (see Fig. 3.15). The damage in the second floor slab was similar to that observed in the first floor, though much less severe.

The beams located on the perimeters of each wing in the first and second floors suffered substantial cracking. Shear cracking and failures were also observed in some of these joint regions. The distress to these beam-column joints can be seen in Figs. 3.1, 3.11 and 3.12.

Structural Walls.- There were no structural, reinforced concrete walls in the ground story. In the first story, however, walls were located around the elevator shafts and stairtowers (Figs. 2.1 and 2.2). The stairtowers were not connected to the building above the first floor slab, and the elevator walls were separated from the first floor slab and the adjacent columns by a 1-in. gap; thus, these walls were not intended to contribute to the lateral stiffness of the first story. As discussed, ground story tied columns supporting the stairtowers failed, resulting in the collapse of the latter (see Fig. 3.1). Further details regarding the damage to the stairtowers may be found in Reference 1.2.

Although the walls around the elevator shafts in the first story were not monolithically cast with the adjacent columns, the damage to the first story walls was substantial (Figs. 3.16). This damage occurred because the gap between the columns and wall was insufficient to accommodate the large drifts that actually developed. Furthermore, these walls were actually bolted to the first story columns (see Fig. 3.17), restraining relative deflection between the columns and wall in the N-S directions. The large drifts and damage in the first story of the elevator shafts severely disrupted access to the upper stories. The brick veneer on these walls spalled in many places, posing a potential threat to life safety.

Nonstructural Elements. - There was, of course, tremendous nonstructural damage in the portions of the ground story that suffered partial or complete collapse. There was also extensive damage to nonstructural elements and to contents of the building throughout the remainder of the bottom two stories. This nonstructural damage included the breaking of nearly all window panels, the cracking and/or collapse of most partitions, and the widespread collapse of ceiling panels, lighting fixtures, and heating, ventilation and air conditioning equipment. In many places, large glass panels toppled out into public areas. The general nature of the nonstructural damage can be seen in Figs. 3.8 and 3.10 through 3.15.

Of particular concern was the damage to precast architectural panels and masonry partitions. Precast panels were attached to the parapet at the boundary of the terrace canopy as shown in Fig. 3.18. These panels generally fell from their supports as seen in Figs. 3.7, 3.11 and 3.19. The collapse of these panels posed a serious hazard to public safety. Such nonstructural elements must be securely fastened to the structural system with ductile connectors. The details of the connections used in this case (Fig. 3.18) failed to provide this type of connection.

Another example of poor detailing was the concrete masonry walls used in the ground story of Wing C. As discussed in Chapter 2, these walls were not intended to contribute to the lateral force resisting system of the building. To accomplish this, a continuous horizontal gap was provided between the top of these walls and the bottom of the first floor slab. However, the gap was not continued around the perimeter of beams that extended below the slab; thus the walls were able to resist lateral forces. The resulting damage to some of these walls can be seen in Fig. 3.20.

It is evident that the damage to nonstructural elements posed a serious threat to the safety of the building's occupants and that the design of these elements was inadequate. Nonstructural elements must be designed so that they will not endanger life safety. It is

essential that such elements be securely attached to the structural system and that they be detailed to behave in a ductile manner or be adequately isolated from structural actions that may cause brittle failures (e.g., large relative drifts). As illustrated by the damage to this building, it is necessary to make realistic assessments of the structural behavior if such isolation techniques are to be effective. Although additional protection to occupants may be provided by improved detailing and construction of nonstructural elements, some limit on seismic drifts may be necessary to restrict nonstructural damage to acceptable levels, even in the case of major earthquakes where collapse avoidance is generally considered the primary design criterion. The possibility of injury to occupants and damage to nonstructural elements must be minimized.

3.3.3 Second Through Fifth Stories

The damage observed in the upper stories was relatively minor and generally decreased in intensity towards the top of the building. There was considerable cracking of structural and nonstructural members at these levels.

The most prominent damage occurred in the second story. Many of the exterior channel shaped columns, especially those in Wings A and C, suffered shear failures (Figs. 3.10 through 3.12, 3.20 and 3.21). These channel columns had particularly low shear span-to-width ratios due to the deep spandrel beams and sunshades that framed into them (Fig. 2.12). From the damage shown in Fig. 3.21, it appears that the nonstructural, light-weight wall panels below the second story windows interacted with the columns, causing an additional significant reduction in the clear span of the columns.

Nonstructural damage in the second story was also noticeably more severe in Wings A and C. Plaster used to cover the interior structural members were extensively cracked in some locations. For example, the plaster covering shear wall J-L-12 at the second floor in Wing A was severely cracked (Fig. 3.22). Although this wall was cracked, the width of the cracks was less severe than indicated by the cracks in the plaster.

3.3.4 Penthouses

Little significant damage, structural or nonstructural, was observed in the penthouses. The primary damage that occurred was cracking in the penthouse walls. The pattern of damage observed was similar in each of the penthouses. The most significant cracking typically occurred in the center bent of the interior penthouse wall which coupled the longitudinal shear walls located below them (Fig. 2.1). For more details see Section 3.4.5.

3.4 DETAILS OF DAMAGE TO WING D

The overall damages to Wing D were of the same general nature as those which occurred throughout the main building. Schematic diagrams of the damage distribution in frames 28 and 29 are shown in Figs. 3.23 and 3.24. The most pronounced damages occurred in the first story; this story experienced very large drifts, failures of its tied columns, yielding in its spirally reinforced columns, and shear failures in its floor slab. Although the ground story experienced smaller drifts, these were large enough to cause extensive damages. There were failures in all of the tied columns under the ground story's terrace canopy, courtyard, and stairtower; as a result, the stairtower and parts of the canopy collapsed, while the courtyard and other parts of the canopy partially collapsed. All of the ground story's spiral columns underwent some yielding. There was some cracking in the upper stories, but damage was relatively minor; the interstory deformations in these stories were small due to the presence of numerous shear walls. The damage in the wing's penthouse was also minor; its wall experienced some cracking.

3.4.1 Seismic Joint and Foundation

Wing D impacted the warehouse, causing considerable damage. The separation provided by the seismic joint was clearly insufficient. Details of this damage are shown in Fig. 3.7 and discussed in Reference 1.9.

Cracking in Wing D's ground floor slab was not extensive, but was apparent in a number of locations, particularly where the columns pierced the slab. In some places, subgrade rotations of the columns,

along with other effects of the ground motion, caused considerable horizontal displacements of the ground floor slab. These displacements were particularly noticeable at the slab's construction joints [Fig. 3.8(c)].

3.4.2 Ground Story

There were substantial differences in the nature and severity of the structural damages observed under the terrace canopy and courtyard, and under the highrise portion of the building.

Under the Terrace Canopy and Courtyard. - There were failures in all of the tied columns supporting the terrace canopy and courtyard. Most of the columns failed predominantly in shear due to insufficient lateral reinforcement. Most of these columns were 20 in. square; all of the columns had transverse reinforcement which consisted of #3 ties spaced at 18-in. intervals (except column E-22 which had #3 ties at 14-in. intervals).

After the south exterior columns along column lines E and F.2 (Fig. 2.2) failed, the southern edge of the heavy earth-filled terrace canopy which these columns supported collapsed, falling to the ground floor level (see Figs. 3.11, 3.19, 3.23 and 3.24). Brittle shear failures of the type indicated in Fig. 3.25 occurred in all the relatively stiff, but weak, columns along line E, between column lines 22 and 30 (Fig. 2.2). The columns along line E had relatively short clear heights due to the deep beams which connected them (Fig. 2.11). The columns along line F.2 were larger (Fig. 2.10) and exhibited a different failure mode. These columns rotated on their foundations, but before critical shear stresses developed in them, punching shear failures occurred in the weak flat slabs that they supported (see Fig. 3.11). Column F.2-16 (Fig. 2.2) did not fail due to its close proximity to column F.2-15 and due to a beam that ran along column line 15 (Fig. 2.2). The columns along line F.2 had longer clear heights than those of the columns along line E, since the former supported flat slabs instead of deep beams. Also, unlike the columns along line E, those along line F.2 were not attached to the perimeter grade beams of the building (Figs. 2.10 and 2.11). Thus, it appears that

the differences observed in the column failures along lines E and F.2 (see Figs. 3.11 and 3.25) may be attributed to differences in the strengths and stiffnesses of the columns and of the first floor beams and slabs at these locations.

Most of the columns which supported the terrace canopy on the east side of Wing D (Fig. 2.2), i.e., those columns along lines 30 and 31, failed completely as the stairtower and canopy collapsed on top of them (Fig. 3.1). Of those columns, only E-30, M.5-31, and M.5-30 were not buried.

All the canopy columns on the north-east side of Wing D (i.e., those columns along lines 26, 27, 28, 29, and north of line M), experienced complete diagonal shear failures near their tops and bottoms (e.g., see Figs. 3.26 and 3.27). There was some cracking in the 12-in. thick slabs supported by these columns around the slab-column joints. A shear failure occurred at the construction joint at the top of column P.5-29, as indicated in Fig. 3.24. Columns which had beams framing into only one side (e.g. column N-27) experienced shear failures in their beam-column joints.

The columns in Wing D under the courtyard, columns P-16, P-17, and P-18, suffered shear failures similar to those experienced by the columns of the north-east canopy (see Fig. 3.28). These columns, however, did not fail quite as extensively as those under the north-east canopy. They failed only at their tops and appear to have rotated about their bottom foundations. The courtyard roof slab dropped several feet in elevation as a result of the column failures. There was some cracking in the courtyard slabs around the slab-column joints. As in the case of the rest of the roof of the ground story, the damage to the courtyard slabs was due to the failures of the columns which supported it.

The failure of these tied columns and the subsequent collapse of much of the first floor slab caused extraordinary damage to non-structural elements and contents of these portions of the building. The hazard to occupants was substantial. As previously discussed, failure of exterior precast architectural panels posed an additional

threat to people outside the building.

Under the Highrise Structure. - Though there was substantial cracking and spalling of concrete in most of the ground story columns beneath the highrise portion of the hospital, none of these columns failed completely. Some failures were observed in the joints.

The members of frame 29 suffered the most extensive damage in the ground story of Wing D (Fig. 3.24). A shear failure occurred in the lower portion of the beam-column joint, column M-29 (see Fig. 3.13). This brittle failure was due to the fact that the column spirals did not extend into the beam-column joint. The beam on the north side of this column was substantially deeper than that on the south side. This resulted in a considerable length of column without transverse confinement or shear reinforcement. A somewhat similar shear failure was experienced in the beam-column joint above column G-29; there was also a rotation of this column about its footing. The middle two columns of frame 29 were not as severely damaged. There was some cracking in column K-29's beam-column joint, and column H-29 experienced significant footing rotation [see Fig. 3.8(c)]. Beams 29-M-K and 29-G-H did not suffer much damage, but some large cracks were observed in the middle beam, between columns H-29 and K-29.

The columns of frames 24, 26, 27, and 28 (excluding the columns along column line G) all suffered somewhat similar damage (see Figs. 3.23 and 3.8). Most of them suffered cracking and spalling in their covers and buckling of their corner longitudinal reinforcement. This reinforcement was generally confined by #3 hoops at 18-in. intervals and not by the spiral reinforcement. Plastic hinges formed in the lower halves of some of these columns. It appears that the other columns rotated below grade.

The columns along column line G from column lines 22 to 29 suffered extensive failures in their beam-column joints (see Fig. 3.29). These failures were primarily a result of the collapse of Wing D's

south canopy columns along line E. After the canopy columns failed and the canopy collapsed, the heavy canopy beams which framed into the columns along line G (see Fig. 2.2) rotated about these beam-column joints, thus causing the joint to fail. As can be seen in Fig. 3.29, no shear reinforcement was provided in the joint.

The damages to the spiral columns of frames 16, 17, 18, 19, and 22 were similar to, but slightly greater than, those which occurred in the columns of frames 24, 26, 27, and 28. These columns experienced cracking and spalling of their unconfined concrete covers, especially around their corner longitudinal reinforcement [Figs. 3.8(a) and 3.8(b)]. There were no failures in the beam-column joints of columns G-16, G-17, and G-18 because the south canopy (which collapsed) was connected to these columns by a flat slab which failed before critical stresses could be developed in the joints [see Fig. 3.11(b)].

Tied column N-24 suffered a shear failure, but it was not as severe as the failures of the tied columns under the canopy or courtyard.

Columns H-16 and J.9-16 had wide-flange steel sections as longitudinal reinforcement. These columns were connected by beam 16-J.9-H which had a plate girder within it. The plate girder was connected to the wide-flange sections used for column reinforcement, and these columns and beam were encased in concrete. This arrangement was used to support the loads from column J-16 which was discontinued in the ground story. Significant shear cracking occurred in the concrete encasing these beam-column connections.

Except for the cracking observed in the beams of frame 29 and in the beam-column joints along column line G, there was not much cracking in the first floor beams of Unit D. There was, however, significant damage observed in the flat slab floor system.

Spalling of concrete and cracking in the first floor slab and drop panels were observable from both the ground story and the first story. Around the tops of many of the ground story columns there was evidence of punching through the slab and drop panels (Fig. 3.15).

There were cracks running in the E-W direction in the northern portions of the drop panels (Fig. 3.23). These cracks were consistent with the flexural rotations of the columns at the drop panels. There was a prominent crack (running E-W) in the bottom of the first floor slab near its boundary at column line G where the slab changed elevation (Fig. 3.23). Extensive cracking and shear failure patterns (punching and heaving) were observed in the top of the slab around all of the interior columns (see Fig. 3.15). These damage patterns did not occur around the bottom ends of Wing D's exterior first floor columns, probably because of the large beams supporting the slabs between the exterior columns (Fig. 2.2).

3.4.3 First Story

Wing D's first story experienced greater damage than any other story of this unit, with the exception of the ground story under the terrace canopy and courtyard areas. Not only was there substantial structural damage to the columns, beams, and slabs, there was also a tremendous amount of damage to the wing's nonstructural elements (the partition walls, ceilings, etc.) as shown in Fig. 3.30.

All the columns of the first story underwent permanent lateral drifts greater than 12 in. (Fig. 3.2). Each of the spirally reinforced columns of the wing experienced substantial inelastic deformations, but the only first story columns to fail completely were the three tied corner columns (columns M-29, G-29, and G-16) which had transverse reinforcement consisting of multiple #3 ties spaced at 18-in. intervals. There was also a moderate amount of damage in Wing D's interior second floor slab.

Although all the columns of frame 29 under the shear walls suffered extensive damages (Figs. 3.24 and 3.31), it is interesting to note the differences in these damages. Both of the tied corner columns failed; column G-29 appears to have suffered more damage than column M-29 [compare Figs. 3.31(b) and 3.31(c)]. Since the large residual displacement of the structure was towards the north, the frame's south columns probably experienced pronounced axial tensile forces due to overturning, while the north columns experienced compressive

forces. This difference may explain why most of the concrete spalled from column G-29, yet remained in column M-29 (a consequence of the different properties of concrete in tension and compression). The difference in axial loading may also explain why column H-29 appears to have suffered more cracking and spalling than column K-29. The second floor beam joining columns H-29 and K-29 suffered little cracking.

The exterior spiral columns, along column lines G and M in Wing D, all suffered similar damage, generally consisting of extensive spalling of their outer (unconfined) concrete covers. The beams above the north columns did not suffer much damage, but the beams above the south columns suffered extensive cracking and some spalling (most extensively, around the beam-column joints). The second floor beam-column joints over the south columns suffered considerably more damage than those for the north columns [see Fig. 3.32(a) for typical damage]. This difference in damage was probably the result of the structure's displacement and consequent overturning towards the north.

Wing D's exterior columns facing the central courtyard along column line N suffered damage similar to that of the wing's northern exterior columns along line M [Figs. 2.5 and 3.32(b)]. There was some cracking in the exterior beam of the second floor which ran along the perimeter of the courtyard on a line parallel to and 5 ft north of column line N.

Like the exterior columns, the interior columns generally experienced spalling of part of their outer, unconfined concrete covers [Figs. 3.32(c) and 3.32(d)]. The columns in the western part of the wing apparently suffered more damage than those in the eastern part of the wing; the west columns underwent greater first story drifts (Fig. 3.2). The most highly damaged interior columns in the first story were located under the shear walls (Fig. 2.5). Column L-17, which was under shear wall L-17-18, experienced a shear failure in its beam-column joint because its spiral transverse reinforcement terminated below the bottom of the beam which framed into it on one

side (Fig. 3.33). Column L-16, under shear wall 16-N-J, was also highly damaged, but there was no failure in this beam-column joint because the spirals extended through the beam into the slab above.

As has been pointed out, the spirally reinforced columns throughout the ground and first stories suffered extensive spalling of their exterior, unconfined concrete covers, but no failures were observed in the concrete properly confined within the spiral reinforcement. When each column was subjected to flexure, a surface of weakness was created [3.2] within the column along the boundary of its confined and unconfined concrete (i.e. along the spiral reinforcement). The spalling of the concrete occurred primarily along these planes of weakness [Figs. 3.8(b) and 3.32]; however, the spalling would have undoubtedly been substantially reduced if not for the additional effect of the steel reinforcing bars in the corners of the columns. Practically every spiral column had large, essentially unrestrained steel bars in the corners of its cross section (i.e. outside its confined section) which either extended over its entire length, or acted as dowels that extended through about two-thirds of the column length [Fig. 3.32(a)]. When a column was subjected to bending, the lateral restraint offered by the ties and concrete column cover was insufficient to make the large corner bars conform to the deflected shape of the column. As a result, it was typical for much of the concrete cover outside the spiral reinforcement to spall.

For reasons discussed above, it can be concluded that the corner reinforcement located outside the spirally confined sections of the columns became ineffective once spalling occurred. In a number of the spiral columns, another problem arose with regard to the behavior of the corner reinforcing bars once the unconfined concrete which surrounded them spalled. Where the corner bars extended continuously through a number of stories, mechanical clamping devices were used to splice the bars together. A number of these mechanical connectors failed when the columns underwent substantial bending (Fig. 3.34); the failures added to the ineffectiveness of the corner reinforcement, at least in resisting tensile forces.

3.4.4 Second Through Fifth Stories

Due to the presence of numerous shear walls, the upper four stories of Wing D experienced a comparatively smaller amount of structural damage. The damage was greatest in the second story and generally decreased at each higher level. There was also some nonstructural damage (mostly partition wall cracking) in the upper stories.

The most significant cracking in the wing's shear walls occurred in the second story. This fact was most evident in the cases of exterior walls 16-G-J and 29-G-M (Fig. 3.24). The interior shear walls were enclosed by partitions which in most of the cases did not allow cracking in the actual walls to be observed. Substantial cracking, similar to that shown in Fig. 3.22, was observed in many of the partition walls which enclosed these shear walls. Where the actual walls could be inspected, similar crack patterns were observed, the crack widths were smaller than observed in the partitions. Cracking also occurred in the L-shaped column, M-29, which was poured integrally with the shear wall along column line 29 (Fig. 3.35).

Almost all of the wing's exterior channel columns and thin window partition columns experienced some cracking (Fig. 3.36). Cracking in the interior upper story columns could not be readily observed because the columns were enclosed by partitions. From the few observations of these columns which could be made, it was concluded that little significant cracking occurred in these columns.

The diagonal shear cracking in the channel columns was evidently a result of the wing's movement in the E-W direction. These columns were extremely rigid in this direction; they had deep cross sections and very short clear heights. The channel columns of the fourth and fifth stories (particularly column M-28) seem to have suffered greater amounts of cracking than those of the second story (Fig. 3.36). This distribution of cracking was a consequence of the distribution of stiffness throughout the structure, in particular, the abrupt change in stiffness at the second floor level. This conclusion is based upon computer analyses of the structure which are presented and discussed in Chapter 5.

There was cracking in the slabs of each upper floor. Although the crack patterns were similar in each floor, the magnitude of cracking was greatest in the second floor slab (Fig. 3.37) and decreased at the higher levels. Carpets and ceilings covered much of the slab areas, obscuring many cracks. Of the cracks which were observed, no cracks greater than 1/16 in. in width were found at these levels. Figure 3.38 shows the crack patterns which occurred in the fourth floor slab between column lines K and M, and 28 and 29.

Except for cracking in the exterior second floor edge beams, there was little significant cracking in the wing's upper floor beams. The most noticeable cracking occurred in the exterior edge beams which were adjacent to the wing's most highly cracked upper story column, M-28 [Fig. 3.36(b)]. Only fine hairline cracks occurred in the 42-ft-long exterior beams along column line 24 (beam 24-P-M). There were practically no noticeable cracks in the spandrel beams connecting the shear walls of frame 29.

In each story there was a significant amount of cracking and spalling in the partition walls connected to the exterior channel columns of the wing along column lines M and G (Fig. 3.39). There was also significant cracking in many of the interior partitions. It is evident from the damage that these brittle, nonstructural elements were not capable of sustaining even a slight amount of differential displacement without substantial cracking. The other nonstructural elements -- windows, doors, etc. -- which were subjected to lateral drifts also suffered moderate damage.

3.4.5 Penthouse D

There was little significant damage to the structural and nonstructural (machinery) elements of Wing D's penthouse. The most noticeable cracking occurred in the penthouse's north wall (Fig. 3.40). The west wall also experienced some cracking, but the east and south walls suffered little cracking. Small amounts of cracking could be seen in the columns, beams, and floor slabs of the penthouse.

An examination of the penthouse's structural system can help explain why the walls cracked in particular locations (see Fig. 3.41).

The west wall was the penthouse's most rigid element in the N-S direction; for this reason it developed greater shear and more cracking than the other elements designed to resist lateral forces in the N-S direction. In the E-W direction, the north and south walls were equally rigid, but it appears that the different structural systems below these longitudinal walls caused cracking to occur only in the north wall.

In each penthouse the most significant cracking occurred in the middle panel of the interior longitudinal wall which faced the courtyard (Penthouse D's north wall). There were shear walls below this longitudinal wall in each penthouse (along column line L for the case of Wing D), but no such walls were below the longitudinal walls facing the exterior of the building (see Fig. 3.41). These walls were not present below the middle bent of each inner longitudinal wall (between column lines 19 and 22 in Wing D). Thus, the walls below the penthouse formed a rigid portal frame connected at the top by the middle panel of the interior penthouse wall (wall L-19-22 in Penthouse D). Therefore, the cracking in the middle of the penthouses' interior facing walls (Penthouse D's north wall) was a consequence of the high shear forces which developed due to this frame action.

3.5 CONCLUDING REMARKS

The main building of the Olive View Hospital suffered severe structural and nonstructural damage, including the failure of many structural elements and the collapse of significant portions of the building. The use of four stiff stories with structural walls supported by two relatively flexible stories, without any special means of limiting large deformations in case of a major earthquake, was the primary reason for the severe damage observed in the first two stories. The nature of much of the local failures and damage could be attributed to sudden discontinuities in the depth of girders at the columns and in the shape of columns at the floors, poor detailing of reinforcement splices and of joint connections between slabs and columns, inadequate shear and lateral reinforcement, and errors in anchoring spiral reinforcement. The use of numerous stiff but

brittle tied columns in the ground story resulted in substantial structural damage, and a considerable decrease in the story's overall lateral strength and stiffness. The abrupt loss of the lateral load capacity of the brittle tied columns would suddenly increase the inertial forces and the loads resisted by the remaining members during the earthquake. The use of supplemental bars or dowels without proper lateral reinforcement caused premature spalling of the cover of the spirally reinforced columns. The shear failures observed at many locations in the first floor slabs were caused by the inadequacy of the reinforcement in the slabs and their drop panels to resist shear forces resulting from moment transfer between the slabs and columns.

The large drifts experienced by the building, particularly in the lower two stories, resulted in substantial nonstructural damage. This nonstructural damage represented a significant economic loss and endangered the safety of the occupants. In addition, the seismic joints used at various points throughout the building were not sufficient to accommodate the actual displacements that were developed, and the building hammered against the retaining wall and warehouse at the level of the first floor, generating large additional forces at the first story level. Also, the second floor of Wing C hammered against Stairtower C. This hammering action greatly contributed to the structural damage. Damage control should be explicitly considered in the design of structures. The nature and proximity of adjacent structures should be considered in design in order to provide adequate separation between them.

IV. GROUND MOTION

4.1 INTRODUCTION

More than 250 strong motion accelerograms and 150 seismoscope records were obtained from the San Fernando earthquake, making it the most thoroughly documented seismic event ever. However, there were no strong motion instruments in the immediate vicinity of the Olive View Hospital. Consequently, the exact nature of the ground motion at the building site can only be estimated.

A number of ground motion records have been selected for subsequent seismic evaluations of the main building. These records were either analytically generated or abstracted from other analytical investigations which modified nearby recorded ground motions. As a background for discussion of the various records, the general characteristics of the earthquake and the specific geophysical features of the site are briefly reviewed. The basis and limitations of each of the selected ground motions are then presented.

4.2 GENERAL CHARACTERISTICS OF THE EARTHQUAKE

The nature of the San Fernando earthquake and related aftershocks have already been reported in detail (see References 4.1 through 4.5) so that a thorough presentation of this data will not be attempted in this report. The main shock of the 9 February 1971 earthquake occurred at 6:00:41.6 PST and was initially assigned a 6.6 Richter magnitude. Later a local magnitude of 6.4 and surface wave magnitude of 6.5 were assigned [1.1]. The epicenter was located at 34°24.0'N, 118°23.7'W with a focal depth of thirteen miles. The center of energy release was approximately 1.9 miles southwest of the epicenter (34°23'N, 118°25'W), based on the estimated fault rupture and aftershock data [4.5]. The site of the Olive View facility was 6.0 miles southwest of the epicenter, as shown in Figs. 4.1 and 4.2 and has been given a Modified Mercalli intensity of XI. The duration of the severe ground shaking was about eight seconds. A more complete discussion of the nature of the geological and seismological factors affecting the site are included in Section 4.3.

Of the strong motion accelerograms recorded during the main shock, some of which are indicated in Fig. 4.3, only one was located less than 15 mi. from the epicenter. This recording was taken at Pacoima Dam which was about 3 mi. east of the facility and 5 mi. south of the epicenter. Maximum ground accelerations of 1.25 g in the horizontal direction and 0.70 g in the vertical direction, more than double the largest previously recorded values, were recorded at this station. With the exception of this record, however, the general nature of the ground motion records, i.e. frequency content, time histories, etc., were not substantially different from those recorded in past California earthquakes. This suggested that the ground motion might be represented by a nonstationary stochastic process based on a statistical evaluation of data available for this and previous strong motion earthquakes. This possibility is explored in Section 4.5.

Other records obtained near the facility included the Holiday Inn (8144 Orion Street) accelerogram, and the Lower Van Norman Dam abutment seismoscope trace, which were about 11 mi. south and 3 mi. southwest of the facility, respectively. Attempts to use these or modified versions of these records as representations of the site ground motions are discussed in Sections 4.6 and 4.7.

4.3 SITE CONDITIONS AT OLIVE VIEW

The earthquake has been associated with a thrusting movement along the San Fernando fault. This fault is a part of the E-W oriented system of north-dipping thrust faults which, along with the San Andreas system (including the San Gabriel fault) of right-lateral strike-slip faults, dominates the tectonic structure of the San Fernando Valley area. Although prior to 1971, the region had been one of low to moderate seismic activity, faulting had occurred in historic times, principally on faults related to the San Andreas system.

For the Southern California region, earthquakes of magnitudes similar to the San Fernando event or larger have return periods of about four years [4.6]. Consequently, this event was not particularly exceptional except for its proximity to a large urban center.

The San Fernando area has had only about ten small earthquakes ($M \geq 3$) since 1934, the largest of which ($M = 4.0$) occurred below southern San Fernando in 1964. The most significant historic events were a 1930 shock ($M = 5.2$) which may have occurred near San Fernando (although the epicenter was originally assigned to Santa Monica Bay) and the 1893 Pico Canyon earthquake ($M = 6$) which occurred near Newhall.

Active faulting during the 1971 earthquake was generally limited to the Mission Wells, Sylmar and Tujunga segments of the San Fernando fault zone and the shorter Veteran's fault (Fig. 4.3). As indicated in Fig. 4.2, the fault rupture propagated from the epicenter along the fault surface which dipped towards the north at about a 45° inclination. The fault ruptured the ground surface about 1.2 mi. south of the Olive View facility. The hospital was located above the subsurface fault rupture on the upthrusted block. Residual displacements of about 1.6 ft vertically, and 2.0 ft southward occurred at this site. The complex nature of the fault movement and the proximity of the facility to the fault plane significantly decreases the certainty with which the ground motion may be estimated.

The Olive View Hospital was located at the foot of the San Gabriel Mountains on an alluvial fan of sand and gravel deposits from Wilson Canyon. Several groups [4.7, 4.8] have conducted field investigations of the area including extensive geological surface and subsurface examinations. Six shallow trenches and four test holes up to 60 ft deep have been made, in addition to several seismic and electrical-resistant refraction traverses around the facility. No active faulting was discovered at the site, although there was substantial surface cracking apparently caused by differential settlement. The available data were interpreted to construct soil profiles, such as those shown in Fig. 4.4, representing traverses along the west and south sides of the main building [4.7]. These show that there was generally more than 100 ft of alluvium or consolidated sands and gravel underlying the main building. The various profiles which are available for the site have been compared in order to idealize the local geological site conditions as shown in Fig. 4.5 [4.9].

4.4 ESTIMATION OF GROUND MOTIONS

It must be realized that it is impossible to reconstruct the "exact" ground motion records which occurred at the Olive View Hospital site. This is particularly true in this case because of the relatively small amount of information available regarding near-field motions produced by thrust faulting. Consequently, the objective in selecting ground motions for use in subsequent analyses is not to determine the actual record, but to incorporate, as realistically as possible, the general features which, at least in an average sense, characterize the ground motions which occurred.

The nature of free-field ground motions is influenced by the type and features of the source mechanism, travel paths of the seismic waves, the geology between the source and the site, and the local soil conditions at the site. While studies of the modification of bedrock accelerograms by local soil deposits have illustrated the importance of this factor [4.10], analytical models for soil properties and propagation of seismic waves remain relatively simplistic, particularly for sites close to the causative fault. Several investigations [4.11-4.13] have in fact indicated that site responses may, in many cases, be controlled more by the faulting mechanism and the travel path of seismic waves than by local soil conditions. The nature of ground motion amplitudes, durations and frequency content, and the factors affecting their spatial distribution about a fault needs further study.

For example, one of the main unknowns concerning the ground motion at the facility is the maximum accelerations experienced. The order of magnitude of the peak site acceleration has been estimated by several authors to be about 0.50 g [4.1, 4.2]. However, the certainty with which this parameter can be established is poor in the absence of nearby strong motion accelerograms. For the San Fernando earthquake, the relationship between maximum recorded horizontal acceleration and the distance of that recording from the center of energy release is shown in Fig. 4.6 for sites located on rock or alluvium (see Reference 4.5 for classifications). Two things are apparent: (1) no records were obtained near Olive View, and (2) there

are substantial differences in the peak accelerations obtained at a given distance from the energy center. Trend lines derived to fit these data in Reference 4.5 cannot be used to extrapolate the intensity of motion with certainty because of the large standard deviation associated with the curves. For a distance of 7 km to the energy center, corresponding to the Olive View location, the curve for alluvial sites suggests ground accelerations of about 0.70 g. The reliability of this value is questionable in view of the previous discussions.

Estimations of the peak ground acceleration from the ground motion intensity necessary to produce analytically the damage to simple structures at the site, e.g. the ambulance canopy, are also expected to be unreliable. Studies of the response of simple inelastic systems [4.14, 4.15] indicate that very large variations in the response can occur for ground motions with the same peak acceleration and that predictions of time to collapse involve considerable uncertainty. Therefore, this approach was not followed in this study.

4.5 STOCHASTIC SIMULATION OF ACCELEROGRAMS

Initial attempts to predict suitable ground motion records for the Olive View Hospital site characterized the free-field motion by a nonstationary random process based on a statistical analysis of representative strong motion accelerograms. This technique has been used extensively [4.16-4.18] and gives satisfactory results at sites sufficiently distant from the causative fault so that details of the fault mechanism would not be reflected in the record -- provided that proper parameters are used to define the process.

In this study, a method similar to that developed in Reference 4.16 was employed to simulate the ground motion. The process is schematically illustrated in Fig. 4.7. Gaussian nonstationary shot noise, $a_b(t)$, used to represent the random arrival of seismic waves below the site, is obtained by multiplying a white noise, $w(t)$, times a shaping function, $p(t)$. The shaping function may be derived from a statistical analysis of representative accelerograms. For this investigation, a function of the form shown in Fig. 4.8 was selected

to allow for a rapid build up in intensity over two seconds followed by an eight-second portion with nearly uniform shaking and by a portion with a gradual attenuation of the ground motion similar to that observed in most of the records obtained during the earthquake.

To obtain the desired frequency content in the ground motion record, $a_g(t)$, the shot noise, $a_b(t)$, was passed through a second order linear filter with two adjustable parameters, ω_o and ζ. The first parameter, ω_o, controls the values of the predominant frequencies contained in the record, and the second, ζ, controls the relative amplitudes of the harmonics over the entire frequency range. This model is analagous to a single degree-of-freedom oscillator with a natural frequency of ω_o and a viscous damping ratio of ζ subject to the base accelerations, $a_b(t)$. The resulting acceleration of the oscillator mass is used as the ground motion.

With the exception of the Pacoima Dam records, the recorded accelerograms and their response spectra do not indicate significant differences between the frequency content of this earthquake and those previously recorded on the West Coast. Consequently, the filter parameters (ω_o = 2.5 Hz, ζ = 0.6) were selected to reflect values representative of motions recorded at moderate epicentral distances on relatively firm soil during this type of earthquake [4.16, 4.19].

After a parabolic correction is applied to the base line of the records to let the ground velocity at the end of the earthquake tend to zero, the records are scaled to the desired maximum value of acceleration. In this case an ensemble of ten fifteen-second earthquakes were generated and normalized such that their peak acceleration was 0.50 g. The time history of ground acceleration, velocity, and displacement for three of these records used in subsequent analyses are shown in Fig. 4.9 and their response spectra are shown in Figs. 4.15 and 4.16. From these figures it is apparent that there are significant probabalistic variations between individual records generated by this method.

4.6 MODIFICATION OF RECORDED ACCELEROGRAMS

It would appear ideal to use an accelerogram recorded during

the San Fernando earthquake at a site close to the facility. However, the reliability of this approach is questionable in this case because the site is closer to the faulting than to the nearest accelerographs. Nonetheless, several records have been studied or modified in order to assess the general characteristics of the near-field ground motions. The applicability of these records to the Olive View site will be discussed in the remainder of this chapter.

Since aftershock instrumentation was installed at the site, it might be possible to derive transfer functions to modify recorded main shock motions at other sites so that they could be applied to Olive View. This possibility was investigated in Reference 4.7. Although records obtained at the Holiday Inn were found to be the most suitable for this purpose, it was concluded that the ground motions at the two sites would significantly differ because: (1) the soil conditions were different, (2) there were large differences in the intensities of the main event and aftershocks, and (3) the locations were situated on opposite thrust blocks. It was therefore not possible to construct a reasonable record in this manner.

The Pacoima Dam accelerogram has attracted considerable attention because of the large accelerations recorded. Although this record was the only one obtained in the area of strongest shaking, it may not be directly applicable to other nearby sites. Since the instrument was located on a rocky spine adjacent to the dam, and there was extensive cracking in the rock near the accelerograph [4.1, 4.4], the features of the site could have strongly influenced the record. An extensive analysis of the Pacoima Dam [4.20] including the abutment and basement rock formation has permitted a derivation of the motion which might have occurred on firm rock near the base of the dam.* Using a three-dimensional finite element model, the base rock

---

* After the completion of a substantial portion of the analytical work presented in this report, it was learned that the orientation originally reported for the horizontal components of the Pacoima Dam accelerograms were incorrect [4.21]. The component originally designated S-16°-E should have been S-14°-W, and the S-74°-W component is actually oriented N-76°-W, i.e. a rotation of 30° clockwise. The derived Pacoima Dam base rock record used as the seismic excitation in many of the dynamic analyses was based on the original orientation reported

excitation necessary to produce the Pacoima Dam accelerogram was computed. Since the recorded accelerogram is believed to be an accurate representation of the instrumented site [4.4], the computed base rock accelerogram may be indicative of the characteristics of the shaking at other nearby sites, such as the medical center.

The Pacoima Dam and the computed base rock motion are compared in Fig. 4.10. It is interesting to note that while peak accelerations as large as 1.25 g were found in the original record, the maximum accelerations in the computed rock motion were about 0.40 g (Fig. 4.14) and did not occur at the same time as the recorded maximum. It is therefore apparent that the topography at the dam site had an appreciable effect on the recorded ground motion.

Perhaps the most outstanding feature of these ground motions is not the peak acceleration, but the three large acceleration pulses of 2/3 to one second duration early in the records. In spite of the relatively low peak accelerations associated with these pulses (about 0.7 g in the recorded motion and 0.4 g in the computed rock motion), they give rise to velocity increments of about 4 ft/sec (120 cm/sec) which is very close to the 150 cm/sec value suggested by Ambraseys [4.22] as the upper bound for bedrock velocities near fault breaking. Although this type of motion is relatively uncommon, it has been observed at near-fault sites on firm ground [4.23] and may be derived from considerations of faulting displacements [4.24, 4.25] at near-fault sites. The large residual drifts seen in the displacement graphs (Fig. 4.10) are caused by the absence of baseline correction in these records; this should not have significant structural consequences.

The presence of this type of pulse in the ground motion can result in very severe structural behavior, as will be discussed later.

---

for the accelerograms. No information is available regarding the effect of this misalignment on the reliability of the derived accelerogram. However, it is not believed that the conclusions of this report regarding the overall structural behavior and the significance of intense, long-duration acceleration pulses in the Pacoima and derived Lower Van Norman Dam records would be invalidated because of this error. To avoid confusion, the original orientation reported for the Pacoima Dam records will be used throughout this report.

The response spectra for these motions (shown in Figs. 4.17-4.19) indicate that the elastic behavior would be particularly severe for structures with natural periods between one and two seconds. However, the response of yielding structures can be significantly different than that indicated by the elastic spectra for such excitations.

Another method suggested for estimating the site ground motions was based on the seismoscopic trace obtained on a rock outcropping at the east abutment of the Lower Van Norman Dam (Fig. 4.3). Since seismoscopes are essentially single degree-of-freedom systems, the excitation should be calculable from the response trace. In addition to various numerical problems, however, it is difficult to determine the exact trace sequence because of the overlapping and irregularity of the traces. The N-S component of the ground motion derived [4.26] in this manner for the Lower Van Norman seismoscope is shown in Fig. 4.11, and the corresponding response spectra are presented in Figs. 4.18 and 4.19. While the reliability of the approximations made in the derivations of this record make its reliability uncertain, it is instructive to examine the record for evidence of pulses like those found in the Pacoima Dam records. The high frequency signals in this accelerogram prevent a clear interpretation, but the form of the ground velocity time history and the high spectral values obtained in the one- to two-second period range indicates that this pulse phenomenon also occurred at this location. This is further clarified in Fig. 4.13, where a manually smoothed trace of the Lower Van Norman Dam accelerogram is superimposed on the calculated Pacoima rock motion. The origin of the time scales for the accelerograms was shifted to obtain the best visual correspondence. Although the signals are different, there is a surprising amount of agreement, particularly with regard to the pulses. Since these two records were obtained on different sides of the facility, this type of pulse characteristic might be expected to be present in the ground motions experienced at the facility.

Several attempts to account for the possible effects of the soil at the site (Fig. 4.5) on the free-field ground motion have been conducted [4.9] using the calculated Pacoima Dam base rock motion and

the Lower Van Norman Dam accelerograms as base rock input excitations. The resulting accelerograms and response spectra are shown in Figs. 4.12 and 4.18, respectively. The method used to calculate these ground motions, based on one-dimensional wave propagation and equivalent linear soil properties, has demonstrated good agreement between computed and recorded motions at moderate epicentral distances. In this case, however, many of the assumptions employed in the technique may no longer be applicable. In particular, the complex near-fault surface motion may not be adequately represented by a one-dimensional wave propagation model. The proximity of the site to the thrust fault, in this case, may necessitate more complex assumptions regarding the arrival of seismic waves below the site. Furthermore, the large pulses in the initial portions of the wave train may invalidate the use of linearized soil properties.

On the basis of the one-dimensional wave propagation model, it appears that the effect of the soil is generally to amplify the intensity of the original motions as indicated by the response spectra as well as by the accelerograms. At the frequency range of interest for the main treatment facility ($T \simeq 0.6$ sec), however, the elastic response spectrum values are not appreciably affected. Consequently, these soil models will not be used extensively in the following elastic analyses.

4.7 CONCLUDING REMARKS

Since the damage to the Olive View facility was a consequence of ground shaking rather than surface faulting, it is of the utmost importance that the nature of the ground motions be characterized accurately. From a review of the site conditions and nearby accelerograms obtained during the earthquake, it was possible to generate appropriate records both deterministically and nondeterministically. The actual peak accelerations at the site are uncertain and will be discussed later with the results of the analyses of the facility. Since a record of the actual ground motions at the site is not available, the reliability of these generated records remains speculative.

V. ELASTIC ANALYSES

5.1 INTRODUCTION

The general dynamic characterisitics and responses of the building to possible ground motions are examined in this chapter, assuming linear-elastic behavior. A three-dimensional dynamic analysis of a model incorporating all structural members was performed using an existing computer program. This analysis provided considerable information regarding the dynamic characteristics and initial dynamic response of the building, including the effect of two simultaneous horizontal ground excitations and of torsional eccentricity. The results of elastic analysis were interpreted to determine the probable mode of structural failure.

It is obvious from the structural damage, as well as the results of this analysis, that the building did not remain elastic, but in fact sustained large inelastic deformations. Unfortunately, it is not currently feasible to calculate the inelastic response of a three-dimensional structure of the size and complexity of the main building. A model of a portion of the building suitable for additional elastic and inelastic analyses is discussed in the last part of this chapter. The adequacy of this model was checked by comparing its response to that of the whole building. The response of this two-dimensional model was then compared with those of two comparable models of alternative structural systems for the building. In the two alternative systems considered: (1) shear walls were continued down to the foundation level, and (2) shear walls were removed entirely.

5.2 COMPUTER PROGRAM

The TABS (Three-dimensional Analysis of Building Systems) computer program has been developed [5.1] to perform linear-elastic structural analyses of three-dimensional frame and wall buildings subjected to both static and dynamic (earthquake) loadings. The program can accommodate buildings with any number of rectangular frames or walls located arbitrarily in plan, providing each forms a continuous vertical plane [see Fig. 5.1(a)]. Floor elevations must be the same in each frame,

and the frames are assumed to resist forces only in their own plane. Frames can be composed of column, beam, wall, and shear panel (infill) elements. For columns and walls, bending, axial and shear deformations are considered. Beams may be nonprismatic, but only their flexural deformations are accounted for. Only shear deformations are allowed in the shear panels. The beam-column joints (panel zones), shown in Fig. 5.1(b), are assumed to be rigid. The torsional stiffnesses of members are disregarded.

The computer program assumes that frames and walls are interconnected at each floor level by a horizontal floor diaphragm that is rigid in its own plane. Thus, in formulating the equations of motion, the horizontal displacement of each floor level can be described in terms of only three degrees-of-freedom; two lateral and one torsional. Because frames are assumed to act only in their own plane, axial deformations in columns common to more than one frame are not necessarily compatible.

The three-dimensional mode shapes and natural frequencies, and the responses due to gravity loads and earthquake time histories are calculated. The computer program has been modified to account for an earthquake excitation consisting of time histories of two horizontal components of ground acceleration. These components can be applied in arbitrary directions with respect to the orientation of the building. Other program modifications were made to obtain output of the maxima and time histories for story shears and torques, floor displacements and rotations, frame displacements, and member forces.

5.3 MATHEMATICAL MODELING OF STRUCTURE

The Olive View Hospital was analytically modeled for seven stories to include the penthouse level. The model consisted of 70 frames (69 of which were different) which intersected each other in the orthogonal grid shown in Fig. 5.2. Only beam and column elements were used to model the structure; there were more than 4600 such elements in the final model. The walls and columns were modeled by column elements while the beams and slabs were modeled by beam elements. The geometric model of the structure was then formed by assigning the

appropriate beam and column elements to the various frames. In defining certain frames, it was necessary to neglect the lateral offsets present in the actual structure as can be seen by comparing Fig. 5.2 with Fig. 2.1.

The mass and rotational mass moments of inertia about the center of mass of each floor were calculated. In modeling the hospital it was assumed that the entire mass of each stairtower (except for Stairtower C which was not directly connected to the main building) could be concentrated at its point of attachment to the first floor level. This assumption is reasonable (see Reference 1.2) because the stairtowers were very rigid above the first floor slab. Since the overturning effects of the towers are disregarded, forces in members directly adjacent to the towers may not be reliable. This idealization was necessary because the relatively rigid upper stories of the stairtowers were not structurally connected to the rest of the main building's upper stories, and the computer program could not account for relative movement between the stairtowers and the rest of the building at these levels. The first floor slabs and beams and the ground story columns under the stairtowers were integral with the main structure, and thus were included in the structural model.

Throughout the analysis and in the interpretation of the results, the material properties assumed were average values obtained from the tests discussed in Chapter 2. The average modulus of elasticity, E, for the specified 5000 psi strength concrete was 3540 ksi; the average for the 3000 psi concrete was 3080 ksi. Note that 3000 psi concrete was used throughout the building except in the ground and first story columns where 5000 psi concrete was used.

A more detailed explanation of the structure modeling follows.

5.3.1 Columns

Each column was a member of two orthogonal frames; a frame with a vertical plane in the N-S direction and a frame with a vertical plane in the E-W direction. Therefore, unlike the beams, each prototype column was represented in the structural model by two column elements. Each column element was assigned a moment of inertia, an area, and a

shear area corresponding to the actual member along the appropriate axis. For each column element, the moment of inertia was based on the uncracked transformed section oriented in the appropriate direction, the axial area was based on the transformed area, and the shear area was taken to be the gross area reduced by 5/6. An example of how these parameters were calculated is provided in Appendix B.2.

The actual width of each column was specified to define dimensions for the rigid beam-column joints assumed in the analysis. Appropriate transformations are made by the computer program to modify (increase) element stiffnesses to account for these zones of rigidity. The column width affected the stiffness of the adjacent beam elements, as can be seen from Fig. 5.1(b), by reducing their effective clear spans. Correspondingly, the depths of the adjacent beam elements were specified in the computer input data to calculate the clear length of the columns. In this case, the clear span was assumed to extend from the top of the floor slab at the bottom of the column to the bottom of the lowest beam framing into the top of the column. Additional comments are made in Section 5.3.3 regarding the importance of these beam depths.

5.3.2 Structural Walls

The reinforced concrete walls shown in Fig. 2.1 extended between the second floor and the roof. The walls around the elevator and stair shafts adjacent to the courtyard actually continued down to the first floor, although they were not structurally connected to that level. The penthouses on the roof were also constructed using one-story-high walls.

Since the walls did not extend through the full height of the building, they could not be modeled as wide columns and still provide reliable values for the forces acting in their supporting columns. Consequently, it was necessary to model a wall as an equivalent frame in which beam and column properties were selected so the frame would develop equivalent dynamic properties [5.2]. The equivalent beam elements were assumed to be rigid. The moments of inertia and the axial areas of the equivalent columns were determined using the following

assumptions: the columns had only axial and flexural deformations; the lateral story displacement of the equivalent frame equaled the story displacement of the actual wall for a given story shear; and the story rotation of the equivalent frame was the same as the rotation of the wall for a given overturning moment. The details of these calculations are shown in Appendix B.3 for a single-bay wall. Although this idealization precludes exact duplication of the stiffness properties of shear walls, a comparison of results based on the approximations used with those based on more refined (and more complex) methods indicated this idealization to be adequate. The shear area of a wall was taken to be equal to its length multiplied by its nominal thickness. The effects of small openings in the walls (for ventilation, piping, etc.) were not considered in determining the walls' stiffness properties. However, walls separated by larger openings (for doors and hallways) were modeled as separate walls connected by coupling beams.

5.3.3 Beams and Slabs

The building's floor system consisted of monolithic structural slabs, drop panels, and beams. In order to idealize the floor slab as equivalent beam elements it was necessary to determine effective moments of inertia for various slab configurations. In doing so, it was assumed that the effects of steel reinforcement and torsional rigidities of transverse beams and slabs were negligible.

To determine the properties of equivalent beam elements, a series of finite element analyses was performed. Although the scope of these analyses, described in Appendix B.4, was limited, it was found that design charts constructed by Khan and Sbarounis [5.3] could be applied, if properly interpreted. These charts considered only the general case of uniform flat slabs without drop panels or edge beams. For cases investigated in Appendix B.4, slabs with drop panels had nearly the same flexural stiffness as uniform flat slabs with depths equal to that of the slab plus that of the drop panel. Thus, by using these design charts, it was possible to approximate the effective widths of flat slabs and drop panels with a significant savings of computation. In these cases the depth of the rigid beam-column joint was taken to

be the depth of the slab plus that of the drop panel.

In many locations, beams were cast integrally with the floor slabs. These flanged beams had various shapes (most were either T, L, or Z sections); their stiffness properties were evaluated assuming ideal beam action with effective flange widths generally based on the strength provisions of Section 2609(3) of the 1967 UBC [2.7]. To simplify the analysis, moments of inertia were based on the untransformed and uncracked section of the effective beam.

The depth of each beam element was generally taken as the distance between the top of the slab and the lowest fiber of the beam or drop panel. Special treatment was required for the beams and slabs in the courtyard and terrace canopy of the ground story because they were located 21 in. below the top of the first floor slab in the highrise portion of the building.

It is significant to note that exterior spandrel beams in the upper four stories had depths of 67 in., while many interior flat slabs had depths of 13 in. Thus, there was a substantial difference in the clear heights of the interior and exterior columns at these floors.

5.3.4 Masses and Mass Moments of Inertia

At each floor level, the masses of all structural elements were calculated in this investigation by determining their volumes and assuming the density of the concrete to be 150 lb/ft^3. Fifty percent of the mass of walls and columns between floor levels was lumped at the floor level above, and the remainder was lumped at the floor level below. The other masses (roofing, masonry veneer, ceilings, machinery, partitions, concrete and earth fills, mechanical equipment, etc.) were determined using design loading assumptions. For example, the density of the earth fill was assumed to be 110 lb/ft^3.

At each floor level, the masses that were calculated and their spatial distribution were used to calculate the rotational mass moment of inertia about the floor level's center of mass. Since the stories above the first floor were point symmetric, the centers of mass coincided with the point of symmetry (the intersection of column lines

17 and S as shown in Fig. 2.1). The center of mass at the first story level was calculated to be 25.9 ft west of column line 17 and to be 33.5 ft south of column line S.

Table 5.1 summarizes the weights, masses, and mass moments of inertia that were calculated for each floor level. At the first floor level, the earth fill contributed a significant portion of that floor's total mass. The resulting floor mass was more than three times larger than that of any other floor level.

5.3.5 Foundation Conditions

The computer program requires a horizontal base plane for the structure to rest on. In the Olive View Hospital's main building, the ground story slab was such a horizontal plane; however, the ground story columns extended from zero to 10 ft below this slab to spread footings. As discussed in Section 2.2, the ground floor slabs were poured directly on grade (earth fill) except in the northern halves of Wings B and C where an 8-ft-deep access space was constructed under the slab. In the structural model of the hospital, it was assumed that all ground-story columns were fixed at their base to an imaginary horizontal plane 12 in. below the top of the actual ground floor slabs; in other words, the height of the ground story was increased by 12 in. to 17'-6". Preliminary computations indicated that this assumption approximately compensated for the flexibility of the columns between the ground slab level and their footings.

5.3.6 Structural Configuration

In order to construct a mathematical model of the hospital suitable for the TABS computer program, the coordinates of all member elements were assigned to frames which lay in continuous vertical planes. The frames, in turn, were located in their appropriate positions for the analysis. Many of the columns in the actual building were slightly offset from the imaginary vertical planes used to model the frames. In the mathematical model, the positions of some elements and discontinuous framing planes were slightly altered where frame action was likely to occur so that the columns would lie in continuous planes extending across the entire model. For example, columns along column

line 12 (Fig. 2.1) were assumed to lie 2.43-ft east of their actual positions while columns along column line 13 were assumed to lie 5.07 ft west of their actual position; thus, the columns along these two column lines were assumed to lie in a common, continuous, vertical plane and form a frame which extended across the entire building, as seen in Fig. 5.2(a).

In other cases where frames did not extend across the entire building, they were assumed to terminate near their points of discontinuity. For example, the frame formed along column line Y (see Fig. 2.1) was assumed to terminate at a position 12.5 ft (one-half span) east of column Y-9. To account for the flexural restraints of actual slabs at the points of termination, roller supports were assumed at the far end of the beam elements representing these slabs. These beam elements typically extended one-half span beyond the frame's last column (in this case, column Y-9). The calculated member forces in elements located in the region where these framing assumptions were made may not be reliable, but this should not substantially affect the overall characteristics of the model or the forces in other elements.

5.4 THREE-DIMENSIONAL ANALYSIS OF ENTIRE BUILDING

5.4.1 Periods, Mode Shapes, and Participation Factors

Numerical values were calculated for the first twelve mode shapes, periods and participation factors for the three-dimensional model; some of these values are listed in Tables 5.2 through 5.4. The mode shapes in Table 5.4 are normalized to give a generalized mass of unity in each mode. The first mode of the hospital model was oriented primarily in the E-W (x) direction with a period of 0.607 seconds; the second mode was primarily in the N-S (y) direction with a period of 0.589 seconds; and the third mode was primarily torsional with a period of 0.503 seconds.

The three-dimensional shapes of these three modes are schematically illustrated in Fig. 5.3. The closeness of the translational and torsional periods indicates that disregarding torsional effects in the analysis might result in an underestimation of the response. The small relative displacements between the upper levels, as inferred from

the mode shapes, is a consequence of the high rigidity (due to numerous walls) of the building's upper four stories. The large relative displacements indicated in the lower levels by the mode shapes results from the relatively low rigidity of the building's bottom two stories and the large concentration of mass at the first floor level. The first three mode shapes were similar to the overall pattern of permanent deformation which occurred in the actual building; large lateral deformations occurred in the building's lower two stories while there were negligible interstory lateral deformations in its upper stories.

The UBC seismic design provisions are based on the assumption of a triangular first mode shape; as can be seen, this assumption is not appropriate for buildings with soft stories or other irregular stiffness and mass distributions.

The modal participation factors [4.23] for the three floor level degrees-of-freedom are listed in Table 5.3. These participation factors provide useful information regarding the potential elastic response of the model. For example, plots in Fig. 5.4 show the components of a particular mode shape along each of the three structural degrees-of-freedom where each of the modal components have been normalized by the ratio of the mode's participation factor for the component considered to the maximum of the participation factors for the component occuring in any mode. The curves in Fig. 5.4 indicate that each of the first three modes responded essentially in only one of the lateral degrees-of-freedom, and thus, were nearly uncoupled. On the other hand, higher modes had significant components along at least two of the degrees-of-freedom. Even for the higher modes, interfloor deformations are concentrated in the lower two stories. According to this figure, the first three modes would likely control the response. The actual modal response, however, depends on the relative spectral values for the actual earthquake in addition to the relative magnitude of participation factors. Based on an examination of these participation factors and response spectra presented in Chapter 4, it is believed that the first nine modes of the model may have significantly contributed to the response. These modes were therefore included in subsequent three-dimensional analyses.

5.4.2 Dynamic Response Analysis

A time-history analysis of the entire structure was performed using the three-dimensional elastic model and the computer program discussed. The results of this analysis are presented in this section.

(a) Ground Motions.

In the analysis of the hospital building, both horizontal components of the derived Pacoima Dam base rock motion (S-16°-E and S-74°-W) were used as earthquake excitations. The accelerations of both components were scaled upward by a factor of 0.65/0.40 = 1.625 so that the maximum acceleration in each component was 0.65 g instead of 0.40 g. As discussed in Chapter 4, there is great uncertainty regarding the peak acceleration experienced at the site. On the basis of soil amplification studies and extrapolation from peak acceleration data obtained at sites farther from this source, it is believed that the derived Pacoima Dam base rock motion scaled to a maximum acceleration of 0.65 g may be a reasonable estimate of the maximum ground motion at the site. Since the analysis assumes linear-elastic response, however, the magnitude by which input ground accelerations were scaled is not crucial; the resulting values of response can easily be scaled to correspond to any other value of maximum acceleration.

In order to simplify the analysis, each component of the ground motion was applied along one of the principal horizontal axes of the hospital model. Thus, the S-16°-E component was applied along the model's N-S axis, and the S-74°-W component along its E-W axis. This procedure was reasonable in light of the many uncertainties regarding actual ground motion characteristics at the site.

Only the first six seconds of each component of the derived Pacoima Dam base rock motion were used for the time-history analysis. This was because preliminary elastic analyses of a simplified structural model indicated that the maximum responses would occur between the second and fourth seconds of the ground motion. Furthermore, it was clear from these preliminary elastic analyses and from the actual deformations sustained by the building that inelastic yielding was initiated well before reaching maximum displacements. For these

reasons an elastic time-history analysis beyond six seconds was not performed.

(b) General Structural Response.

The envelope of the structural model's maximum floor displacements, rotations, shears, and torques at each floor's center of mass due to the N-S component of the ground motion (i.e., the S-16°-E component of the derived Pacoima Dam base rock motion at 0.65 g) are listed in Table 5.5. The maximum responses to both components of the ground motion (S-16°-E and S-74°-W at 0.65 g) acting simultaneously are also listed in this table and plotted in Fig. 5.5. The tabulated results show that the N-S component caused insignificant responses in the E-W direction while the E-W component caused negligible responses in the N-S direction. Results also indicate that the N-S component was primarily responsible for the model's maximum rotations and story torques.

The maximum responses in the N-S direction were generally about 35 percent greater than those in the E-W direction. On the basis of the dynamic characteristics of the model and the response spectra of the ground motions, one would expect the response to be largest in the E-W direction. This discrepancy between expected and computed response was probably due to the fact that the duration of the ground motion used in the analysis was limited to six seconds, during which time the maximum acceleration of the N-S component was about 33 percent greater than that of the E-W component (Fig. 4.10). Had the response been obtained for the entire record, the computed response would undoubtedly agree with that inferred from the response spectra.

The story shears and static lateral displacements obtained by applying the UBC forces used in the design (listed in Tables 2.1 and 2.2) have also been plotted in Fig. 5.5. Note that there are large differences between the design values and those obtained for the elastic dynamic analysis.

The floor displacements for two of the model's N-S frames at the instant of time at which the model experienced its maximum N-S responses to simultaneous components of ground motion are illustrated in

Fig. 5.6. The maximum floor displacements of frames 7 and 26 (i.e., the frames along column lines 7 and 26, see Fig. 2.1) towards the north occurred at 3.40 seconds, and towards the south, at 2.70 seconds. The differences in the values of displacements of these frames are due to torsional rotation of the floor diaphrams. Note that the curves are similar in shape to those of the model's fundamental modes.

The displacements and rotations of the model's first and second floors at the times (t = 3.40 seconds, and t = 2.70 seconds) at which the model experienced its maximum N-S responses to simultaneous ground motions are illustrated in Fig. 5.7. This figure illustrates (in an exaggerated form) the effects of torsion on the model's maximum responses. At both of these times, exterior frames on opposite sides of the model experienced significantly different displacements. For example, at t = 2.70 seconds, the total lateral displacement of point d at the second floor of an exterior frame of Wing D was 37 percent greater than that of point b at the second floor of Wing B on the opposite side of the model.

The large inelastic deformations which the building actually suffered are not implied by this analysis. The elastic analysis, even considering severe earthquake ground motions simultaneously applied along both principle axes of the building, predicted maximum displacements at the second floor of about 4-in. while the actual permanent displacements at the building's second floor were over 20 in. However, some insight can be gained into the probable response of the building from the results of the elastic analysis. The envelopes of maximum displacements were similar in shape to the pattern of permanent lateral deformations in the building; i.e., relatively high differential displacements were predicted in the bottom two stories. It is also evident that the building was not adequately isolated--to preclude the possibility of pounding--at its upper stories from the stairtowers (with a 4-in. design separation) and at its ground story from the retaining walls (with a 2-in. effective separation).

The elastic analysis also shows that the design base shear

coefficient (0.08 W) was very low in comparison to the maximum base shear coefficients obtained in the dynamic analysis. Under the simultaneous ground motions a maximum coefficient in the N-S direction of 0.98 W was required for elastic behavior; if coefficients along each principal axis of the hospital are added vectorially, the resultant is 1.22 W. This is not to say that the building should have necessarily been designed for such a high value; it only points out that the building was likely to suffer significant inelastic responses when subjected to a large earthquake.

The three-dimensional elastic analysis of the building also indicated the possible effects of torsion on the response. Although the distribution of mass and stiffness in the building above its first floor was point symmetric about a vertical line through the intersection of column lines S and 17 (Fig. 2.1), its ground story and first floor slabs were not symmetric about this point. In the analysis, this nonsymmetry resulted in significant torsional vibrations being excited throughout the model by the ground motions. Torsion caused larger maximum displacements in the model's exterior frames than would have been expected had its effects been disregarded. When the model underwent its maximum displacement towards the north at t = 3.40 seconds [see Fig. 5.7(c) and (d)], both its first and second floors had rotated counterclockwise. The first floor of the actual building suffered a permanent counterclockwise rotation, but the second floor rotated clockwise. This discrepancy between the predicted and observed behavior was undoubtedly due to the presence of Stairtower C which did not collapse during the earthquake (Fig. 3.5). The building pounded violently against this stairtower (mainly at the second floor level). The tower restrained the upper portion of the building (including the second floor) from rotating couterclockwise and probably resulted in its clockwise rotation.

The time histories of displacements and rotations at the centers of mass of the first and second floors were obtained for the two components of the derived Pacoima Dam base rock motion ($\ddot{u}_{g_{max}}$ = 0.65 g) and are shown in Figs. 5.8 and 5.9. The roof deformations are not shown because the model's rigidity above the second floor resulted in

deformations at the roof that were similar to those at the second floor [see Fig. 5.5(a)].

A comparison of Figs. 5.8(a) and 5.8(b) and a similar comparison of Figs. 5.8(c) and 5.8(d) reaffirms that when both components of the ground motion act simultaneously, neither component has any significant effect on the displacement responses of the model (at its centers of mass) in the direction perpendicular to the component's line of action. The model's responses in each direction are almost solely a consequence of the component acting in that direction. This conclusion is further illustrated by Fig. 5.10. A biaxial plot of the model's second floor displacements (at its center of mass) due to each component of the ground motion acting simultaneously is shown in Fig. 5.10(a). Figures 5.10(b) and 5.10(c) show biaxial plots of the displacement at the second floor center of mass due to both components acting separately; the simultaneous occurrence of significant displacements along both axes of the building emphasizes the importance of considering the biaxial structural responses.

The time-histories of rotations at the centers of mass of the first and second floors shown in Fig. 5.9 were obtained from the two components of the ground motion for cases when they are assumed to act simultaneously or separately. A comparison of the time-histories shown in this figure reveals that the N-S component had the largest effect on the rotation (torsion) of the model. The E-W component created relatively little torsion in the model.

The time-histories of second floor displacements of the N-S oriented frames (Fig. 2.1) along column lines 3 (the west end of the second floor), 17 (the second floor's center of mass), and 29 (the east end of the second floor) were obtained from the N-S component of the ground motion and are shown in Fig. 5.11. The differences in the responses of these three frames were due to the effects of torsion. As can be seen from Fig. 5.11, torsion did not have a large effect on the overall responses of these frames; frame 29 had slightly greater peak displacements than frame 17, while those for frame 3 were slightly smaller.

(c) Distribution of Member Forces.

Even though the actual building behaved inelastically, it is

important to consider the distribution of member forces that were obtained in the elastic analysis. By studying the distribution of maximum forces throughout the elastic model, it is possible to determine which members may have been seriously overstressed. Those members which initially yielded or failed, and the sequence in which these events occurred, can be identified by examining the time histories of member forces.

Although internal forces were obtained for all members, shear forces in the columns will be emphasized here in view of the large number of column shear failures. Forces in beams and slabs will not be discussed for two reasons: (1) it was apparent from the actual damage to the building that the damage to the columns was generally more significant; and (2) the building damage and the results of the elastic analysis indicated that nearly all of the building's tied columns suffered shear failures before significant yielding occurred in any of the other members.

The capacity studies (see Appendix B) indicated that due to their lack of adequate transverse reinforcement, practically all of the building's tied columns would fail brittly in shear rather than yield in flexure when the building was subjected to severe seismic excitations. A brittle member whose capacity is controlled by shear may generally be assumed to remain elastic until it suddenly fails. Elastic analyses of buildings containing such brittle members can sometimes be used to predict the relative times and the order in which initial shear failures and other nonlinear events might occur for a particular earthquake ground motion. Such predictions are valid only if the model's primary lateral force resisting system is not subjected to forces which would cause it to yield prior to the initial shear failures; after the initial shear failures or the yielding of a few members, the computed elastic internal forces lose their significance because they do not account for the redistribution of forces which would occur in the real structure.

Only components of shear forces and stresses along the columns' N-S axes are considered in most of the discussions which follow; the

effects of biaxial forces on the columns will be briefly discussed at the end of this section. The uniaxial shears presented below were due to both components of the ground motion acting simultaneously; but, as previously discussed, the E-W component had little effect on the response of the elastic model in the N-S direction.

After examining the results of the elastic analysis and carefully checking the maximum forces in the columns throughout the model, it was observed that the highest column forces occurred in the ground and first stories, and in the upper story channel columns and shear walls. Particularly high forces occurred in the first story columns directly under the shear walls and in the ground and first story columns directly along the exterior outline of the six-story portion of the structure, due to the large, stiff perimeter beams which framed into these columns. The maximum forces in the N-S direction occurred in most of the columns at 3.40 seconds; the time at which the model reached its peak displacement towards the north (see Fig. 5.12). Other maximum forces occurred at 2.70 seconds; the time at which the model reached its peak displacement towards the south. In many of the model's columns (especially those of the ground and first stories), the maximum elastic forces which occurred at these two time instances were much higher than their actual ultimate capacities. For example, at t = 3.40 seconds, ground story spiral column M-29 had an elastic shear force of 1171 kips, bending moment of 109,300 kip-in., and axial force of 5075 kips (compression including dead load); the bending forces were 2.5 times greater than the column's ultimate capacity for the given axial load (see Fig. 5.13). Many of the model's tied columns developed elastic forces greater than their actual capacities during even the displacement excursion to the north which peaked at t = 2.35 seconds (Fig. 5.12); therefore, after this time the predicted forces in the model's members were not realistic.

The nominal elastic shear stresses which occurred in the model's ground and first story columns along their N-S axes at t = 2.30 seconds are shown in Figs. 5.14(a) and 5.14(b). These nominal stresses were calculated [as specified in Section 1701(a) of the ACI 318-63 Code] by dividing the shear force in each column, at t = 2.30 seconds, by

the column's effective shear area. All of the columns which reached their ultimate capacities during the displacement excursion which peaked at t = 2.35 seconds (Fig. 5.12) are noted in Figs. 5.14(a) and 5.14(b). These figures indicate that almost all of the model's ground and first story tied columns had reached their ultimate shear capacities by t = 2.35 seconds. A few of the tied columns (including some of the first story corner columns) reached their ultimate capacities during the earlier displacement excursion to the south which peaked at t = 2.05 seconds. Each tied column had an approximate shear stress capacity of 155 psi; this value was obtained from the formula for the contribution of concrete to a member's shear strength: $v_{uc} = 1.9 \sqrt{f'_c}$, using f'_c = 6670 psi (an average value obtained from the laboratory tests). As can be seen in Figs. 5.14(a) and 5.14(b), most of the tied columns had stresses which exceeded this shear capacity before t = 2.30 seconds; in most of these columns, this stress was exceeded between t = 2.20 seconds and t = 2.30 seconds. Even though the capacity of each tied column was exceeded at a slightly different time, these results show that a great majority of the model's first and ground story tied columns would have failed at nearly the same time (about t = 2.25 seconds).

As can be seen in Figs. 5.14(a) and 5.14(b), many of the model's spiral columns suffered very high shear stresses at t = 2.30 seconds. These stresses, in themselves, cannot be used to determine whether ultimate capacities of the spiral columns were exceeded at the given instant of time. Unlike the tied columns, the capacities of the spiral columns were controlled by flexure; due to their large amounts of transverse reinforcement (spirals) they were expected to yield in flexure (forming plastic hinges), rather than fail in shear, when overstressed (see Appendix B). To determine whether significant yielding occurred in any of the spiral columns of the model during its displacement excursion to the north, which peaked at t = 2.35 seconds, the maximum moments and axial forces which occurred in each column during the excursion were checked against the column's ultimate strength capacity as represented by a bending moment-axial force interaction diagram. After checking these forces, it was concluded that before significant

inelastic deformations occurred in the model's spiral columns, the tied columns supporting the ground story canopies, the stairtowers, and the corners of the first story would have failed in shear.

Ground story columns E-29 (a tied column) and M-29 (a spiral column) are two columns which were highly stressed during the elastic model's displacement excursion which peaked at t = 2.35 seconds. The capacities of these two columns are shown in Fig. 5.13. At t = 2.30 seconds, column E-29 had a shear stress of 371 psi versus its 155 psi capacity. Consequently, column E-29 would have failed at about t = 2.21 seconds. At this time, column E-29 had a differential horizontal displacement of 0.27 inches, a maximum moment of 4100 kip-in., a shear of 55 kips, and an axial compressive force (including dead load) of 108 kips.

During the same displacement excursion, column M-29 was subjected to its maximum elastic forces at t = 2.35 seconds; at which time it had a differential horizontal displacement of 0.68 inches, a maximum moment of 38,100 kip-in., a shear of 421 kips, and an axial compressive force (including dead load) of 2210 kips. As can be seen from the interaction diagram shown in Fig. 5.13, this column did not exceed its ultimate flexural capacity during this displacement excursion. A check of the column forces in the rest of the building indicated that very few of the spiral columns would have yielded prior to the failure of the tied columns.

It has been shown [1.2] that the tied columns supporting the stairtowers would also have failed brittly in shear for the derived Pacoima Dam base rock motion (S-16°-E) during the displacement excursion that peaked at 2.35 seconds. These column failures would have resulted in the collapse of the stairtowers they supported, as observed in the building.

As discussed in Appendix B, these brittle failures in the tied columns of the ground and first stories were a consequence of their inadequate shear capacity and lack of confinement provided by their transverse reinforcement. Had these columns been provided with transverse reinforcement meeting current code requirements [2.5], their

shear capacity and flexural ductility would have been substantially increased as discussed in Appendix C. Such transverse reinforcement would probably have mitigated the damage to these columns and thereby reduced the likelihood of structural collapse (resulting from their failure.)

According to the elastic analysis, all of the model's third, fourth, and fifth story channel columns with their longitudinal cross-sectional axes (see Fig. 5.15) aligned in the N-S direction would have failed in shear during the displacement excursion which peaked at t = 2.35 seconds. The locations of these columns are illustrated in Fig. 5.15; the elastic shear stresses which occurred along the N-S axes of the third story channel columns at t = 2.30 seconds are also shown in the figure. These columns would have failed at about the same time as the model's ground and first story tied columns and before significant inelastic deformations would have occurred in the spiral columns. The channel columns had shear stress capacities even lower than those of the tied columns of the ground and first stories; not only did they lack adequate lateral reinforcement, but their concrete had a lower compressive strength (5040 psi versus 6670 psi) as well. As has been previously noted, each channel column was very stiff in the direction of its longitudinal axis (i.e., parallel to the exterior edge of the building); this stiffness was due to the column's large width in that direction and its relatively short effective length caused by the deep spandrel beams which framed into it (see Fig. 5.16). The columns were not nearly as stiff along their transverse axes; for this reason those channel columns (Fig. 5.15) with transverse axes oriented in the N-S direction did not suffer such high shear stresses. However, in a similar manner, the E-W component of the earthquake induced high shear stresses along the longitudinal axis of these columns with their transverse axes in the N-S direction.

According to the elastic analysis, the channel columns in the second story did not suffer high elastic shear forces along their longitudinal axes and probably would not have failed like the channel columns in the higher stories. This can be explained by examining the distribution of maximum elastic shear forces and moments at t = 3.40

seconds along a row of typical channel columns and its adjoining members. For example, Fig. 5.16 shows the shear force and moment distribution at column L-7. As the structure deformed laterally, the second story channel columns did not develop a point of contraflexure (i.e., they were bent in single curvature) whereas the upper columns did. This was partially a consequence of the relative rigidities of various members. The edge beams which framed into the channel columns at the second floor were not nearly as stiff as those in the upper floors. However, another and perhaps even more significant factor was the severe change in the deflected shape of the structure that occurred at the second floor level due to the presence of shear walls above this level. The deflected shape of the columns necessary to accommodate the large reduction of interstory drifts at the second story is shown in Fig. 5.16. This resulted in relatively low shear stresses in the second story channel columns, and in a number of cases the local distribution of stresses was actually such that the sense of the resulting column shear forces opposed that acting in the shear walls and the building as a whole. On the other hand, the deep and nearly rigid spandrel beams in the upper floors forced the upper story channel columns into double curvature and into carrying much higher shear forces.

The second story shear walls suffered disproportionately high shear forces because of the low shears carried by the second story channel columns and, as noted, shears in some of these columns acted in a direction opposite to that of the total second story shear. As a result, the second story walls had to carry a much larger proportion of the story shear than walls in the upper stories. In the top three stories, channel columns resisted a substantial portion of the total story shears.

The nominal shear stresses in the elastic model's second and third story N-S shear walls at t = 2.30 seconds are shown in Fig. 5.15. The shear stresses indicated in the second story walls are about 2.5 times greater than those in the third story walls while the maximum story shear in the second story was only 1.28 times that in the third story. Also note that shear stresses in the longer walls (i.e.

longer than 50 feet) of the second story exceeded the value calculated in Appendix B.3 to be their cracking shear stress, i.e. 429 psi. Therefore, the elastic analysis also indicates that these second story shear walls might have experienced some cracking during the model's displacement excursion which peaked at t = 2.35 seconds. Cracking would have occurred at about the same time as failure of most of the model's ground and first story tied columns and before significant inelastic deformation could have occurred in the spiral columns.

Thus far, only the elastic column force components along the N-S axis of the model have been discussed. For this ground motion the maximum elastic shears along the E-W axis of the ground and first story columns were about 75 percent of the maximum shears along their N-S axes. The same columns, which would have failed due to the uniaxial shear components in the N-S direction (Fig. 5.14), would also have failed due to biaxial shears during the model's displacement excursions to the north and east which peaked at t = 2.35 seconds and t = 2.45 seconds, respectively. Since there was a 0.10 second lag in the model's displacements towards the east [Figs. 5.8(a) and 5.8(b)], the components of the resultant biaxial shears at the onset of failure would have been substantially greater toward the north; however, the addition of eastward components would have caused the resultant shears in columns to reach the failure level (assuming an elliptical biaxial shear failure surface) at times slightly before they would have considering only the northward component of shear. Therefore, even considering the high forces due to the ground motion in the E-W direction, the failures of the model's ground and first story tied columns would have been caused primarily by the N-S component due to the lag in the response of the structure in the E-W direction. The observed pattern of damages to columns throughout the whole building indicated that they failed principally in the N-S direction.

If the elastic analysis had been run using the original Pacoima Dam base rock motion which had a maximum acceleration of 0.40 g instead of 0.65 g, the same general conclusions would have been reached. The shears in the tied columns still would have exceeded their ultimate capacities--but at times later in the ground motion. This observation

was evident from the fact that maximum uniaxial shear forces induced in the model's tied columns were more than three times their shear capacities according to elastic analyses based on the 0.65 g peak ground acceleration. Thus, even if the maximum ground acceleration were reduced to 0.40 g, shear stresses would still have been nearly twice their capacities. Consequently, many of these members would have failed even if the peak acceleration had been only 0.20 g.

Again it should be pointed out that the response predicted by the elastic analysis is unreliable once members begin to fail or yield. Consequently, while the results presented indicate that many members would be stressed to levels exceeding their shear capacities, the actual forces developed in the building depends on the sequence of member failure and the ability of the remaining elements to redistribute the loads acting on the structure. As members fail or yield, the resisting system and the inertial and damping forces change, and the subsequent response would be substantially altered--intensifying or mitigating the structural distress.

5.5 TWO-DIMENSIONAL ANALYSIS OF WING D MODEL

Due to the size of the structure and the current unavailability of computer programs for realistic three-dimensional structures, inelastic analysis of the entire building was not feasible. However, a simplified inelastic analysis of an isolated portion of the building was believed possible. For the predicted response of the isolated part of the building to represent adequately the actual nonlinear dynamic response of the building, it is necessary, although not sufficient, that the dynamic characteristics and elastic responses of the isolated portion be similar to those of the building as a whole. To model correctly inelastic mechanical behavior, the structural model considered must also incorporate, in the correct proportion, all of the building components which significantly affect the response. This will generally necessitate relatively large structural models.

A survey of the building's damages and subsequent preliminary analyses suggested that it would be useful to analyze the inelastic behavior of Wing D. In order to establish a model for such an analysis, a portion of Wing D was idealized as a two-dimensional framed

structure with frames running in the N-S (transverse) direction. This model was then analyzed using the dynamic elastic TABS computer program to determine its adequacy.

5.5.1 Mathematical Modeling of Wing D

The portion of Wing D modeled for the analysis is shown in Fig. 5.17; this model shall hereafter be referred to as the "Wing D model." Its structural system consisted of five frames with the same structural configurations and properties as the frames of the three-dimensional model along the N-S oriented column lines 24, 26, 27, 28, and 29. These frames were assumed to be completely isolated from the rest of the building at the boundaries indicated in Fig. 5.17. As before, the frames were connected at the floor levels by diaphragms which were assumed rigid in their own plane. However, in this case, the floor diaphragms were not allowed to rotate; thus, each frame had the same lateral floor displacements in the N-S direction. Deformations in the E-W direction were not allowed. As can be seen by comparing Figs. 2.1 and 5.17, only the southern portions of frames along column lines 24, 26, and 27 were included in the Wing D model; columns M-24, N-26, and S-27 were included in the model but the structural members of frames 24, 26, and 27 to the north of these columns were not. Also, the penthouse was not explicitly accounted for in the model. The model's masses were calculated for the tributary regions shown in Fig. 5.17 with the same loading assumptions used for the three-dimensional model of the total structure.

5.5.2 Mode Shapes and Periods

The Wing D model had a slightly lower fundamental period, 0.569 seconds, than that of the total structural model (0.589 seconds) in the N-S direction. (Compare Tables 5.2 and 5.6.) The first and second mode shapes of the Wing D model were very similar to the N-S component of the first two primarily N-S mode shapes (actually, the second and sixth modes) of the total structural model (see Fig. 5.18 and compare Tables 5.4 and 5.7).

5.5.3 Dynamic Response Analysis

(a) Ground Motion.

The S-16°-E component of the derived Pacoima Dam base rock motion was used as the earthquake loading in the analysis of the Wing D model. As was done in the three-dimensional analysis, accelerations of ground motion were normalized so that the maximum acceleration was 0.65 g.

(b) General Structural Response.

In Fig. 5.19 the envelopes of maximum floor displacements obtained in the elastic analysis of the Wing D model are compared to the maximum displacement envelopes obtained for the N-S direction in the analysis of the total structure (at its centers of mass and at frame 29) due to the S-16°-E component of the derived Pacoima Dam base rock motion acting only in the N-S direction. The envelopes were very similar. The slightly smaller displacements of the total structural model at its centers of mass could be attributed to the difference in the two model's fundamental periods; the increased displacements at frame 29 in the total structural model could be attributed to the effect of torsion on the whole building. The maximum floor displacements and story shears obtained in the analysis of the Wing D model are listed in Table 5.8.

The time histories of first and second floor displacements obtained in the analysis of the Wing D model are compared in Fig. 5.20 with the time histories in the N-S direction obtained for the total structural model at its centers of mass and at frame 29 due to the S-16°-E component of the derived Pacoima Dam base rock motion acting only in the N-S direction. During the first six seconds of ground motion, the displacements of the Wing D model and the total structural model at its centers of mass were practically identical. The peak displacements of frame 29 in the total structural model were slightly greater than those of the Wing D model due to the effect of torsion on the total structural model.

(c) Distribution of Member Forces.

The maximum elastic shear and axial forces in the columns of the bottom two stories and the maximum shear stresses in the structure of the upper four stories obtained for the two models are compared in

Fig. 5.21 for frame 29. The distribution and magnitude of forces in columns of the two models were generally found to be similar. The ground and first story columns of the total structural model had slightly greater shear forces; this difference can probably be attributed to the effect of torsion on the total structural model. In both models, the maximum member forces were developed at about the same time (t = 3.40 seconds).

The only significant differences in the distribution of maximum forces throughout the two models occurred in the members near the joints where the frames of the Wing D model were separated from the rest of the structure, i.e., near columns M-24, N-26, and S-27.

Although the distributions of forces throughout the corresponding columns of each model were similar, distributions of shear forces in the upper story shear walls of each model were quite different. This can be seen by comparing the maximum shear stresses occurring in the walls of frame 29 in the two models as shown in Fig. 5.21. In Table 5.9 the maximum of the combined shear forces in the walls of frames 24 and 29 in the Wing D model are compared with shear forces in the corresponding walls in the total structural model.

The differences in shears taken by the walls can be attributed primarily to the absence of channel columns in the Wing D model with their longitudinal cross-sectional axes oriented in the N-S direction (see Fig. 5.17). As previously discussed, the channel columns and their deep, connecting beams resisted a large portion of the story shears in the third, fourth and fifth stories of the total structure. In the second story of the total structural model, the shear walls resisted a much greater portion of the story shear than did the walls in the upper stories because shears in the model's columns were small or acted in a direction opposite to those in the walls. In the Wing D model, the walls carried most of the story shears at all levels since the channel columns in this wing were oriented such that they did not contribute significantly to its N-S stiffness.

5.5.4 Adequacy of Wing D Model

After comparing results of the elastic analysis of the three-

dimensional model of the entire building with those of the two-dimensional model of an isolated portion of Wing D, it is believed that in the elastic range the response of the Wing D model adequately represents the overall response of the corresponding portion of Wing D acting as part of the total structural model in the N-S direction. This conclusion was drawn based on the similarities observed between the two models in their (1) dynamic characteristics, mode shapes, and periods; (2) general responses (e.g. time histories of floor displacements, etc.) to the S-16°-E component of the derived Pacoima Dam base rock motion; and (3) overall internal force distributions.

Analyses using the Wing D model do not accurately predict the elastic forces in certain members. This is primarily true for members located where the model was isolated from other parts of the building and for the shear walls. However, these limitations should not seriously distract from the objectives of this investigation since the overall inelastic response was apparently controlled by members of the ground and first stories which were adequately represented by the proposed model.

5.6 RESPONSE OF ALTERNATIVE STRUCTURAL SYSTEMS

Results of the two- and three-dimensional elastic dynamic analyses have indicated that many features of the observed dmage in the main building could be attributed to its unusual structural system. In particular, the presence of shear walls in only the upper four stories resulted in much larger drifts in the bottom two stories than in the stories with walls. Had a more conventional structural system been used, the structural behavior might have been substantially different. While it is beyond the scope of this report to redesign completely the building using different structural systems and design philosophies, a series of simple examples based on the Wing D model can be used to gain insight into the effect of the type of structural system on the behavior of the building.

To assess the effect that the abrupt change in stiffness at the second floor level had on overall structural performance, two alternative

models, viz., a shear wall and frame model, were formulated for Wing D. A response spectrum analysis was performed on the original Wing D model developed in Section 5.5 and on the modified structural systems developed for Wing D.

For the first alternative structural system, the shear walls in the original Wing D model were continued down through the ground and first stories to the foundation. This model, referred to as the shear wall model, was identical to the standard model with the exception of the presence of walls in the bottom two stories. The thicknesses of these walls were selected to be 14 in. in the first story and 16 in. in the ground story in order to provide for a smooth variation of wall thicknesses from the top to the bottom of the building (see Fig. 2.5 for wall thicknesses in the upper stories.)

For the second alternative structural system, the shear walls were removed entirely from the original Wing D model. In this frame model, columns used in the upper four stories were assumed to have the same cross-sectional dimensions as the columns that supported them in the first story of the original Wing D model. No attempt was made to detail the reinforcement for any of these members.

5.6.1 Ground Motion Characteristics

A smoothed type of response spectrum was used in these analyses so that the computed structural response would not be unduly influenced by unusual frequency characteristics of a specific ground motion. The elastic response spectrum considered in this section was constructed using methods suggested by Newmark and Hall [5.4] for a maximum ground acceleration of 0.5 g, ground velocity of 24 in./sec and a critical damping ratio of five percent. The resulting spectrum used in the analyses is shown in Fig. 5.22(a).

5.6.2 Dynamic Characteristics

As would be expected, the frame model was more flexible, and, consequently, had a longer fundamental period than the original Wing D model; the shear wall model had a period that was shorter. The first mode periods of the shear wall, original Wing D, and frame models were 0.322 seconds, 0.568 seconds and 0.744 seconds, respectively. The periods for higher modes are tabulated in Table 5.10. The mode

shapes for the alternative structural systems did not exhibit the abrupt change in shape that was detected for the original Wing D model (Fig. 5.18).

5.6.3 Comparison of Response Parameters

The root-mean-square (RMS) lateral floor displacement envelopes computed for the response spectrum in Fig. 5.22(a), considering the first three modes of vibration of the models, are shown in Fig. 5.22(b). While the roof displacement of the more flexible frame model was 37 percent greater than that of the original Wing D model, its displacement at the second floor was 23 percent less. As indicated in Fig. 5.22(b), high interstory drifts were required by both the frame and original Wing D models, especially in the bottom two stories of the latter. On the other hand, the lateral displacements of the shear wall model were considerably smaller than those computed for either of the other two models. In fact, the interstory drifts were similar to those computed for the Wing D model in the upper four stories where the observed damages were only moderate. Thus for elastic behavior, a building with continuous shear walls would have more likely suffered the least damage (as inferred from the severity of the interstory drifts) while a building resembling the actual building, with discontinuous shear walls, would have had the largest degree of damage.

The story shear requirements for elastic behavior were also largest for the original Wing D model (except in the top two stories) as shown in Fig. 5.22(c). The smallest base shear was computed for the shear wall model. It is also interesting to note that the large mass located at the first floor level in the models resulted in large increases in story shears between the first and ground stories in all of the systems.

These results cannot be used to predict the behavior of the actual building using alternative structural systems because the effect of inelastic action has been ignored and the actual ground motion record is unknown. However, it is clear that if control of damage by limiting inelastic deformations and interstory drifts had

been a principal design objective, it would have been desirable to continue the shear walls down through the bottom two stories.

5.7 SUMMARY AND CONCLUDING REMARKS

The TABS computer program was used to analyze the dynamic characteristics and the initial elastic responses of the Olive View Hospital's main building to earthquake loading. The assumptions used to formulate the computer program and those used to model the hospital, while simplifying the actual structural configuration and behavior, were reasonable, given the objectives of this investigation and the complexity of the structural system. More accurate analyses are possible using certain finite element programs [5.5]. Such analyses were attempted, but the largeness of the building resulted in prohibitive storage and computational requirements. It is believed that any inaccuracies introduced in modeling the building did not substantially affect the overall response. The analytical results for local regions of the structure may, however, be affected by the analytical idealizations as well as by other characteristics of the building which were not taken into account in the elastic analysis (such as nonstructural elements, variations in the distribution of mass, changes in stiffness due to cracking and spalling, and inelastic behavior.)

A number of significant insights into the seismic behavior of the building were gained from the results of the elastic analyses. First, the results provided an estimate of the building's initial dynamic characteristics; e.g., its fundamental translational periods were approximately 0.60 seconds. Secondly, torsion did not have a major effect on the overall elastic response of the structure, although it did significantly increase displacements and member forces in frames located near the exterior of the building. This conclusion makes a two-dimensional analysis of the structure or an isolated portion of the structure reasonable. Thirdly, interpretation of the response of the building--in particular, the time histories of member forces--indicated that most of the ground and first story tied columns (and third, fourth, and fifth story channel columns) would have probably suffered brittle failures due to shear during the early part of the ground motion before the building's spiral columns yielded. Fourthly,

the response of a two-dimensional model of a portion of the building (the Wing D model) adequately represents the overall unidirectional elastic response of the corresponding portion of the building acting as part of the three-dimensional model of the entire building. This conclusion was reached because the dynamic characteristics and the elastic structural responses of the Wing D and total structural models were quite similar in the N-S direction.

Another important conclusion can be derived from these analyses. Elastic dynamic analysis of a large, complex building can be performed practically using existing computer programs such as TABS. The model of Olive View Hospital had more than 4600 members; it had 69 different frames, the largest being 29 bays wide and seven stories high; and the dynamic responses of the total structure (including all of its members) were obtained at 120 points in time. The total computational cost using the University of California's CDC 6400 computer was about $160; due to the complexity of the building, the largest expense was for the labor required to prepare the input data and to interpret the results.

Results obtained in these analyses provided invaluable guidelines regarding the seismic behavior of the structure and indicated numerous weaknesses in its structural design. It must be recognized, however, that the tremendous uncertainties and simplifications involved in modeling the building and describing the ground motion it experienced preclude exact prediction of the response. In this case, it was not possible to predict the large inelastic deformations that the actual building experienced.

VI. INELASTIC ANALYSES

6.1 INTRODUCTION

The maximum dynamic displacements obtained assuming linear-elastic behavior were substantially lower than the actual residual displacements observed in the building after the earthquakes. Nonetheless, the elastic analyses provided an indication of the initial dynamic response characteristics of the building and identified some of the principal deficiencies of the structural system. However, it is clear from the extensive structural damage discussed in Chapter 3 and the substantial overstresses that occurred in many members for the elastic analysis presented in the last chapter, that it is essential to consider explicitly the nonlinear nature of the seismic response of the building. By investigating the post-elastic behavior of the building, it may be possible to identify the particular features of the structural system and/or ground motion that controlled the response.

At present, analytical methods available for investigating inelastic behavior of structures are limited, particularly for reinforced concrete structure with complex structural systems. One approach to this problem is to represent the gross interstory force-deformation characteristics of a structure by an equivalent shear building model. Several investigators (1.4-1.6) have applied this technique to the main building. The advantage of this type of idealization is that the analytical formulation of the problem can efficiently account for the overall three-dimensional structural response and stiffness degrading mechanical behavior. The principal disadvantages are that the interstory force-deformation relationships are difficult to determine--requiring simplified structural models or loading distributions which may not be compatible with the actual structural response--and their use generally makes it difficult to evaluate local member behavior.

Because of the success achieved in isolating a portion of the building which had essentially the same elastic dynamic characteristics as the building as a whole, an alternative approach to the nonlinear problem was pursued in this investigation. Individual members, with simplified nonlinear mechanical characteristics, were combined to form

the various frames of the Wing D model discussed in the last chapter. Thus, the problem could be evaluated using existing nonlinear dynamic frame analysis computer programs. In this way, the behavior of individual members would be accounted for directly, but other features such as stiffness degradation and three-dimensional structural modeling remained untractable for the complexity and size of the building.

Based on this approach, several models of Wing D were constructed and analyzed using a modified inelastic dynamic analysis computer program for various ground motion records. The assumptions and limitations inherent in this method are examined below. In this way, the basic features of the structural system controlling the failure mechanism were identified. An attempt was also made to interpret the results to identify the effect on the response of different ground motions; of variations in the assumed member properties; and of member failure and hammering of the first floor against the warehouse and retaining wall.

6.2 COMPUTER PROGRAM

An existing nonlinear analysis computer program [6.1] was extended [6.2] to incorporate some of the mechanical characteristics of frame structures similar to the Wing D model when subjected to severe earthquakes. Two-dimensional rectangular frames may be analyzed for the combined effects of gravity loads, and horizontal and vertical ground excitations. Beam-column joints were considered to be rigid. All shearing deformations were disregarded. While beam elements were assumed to be inextensible, axial deformations were accounted for in column elements. Thus, every joint was associated with a vertical and rotational degree-of-freedom, and all joints at a floor level were associated with a single horizontal degree-of-freedom. In this investigation, only horizontal ground motions were considered, and the geometry was specified using center-to-center dimensions.

The computer program was based on a bilinear, hysteretic moment-curvature relationship for members in which inelastic deformations were concentrated at member ends. This formulation employs the well-established two-component element idealization [6.3]. The yield

criteria are sufficiently general to allow for unsymmetrically reinforced members, and to account for appropriate flexural capacity-axial load interaction equations for columns. Element limitations are discussed in Reference 6.2.

Gravity load effects may be included in the analysis for the purpose of initializing member internal forces and for calculating so-called P-Δ effects. Both horizontal and vertical base level acceleration time histories may be specified.

Since structural response will in general be nonlinear, the equations of motion are expressed in an incremental form and solved using an unconditionally stable, constant average-acceleration algorithm. Viscous damping of the Rayleigh type is employed. By summation of the incremental displacements and member forces, the structural response, including member forces and yield conditions, is determined at each time step. Whenever the yield condition of a member changes, the stiffness matrix for the structure is reassembled to account for the modified stiffness distribution.

The program tabulates the internal force distribution and displacements under specified static loads. Time histories and envelopes of maximum floor level displacements and overturning moments, interstory drifts and shears, member forces, plastic rotations, and curvature ductilities are used as output.

Additional information about the assumptions and computational procedures employed in this program is available in Reference 6.2. While most of the terminology used for the various input and output parameters is consistent with standard engineering practice, it is of value to discuss briefly the definition used for ductility. Ductility as it is used here is a measure of the inelastic deformations that occur in the structure, and is generally presented as the ratio of the maximum deformation to the corresponding yield deformation. Consequently, displacements, rotations, curvatures, and strains can be used as the basis of ductility indices. However, ductility ratios based on different deformational parameters cannot usually be compared directly. For example, ductility ratios based on displacement or

rotation measurements depend on the loading distributions and structural configuration. Curvature ductilities, on the other hand, are based on cross-sectional configuration and material properties so that they may be more useful comparative indices of inelastic deformation.

It is for these reasons that unnormalized plastic rotations or cyclic curvature ductilities will be used in this presentation as indices of the severity of inelastic deformations. For bilinear hysteretic systems a cyclic curvature ductility factor, as illustrated by Fig. 6.1, may be expressed in terms of the maximum moments developed at a section [6.2]:

$$\mu_\phi = 1 + \frac{\sum|M_{max} - M_p|}{pM_p} \tag{6.1}$$

where the summation is performed for each sense of bending in which yielding has occurred, and in which M_{max} is the maximum moment at section; M_p is the plastic moment capacity; and p is the rate of strain hardening.

This ratio may be calculated directly for symmetrically reinforced sections. However, for unsymmetrically reinforced sections, the ratio must be calculated at each time step, using the appropriate plastic moment capacity for the sense of yielding.

In order for column internal forces to remain near the interaction curve during yielding, any change in the axial load requires a corresponding change in the moment. This complicates the definition of ductility since the plastic moment may be different each time the member yields and may change substantially while yielding (Fig. 6.2). To solve this problem, the average plastic moment, $\bar{M}_p$, occurring at a plastic hinge location is calculated by the relation:

$$\bar{M}_p = \frac{\sum|M_p \cdot \Delta\theta_p|}{|\Delta\theta_p|} \tag{6.2}$$

where the summation is carried out for each analysis time step in which yielding occurs, and M_p and $\Delta\theta_p$ are the plastic moment and

incremental plastic rotation during a particular time step. This method then proceeds as for the case of beams (Eq. 6.1), except since the calculation of $\bar{M}_p$ is performed at the end of the response, only the absolute value of the maximum cyclic curvature ductility factor can be determined.

These definitions are more general than those commonly used in the literature in order to account for members with unsymmetric moment capacities, yield reversal and axial load variations during yielding. Further clarification of this terminology may be found in Figs. 6.1 and 6.2 and in Reference 6.2.

6.3 MATHEMATICAL MODELING OF STRUCTURE

The basic analytical model used for simulating the nonlinear response of the main building was similar to the two-dimensional model developed in Chapter 5 for Wing D. The idealized portion of the building is shown in Fig. 5.17. Its structural configuration and dimensions and the boundary conditions that were assumed in separating it from the rest of the structure have been discussed previously. Again the investigations were confined to the hypothetical two-dimensional response in the N-S direction; torsional effects were disregarded.

The inelastic analyses were conducted in two phases. Initially, member properties were assumed to remain constant throughout the earthquake. This was a consequence of the member behavior assumed by the computer program. Thus, member spalling and failure were not accounted for, nor was the hammering of the building against the retaining walls or warehouse considered at this stage. These studies were used to identify the basic nature of the seismic response and to clarify the effect of various modeling and loading assumptions on the building's behavior. Once this was done, the inelastic computer program was modified in the second phase to allow member properties to change during the excitation and to consider hammering. These modifications which approximately account for these factors and the analytical results are examined in Section 6.6.

The results of the elastic analysis have indicated that the tied columns supporting the terrace canopy probably failed very early in

the seismic response and prior to any significant inelastic action in the rest of the building. Drifts of only 0.3 in. in the ground story (a story drift index = 0.0016) would have induced shear failures in most of these tied columns. Moreover, the acceleration intensity necessary to produce these failures (about 0.2 g) was much smaller than the peak values estimated for the site. It would appear that the stiffness of these canopies had no controlling influence on the inelastic response of the building. Since the initial analysis will be based on the original member properties and assuming that no member failures occur, the contribution of the terrace canopy to the stiffness of the building will be neglected. However, the mass of these areas will be included since even after failure the canopy moved with the first floor. The largest uncertainty in this regard is the stiffness and energy dissipation provided by the collapsed canopies.

The modeling of members used for elastic and nonlinear analyses was essentially the same except that the appropriate yield criteria had to be specified for the inelastic analyses. However, differences between the elastic and nonlinear computer programs required substantially different mathematical representations for the same structure. In both cases only two-dimensional response was considered; no torsion of the building was allowed. Initially, only cases using invariant member properties will be examined and members will be assumed to have unlimited ductility capacities. Section 6.6 considers member spalling or failure and hammering of the building against adjacent structures. The modifications and refinements of the basic analytical model required to perform the first phase of the nonlinear analyses are described below. The initial model described here is designated as the standard nonlinear model of Wing D.

6.3.1 COLUMNS

Since the nonlinear program disregarded shearing deformations, only the transformed cross-sectional area and the uncracked transformed moment of inertia were specified for each column. These values were the same as those used in the elastic analyses except they were modified to account for two additional factors. Firstly, the computer

program used in these analyses considered center-to-center dimensions to define the structural geometry and member stiffnesses. To compensate for the finite size of the beam-column joints, which were accounted for directly in the elastic analyses, the column moments of inertia were multiplied by the cube of the ratio of the center-to-center span to the clear span. Because the modulus of elasticity is assumed to be constant for all members by the computer program, a second transformation was required to account for the different moduli associated with the different strength concrete used in the ground and first story columns (see Sections 2.4.1 and 5.3). Consequently, the moments of inertia and areas were also multiplied by the ratio of their actual modulus divided by the value assumed in the analysis for the entire building. Thus:

$$A_{equiv} = \frac{E_{actual}}{E_{assumed}} \cdot A_{actual} \tag{6.3}$$

$$I_{equiv} = \frac{E_{actual}}{E_{assumed}} \cdot \left(\frac{L_{center\ to\ center}}{L_{clear\ span}}\right)^3 \cdot I_{actual} \tag{6.4}$$

In order to account for the effect of axial load on the flexural moment capacity of columns, the computer program assumes an interaction curve of the form shown in Fig. 6.2. While the flexural stiffness is affected by yielding, the axial stiffness is assumed invariant by the program. During yielding, internal forces are constrained to remain on the interaction curve except for small deviations caused by strain hardening. While the mechanical properties assumed for columns account for the interaction of axial and bending forces, these properties are based on the characteristics of monotonically loaded members; they do not account for any stiffness deterioration or yielding associated with the closing of flexural cracks as discussed by Aoyama [6.4] for reversed plasticity.

To determine the required interaction curves, moment-curvature relations were developed for each column cross section at a variety of axial loads assuming monotonic loading. This was done using a computer program described briefly in Appendix B and in Reference 6.2.

This program computes the moment carried by any cross section which is loaded along an axis of symmetry for a given axial load. Arbitrary nonlinear steel and concrete material properties may be specified. In this case the actual geometry of each section was used and material properties were based on experimental data (see Section 2.4). A family of interaction curves can be constructed from these moment-curvature relationships based on an assumed ultimate concrete strain. Details of the method used to calculate the moment-curvature relationships are described in Appendix B.2. On the basis of these relationships, a rate of strain hardening of 0.03 was used in the nonlinear dynamic analyses.

The computer program also calculates the shear strength and ductility capacity of each column considered. These values will be discussed later when the analytical results are evaluated.

6.3.2 STRUCTURAL WALLS

The shear walls were treated as elastic elements. Consequently, their properties were the same as those in the elastic analysis (see Section 5.3.2 and Appendix B.3). This assumption was based on a number of considerations; cracking in the shear walls in the actual structure was relatively minor, and possible methods for representing the nonlinear behavior of these walls by a frame analogy did not seem realistic in this case. Furthermore, it is not believed that the nonlinear behavior of these walls significantly affected the overall response of the actual structure.

6.3.3 Beams and Slabs

Floor slabs of the type encountered in Wing D were investigated using elastic finite element computer programs. Consequently, elastic stiffness characteristics of equivalent beams used to represent slab properties in nonlinear simulations were based on these analyses. The methods used to determine these equivalent beam stiffnesses are discussed in Appendix B.4. The approximate values used in the preceding elastic simulations were not substantially different from the more refined values used here.

Since these computations considered the rigidity of the slab-column joints, no transformation of the stiffness to account for clear spans was required. To establish the yield criteria for the slabs, the moment capacities of various yield lines running perpendicular to the direction of the frames were calculated. These yield lines were assumed to extend across the full width of the slab, i.e., between points bisecting the span separating adjacent frames. Critical locations were assumed at the face of the columns, at the edge of the drop panel, and at any cut-off point for reinforcement. Since the beam elements used in the computer program can yield only at their ends, and subdividing each slab into sufficient elements to allow yielding at critical yield lines located within the span would make the problem computationally prohibitive, equivalent yield moments at the element ends were computed. These were derived by fitting a linear moment variation with reversal through the envelopes of critical yield line moment capacities. Since slabs have different amounts of reinforcement on the top and bottom, these computations were carried out for each sense of slab bending. Details of these calculations are briefly outlined in Appendix B.4.

It is interesting to note that in many upper floors the positive slab reinforcement was terminated at column lines without laps or splices (see Fig. 2.16). Consequently, the positive moment capacity of these locations was that required to overcome gravity loads.

In frame 29 all of the slabs were cast integrally with beams running parallel to the frame. The moments of inertia used were the same as those in the elastic analyses except that transformations similar to those described for the columns were required to compensate for joint rigidity. The moment capacities of these T-beams were evaluated using the computer program used to determine the moment-curvature relationship for columns except that zero axial loads were specified. Since the joint dimensions were relatively small at the first floor level, no modification of yield moments was made to compensate for differences in moments at the centerline and face of supporting members. However, in the case of spandrel beams connecting the two shear walls in frame 29, a special idealization was required. In this case, shear walls extended appreciably beyond the column lines

and, consequently, the moment capacity at the ends of the beam element connecting these walls had to be increased substantially in order to model realistically the actual behavior of these members. An example of these calculations is presented in Appendix B.4.

6.3.4 Structural Idealization

Once the various member properties had been determined, they were assigned to the appropriate locations in a rectangular two-dimensional framework as required by the computer program. In this case the structure to be idealized (Fig. 5.17) consists of five parallel frames. As discussed previously, the stiffness of terrace canopies will be disregarded for the time being. Since the structural model developed for Wing D in Chapter 5 assumes that different frames have the same lateral displacement at each floor level, the two-dimensional frame idealization schematically illustrated in Fig. 6.3 can be employed to model the in-plane deformations of the actual three-dimensional multi-frame building. In this analogy, frames are connected at each floor level by inextensible link elements. These can be analytically represented by axially rigid, pin-ended rods; computationally, they are treated as elastic elements with nearly zero flexural stiffness.

A further computational simplification of the model is possible by recognizing that, for all practical purposes, the strength and stiffness characteristics of frames 26, 27, and 28 were identical. By appropriate transformations of mass, stiffness, and strength, these three frames can be represented by a single equivalent frame. In this case, the three frames with similar properties (frames 26, 27, and 28) were replaced by a single frame with the same geometrical dimensions and modulus of elasticity as the original frames. However, the member moments of inertia, areas and yield moments (or interaction curves), the gravity loads, and the floor level masses for the equivalent frame were taken to be three times those of frame 28. The equivalent frame will be designated frame 28*.

The structural system analyzed in the nonlinear analyses consisted of the three frames (frame 24, 28*, and 29) is shown in Fig. 6.3. Although the actual foundation footings may have been slightly flexible,

columns were assumed fixed at their base as they were for the elastic analyses. In the real structure there was substantial yielding near the base of the columns at the ground floor level, indicating sufficient rigidity at the footings to develop the flexural capacity of the columns. The base of the columns were assumed to be slightly below the elevation of the actual floor slab. This is similar to the idealization used in the elastic analyses and approximates the foundation flexibility.

The actual masses of the Wing D model, as defined in Section 5.5.1, were used. Rather than the modal damping used in the elastic analyses discussed in Chapter 5, the nonlinear analyses assumed that viscous damping forces were proportioned to the mass matrix. Damping was taken to be equal to five percent of critical in the first elastic mode of vibration of the structure. This resulted in damping equal to 1.5 percent and 0.85 percent in the second and third elastic modes of vibration, respectively.

6.3.5 Gravity Loads

The principal of superposition is not generally valid for nonlinear behavior; therefore, seismic and gravity loading cannot be considered separately, as is often done in the case of elastic analyses. In these investigations it was considered essential to include the effects of gravity loads because the associated geometric nonlinearities could be substantial for the anticipated displacements, and it was necessary to initialize the internal forces in members which might yield, particularly in columns where the flexural capacity is controlled by axial loads.

In addition to loads from the structure, fixtures and partitions used in calculating the mass of the building for the elastic dynamic analyses, the effects of live loads reduced as allowed by code requirements were included as part of the gravity loads acting on the building. The beam elements were acted upon by the distributed loads acting on the slab column strips. The remaining tributary loads from the columns, slabs and beams were applied as concentrated vertical loads at the beam-column joints.

Special treatment was required at locations where the idealized

frames were isolated from the remainder of the building. Gravity load forces acting at the points of discontinuity were estimated using a simple moment distribution procedure. These forces were then applied to the frames as concentrated external joint loads and moments.

6.3.6 Dynamic Characteristics of Standard Nonlinear Model

In order to determine the effect of modifications of member stiffnesses made in formulating the standard nonlinear model just discussed, as well as the effect of disregarding the terrace canopy, the elastic dynamic characteristics of the proposed nonlinear model were compared with those for the elastic model of Wing D presented in Chapter 5. The natural periods of the two Wing D models and of the entire three-dimensional model are shown in Table 6.1. It is clear from these values that the loss of the stiffness contributed by the terrace canopy results in a structure slightly more flexible than the original model. The mode shapes for the proposed nonlinear model are presented in Table 6.2 and are compared with values obtained for the Wing D model (Table 5.7) in Fig. 6.4. In this figure, the mode shapes for both models were normalized to unity at the roof level to facilitate comparison. Because the dynamic characteristics of the two models are similar, their computed maximum displacements (Table 6.3) to the derived Pacoima Dam base rock motion (0.65 g) were also similar as shown in Fig. 6.5. While the elastic displacements of the more flexible standard nonlinear model were just slightly smaller than those for the original Wing D model at the upper four floor levels, the opposite was true at the first floor. Because of the smaller displacements and the reduced ground story stiffnesses, the story shears developed by the standard nonlinear model were less than those for the original Wing D model as shown in Fig. 6.5. The distribution of maximum elastic member shear forces in vertical elements is shown in Fig. 6.6. Comparison of Fig. 6.6 with Fig. 5.21 for the Wing D and three-dimensional models reveals that the modified member stiffnesses and the loss of canopy stiffnesses results in a slightly different distribution of internal forces. It is believed, however, that the reliability of the model is sufficient for the purposes of this investigation.

6.4 NONLINEAR DYNAMIC RESPONSE OF WING D

To illustrate the basic nonlinear behavioral characteristics of the structure, the computed response of the standard nonlinear model of Wing D to simulated ground motion number 6 (Fig. 4.9) will be examined. As discussed in Chapter 4, the frequency content of this ground motion is representative of other strong motion accelerograms recorded in the western part of the United States on firm soil sites at moderate epicentral distances. In this case, the peak ground acceleration was set equal to 0.5 g.

The sensitivity of nonlinear response to different modeling assumptions and ground motions will be examined in subsequent sections and in Appendix D.

6.4.1 Story Shears

The envelope of maximum story shears developed during the response is shown in Fig. 6.7. Substantial inelastic action occurred during the response, involving numerous critical regions throughout the structure as indicated in Fig. 6.8. Although all of the plastic hinges indicated in this figure do not develop simultaneously, a complete panel mechanism, like that shown in Fig. 6.9, does occur throughout the bottom two stories at certain times. Because of this, the shears indicated in Fig. 6.7 for the ground and first stories are close to the story capacities.

The seismic resistance coefficient of a story is defined as the shear capacity of a story divided by the weight of the structure above that story. In this case, the computed shears imply seismic resistance coefficients of 0.38 and 0.55 for the ground and first stories, respectively, of the standard nonlinear Wing D model.

It is interesting to note that the coefficient for the ground story is less than that for the first story. This is because of the extremely large mass of the terrace canopy and because the standard model disregards the strength and stiffness of the structural framing under the canopy. These tied columns failed prematurely and their strength was therefore discounted in the analysis.

The member strengths and stiffnesses used to compute these story shears are based on the initial cross-sectional properties (see Appendix B) and would consequently overestimate the story shears that could be developed after spalling. To account for this, an analysis was performed (see Appendix D) in which member mechanical characteristics were based on their condition after substantial spalling may have occurred. Seismic resistance coefficients for this modified model of Wing D are slightly greater than 0.25 and 0.36 for the ground and first story, respectively. Table 6.4 compares the values of seismic resistance coefficients obtained by other investigators with those discussed above. The values by Selna, et al. [1.8] are between those computed here for the initial and confined sections, as might be expected. While the value suggested by Aoyama and Sozen [1.9] at the first story is similar to the other values predicted for this level, the value at the ground story is much larger than would be expected on the basis of the other values. This is apparently because they assumed that the tied columns in the ground story also yielded in flexure and thus contributed to the seismic resistance coefficient, rather than failed brittly in shear as observed.

While it is clear from these values that estimates of the strength of the structure varied substantially depending on member mechanical models and overall analytical procedure, these estimated values were all relatively greater than expected on the basis of the design code requirements existing at the time of construction. For example, the working stress level story shears computed for the Wing D model according to the original design procedure used for the design of the building are shown in Fig. 6.7. Assuming an ultimate seismic load factor of 1.4, the strength of the standard nonlinear Wing D model is more than 3.2 times that required by the design code; considering only the confined section member properties, the model is still 2.3 times stronger than that prescribed. In fact, if the building were redesigned with the seismic coefficient based on a K value of 1.0 and a C value based on the actual period of the building (as substantiated by the three-dimensional analysis of the building), the required design forces could be reduced from the actual values used in the design by about

25 percent. The working stress level seismic coefficient would drop in this case from a value of 0.08 to about 0.06.

Even in the event that newer earthquake regulations of TITLE 17 of the California State Administrative Code [2.8] related to static analyses (Method B) were applied to the structure, the basic design forces required would be significantly less than the capacity of the structure. For example, in this case for K = 3.0 and C = $0.05 \cdot T^{-1/3}$ 0.06, a design base shear equal to 18 percent of the building's weight or, for a load factor of 1.4, a required seismic resistance coefficient of 0.25 is obtained. The estimated values of the building's seismic resistance coefficient are equal to or greater than this value. Under TITLE 17, the adequacy of the hospital would now have to be verified in a computer analysis and much more attention given to drift and damage control, as well as to detailing to achieve ductile behavior. It is clear, however, that the building had a substantially higher strength than that required, even in the context of current seismic requirements.

6.4.2 Lateral Floor Displacements and Story Drifts

The envelopes of maximum inelastic floor displacements and story drifts computed for the standard nonlinear Wing D model subjected to simulated record number 6 are shown in Fig. 6.10. While the maximum roof displacement of 4.12 in. was considerably smaller than the residual displacements observed in the building (Fig. 3.2-3.4), the pattern of displacement indicates that large story drifts [Fig. 6.10(b)] were concentrated in the lower two stories. The structural walls in the upper four stories successfully limited the drifts in these stories. However, the computed drifts in the lower two stories were similar in magnitude, in contrast to the permanent drifts due to the earthquake which were much larger in the first story than in the ground story (see Figs. 3.2 and 3.3).

Another inconsistency between the analytical results and the observed damage can be seen in the time histories of floor displacements shown in Fig. 6.11. These computed histories indicate that the building would have suffered a large number of oscillations with reversal of drifts with about the same magnitude. This is inconsistent with the

damage shown in Chapter 3 which indicated that the main features of the damage were produced by one or a few cycles of large inelastic drift without significant reversal.

It is also interesting to note that the nonlinear displacements of the building are not substantially larger than those computed on the basis of elastic behavior (Fig. 6.10). For this figure, the elastic values were obtained by a RMS spectral analysis of the model for five percent viscous damping. The elastic drifts in the upper four stories are greater than the corresponding nonlinear values since it appears that a significant portion of the elastic lateral displacements was attributable to column axial deformations in the bottom two stories. In the nonlinear case, the formation of a panel collapse mechanism resulted in larger drifts in the lower two stories and larger overall displacements throughout the height of the building. The drift indices computed by the elastic dynamic analyses for the simulated record are just slightly larger than the value of 0.5 percent suggested in Reference 6.5 as the permissible story drift for working stress level static lateral forces. Because the intensity of this ground motion is much more severe than that represented by working stress level design forces, one might infer, on the basis of these analyses, that the drifts in the building would be acceptable. Even if the actual drifts in the building were as small as those indicated by these analyses, it is believed that the irregular distribution of drifts which concentrates drift related damage in just these stories is undesirable. Furthermore, it may be necessary to impose even lower drift limits in cases (such as hospitals) where nonstructural damage must be limited to assure functional integrity after an earthquake.

6.4.3 Inelastic Deformations

The nonlinear analyses of the building indicated that the slabs and columns of the lower two stories would have started to yield during the first two seconds of simulated record number 6. As shown in Fig. 6.11, yielding initiated very early in the response before the ground motion reached its maximum intensity (Fig. 4.9). Elements with low shear capacities, such as the first floor slabs and the first story tied columns, would have failed soon thereafter. As discussed, this

analysis did not account for the effect of the failure of these elements or the spalling of the concrete covers indicated for many columns on the subsequent response.

As indicated in Fig. 6.8, yielding also occurred in the upper story slabs which were relatively weak. The shear stresses computed for the walls did not exceed their cracking stress (see Appendix B.3). However, as indicated in Section 5.5.3(3), the Wing D model tends to underestimate substantially the wall stresses in the second story. Cracks were observed in these walls (Fig. 3.24).

The ductility requirements for the girders, slabs, and columns in the model are shown in Fig. 6.12. For the slabs and girders, the maximum cyclic curvature ductility factor (Eq. 6.1) developed anywhere at a floor level in a frame are plotted. For the columns, the maximum value of cyclic curvature ductility factors based on the curvature corresponding to the average plastic moment (Eq. 6.2) developed at the critical region are plotted for each story in a frame. As seen in Fig. 6.12(a), the largest column ductilities were required in the two stories under the structural walls in frame 29. Significantly smaller column ductility requirements were computed at other locations in the bottom two stories and, with only two exceptions, the columns in the upper four stories remained elastic (Figs. 6.8 and 6.12). The maximum column curvature ductility computed was less than five in all cases. Although it is generally recommended that yielding in ductile frames occur in girders rather than columns [6.5] because of the limited ductility capacities of axially loaded members, it is apparent that the predicted ductilities are considerably smaller than those that the spiral columns were actually able to develop.

The columns yielded numerous times; on the average, the columns that yielded did so eight times with some ground story columns below the structural walls yielding more than 40 times at their base. Again this number of inelastic events is not consistent with the observed damages which indicated that only a few inelastic excursions occurred.

The ductilities predicted in the slabs and girders also indicate a concentration of inelastic behavior in the bottom two stories. The

first floor beam in frame 29 required curvature ductilities up to thirteen. It is interesting to note that the coupling spandrel beams in frame 29 generally did not yield, and where they did, the ductility demands were quite small. Because the structural walls in the upper stories limited the story drifts, the slab ductility requirements were considerably reduced at these levels despite the relative weakness of the slabs.

Like the columns, the slabs and girders that yielded would have done so numerous times. This is particularly true for the slab in frame 24 adjacent to the structural walls in the upper stories (Fig. 6.8) and for the first floor slab throughout the building. The average number of yield events per slab critical region was nearly 20 for the entire building, but the first floor slab hinges yielded on the average 31 times.

With the exception of the tied columns in the first story and the flat first floor slabs which had limited shear capacities, it is believed that the building members had ductility capacities in excess of the demands predicted for this earthquake record. However, there still would have been significant structural (as well as nonstructural) damage even at these relatively low displacement amplitudes.

6.4.4 Comparison of Computed and Observed Damage

Although the nonlinear response of the standard Wing D model correctly identified some of the features of the damage that occurred in the earthquake (e.g., concentration of inelastic deformations in the bottom two stories), there are a number of significant discrepencies between the observed and computed damage. For example, the computed displacements are much smaller than the permanent displacements caused by the earthquake. Also, as mentioned, the computed drifts were similar in the bottom two stories which was not the case in the actual building. Finally, the response histories indicate a large number of inelastic cycles including reversal which is not consistent with the observed damage.

Two principal reasons can account for these differences. First, there is a substantial amount of uncertainty regarding the modeling

of the nonlinear mechanical characteristics of the structure. This not only concerns the reliability of the predicted member strengths and stiffnesses and the adequacy of the Wing D model itself in the inelastic range, but it also concerns the assumption of invariant nonlinear characteristics. It is clear from the previous results that some members should fail or substantially alter their characteristics during the response. Thus, damage to some beam-column joints on lines G and M resulting from the collapse of the terrace canopy, the drastic decrease in the resistance of some of the flat slabs which failed prematurely, the sudden release of energy and transfer of load from the failed first story tied columns to the spirally reinforced columns, the decrease in the ground story's seismic resistance coefficient due to the brittle failure of its tied columns, the decrease in capacity of the spirally reinforced columns due to spalling of their outer cover, and so on, were not considered in this analysis. Furthermore, biaxial seismic excitations and torsional action due to unsymmetric distributions of strength, mass, and/or stiffness could have had a significant effect on the actual nonlinear response that was not detected in these analyses.

A number of analyses have been performed to determine the sensitivity of the response to some of the modeling assumptions. These are briefly examined in Appendix D. It was found that while variation of member properties had some effect on the response, the computed responses were still significantly different from the observed damage. An analysis which includes some member failure and hammering against the warehouse is examined in Section 6.6.

The second principal source of uncertainty in these analyses is that the actual ground motion experienced at the site is unknown. Once a panel mechanism, such as that shown in Fig. 6.9, formed, the subsequent response was very sensitive to the characteristics of the ground motion at that time.

6.5 EFFECT OF GROUND MOTION CHARACTERISTICS ON NONLINEAR RESPONSE

A number of hypothetical ground motion records for the site were discussed in Chapter 4. The inelastic responses of Wing D models have beem computed for several of these records and they are briefly

discussed in Appendix D. To illustrate the sensitivity of the nonlinear response to different ground motions, the response of the standard nonlinear Wing D model to the simulated ground motion record (number 6) will be compared to that for the S-16°-E component of the derived Pacoima Dam base rock record. The simulated record is believed to be representative of strong ground motions experienced on firm soil sites located at moderate epicentral distances. The derived Pacoima Dam record is believed to be representative of ground shaking in the immediate vicinity of the faulting.

To study the effect of ground motion intensity on nonlinear response, both of the records considered in this section were also arbitrarily amplified by a factor of two. As discussed in Chapter 4, there is considerable uncertainty regarding the peak acceleration at sites near fault ruptures.

6.5.1 Story Shears

As discussed in Section 6.4.1, a collapse mechanism was formed in the bottom two stories under the simulated ground motion. Because the same collapse mechanism was formed for the derived Pacoima Dam base rock record, the story shear forces in the bottom two stories are very similar for both records as seen in Fig. 6.13. Even for the amplified ground motion records, the story shears are similar. The slight differences in values are due to greater amounts of strain hardening caused by the larger ductilities developed by the derived Pacoima Dam record and the amplified records. In the case of ground motions severe enough to form a collapse mechanism the story shears are controlled by member strengths.

6.5.2 Lateral Floor Displacements and Story Drifts

The maximum lateral displacements developed by the model for the derived Pacoima Dam base rock record at 0.4 g are substantially larger than those based on the simulated record as shown in Fig. 6.14. They are still considerably less than the actual residual displacements observed in the building. When the ground motions are arbitrarily amplified by a factor of two, the displacements for the amplified simulated record (1.0 g) are just larger than those for the unamplified Pacoima Dam base rock record. Doubling of the intensity of the

Pacoima record increases the lateral displacements by nearly a factor of four. It is the only one of the four records considered here in which the first floor displacements would have been large enough to result in hammering against the warehouse as observed in the actual building.

It is interesting to note that unlike the responses for the simulated record, there are significant differences between the elastic and nonlinear responses for the derived Pacoima Dam base rock record. This is illustrated in Fig. 6.15. The maximum nonlinear displacements are more than twice as large as the elastic values at a peak acceleration of 0.4 g, and when the acceleration amplitudes are doubled, the difference increases to a factor of almost four.

The displacement response histories for the derived Pacoima Dam base rock record and the amplified records are shown in Figs. 6.16 through 6.18. It is interesting to note that the response to the Pacoima record is dominated by a single large displacement cycle early in the response that results in a small permanent northward displacement (Fig. 6.16). While these displacements are still smaller than the permanent drifts observed, the presence of a single large excursion agrees with the observed damage. The large cycle corresponds to the long-duration acceleration pulses in the beginning of the record (Fig. 4.10) that were discussed in Section 4.6.

Even when the simulated record is amplified, the displacements (Fig. 6.17) remain relatively small and oscillate numerous times with reversal. On the other hand, the response for the amplified Pacoima record exhibits a single large displacement excursion. However, the largest displacement is to the south (rather than to the north as in the actual structure) where reversal of displacement occurs, bringing the building back to about its original position. The response of the structure when a collapse mechanism occurs is very sensitive to the shape and duration of the acceleration pulse(s) immediately thereafter, to the response of the structure leading up to the formation of the collapse mechanism, and to the strength and stiffness characteristics of the structure. Thus, slight modifications to the

accelerogram leading up to the pulse and to the pulse itself could result in larger transient or permanent displacements to the north, in larger southward displacements, or any other desired response. It is believed, however, that strong, long-duration acceleration pulses like those of the derived Pacoima Dam base rock record or the Van Norman Dam record were the cause of the large lateral drifts observed in the building. While the computed responses do not exactly reflect the observed damages, it is clear from the drifts computed in the nonlinear analyses (Fig. 6.19) that the response would result in undesirably large amounts of structural and nonstructural damage. Drift indices ranging from 1 to 5 percent are too large, particularly for hospital or other essential facilities.

6.5.3 Inelastic Deformations

In general the locations of plastic hinges and the distribution of curvature ductility requirements for the derived Pacoima Dam base rock record and the amplified records are similar to those for the simulated record discussed in Section 6.4.3. Envelopes of the maximum cyclic slab curvature ductilities and of the maximum cyclic column curvature ductility (based on the average yield moment) are shown in Figs. 6.20 through 6.22 for these other ground motions. Comparison of Figs. 6.12 and 6.20 indicates that the curvature ductility requirements generally increase by more than a factor of three when the ground motion is increased from 0.5 g to 1.0 g. Although the main inelastic deformations controlling seismic response are still concentrated in the lower two stories, the seismic internal moments developed in the upper floor slabs are sufficient to overcome initial gravity load moments so that yielding in a positive bending sense occurs at the supports. Since the positive slab reinforcement at slab supports is not continuous, only minimal yield moment capacities were assumed for the case where tensile forces develop at the bottom of the slab. Because of this the computed ductilities at these locations are not representative of the behavior and as such are neglected in the figures.

The cyclic curvature ductility requirements for the model subjected to the original and amplified derived Pacoima Dam base rock

motions are shown in Figs. 6.21 and 6.22. The values for the original Pacoima record are about twice those for the unamplified simulated record, and the amplified Pacoima values are about twice those for the amplified simulated record.

All of these analyses indicate that the columns and slabs would have sustained numerous cycles of large inelastic deformation including reversal. Although spiral columns, as discussed in Appendix B.2, have substantial ductility capacities and could have sustained the required inelastic deformation, it is doubtful that the slabs could have done so. The ductility requirements in the first floor slab are generally much higher than those in the columns. Furthermore, analyses indicate that the slabs yielded more often than the columns. Consequently, it is doubtful that the slabs, particularly at the first floor level, could have sustained the required inelastic deformations in a ductile manner.

6.5.4 Comparison of Computed and Observed Damage

While the maximum computed displacements for the ground motions considered in this section are not as large as the observed permanent drifts, even when the peak ground accelerations were raised, characteristics of the structural behavior and the distribution of damages are correctly identified. It has been shown that the response is very sensitive to the ground motion considered in the analysis. In particular, the lateral displacements can become very large if a collapse mechanism forms during intense, long-duration acceleration pulses like those found in the Pacoima and Van Norman Dam records. Since the exact ground motion is not known at the building site, it is not possible to compute accurately the structural response. Furthermore, the response is likely to be sensitive to the type and sequence of member failures that occur and to the hammering of the building against the warehouse and retaining wall. The effect of such events on the response is briefly examined in the next section.

6.6 EFFECT OF MEMBER FAILURES ON NONLINEAR RESPONSE

To assess the effect that failure of various members throughout the building had on its seismic behavior, a simplified "Failure Model"

was devised. This model was similar to the standard nonlinear model of Wing D described earlier in this chapter, except that it incorporated a number of additional features to model member failure and hammering against the warehouse.

6.6.1 Failure Model

The model used is schematically illustrated in Fig. 6.23. The model incorporates options for: (1) brittle failure of the terrace canopy; (2) shear failure of the first story tied columns; (3) spalling of the concrete cover from the columns; and (4) hammering against the warehouse and retaining walls. The failure of the slabs were not accounted for. Details regarding the modeling assumptions are discussed below.

(a) Failure of Terrace Canopy.

The terrace canopy tributary to the original Wing D model (see Fig. 5.17) was represented by a single nonlinear spring. The stiffness of the spring was determined by summing the lateral stiffnesses of all tied columns supporting this portion of the canopy, assuming complete fixity at top and bottom. The lateral resistance of the spring was determined by summing the shear capacities of the individual tied columns based on axial force corresponding to their loads, again assuming fixed-end conditions (see Appendix B.2.2 for discussion of shear strength determination). Once this lateral force is reached in the spring, it fails brittly, transferring its load to the main structure, and no longer contributes to the structural stiffness or strength. Ductile behavioral modes for the canopy which might have resulted had these columns been properly confined (see Appendix C) have not been considered in the analyses.

(b) Shear Failure of First Floor Tied Columns.

These L-shaped tied columns suffered very severe damage during the earthquake (Fig. 3.31) and had relatively low shear strengths. In this case, their shear capacity was estimated to be 127 kips. Once this value was reached in one of these columns, its mechanical properties were significantly reduced (to a value based on the summation

of the individual reinforcing bar properties) and its internal forces were distributed to the rest of the structure.

(c) Spalling in Spiral Column.

Although spiral columns could sustain large inelastic deformations, it was shown in Appendix B.2.1 that the stiffness and strength of a spiral column can decrease significantly due to spalling. To account for this, two interaction curves were specified for each column; one corresponding to the initial cross-sectional shape and the other to the confined section characteristics at a maximum concrete compressive strain of about 0.01. This procedure is illustrated in Fig. B.8. Spalling was assumed to occur at a curvature ductility of two in all members. This approximation was based on an inspection of moment-curvature relationships of the critical sections for the range of axial loads anticipated. Once the curvature ductility at either end of a member reached a value of two (indicating spalling), the stiffness parameters and interaction curves for the member were replaced by ones corresponding to the confined section. Thus, the stiffness of the structure is reduced and some of the internal forces acting in the columns are transferred to the rest of the structure when spalling occurs.

(d) Hammering against Warehouse and Retaining Wall.

The seismic joint was idealized by a nonlinear elastic spring with an arbitrarily high stiffness that would not contact the first floor until the floor displaced 4 in. to the north. As previously mentioned, the seismic joint was only 2 in. wide in some locations. However, next to the warehouse the gap was closer to 4 in.

(e) Ground Motion

As discussed in Appendix D, a number of ground motion records were used. However, in most cases the first floor displacements were not sufficient to make contact with the retaining wall. In the following discussions the response of the structure to the S-16°-E component of the filtered Pacoima Dam base rock motion shown in Fig. 4.12 was

used. This record retains the intense, long-duration acceleration pulses found in the original record with a peak acceleration of 0.66 g.

6.6.2 Lateral Floor Displacements and Story Drifts

The displacement time histories and the time when significant events occur during the response are shown in Fig. 6.24. The maximum northward and southward displacements are both large in this case.

As shown in Fig. 6.24, the tied columns on the first story failed very early in the response. The terrace canopy fails soon thereafter, prior to the imposition of large, long-duration acceleration pulses. While some slab yielding in the first floor occurred during the northward displacement excursion at 1.70 seconds, spiral column yielding did not occur until the arrival of the first major acceleration pulse which resulted in a southward deflection of the building. During this first pulse, yielding rapidly propagated throughout the lower two stories so that the analysis indicates that within 0.12 seconds of the first yielding in a column, a complete soft story (panel) collapse mechanism formed. Spalling was predicted in all of the columns within 0.1 seconds after the formation of the collapse mechanism. During the second major acceleration pulse the building displaced towards the north and the first floor impacted against the warehouse spring. While this spring precluded further significant northward deflection of the first story, the upper stories continued to move toward the north, significantly increasing the drifts in the first story. Subsequent acceleration pulses moved the structure toward its original base line and the first floor moved away from the warehouse spring.

The maximum floor displacement envelopes for the failure model are shown in Fig. 6.25. In this case the displacements to the north are generally greater than those developed toward the south. At the first floor, northward displacements are limited to about the width of the seismic joint so that the first floor deflects further to the south than the north. The displacement pattern to the north is close to that observed in the actual building. The actual permanent drifts in the first story were substantially larger than those developed in the ground story as shown in Figs. 3.2, 3.3 and 6.26. The impact of

the first story in the failure model against the warehouse retaining wall spring limited the ground story drifts resulting in relatively larger maximum drifts in the first story. While the maximum computed northward drifts are similar to the permanent drifts observed in the first story, they were smaller in the ground story. This was a consequence of the elastic behavior of the warehouse spring; the actual warehouse was substantially damaged and displaced permanently, significantly to the north [Figs. 3.3 and 3.7(b)].

6.6.3 Comparison of Observed and Computed Damages

While the maximum computed northward displacements are similar to the observed permanent displacements in the structure, there are significant discrepancies between the observed and computed behavior. The first of these is that the computed response indicates a large displacement excursion to the south with roof displacements exceeding 14 in. The damage to the building does not indicate that the building suffered such large displacements to the south. Secondly, the computed maximum displacements are not permanent; the building continues to oscillate about its original position.

It should also be noted that the failure model implemented here is much simpler than that expected of real structures. It would be expected that the response would be sensitive to this modeling. Furthermore, a number of failures observed in the structure were disregarded in this analysis. In particular, the shear failure of the first floor slabs and the shear failure in the first floor beam-column joints along column line G (as well as in column M-29) may have significantly affected the response. Furthermore, the nonlinear behavior of the rest of the building (not modeled here) could considerably affect the nonlinear behavior of Wing D, especially the response to possible torsional effects.

6.7 SUMMARY AND CONCLUDING REMARKS

A nonlinear dynamic analysis computer porgram was used to compute the response of a simplified planar idealization of Wing D of the Olive View Hospital main building. The basic assumptions used for the structural idealizations in the computer program and appropriate

definitions of cyclic curvature ductility factors were reviewed. The nonlinear mechanical characteristics of the individual members are discussed. While the structural model is much simpler than the actual structure, it is believed that it incorporates most of the parameters controlling the response of the Wing D structure.

The presence of numerous, relatively stiff and strong structural walls in the upper four stories resulted in a concentration of story drifts and inelastic deformations in the bottom two stories. A panel collapse mechanism formed in these two soft stories for all ground motions hypothesized for the site. While the response of the structure was found to be somewhat sensitive to the modeling parameters, the most significant parameter affecting the response was the ground excitation. Once a collapse mechanism formed, the subsequent response was markedly affected by the time history of the accelerogram.

In particular, it was found that simulated records representative of strong ground motion accelerograms obtained on firm soil sites at moderate epicentral distances would not produce displacements as large as the permanent structural drifts observed. They also resulted in numerous cycles of reversed inelastic deformation of moderate intensity which is not consistent with the observed damage.

Records derived from accelerograph or seismoscope recordings during the San Fernando earthquake obtained at sites close to the fault rupture contained large amplitude, long-duration acceleration pulses. Such pulses were found to have a significant effect on the nonlinear structural response of the building, though not on its elastic response. Computed nonlinear displacements consistent with measured drifts were obtained by considering such ground motions. The computed response histories were characterized by a few large inelastic excursions as was the case for the observed damage.

The inelastic analyses were unable to provide reliable estimates of the permanent drifts and damage observed in the building. The structural model considered incorporated only a small part of the entire structure and numerous simplifying assumptions were made.

Furthermore, the effects of biaxial ground motions and torsional response were disregarded. However, the largest source of error remains the uncertainty regarding the ground motions experienced at the site.

The nonlinear analyses indicated large curvature ductility requirements throughout the bottom two stories, particularly in the first floor slabs. For all of the ground motions considered, numerous cycles of inelastic deformation, including reversal, would be required at the critical regions in these stories. While spiral columns had large ductility capacities, the tied first story columns and first floor slabs had low shear strengths and would have failed. The analytical results generally confirm the observed distribution of damages.

An analytical model was implemented which considered failure or spalling in members and hammering of the first floor against the warehouse. This analysis confirmed the sequence of damage predicted from the elastic analyses. It is believed that the first floor tied columns and the tied columns supporting the terrace canopy failed very early in the response and at low displacement amplitudes. Yielding in the slabs and spiral columns of the bottom two stories followed thereafter. After the formation of a collapse mechanism, the response was controlled primarily by the form of the ground motion and the impact of the building against the warehouse and retaining wall. Because of the sensitivity of inelastic response to the detailed dynamic characteristics of a ground motion, it was not possible, even with the analytical model that incorporated changes in stiffness and strength (or failure) of members and hammering of the building against the warehouse, to predict a history of deformation that was entirely consistent with the observed damages and permanent story drifts. However, results of inelastic analyses did identify the severity and overall pattern of the observed damage.

These results also indicated that the ground motion experienced by the building must have been very severe; i.e., its effective peak acceleration was very large. More importantly, the results indicate that the type of damage observed in the building could only be justified by considering ground motions containing intense, long-duration acceleration pulses of the kind found in records obtained or derived

for sites near the fault rupture (see Figs. 4.10-4.12). In this regard, it is interesting to note that the peak ground velocities (or peak incremental ground velocities) produced by these severe, long-duration acceleration pulses (Figs. 4.10-4.12) are close to 40 to 60 in./sec. which has been suggested [5.4, 6.6] as the probable maximum particle velocity that can be developed.

The basic characteristics of the response of the building could also be ascertained from the results of the elastic analyses. However, such analyses cannot adequately predict quantitative information regarding the seismic response of yielding structures (including displacements, shears, inelastic deformations, etc.) that may be subjected to ground motions containing severe, relatively long-duration acceleration pulses like those found in the near-fault San Fernando earthquake records.

The inelastic dynamic analysis methods substantially simplified the mechanical behavior of the structure. Mechanical models are needed (1) to account for the effect of spalling, stiffness and/or strength deterioration that may occur with deformation reversal, and nonlinear shearing deformations in beam-column type members; and (2) to idealize realistically the behavior of structural walls and floor systems. In particular, computational methods are needed to account for the torsional effects that can be induced by unsymmetric distributions of stiffness and mass, or by nonuniform distributions of plastic hinging, throughout a structure.

The nonlinear results obtained indicate that the building had substantial strength (larger than required) even in the context of current seismic requirements. Furthermore, these results clearly point out the necessity for imposing more restrictive (i.e. lower) drift limits for essential facilities such as hospitals.

VII. SUMMARY AND CONCLUSIONS

7.1 SUMMARY

The six story, cast-in-place, reinforced concrete main building of the Olive View Hospital Medical Treatment and Care Facility sustained such extensive damage during the 1971 San Fernando earthquake that it had to be demolished. Since this modern building was completed just four months prior to the earthquake, the observed structural damage was compared with that predicted in a quantitative analytical investigation of the building's dynamic behavior in order to assess current seismic-resistant design, analysis, and construction practices. From results of linear-elastic and inelastic dynamic analyses of various mathematical models it was possible to identify the factors controlling the seismic behavior of the building.

A complex structural system was used for the building. It consisted of four wings located around a central courtyard. Numerous structural walls were located in the top four stories, but these did not continue down through the bottom two stories to the foundation. This resulted in a concentration of lateral drifts and inelastic deformations in the slabs and columns of the bottom two stories. The building appeared to be designed in accordance with the governing design codes; however, it would not meet current detailing requirements for ductile moment-resisting reinforced concrete space frames.

A thorough field inspection of damages to the building was reported. The main features of structural damage appeared to be a consequence of the severity of ground shaking, not due to soil or foundation failure, faulty materials or poor workmanship.

Because no ground motion records were obtained near the building site, several accelerograms were numerically simulated or derived from recordings obtained at other sites in order to perform the seismic analyses. Ground motions obtained near the fault rupture were found to contain high amplitude, long-duration acceleration pulses which could account for the type of building damage observed.

A complete three-dimensional model of the building was analyzed for biaxial horizontal ground accelerations in order to assess the structure's overall dynamic characteristics and to identify initial member failures. This analysis, in conjunction with member capacity studies, identified the brittle type of failure observed in the tied columns of the first and ground stories. It also indicated that the horizontal, translational degrees-of-freedom of the building were essentially uncoupled and that torsion probably had an insignificant effect on the overall linear-elastic response. Thus, it was believed that a two-dimensional nonlinear model of part of the building could be used to obtain "guidelines" regarding the actual inelastic response of the whole building.

Analytical results for the two types of nonlinear models which were considered are discussed in detail. The first of these types was denoted the standard nonlinear model, and the second, the failure model. The standard model disregarded the possibility of member failures, but the failure model accounted for failure of brittle members, spalling of the concrete covers from the ductile, spirally reinforced concrete columns, and hammering of the first floor slab against the adjacent warehouse structure.

7.2 CONCLUSIONS

Some concluding remarks regarding each of the phases of this investigation have already been presented at the ends of the relevant chapters. Some of the more important of these conclusions are summarized below along with some additional overall comments.

7.2.1 Adequacy of Structural System

The building was designed for lateral forces substantially higher than those required by then-existing and current code requirements. In spite of this, the building suffered severe damages during the earthquake, a consequence of the inadequate structural system and details, and the severity of the ground motion experienced at the site. Discontinuation of the shear walls in the bottom two stories resulted in a "soft" story type of response which concentrated the inelastic deformations at relatively few locations. The inadequate shear reinforcement

provided in the tied columns resulted in their premature, brittle failure. The large mass concentrated on the roof of the ground story terrace resulted in high axial loads in the tied columns and large inertial forces at this level.

A study of the elastic response of alternative structural systems relying on shear walls or moment-resisting frames for their lateral resistance was performed. This indicated that, from the point of view of controlling damage by limiting interstory drifts, better seismic performance would have resulted had the structural walls been continued down through the bottom two stories to the base.

7.2.2 Failure Mechanism

From results of the elastic and inelastic analyses of the building, it is believed that the first story tied columns, the tied columns supporting the massive terrace canopy and courtyard, and some of the tied channel-shaped columns in the upper three stories would have failed in shear very early in the seismic response, before yielding occurred in the slabs and spiral columns supporting the high-rise portion of the building. These tied column members were not detailed to withstand the shears corresponding to their ultimate flexural strength. Yielding in the first floor beams and slabs, and the ground and first story spiral columns resulted in a panel type of collapse mechanism. The ground motion must have been such that large inelastic displacements occurred once this mechanism formed. The first floor slab hammered against the retaining wall and warehouse, causing significant local damage where the impact occurred, and inducing a considerable increase in the drifts in the first story.

7.2.3 Mechanical Characteristics of Materials

The materials used in the building were of good quality. In most cases, the strength of the materials, as obtained from field or mill tests performed prior to the earthquake, and those from laboratory tests performed after the earthquake, equalled or exceeded the values specified by the designers. There was a wide variation in the properties obtained for the materials, especially the concrete. This points out the need

for careful quality control of materials during construction. Because overstrength of materials can result in considerably greater member strengths than expected on the basis of the specified minimum material strengths, it is necessary to use realistic, rather than specified minimum, material properties in design, or to specify maximum as well as minimum material strengths.

7.2.4 Adequacy of Failure Predictions based on Elastic Methods

The elastic analyses permitted evaluation of the three-dimensional response characteristics of the structure, as well as modeling of many of the structural irregularities that could not be considered with available nonlinear computer programs. These elastic analyses could also be interpreted to detect brittle failures of the tied columns (when the results were compared with the estimated shear capacities) and the concentration of deformations in the bottom two stories. However, identification of many details of the response, such as the severity and distribution of inelastic deformations, and the significant increase in lateral displacements when an inelastic panel mechanism formed, was not possible from the results of the various elastic analyses performed in this investigation.

7.2.5 Inelastic Structural Response

The inelastic analysis procedures necessitated elaborate computations to determine the yield strength of the various members before the dynamic analyses could be performed. There was considerable uncertainty regarding the strengths of some members, e.g., walls and slabs.

The maximum story shears obtained for the standard nonlinear model subjected to the different ground motions considered were similar in value and about equal to the lateral shear capacity of the structure in the bottom two stories. They were about four times larger than the working stress level shears used in the design of the building. The results indicate that the multi-story portion of the building was detailed to be strong enough to meet the strength requirements of most current codes. The inelastic story shear capacities were significantly smaller than the story shear forces predicted using elastic methods.

The smaller stiffness and strength of the bottom two stories resulted in a sidesway (panel) type of collapse mechanism in which displacements and inelastic deformations were concentrated in these stories. Substantial ductilities were required in the slabs and columns of the bottom two stories. While the tied columns had low shear capacities and failed, the spiral columns had very large curvature ductility capacities and probably would not have failed under the computed response. The slabs had to undergo many more inelastic cycles to larger ductilities than any other type of member in the building. Consequently, these elements were expected to fail as they eventually did.

Although changes in the structural modeling parameters only moderately affected the response, ground motion characteristics were found to have had a very significant influence.

7.2.6 Effect of Ground Motion Characteristics

For the simulated ground motion, the pattern of lateral deformation obtained in the nonlinear analyses clearly revealed the weakness of the bottom two stories. However, the displacement amplitudes were not nearly as large as those observed in the actual building, even when the peak acceleration was increased to 1.0 g. These results still indicated unacceptably large story drifts for facilities such as this building. For hospitals and other essential facilities, damage control should govern design.

Once a collapse mechanism forms, the subsequent response is apparently very sensitive to the ground motion time history (in particular, the duration and characteristics of individual pulses). Thus, the response to the derived Pacoima Dam base rock motion, which contained intense, long-duration acceleration pulses, was much more severe. Careful consideration should be given to the design of structures located close to potential earthquake faults, since severe, long-duration acceleration pulses may be associated with the faulting process.

7.2.7 Reliability of Dynamic Analysis Procedures

Elastic analysis procedures are currently available for efficiently determining the response of complex, three-dimensional buildings.

Information obtained from such analyses offers many useful insights into the dynamic characteristics of structures as well as to their initial dynamic response. However, the results presented in this report indicate that once substantial yielding occurs, elastic analysis can no longer be considered a reliable indicator of internal forces (as evidenced by story shears) and of deformations in general. Considerable judgment and effort are required to interpret results of elastic analyses that indicate that substantial yielding might occur.

Proper interpretation of results of nonlinear analyses can give indications of the actual nonlinear seismic response that are not otherwise obtainable. However, it should be recognized that it may be necessary to idealize complex structural systems in order to perform nonlinear analyses, thereby sacrificing accuracy for practicability. Moreover, most nonlinear mechanical models for members are simpler than the actual physical behavior they represent, especially in the case of reinforced concrete. Consequently, results of nonlinear analyses should be used only as general design guidelines rather than as definitive predictions.

It is generally difficult to estimate member mechanical characteristics with great confidence or to determine the energy dissipation capacity of critical regions with certainty. Further refinements in analytical techniques for predicting the hysteretic behavior of members, as well as for experimental corroboration, are needed, particularly for slabs, walls and column members.

7.2.8 Adequacy of Mathematical Structural Idealizations

Structural idealizations must be as realistic as possible. Mathematical models should reflect the actual behavioral characteristics of the structure, as constructed, and not simply those desired or assumed by the designer. This is particularly important for idealizations of boundary or support conditions. To account for uncertainties that exist in modeling, bounds should be considered for the range over which the controlling parameters can vary. For example, in this investigation, nonlinear analyses were performed to identify the effect on the seismic response of modifying the column support conditions,

member stiffnesses and strengths (as affected by spalling and member failure), the effect of hammering against adjacent structures, rate of strain hardening, and so on.

Models should also account for nonstructural elements if their mechanical behavior is such that it can actually influence the behavior of individual members or the structure as a whole. Appropriate techniques accounting for the effect on nonstructural elements should be devised and verified.

Analytical and experimental investigations are needed to assess the best method of modeling the nonlinear behavior of slab floor systems and structural walls. Current models are generally much simpler than actual behavior.

Nonlinear analytical techniques should be developed to account for the effect of torsion on dynamic structural response. Not only can torsional vibrations be induced by unsymmetric distributions of elastic stiffness and/or mass, but it can also result from the asymmetric occurrence of plastic hinges in a structure during the response. In addition, more refined analytical models are needed to study realistically the nonlinear behavior of columns subjected to axial load, bending moments and shear forces and that can undergo substantial inelastic deformations and large overall displacements.

7.2.9 Member Mechanical Characteristics

An analytical study comparing the flexural and shear capacities of column sections has been presented. This study indicated that the use of material stress-strain relationships based on specified, rather than realistic or ultimate, stresses can result in significant underestimation of the moment capacity of a section and, as a consequence, in the underestimation of member shear forces. Because of this, the amount of transverse reinforcement provided in a member to prevent shear failure may be inadequate.

Differences between ACI and UBC shear strength provisions were examined. The large discrepencies between the shear strengths predicted by these codes as well as by other recommendations clearly indicate the

need for further experimental and analytical research to develop reliable methods for determining the required amounts of transverse shear reinforcement for members subjected to axial load, bending moments and shear forces. This is particularly crucial in view of the need to detail members so that they yield ductilely in flexure rather than fail brittly in shear. Research is needed on both spiral and tied columns.

It is also believed that for the case of reversed inelastic deformation, the contribution of concrete should be disregarded at low axial loads as suggested by the UBC. However, the best method for discounting the contribution of concrete to the shear strength as a function of axial load and for proportioning the transverse reinforcement is not known in this case and requires further investigation.

The analytical results presented also indicate that further experimental research is required to establish the amount of special transverse reinforcement needed to obtain ductile flexural behavior. The analytical results presented for tied columns show that current UBC requirements may be unnecessarily conservative at low axial loads, but a number of factors such as load reversal and buckling of longitudinal reinforcement were not considered.

One of the most convincing lessons to be learned from the behavior of the main building is that excellent ductility can be provided by spirally reinforced columns designed and constructed according to current seismic code requirements. The closely spaced continuous spiral reinforcement in the spiral columns of the building provided enough shear resistance, confinement for the concrete core, and lateral restraint for the longitudinal reinforcement to allow the columns to develop very large inelastic deformations. This excellent behavior is in marked contrast to that exhibited by the tied columns in the building which were designed for nominal minimum tie requirements.

7.2.10 Effect of Detailing and Workmanship

The collapse of several parts of the building was primarily a consequence of inadequate confinement of tied columns. These members were not able to develop their full flexural capacity in a ductile

manner. Detailing should be based on ultimate strength and ductility capacity considerations. Reinforced concrete space frames of this type must currently be detailed in accordance with ductile moment-resisting frame requirements if they are part of the lateral force resisting system or located on the perimeter of a building.

In a number of instances failures occurred in joint regions where beams of different depths framed into the same column. In these cases column transverse reinforcement terminated below the lowest member framing into the column. These failures could have been prevented had transverse reinforcement been continued through the joint region.

In some cases, the column spiral reinforcement was inadvertently terminated a few inches below the top of the column, resulting in substantial shear failures in these regions. This points out the need for careful workmanship and thorough inspection.

Sudden transitions from one type of structural member to another type should be avoided. For example, in frame 29, the corner columns changed from spirally reinforced in the ground story, to tied in the first story and to captive wall boundary elements in the upper four floors. Also, dowels required to develop the anchorage length of column longitudinal reinforcement terminating in adjacent stories must be adequately restrained laterally to avoid early splitting and spalling of the concrete. Since a large portion of the gross area of the spiral columns was not confined, such spalling resulted in a substantial loss of their strength and stiffness.

The seismic joints used to separate the first floor from the retaining wall and warehouse, and the stairtowers from the upper stories of the main building were generally insufficient to prevent contact. In addition, seismic gaps provided between the first floor slab and the masonry walls in the ground story, and between the first story elevator walls and the structural members below the second floor level, were not large enough or detailed to achieve the desired degree of isolation. Considerable damage resulted from the pounding or interaction of adjacent components that were intended to be separated. Careful detailing and realistic assessments of relative deformations are required to achieve effective seismic separations.

Considerable damage occurred as a result of inadequate connection of nonstructural elements to the structural system. For example, many large precast concrete panels and glass panels fell from position during the earthquake. These posed a serious safety hazard to occupants. Nonstructural elements must be adequately attached to the structural system.

7.2.11 Suggestions for Improving Seismic Resistant Design Procedures

1. Special emphasis must be placed on selecting a structural system that will prevent or minimize undesirable structural response characteristics, such as excessive drifts, large displacements and substantial torsional vibrations. The basic principles of seismic design must be followed. To this end, commentaries to building codes should emphasize the desirability of structural systems in which sudden changes in the strength, stiffness and ductility of structural components are precluded. Whenever possible, structures should be symmetric, and all unnecessary masses should be avoided.

2. Building codes should require "rational" dynamic analyses of unusual and/or important structures, so that deficiencies in their structural systems can be identified during the design process by properly interpreting the analytical results. Design forces recommended by the UBC may be too low for sites close to active faults if damage control is a design consideration. The values of the UBC coefficients, K and C, should be re-evaluated in terms of the expected ground motion intensity, the site conditions and the acceptable level of structural and nonstructural damage.

3. In cases where simple analytical methods are used, uncertainties regarding the expected seismic behavior of a structure should be compensated for by providing the structure with a large ductility capacity. In particular, the use of spirally reinforced columns appears to be an effective method for achieving ductility in columns.

4. Where damage due to large drifts and/or inelastic deformations are to be limited, it it necessary to select and construct structural systems that are generally stiffer and stronger than required by present codes. Buildings with "soft" stories or flexible structural systems

located near active faults should have secondary structural systems to prevent excessive lateral displacements. To reduce drifts in moment-resisting space frames, stiff floor systems with integral beams should be used instead of flat slabs.

5. Members in moment-resisting space frames must be detailed to remain ductile at their ultimate flexural capacities. Specifically, sufficient transverse reinforcement must be provided to avoid a shear failure before considerable flexural yielding occurs. The design of shear reinforcement should be based on flexural capacity estimates obtained using realistic material properties rather than code specified minimum values. Special care must be paid to the design and detailing of tied columns.

6. To protect a building's occupants, nonstructural elements must be securely attached to the structural system. This requires the use of realistic design forces and ductile connections.

REFERENCES

CHAPTER I

1.1 U. S. Department of Commerce, San Fernando, California, Earthquake of February 9, 1971, Murphy, L. M., Scientific Coordinator, NOAA, Washington, D. C., 1973.

1.2 Bertero, V. V. and Collins, R. G., "Investigations of the Failures of the Olive View Stairtowers during the San Fernando Earthquake and their Implications on Seismic Design," Earthquake Engineering Research Center Report No. EERC 73-26, University of California, Berkeley, 1973.

1.3 Chopra, A. K., Bertero, V. V., and Mahin, S. A., "Response of the Olive View Medical Center Main Building during the San Fernando Earthquake," Proceedings, Fifth World Conference on Earthquake Engineering, Paper No. 4, Rome, 1973.

1.4 Selna, L. G., Cho, M. D., and Ramanathan, R. K., "Evaluation of Olive View Hospital Behavior on Earthquake Resistant Design," Proceedings, Fifth World Conference on Earthquake Engineering, Paper No. 5, Rome, 1973.

1.5 Aoyama, H. and Sozen, M. A., "Dynamic Response of a Reinforced Concrete Structure with 'Tied' and 'Spiral' Columns," Proceedings, Fifth World Conference on Earthquake Engineering, Paper No. 15, Rome, 1973.

1.6 Pecknold, D. A. W. and Sozen, M. A., "Calculated Inelastic Structural Response to Uniaxial and Biaxial Earthquake Motions," Proceedings, Fifth World Conference on Earthquake Engineering, Paper No. 223, Rome, 1973.

1.7 Karlsson, B. I., Aoyama, H. and Sozen, M. A., "Spirally Reinforced Concrete Columns subjected to Loading Reversals Simulating Earthquake Effects," Proceedings, Fifth World Conference on Earthquake Engineering, Paper No. 93, Rome, 1973

1.8 Bertero, V. V., "Investigations of the Failure of the Olive View Medical Center Ambulance Canopy during the San Fernando Earthquake and its Implication on Seismic Design," University of California, Berkeley, in-house report.

1.9 Bertero, V. V. and Edgar, L., "Investigation of the Failure of the Olive View Medical Center Warehouse during the San Fernando Earthquake and its Implication on Seismic Design," University of California, Berkeley, in-house report.

1.10 Tashkandi, M. A. and Selna, L. G., "Failure Analysis of the Olive View Psychiatric Day Clinic," Report No. UCLA-ENG-7268, University of California, Los Angeles, 1972.

1.11 Ogawa, Y. and Selna, L. G., "Behavior of the Olive View Hospital Exhaust Pavilion during the San Fernando Earthquake," Report No. UCLA-ENG-7226, University of California, Los Angeles, 1972.

1.12 Bertero, V. V., et al., "Design Implications of Damage Observed in the Olive View Medical Center Buildings," Proceedings, Fifth World Conference on Earthquake Engineering, Paper No. 6, Rome, 1973.

1.13 Bertero, V. V., "Studies of Olive View Building Damage," Proceedings, U. S. - Japan Seminar on Earthquake Engineering, September 4-9, 1973, Berkeley, California.

CHAPTER II

2.1 International Conference of Building Officials, Los Angeles County Building Laws, 1965 edition, Pasadena, California.

2.2 International Conference of Building Officials, Uniform Building Code, 1964 edition, Pasadena, California.

2.3 ACI Committee 318, Building Code Requirements for Reinforced Concrete (ACI 318-56), ACI, Detroit, Michigan, 1956.

2.4 Seismology Committee, Recommended Lateral Force Requirements and Commentary, Structural Engineers' Association of California, San Francisco, California 1973.

2.5 International Conference of Building Officials, Uniform Building Code, 1973 edition, Whittier, California.

2.6 Seismology Committee, Recommended Lateral Force Requirements, Structural Engineers' Association of California, San Francisco, California, 1966.

2.7 International Conference on Building Officials, Uniform Building Code, 1967 edition, Pasadena, California.

2.8 State of California, "Safety of Construction of Hospitals," California Administrative Code, TITLE 17, Public Health, Register 73, No. 15--4-14-73, revised 3-18-74.

2.9 Bresler, B. and Bertero, V. V., "Olive View Medical Center Materials Studies - Phase I," Earthquake Engineering Research Center Report No. EERC 73-19, University of California, Berkeley, December 1973.

CHAPTER III

3.1 Collins, R. G., Mahin, S. A., and Bertero, V. V., "Olive View Hospital Damage Survey," unpublished field notes.

3.2 Kent, D. C., "Inelastic Behavior of Reinforced Concrete Members with Cyclic Loading," Ph.D. Dissertation, University of Canterbury, Christchurch, New Zealand, 1969.

CHAPTER IV

4.1 Jennings, P. C., ed., "Engineering Features of the San Fernando Earthquake: February 9, 1971," Earthquake Engineering Research Laboratory Report No. EERL 71-02, California Institute of Technology, Pasadena, California, June 1971.

4.2 Lew, H. S., Leyendecker, E. V. and Dikkers, R. D., Engineering Aspects of the 1971 San Fernando Earthquake, National Bureau of Standards, Building Science Series 40, U. S. Department of Commerce, Washington, D. C., December 1971.

4.3 U. S. Government Printing Office, The San Fernando, California Earthquake of February 9, 1971, Geological Survey Professional Paper 733, Washington, D. C., 1971.

4.4 Hudson, D. E., ed., Strong-Motion Instrumental Data on the San Fernando Earthquake of February 9, 1971, Earthquake Engineering Research Laboratory and U. S. Seismological Field Survey, California Institute of Technology, Pasadena, California, September 1971.

4.5 Duke, C. M., et al., "Effects of Site Classification and Distance on Instrumental Indices in the San Fernando Earthquake," Report No. UCLA-ENG-7247, University of California, Los Angeles, June 1972.

4.6 Allen, C. R., et al., "Relationship between Seismicity and Geologic Structure in the Southern California Region," Bulletin of the Seismological Society of America, Vol. 55, 1965.

4.7 Woodward-McNeill and Associates, Report of Site Studies, Olive View Hospital, Los Angeles County, Report No. 71107, Los Angeles, California, December 1971.

4.8 Duke, C. M., et al., "Subsurface Site Conditions and Geology in the San Fernando Earthquake Area," Report No. UCLA-ENG-7206, University of California, Los Angeles, California, December 1971.

4.9 Personal communication, H. B. Seed.

4.10 Schnabel, P., Seed, H. B., and Lysmer, J., "Modification of Seismograph Records for Effects of Local Soil Conditions," Bulletin of the Seismological Society of America, Vol. 62, No. 6, 1972.

4.11 Hall, W. J., Newmark, N. M., and Mohraz, B., "Comments on Earthquake Transmission from Basement Rock to Surface," Proceedings, Fifth World Conference on Earthquake Engineering, Paper No. 83, Rome, 1973.

4.12 Hudson, D. E., "Local Distribution of Strong Earthquake Ground Motions," Bulletin of the Seismological Society of America, Vol. 62, No. 6, 1972.

4.13 Udwadia, F. E., "Investigation of Earthquake and Microtremor Ground Motions," Earthquake Engineering Research Laboratory Report No. 72-02, California Institute of Technology, Pasadena, California, May 1972.

4.14 Jennings, P. C. and Husid, R., "Collapse of Yielding Structures during Earthquakes," Journal of the Engineering Mechanics Division, ASCE, Vol. 94, No. EM5, October 1968.

4.15 Adu, R., "Response and Failure of Structures under Stationary Random Excitations," Earthquake Engineering Research Laboratory Report No. EERL 71-03, California Institute of Technology, Pasadena, California May 1971.

4.16 Ruiz, P. and Penzien, J., "Probabilistic Study of the Behavior of Structures during Earthquakes," Earthquake Engineering Research Center Report No. EERC 69-3, University of California, Berkeley, March 1969.

4.17 Jennings, P. C., Housner, G. W., and Tsai, N. C., "Simulated Earthquake Motions," Earthquake Engineering Research Laboratory Report No. 68-40, California Institute of Technology, Pasadena, California, April 1968.

4.18 Donovan, N., "Earthquake Hazards for Buildings," Building Practices for Disaster Mitigation, National Bureau of Standards, Building Science Series 46, U. S. Department of Commerce, Washington, D. C., 1973.

4.19 Housner, G. W., "Behavior of Structures during Earthquakes," Journal of the Engineering Mechanics Division, ASCE, Vol. 85, No. EM4, October 1959.

4.20 Reimer, R. B., Clough, R. W., and Raphael, J. M., "Evaluation of the Pacoima Dam Accelerogram," Proceedings, Fifth World Conference on Earthquake Engineering, Paper No. 293, Rome, 1973.

4.21 Trifunac, M. D., "A Three-Dimensional Dislocation Model for the San Fernando, California, Earthquake of February 9, 1971," Bulletin of the Seismological Society of America, Vol. 64, No. 1, 1974.

4.22 Ambraseys, N. N., "Dynamics and Response of Foundation Materials in Epicentral Regions of Strong Earthquake," Proceedings, Fifth World Conference on Earthquake Engineering, invited paper, Rome, 1973.

4.23 Newmark, N. M. and Rosenblueth, E., Fundamentals of Earthquake Engineering, Prentice-Hall, Inc., Englewood Cliffs, New Jersey, 1971.

4.24 Trifunac, M. D., "Analysis of Strong Earthquake Ground Motion for Prediction of Response Spectra," Earthquake Engineering and Structural Dynamics, Vol. 2, March 1973.

4.25 Tsai, Y. B. and Patton, H. J., "Near-Field Small Earthquakes - Dislocation Motion," Texas Instruments, Inc., November 1972.

4.26 Scott, R. F., "The Calculation of Horizontal Accelerations from Seismoscope Records," Bulletin of the Seismological Society of America, Vol. 63, No. 5, October 1973.

CHAPTER V

5.1 Wilson, E. L., and Dovey, H. H., "Static and Earthquake Analysis of Three-Dimensional Frame and Shear Wall Buildings," Earthquake Engineering Research Center Report No. EERC 72-1, University of California, Berkeley, May 1972.

5.2 Keith, E. J., "Effect of Shear Walls on High Rise Buildings subjected to Seismic Loadings," SEAONC Seminar on Design of Earthquake Resistant High Rise Buildings, San Francisco, California, November 1967.

5.3 Khan, F. R. and Sbarounis, J. A., "Interaction of Shear Walls and Frames," Journal of the Structural Division, ASCE, Vol. 90, No. ST3, June 1964.

5.4 Newmark, N. M. and Hall, W. J., "Proceedings and Criteria for Earthquake Resistant Design," Building Practices for Disaster Mitigation, National Bureau of Standards, Building Science Series 45, U. S. Department of Commerce, Washington, D. C., February 1973.

5.5 Wilson, E. L., "SAP, A General Structural Analysis Program," Structural Engineering Laboratory Report No. 70-20, University of California, Berkeley, September 1970.

CHAPTER VI

6.1 Bertero, V. V. and Kamil, H., "Nonlinear Seismic Design of Multistory Frames," Canadian Journal of Civil Engineering, Vol. 2, Ottawa, December 1975.

6.2 Mahin, S. A. and Bertero, V. V., "An Evaluation of Some Methods for Predicting Seismic Behavior of Reinforced Concrete Buildings," Earthquake Engineering Research Center Report No. EERC 75-5, University of California, Berkeley, February 1975.

6.3 Clough, R. W., Benuska, K. L., and Wilson, E. L., "Inelastic Earthquake Response of Tall Buildings," Proceedings, Third World Conference on Earthquake Engineering, Wellington, New Zealand, 1965.

6.4 Aoyama, H., "Moment-Curvature Characteristics of Reinforced Concrete Members subjected to Axial Load and Reversal of Bending," Proceedings, International Symposium of Flexural Mechanics of Reinforced Concrete, Miami, Florida, November 10-12, 1964, ACI-ASCE SP-12, Detroi, 1965.

6.5 Seismology Committee, Recommended Lateral Force Requirements and Commentary, Structural Engineers' Association of California, San Francisco, 1974.

6.6 Brune, J. N., "Tectonic Stress and the Spectra of Seismic Shear Waves from Earthquakes," Journal of Geophysics Research, Vol. 75, 1970.

TABLE 2.1

FLOOR WEIGHTS AND SEISMIC FORCES

USED IN THE DESIGN OF THE UPPER FOUR STORIES

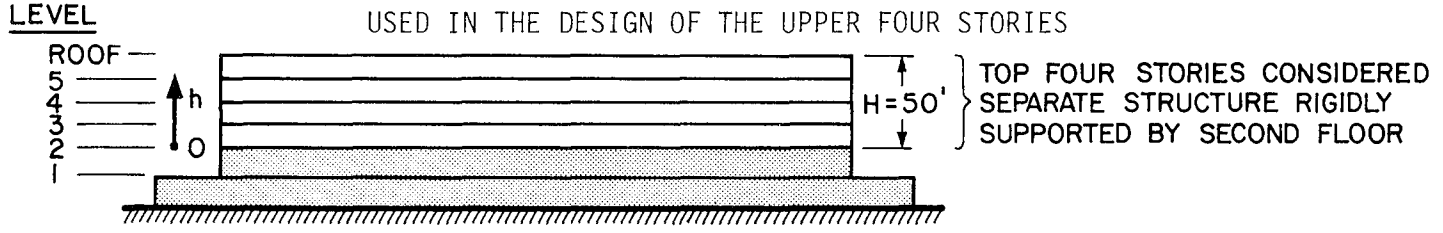

NOTE: V_{BASE} = ZCKW = 1.0 (0.097)(0.80) 67356 = 5210 KIPS

Floor Level i	Floor Weight[a] w_i (kips)	Height h_i (feet)	$w_i h_i$ (kip-ft)	Force $F_i = V\left(\frac{w_i h_i}{\Sigma wh}\right)$ (kips)	Story Shear (kips)	$F_i h_i$ (kip-ft)	$\frac{H-h}{H}$	Over-turning Moment $M_j = \frac{H-h}{H}\Sigma F_x h_x$ (kip-ft)	Accidental Eccentricity[b] (feet)	Horizontal Torsional Moment[b] (kip-ft)
roof	21436	50.0	1075000	2530	2530	126500	0	0	16.5	41700
5	14964	37.5	561000	1320	3850	49500	.25	51000	16.5	63500
4	15356	25.0	384000	900	4750	22500	.50	102100	16.5	78400
3	15600	12.5	195000	460	5210	5700	.75	153100	16.5	86000
totals	67356		2215000	5210		204200		204200		

note: (a) Weight of penthouse lumped at roof level.
(b) Minimum of 5% of maximum building dimension at level times story shear controls.

TABLE 2.2

FLOOR WEIGHTS AND SEISMIC FORCES

USED IN THE DESIGN OF THE BOTTOM TWO STORIES

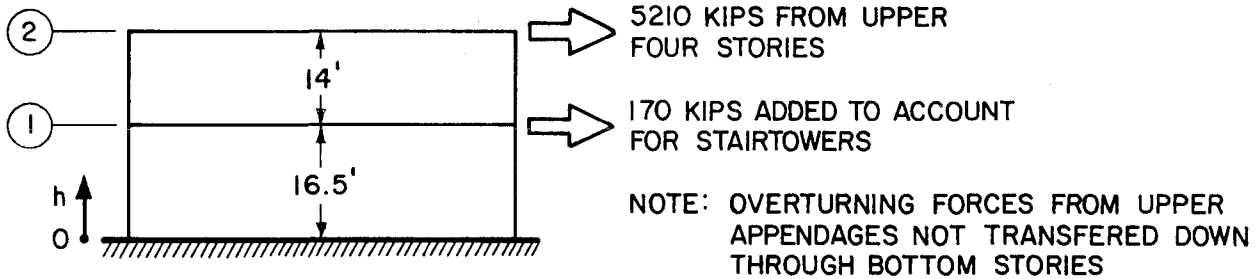

V_{BASE} = ZCKW = 1.0 (0.1185) (0.67) 61989 = 4960 KIPS + CONCENTRATED LOADS

Floor i	Floor Weight w_i (kips)	Height h_i (feet)	$w_i h_i$ (kip-ft)	Force[a] $F_i = V\left(\frac{w_i h_i}{\Sigma wh}\right)$ (kips)	Story Shear (kips)	$F_i h_i$[a] (kip-ft)	$\frac{H-h}{H}$	Over-turning Moment $M_i = \frac{H-h}{H}\Sigma F_x h_x$ (kip-ft)	Accidental Eccentricity[b] (feet)	Horizontal Torsional Moment[b] (kip-ft)
2	15292	30.5	466000	1865 (+5210)	7075	57000 (159000)	0	0	16.5	117000
1	46697	16.5	772000	3095 (+170)	10340	51000 (2800)	.46	119000	21.7	224000
	61989		1238000	4960 (5380)		108000 (162000)		270000		

note: (a) Values in parentheses correspond to concentrated loads from upper stories and stair towers.
(b) Minimum of 5% of maximum building dimension at level times story shear controls.

TABLE 2.3 SUMMARY OF CONCRETE FIELD CONTROL TEST RESULTS FROM [2.9]

Location (building)	M T F[2]		PDC[3]
Design Strength, psi	3,000	5,000	3,000
Number of Tests	107	35	17
Time period, Mo/Yr	9/66 to 1/69	11/66 to 3/69	11/66 to 7/67
Type of Concrete (aggregate)	normal weight	normal weight	light weight
Average Strength Value, psi	4,070	5,530	4,000
Standard Deviation (σ) psi	415	580	372
Coefficient of Variation, (V)	0.102	0.105	0.093
Excess strength ratio t[1]	2.45	0.93	2.68
Estimated % below Specified Strength	0.75	17.5	0.75

(1) t = (Average value - Design value)/σ

(2) MTF = Main Treatment and Care Facility

(3) PDC = Psychiatric Day Clinic

TABLE 2.4 SUMMARY OF STATISTICAL EVALUATION OF MILL TEST DATA FROM [2.9]

Grade of Steel	Average Value $\bar{x}$	Standard Deviation σ	ASTM Specified Minimum x_{min}	Excess Ratio (1) t	% Below Specified Minimum (estimated)
A-15 Grade					
Yield Strength ksi	52.6	3.22	40	4.33	< 0.5
Tensile Strength ksi	79.5	4.15	60	2.35	0.75
% elongation	19.37	3.27	16	1.23	10.0
A-432 Grade					
Yield Strength ksi	71.1	6.7	60	1.66	4
Tensile Strength ksi	112.5	8.8	90	2.56	0.5
% elongation	12.4	2.8	7	1.93	2.4

(1) $t = (\bar{x} - x_{min})/\sigma$

TABLE 2.5 - LABORATORY TEST RESULTS, A-15 INTERMEDIATE GRADE STEEL, MONOTONIC LOADING, FROM [2.9]

Building	Specimen Number	Bar Size No.	f_y ksi	f_{tu} ksi	E_s 10^3 ksi	Elong. %	ε_{sh} in./in.	E_{sh} 10^3 ksi
STA(1)	TA 5	3	51.5	78.2	30.9	22	0.021	0.545
STA	TA 6	3	52.1	78.2	28.6	21	0.0206	0.513
AC(2)	AC 1-5	3	52.2	76.2	28.5	25	0.0198	0.532
AC	AC 3-2	5	50.6	75.5	29.2	*	0.0175	0.645
AC	AC 3-3	5	51.7	76.7	29.4	28	0.0212	0.693
PDC(3)	5-1	7	50.0	76.8	28.6	23	-	-
MTF(4)	13	7	47.5	74.0	28.6	*	-	-
MTF	52-2	7	48.0	76.0	28.6	*	-	-
MTF	50	8	42.7	74.5	29.3	*	-	-
MTF	51-2	8	51.6	83.7	29.9	22	-	-
MTF	51-1	8	57.3	84.2	28.6	20	-	-
AC	2-3(5)	9	50.0	79.6	28.7	*	0.0165	0.835
Average (12 tests)			50.4	77.8	29.1	23.0(6)	0.0194(7)	0.628(7)
Mill Test Average			53.1	79.5		19.4		

* Fracture occurred outside gage length. No representative % elongation could be obtained.

(1) STA = Stairtower A

(2) AC = Ambulance Canopy

(3) PDC = Psychiatric Day Clinic

(4) MTF = Main Treatment and Care Facility

(5) Specimen was designated as A-432 steel. However, laboratory tests indicated that it was actually an A-15 intermediate grade steel.

(6) Average of 7 tests only.

(7) Average of 6 specimens.

TABLE 2.6 - LABORATORY TEST RESULTS, A-432 GRADE STEEL, MONOTONIC LOADING, FROM [2.9]

Building	Specimen Number	Bar Size No.	f_y ksi	f_{tu} ksi	E_s 10^3 ksi	Elong. %	ε_{sh} in./in.	E_{sh} 10^3 ksi
AC(1)	AC 1-1	9	67.3	110	28.1	15	0.00675	1.317
AC	AC 1-2	9	67.4	110	28.1	14	0.00690	1.35
AC	AC 2-2	9	67.5	110	27.9	(*)	0.00675	1.335
STA(2)	TA 1	9	61.4	101.5	28.4	(*)	0.00450	1.06
STA	TA 2	9	67.0	111.1	27.9	14	0.00450	1.30
STB(3)	TB 1	10	67.0	114	29.2	13	0.00503	1.065
STB	TB 3	10	68.8	114	29.1	14	0.00435	1.108
PDC(4)	4	10	66.0	109.1	29.4	(*)	-	-
STD(5)	TD 1	11	63.8	112	25.9	12	0.00300	0.744
STD	TD 2	11	63.8	110	28.9	13	0.00450	0.710
PDC	1	11	63.5	108	29.6	14.9	-	-
MTF(6)	10	11	71.8	114.1	28.1	(*)	-	-
PDC	3	14	61.3	112.6	28.9	16.5	-	-
MTF	3-1	18	71.3	(+)	29.4	(+)	-	-
MTF	1-1	18	70.0	98	29.9	20	-	-
MTF	4-2	18	62.5	(+)	28.8	(+)	-	-
MTF	61	18	63.0(+)	113	29.0(x)	-	-	-
MTF	62	18	60.0(+)	105	29.0(x)	-	-	-
MTF	63	18	64.0(+)	117	33.0(x)			
Average (19 tests)			65.6	109.9(7)	28.54	14.64(8)	0.00516(9)	1.109(9)
Mill Test Average			71.7	112.5		12.4		

(*) Fracture occurred outside gage length. No representative % elongation could be obtained.

(+) Bar did not fracture; capacity of machine exceeded.

(x) Initial loading values from cyclic loadings tests.

(1) AC = Ambulance Canopy

(2) STA = Stairtower A

(3) STB = Stairtower B

(4) PDC = Psychiatric Day Clinic

(5) STD = Stairtower D

(6) MTF = Main Treatment and Care Facility

(7) Average of 17 tests only.

(8) Average of 10 tests only.

(9) Average of 9 tests only.

TABLE 5.1

WEIGHTS, MASSES, AND MASS MOMENTS OF INERTIA
LUMPED AT EACH FLOOR LEVEL OF THE THREE-DIMENSIONAL MODEL

Floor	Weight (kips)	Mass ($K\text{-}sec^2/ft$)	Mass Moment of Inertia* ($K\text{-}sec^2\text{-}ft$)
penthouse	5,090	158.1	1,997,700
roof	16,906	525.0	8,949,100
5	15,228	472.9	8,544,300
4	15,356	476.9	8,601,200
3	15,590	484.2	8,726,900
2	15,240	473.3	8,216,600
1	52,836	1640.7	56,578,600

*Calculated about the center of mass of each floor level. The following diagram locates the centers of mass in relation to column lines 17 and S (refer to Fig. 2.1).

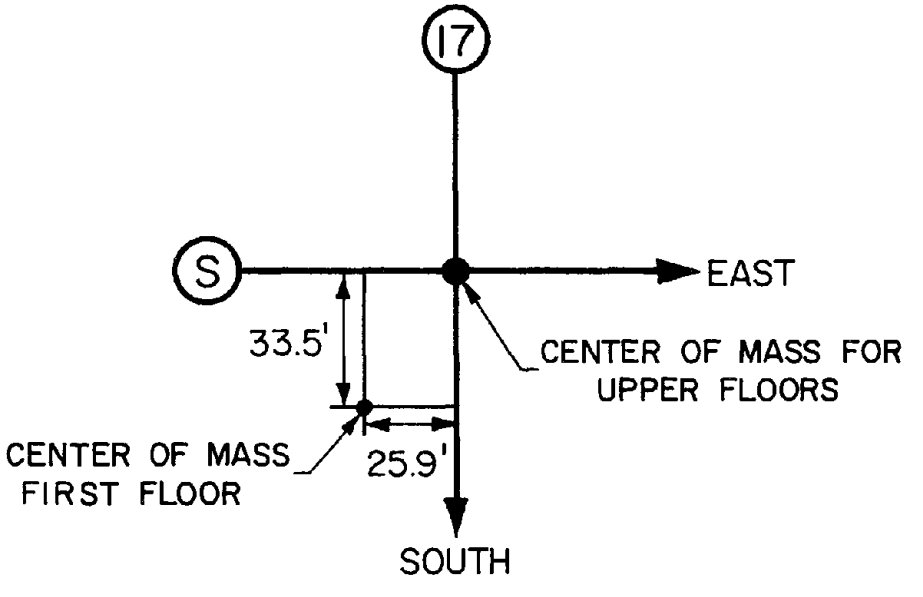

TABLE 5.2

THREE DIMENSIONAL MODEL

Mode Number	Period (sec)
1	.60660
2	.58934
3	.50251
4	.21090
5	.18841
6	.18178
7	.11420
8	.10996
9	.10151
10	.04970
11	.04753
12	.04390

TABLE 5.3

MODAL PARTICIPATION FACTORS

FOR EACH DEGREE OF FREEDOM

Mode Number	Principal Degree-of-Freedom*	North-South Part. Factor (x)	East-West Part. Factor (y)	Rotational Part. Factor (rot.)
1	y	4.0	60.3	570.
2	x	-59.2	5.0	-1890.
3	rot.	13.5	4.1	-8940.
4	rot.	5.7	12.5	-3050.
5	x,y	14.4	-16.1	-1210.
6	x, rot.	-15.0	- 7.9	-2530.
7	y	.3	- 5.9	- 570.
8	x	5.6	.5	540.
9	rot	.1	- .6	- 570.
10	y	.0	.4	60.

* Based on relative values of participation factors in each mode.

TABLE 5.4 THREE-DIMENSIONAL MODE SHAPES OF ELASTIC MODEL OF MAIN BUILDING

Level	Direction*	MODE SHAPES							
		1	2	3	4	5	6	7	8
penthouse	x	.001402	-.020614	.004191	-.003240	-.011821	.014772	.001842	.026913
	y	.021128	.001545	.000551	-.007823	.014204	.010132	-.026144	.001621
	rot	.000008	-.000030	-.000151	.000109	.000033	.000055	-.00023	.000007
roof	x	.001369	-.020105	.004050	-.002764	-.009784	.012098	.001241	.017755
	y	.020611	.001505	.000530	-.006645	.011691	.008249	-.017508	.001062
	rot	.000008	-.000029	-.000148	.000099	.000029	.000049	.000018	.000005
5	x	.001307	-.019141	.003785	-.001899	-.006145	.007344	.000283	.003341
	y	.019624	.001428	.000490	-.004488	.007152	.004862	-.003458	.000166
	rot	.000008	-.000028	-.000140	.000073	.000020	.000033	.000006	.000002
4	x	.001237	-.018060	.003487	-.000974	-.002308	.002357	-.000612	-.000930
	y	.018475	.001338	.000443	-.002122	.002251	.001228	.009668	-.000556
	rot	.000008	-.000027	-.000131	.000046	.000011	.000016	-.000005	-.000002
3	x	.001162	-.016900	.003167	-.000047	.001438	-.002465	-.001315	-.020006
	y	.017204	.001239	.000391	.000294	-.002627	-.002357	.019862	-.001270
	rot	.000007	-.000026	-.000122	.000020	.000001	.000000	-.000014	-.000004
2	x	.001083	-.015682	.002837	.000813	.004775	-.006700	-.001693	-.024954
	y	.015853	.001134	.000336	.002523	-.006945	-.005479	.024983	-.001541
	rot	.000007	-.000024	-.000113	-.000004	-.000007	-.000013	-.000019	-.000006
1	x	.000439	-.007423	.002697	.005262	.013685	-.015062	.000590	.010139
	y	.007461	.000900	.001824	.011516	-.014836	-.009289	-.010361	.000749
	rot	.000004	-.000012	-.000053	-.000094	-.000031	-.000060	-.000009	.000010

* x corresponds to north-south (south is positive)
y corresponds to east-west (east is positive)
rot corresponds to rotation about center of mass (clockwise is positive)

TABLE 5.5

MAXIMUM RESPONSES OF THE THREE-DIMENSIONAL MODEL

AT ITS CENTERS OF MASS DUE TO THE DERIVED PACOIMA DAM BASE ROCK MOTION

Floor Level	Direction	Max. Displacements and Rotations				Max. Story Shears and Torques			
		S-16°-E[b]		S-16°-E and S-74°-W[b]		S-16°-E		S-16°-E and S-74°-W	
		time (sec)	max. value[a] (in or radian)	time (sec)	max. value[a] (in or radian)	time (sec)	max. value (kip or k-ft)	time (sec)	max. value (kip or k-ft)
Penthouse	N-S	3.40	-4.30	3.40	-4.30	3.40	- 5802.	3.40	- 5791.
	E-W	4.25	- .0386	2.80	-3.31	4.25	- 88.	2.80	- 4425.
	Rotation	3.80	.000370	3.80	.000356	3.80	96379.	4.05	- 99640.
Roof	N-S	3.40	-4.20	3.40	-4.20	3.40	- 24919.	3.40	- 24868.
	E-W	4.25	- .0372	2.80	-3.23	4.25	- 358.	2.80	- 18865.
	Rotation	3.80	.000364	3.80	.000350	3.80	519138.	4.05	- 531081.
5	N-S	3.40	-4.01	3.40	-4.01	3.40	- 41728.	3.40	- 41642.
	E-W	4.25	- .0346	2.80	-3.08	4.25	- 561.	2.80	- 31391.
	Rotation	3.80	.000347	3.80	.000334	3.80	899059.	4.05	- 905974.
4	N-S	3.40	-3.80	3.40	-3.80	3.40	- 58189.	3.40	- 58065.
	E-W	4.25	- .0316	2.80	-2.91	4.25	- 721.	2.80	- 43454.
	Rotation	3.80	.000329	3.80	.000316	3.80	1256015.	3.80	1245093.
3	N-S	3.40	-3.58	3.40	-3.57	3.40	- 74376.	3.40	- 74215.
	E-W	4.25	- .0284	2.80	-2.72	4.25	- 837.	2.80	- 55074.
	Rotation	3.80	.000311	3.80	.000298	3.80	1592083.	3.80	1562122.
2	N-S	3.40	-3.34	3.40	-3.33	3.40	- 89716.	3.40	- 89519.
	E-W	3.95	.0252	2.80	-2.51	4.25	- 908.	2.80	- 65312.
	Rotation	3.80	.000293	3.80	.000280	3.80	1884211.	3.80	1830992.
1	N-S	3.40	-1.70	3.40	-1.69	3.40	- 129699.	3.40	- 129179.
	E-W	3.75	- .0508	2.80	-1.26	4.30	- 1835.	2.80	- 89618.
	Rotation	3.80	.000136	3.80	.000127	3.80	2717158.	3.80	2452414.

Note a. A positive value is either to the south or east or clockwise.

b. The values under "S-16-E" are due to the S-16-E component acting alone along the model's N-S axis, the values under "S-16-E and S-74-W" are due to both components acting simultaneously along the model's N-S and E-W axes, respectively.

TABLE 5.6

PERIODS OF WING D MODEL

Mode Number	Period (sec.)
1	.5682
2	.1793
3	.1074
4	.0348

TABLE 5.7

MODE SHAPES - WING D MODEL

Floor Level	MODE SHAPE			
	1	2	3	4
roof	.068800	.060504	.062910	.058162
5	.064481	.034654	.014644	-.053591
4	.060052	.008866	-.030882	-.085756
3	.055848	-.013764	-.064673	-.009362
2	.052008	-.031319	-.081567	.085780
1	.025109	-.065152	.037390	-.002765

TABLE 5.8

MAXIMUM ELASTIC RESPONSES OF THE WING D MODEL

TO S-16°-E COMPONENT OF DERIVED PACOIMA DAM BASE ROCK RECORD

Floor Level	Displacements		Story Shears	
	time (sec)	max. value (inch)	time (sec)	max. value (kips)
roof	3.40	4.42	3.40	2373.
5	3.40	4.16	3.40	4175.
4	3.40	3.90	3.40	5918.
3	3.40	3.64	3.40	7633.
2	3.40	3.41	3.40	9193.
1	3.40	1.71	3.40	13238.

TABLE 5.9

SUMMATIONS OF MAXIMUM SHEAR FORCES IN SHEAR WALLS IN FRAMES 24 AND 29

STORY	SHEAR FORCE		RATIO: $\frac{\text{TOTAL STRUC.}}{\text{WING D}}$
	WING D MODEL (KIPS)	TOTAL STRUCTURE MODEL (KIPS)	
5	1898	610	.32
4	3847	2386	.62
3	5336	5331	1.00
2	8910	12325	1.38

TABLE 5.10

PERIODS OF ALTERNATIVE STRUCTURAL SYSTEMS FOR WING D

Mode	PERIOD (sec)		
	Original Wing D Model	Frame Model	Shear Wall Model
1	0.568	0.744	0.322
2	0.179	0.262	0.0931
3	0.107	0.163	0.0551

TABLE 6.1 COMPARISON OF PERIODS FOR STANDARD NONLINEAR MODEL WITH THOSE FOR ORIGINAL WING D MODEL AND FOR THREE-DIMENSIONAL MODEL (all values in seconds)

MODE	STANDARD NONLINEAR MODEL	ORIGINAL WING D MODEL	THREE-DIMENSIONAL MODEL
1	0.617	0.568	0.589 (a)
2	0.191	0.179	0.182 (b)
3	0.105	0.107	0.110 (c)

note (a) corresponds to mode 2
(b) corresponds to mode 6
(c) corresponds to mode 8

TABLE 6.2 MODE SHAPES FOR STANDARD NONLINEAR MODEL

LEVEL	MODE SHAPES		
	1	2	3
ROOF	.237	.232	.199
5	.222	.134	.029
4	.206	.030	-.132
3	.190	-.063	-.235
2	.174	-.137	-.250
1	.096	-.209	.148

TABLE 6.3 MAXIMUM ELASTIC RESPONSES OF STANDARD NONLINEAR MODEL TO S-16°-E COMPONENT OF DERIVED PACOIMA DAM BASE ROCK RECORD (0.65g)

FLOOR LEVEL	DISPLACEMENTS		STORY SHEARS	
	TIME (sec)	MAX. VALUE (inch)	TIME (sec)	MAX. VALUE (kips)
Roof	2.700	4.375	2.700	2001.
5	2.700	4.122	2.700	3501.
4	2.700	3.848	2.700	4933.
3	2.700	3.575	2.700	6340.
2	2.700	3.295	2.700	7630.
1	2.700	1.877	2.750	11288.

TABLE 6.4 COMPARISON OF SEISMIC RESISTANCE COEFFICIENTS

STORY LEVEL	WING D MODELS		AOYAMA AND SOZEN [1.9]	SELNA, CHO, AND RAMANATHAN [1.8]
	INITIAL SECTIONS	CONFINED SECTIONS		
FIRST	0.55	0.36	0.39	.44
GROUND	0.38	0.25	0.45	.32

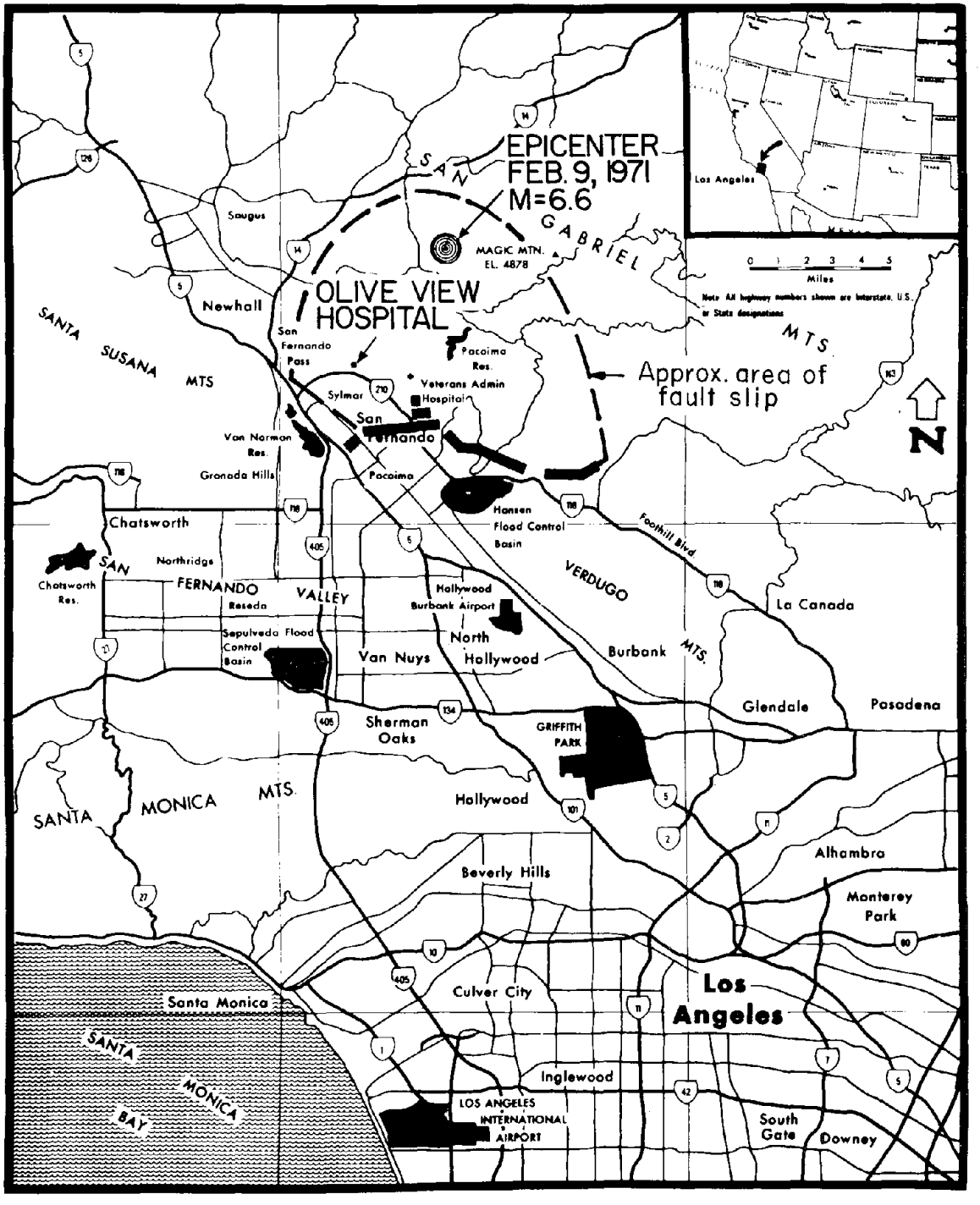

Heavy black lines show the approximate locations of the zone of surface faulting.

FIG. 1.1 LOCATION OF OLIVE VIEW HOSPITAL (REF. 4.2)

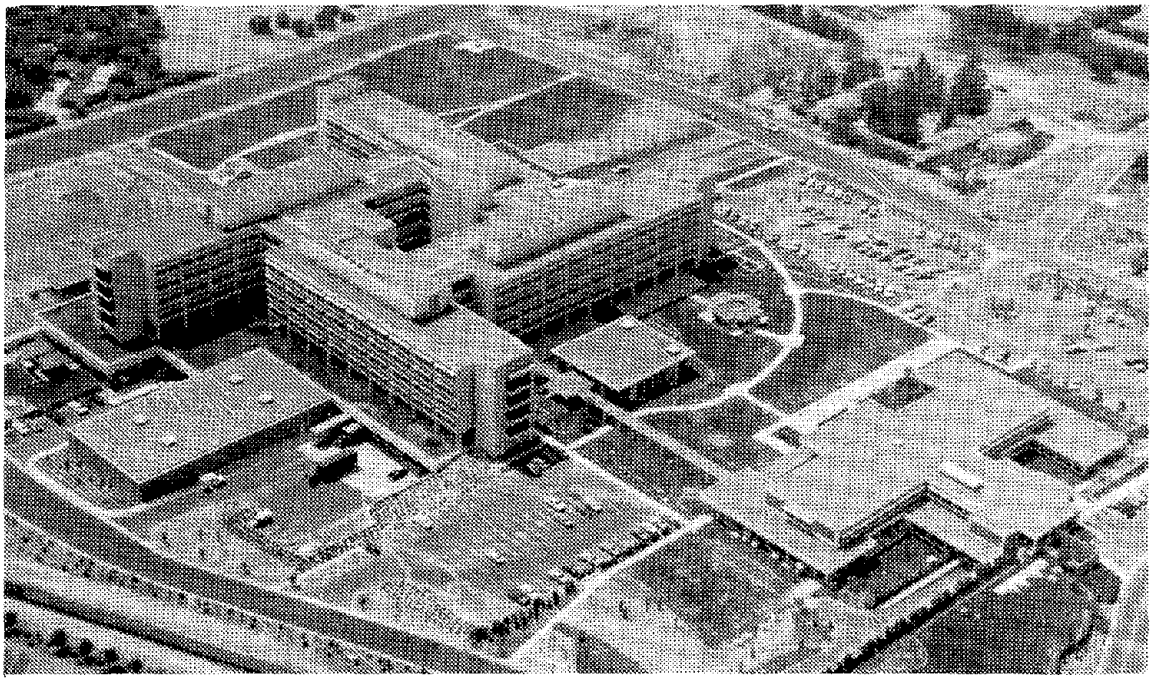

FIG. I.2 OLIVE VIEW MEDICAL CENTER BEFORE EARTHQUAKE VIEWED FROM NORTHEAST

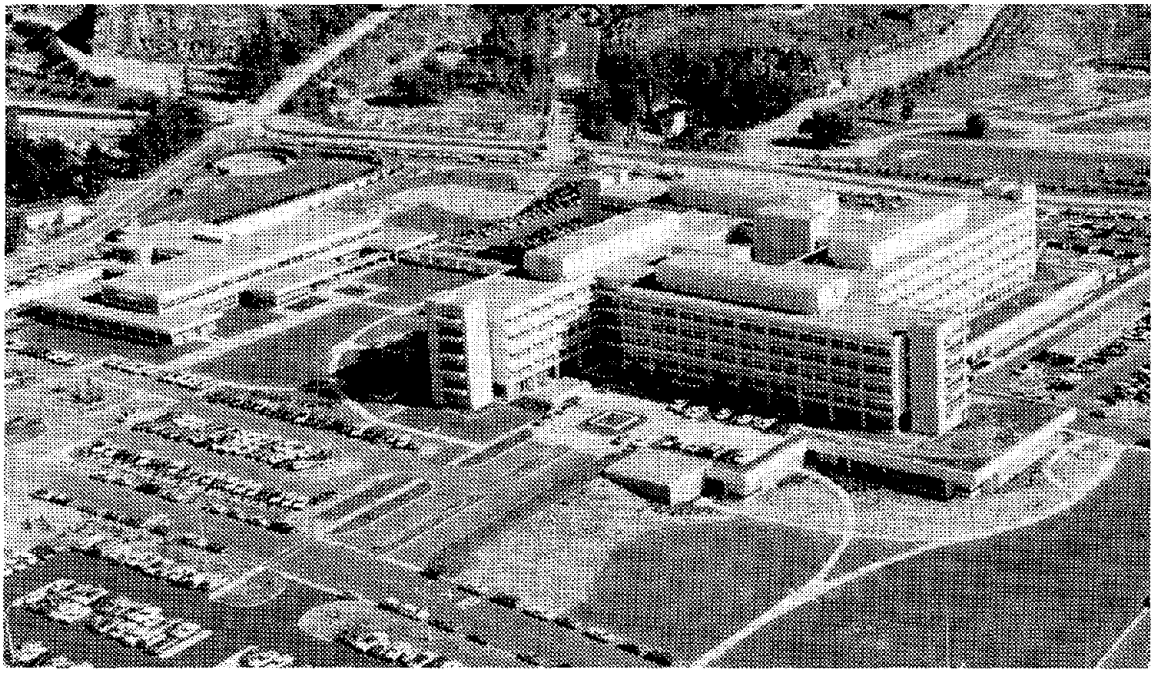

FIG. I.3 OLIVE VIEW MEDICAL CENTER BEFORE EARTHQUAKE VIEWED FROM SOUTHWEST

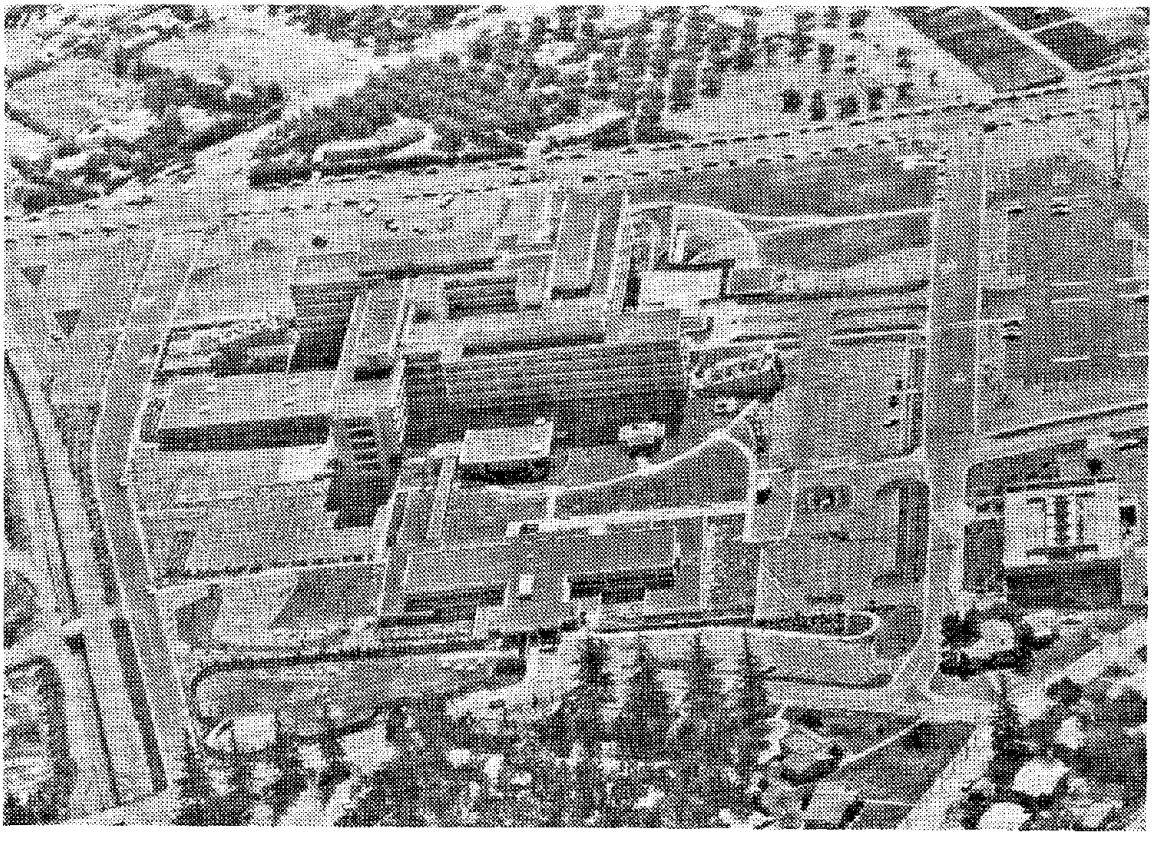

(a) OLIVE VIEW MEDICAL CENTER AS VIEWED FROM THE NORTH

(b) GENERAL VIEW OF DAMAGE TO MAIN BUILDING (WING D IN FOREGROUND)

FIG. 1.4 GENERAL FEATURES OF DAMAGE TO OLIVE VIEW MEDICAL CENTER

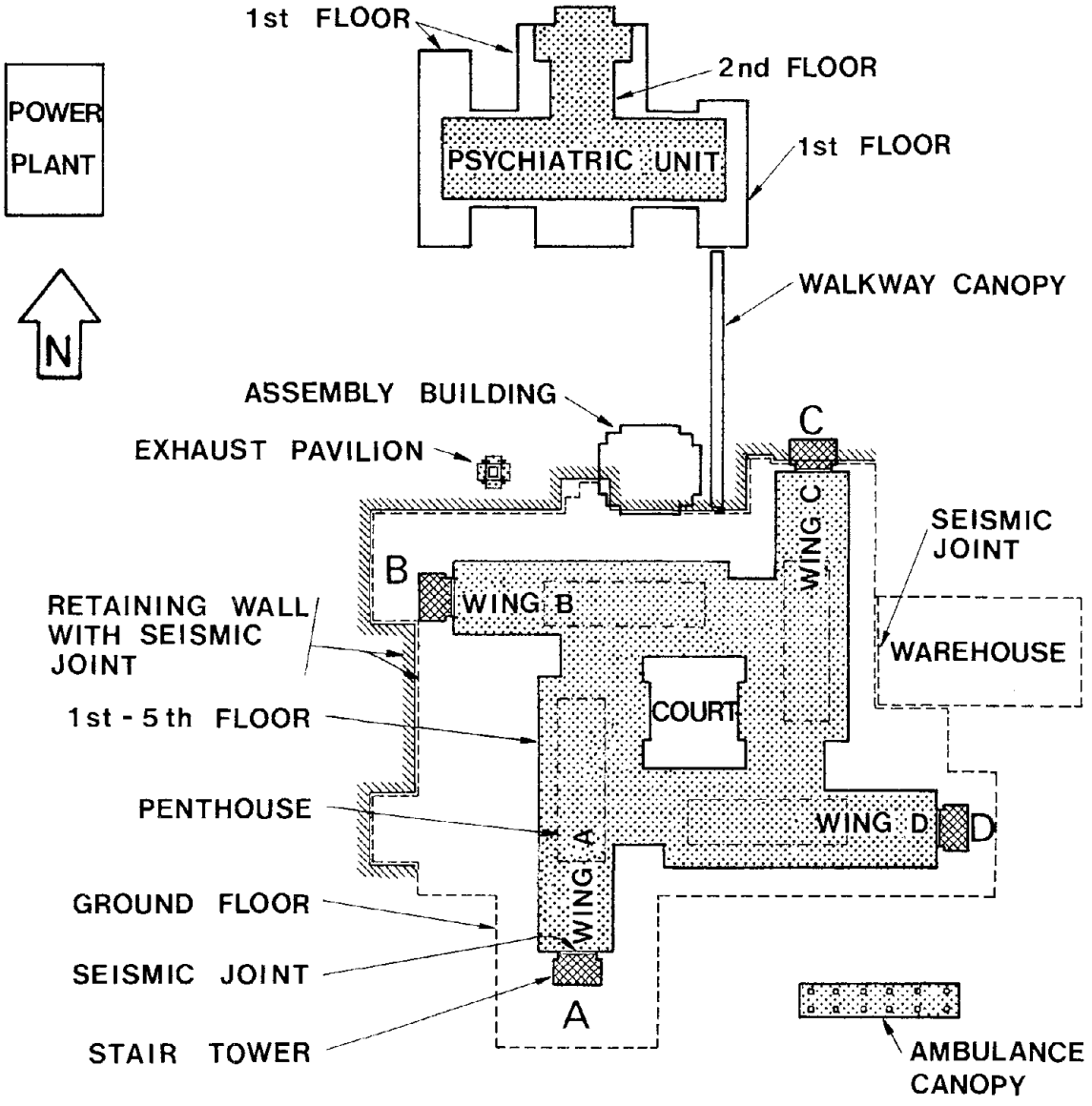

FIG. I.5 SITE PLAN OF THE OLIVE VIEW MEDICAL CENTER

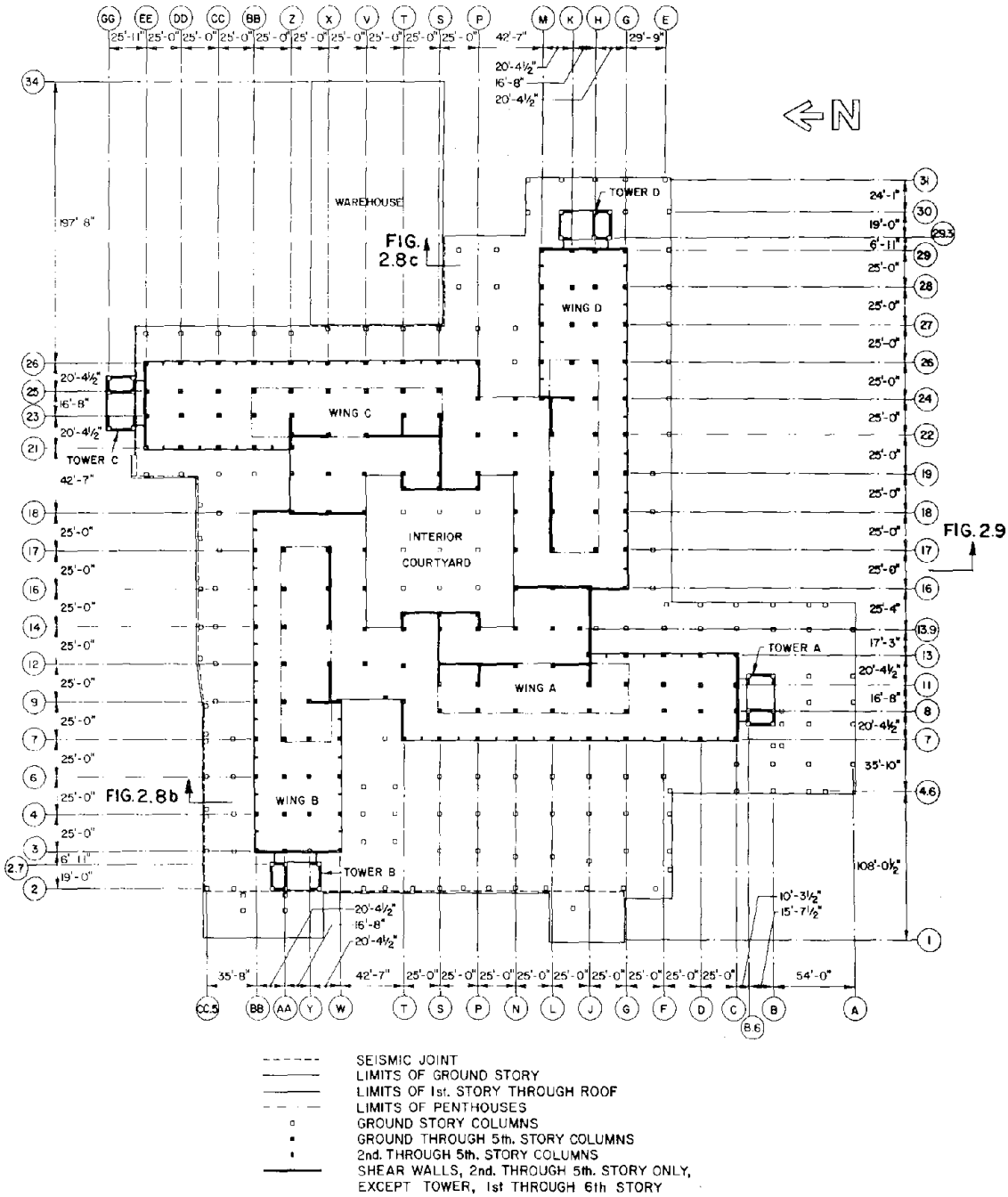

FIG. 2.1 SCHEMATIC FLOOR PLAN OF MAIN BUILDING

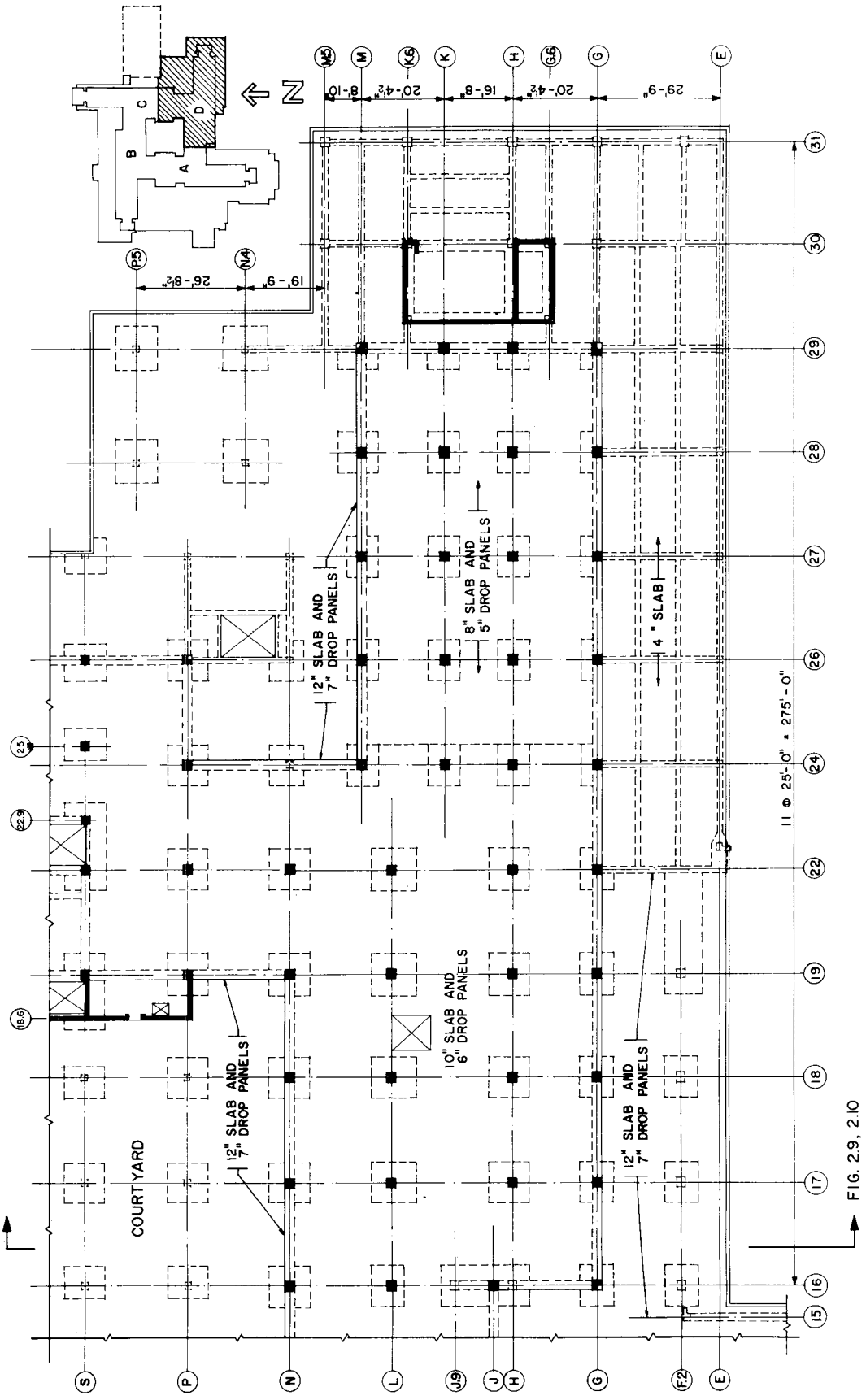

FIG. 2.2 FIRST FLOOR PLAN-WING D

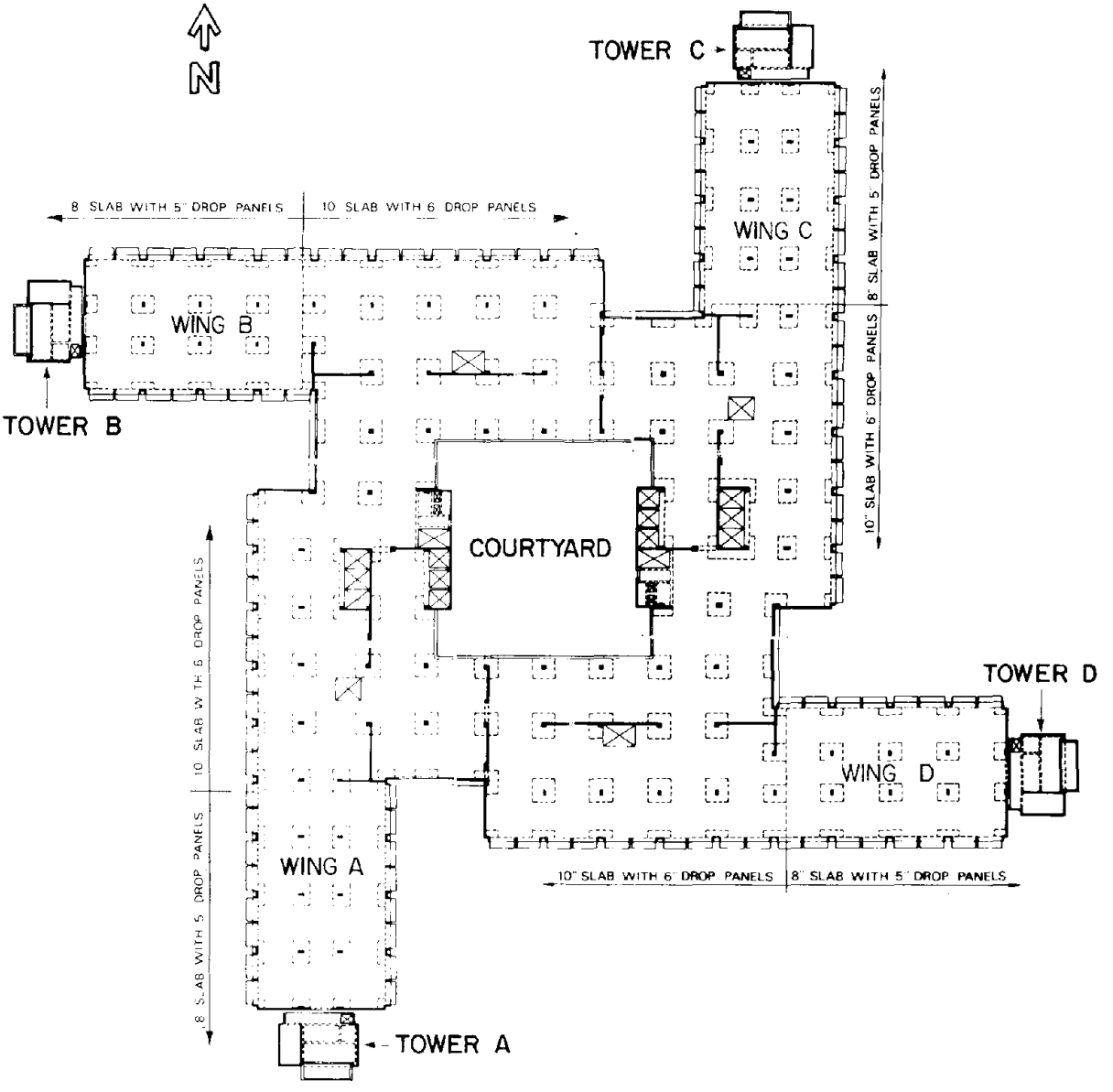

FIG. 2.3 TYPICAL FLOOR PLAN ABOVE SECOND FLOOR

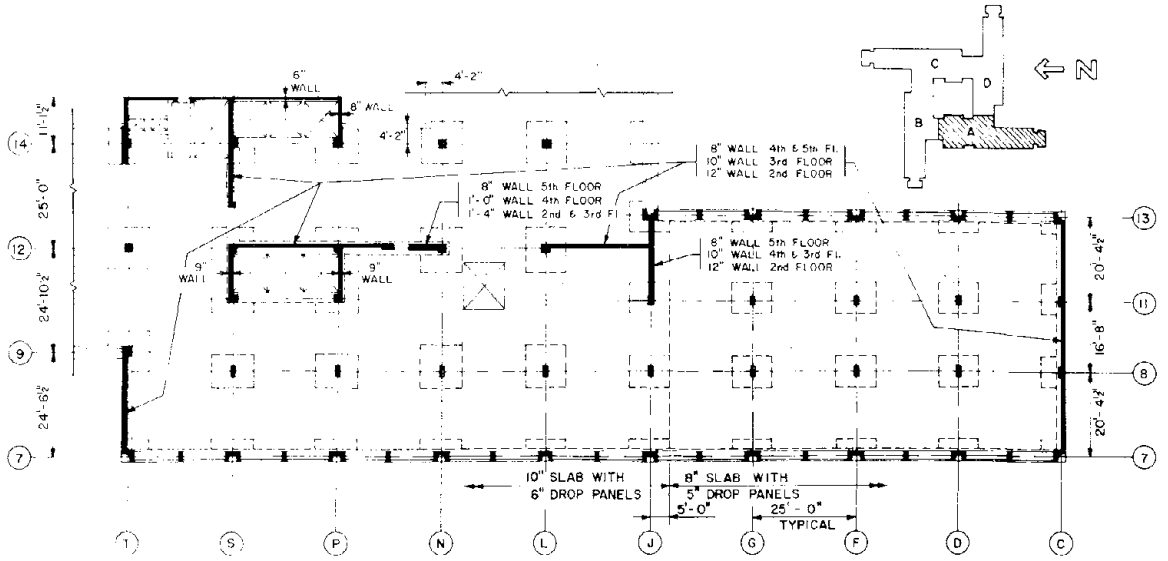

FIG. 2.4 DETAIL OF WING A FLOOR PLAN FOR TYPICAL UPPER STORY (WING C SIMILAR)

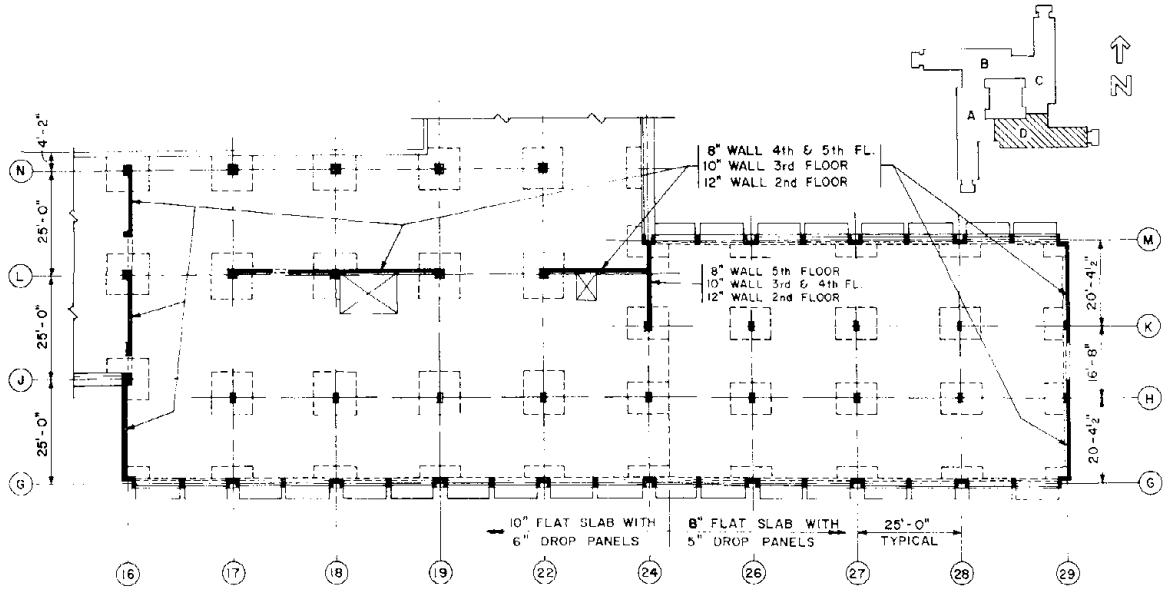

FIG. 2.5 DETAIL OF WING D FLOOR PLAN FOR TYPICAL UPPER STORY (WING B SIMILAR)

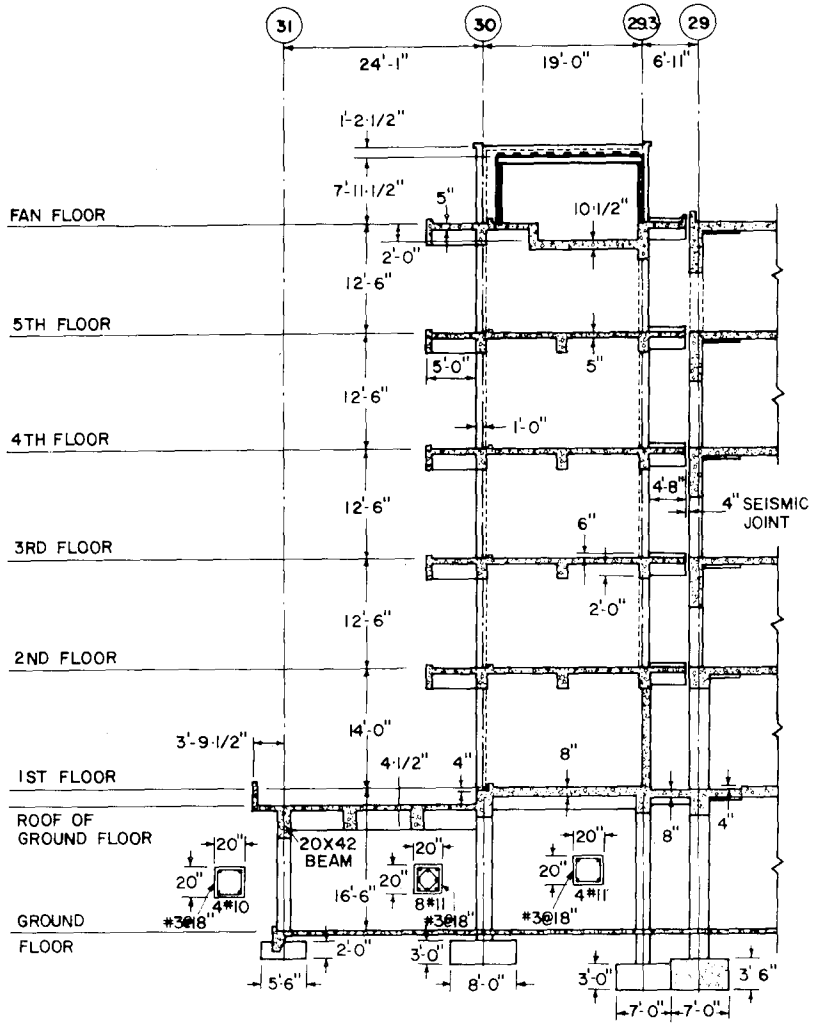

(a) UNIT D-CROSS-SECTION

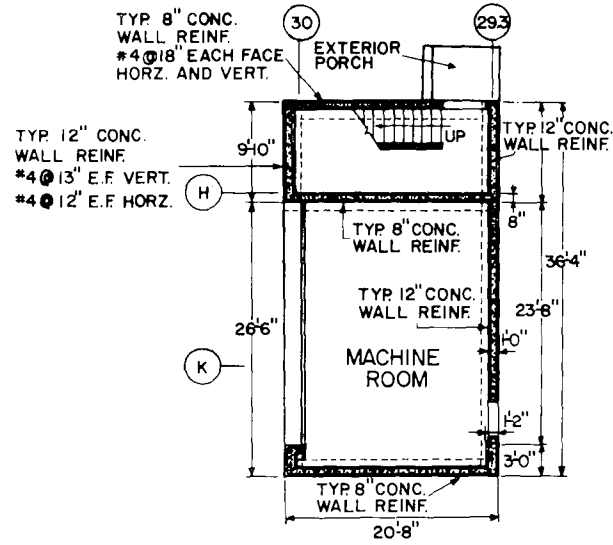

(b) UNIT D-FIRST FLOOR PLAN

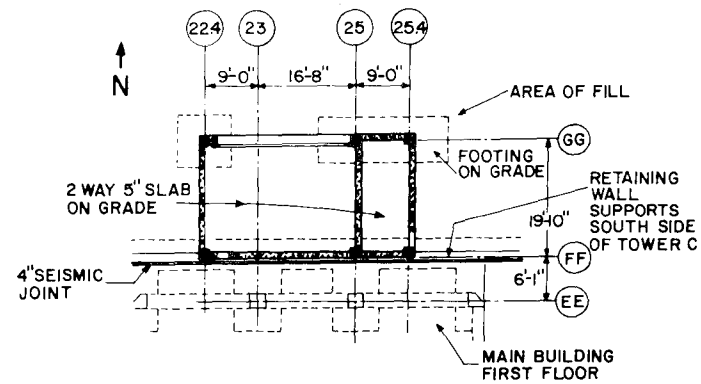

(c) DETAIL AT TOWER C FIRST FLOOR LEVEL

FIG. 2.6 STAIR-TOWER DETAILS

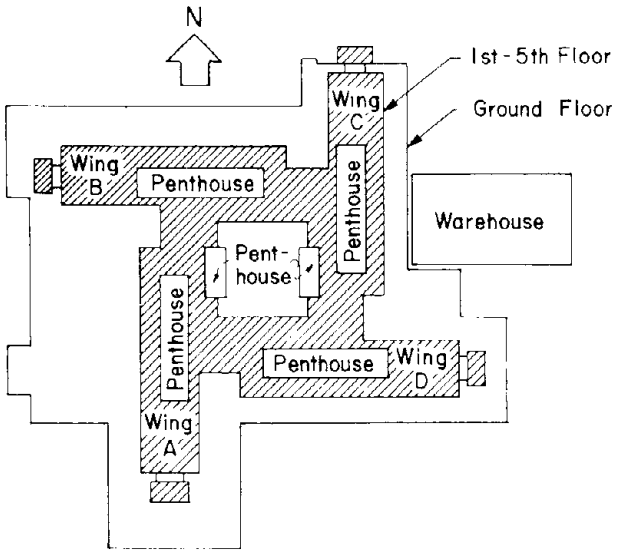

FIG. 2.7 LOCATIONS OF MECHANICAL PENTHOUSES

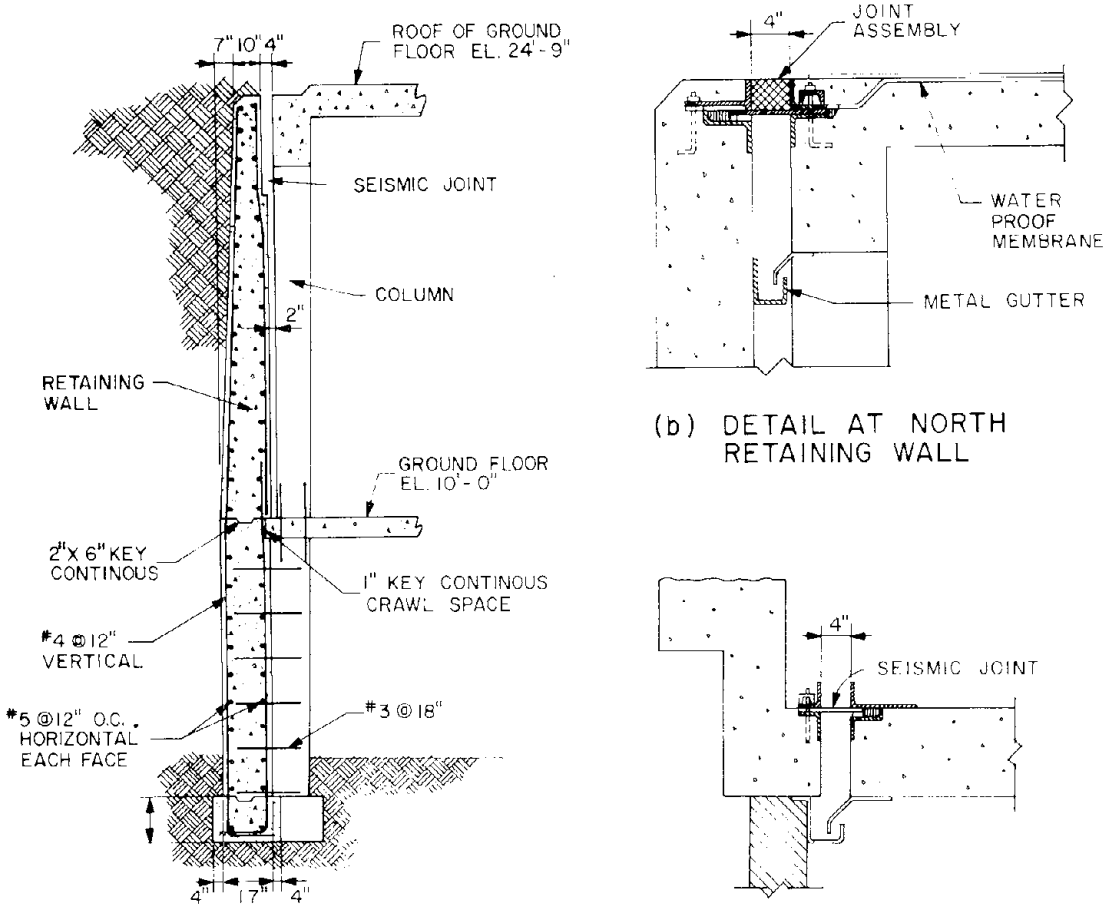

(a) NORTH RETAINING WALL

(b) DETAIL AT NORTH RETAINING WALL

(c) DETAIL AT WAREHOUSE

FIG. 2.8 DETAILS OF SEISMIC JOINT

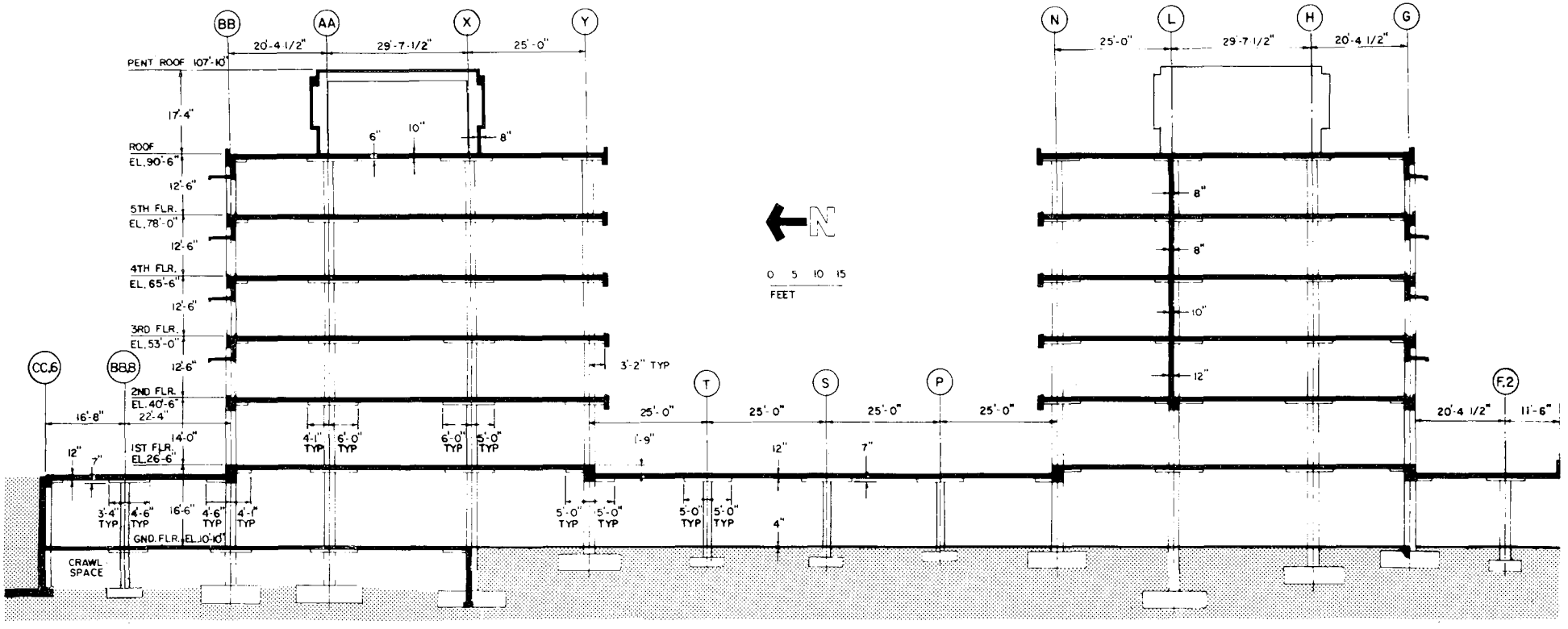

FIG. 2.9 CROSS SECTION ALONG LINE 17 (SEE FIG. 2.1)

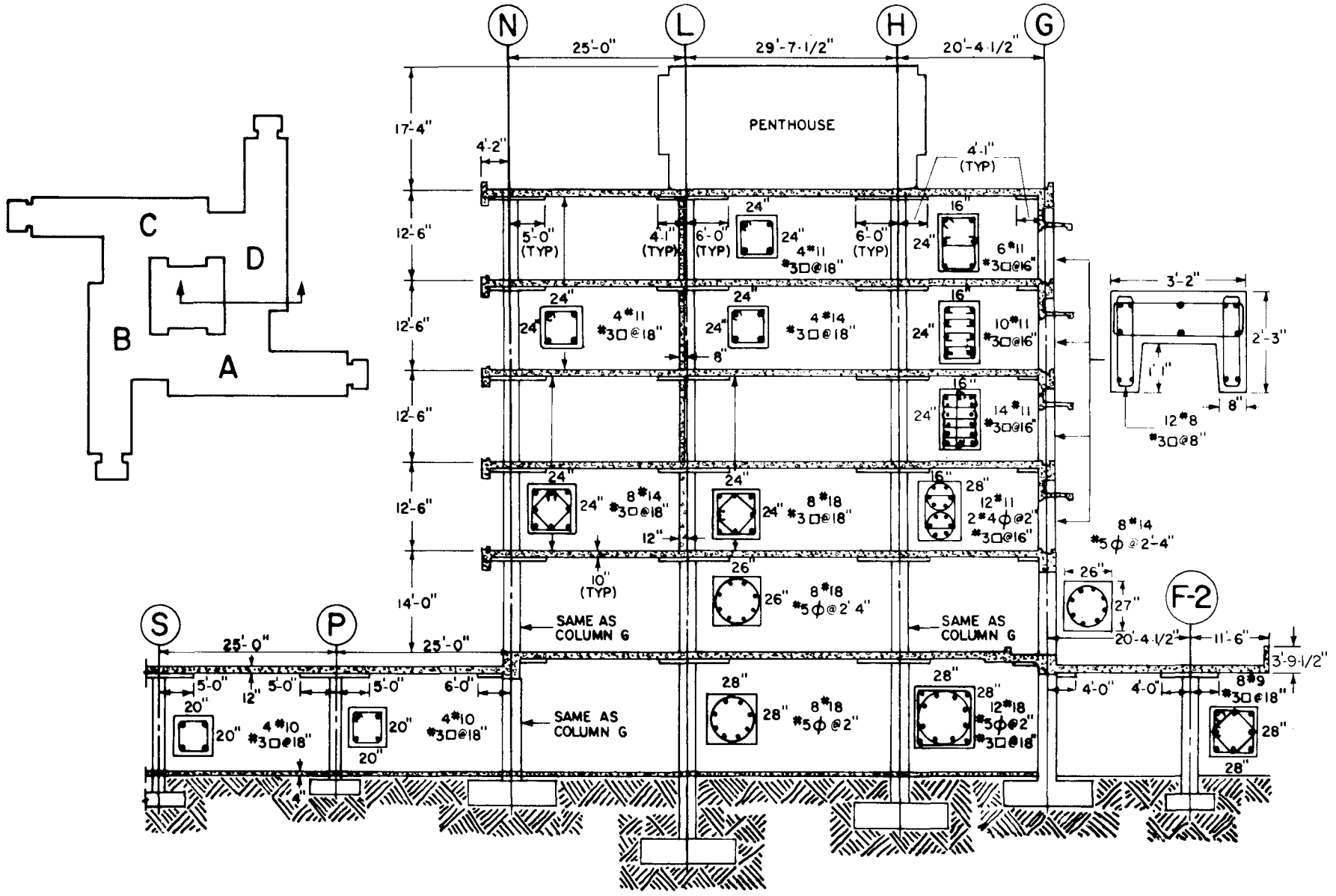

FIG. 2.10 STRUCTURAL DETAIL AT FRAME 17, WING D

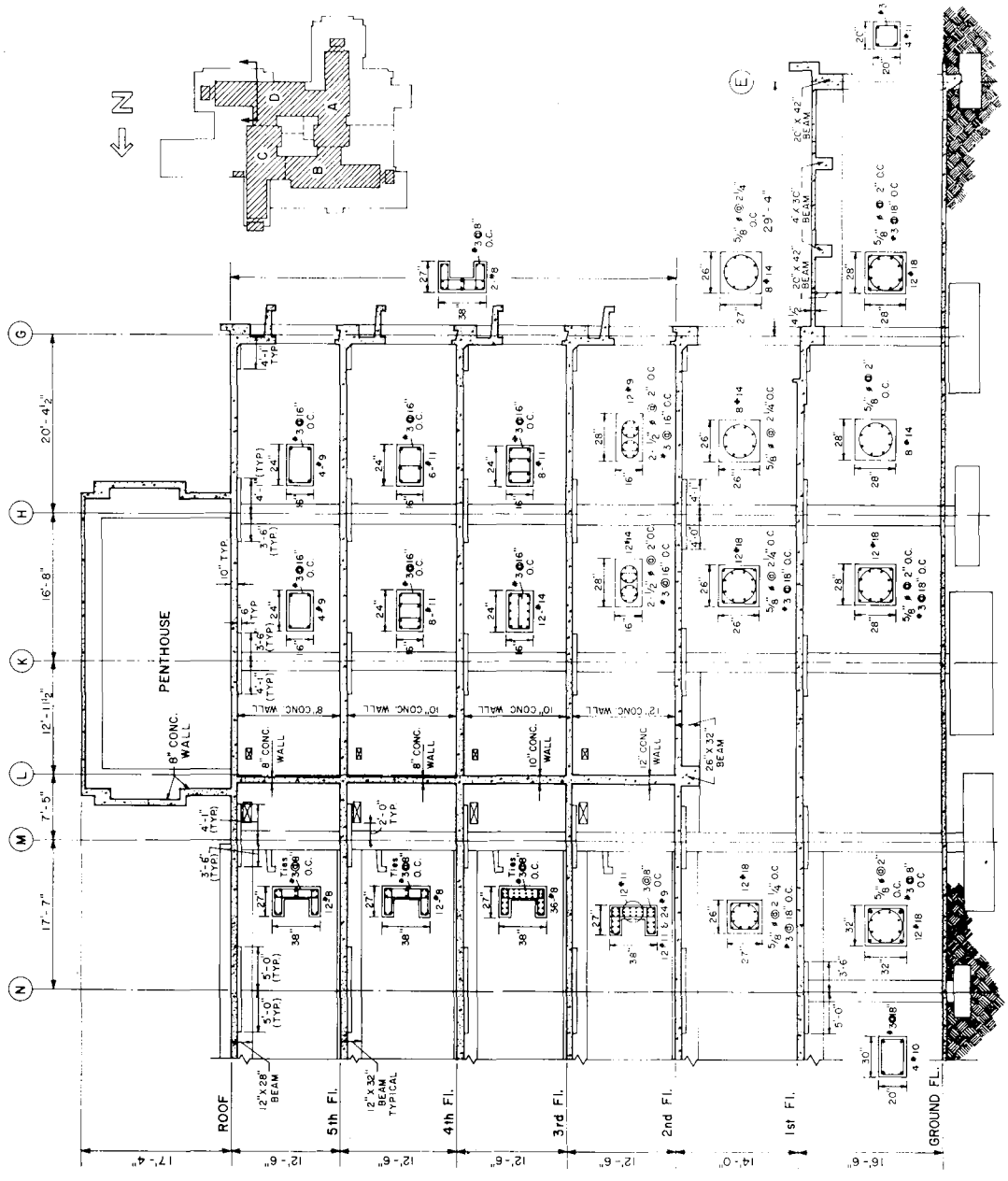

FIG. 2.11 STRUCTURAL DETAILS ALONG FRAME 24, WING D

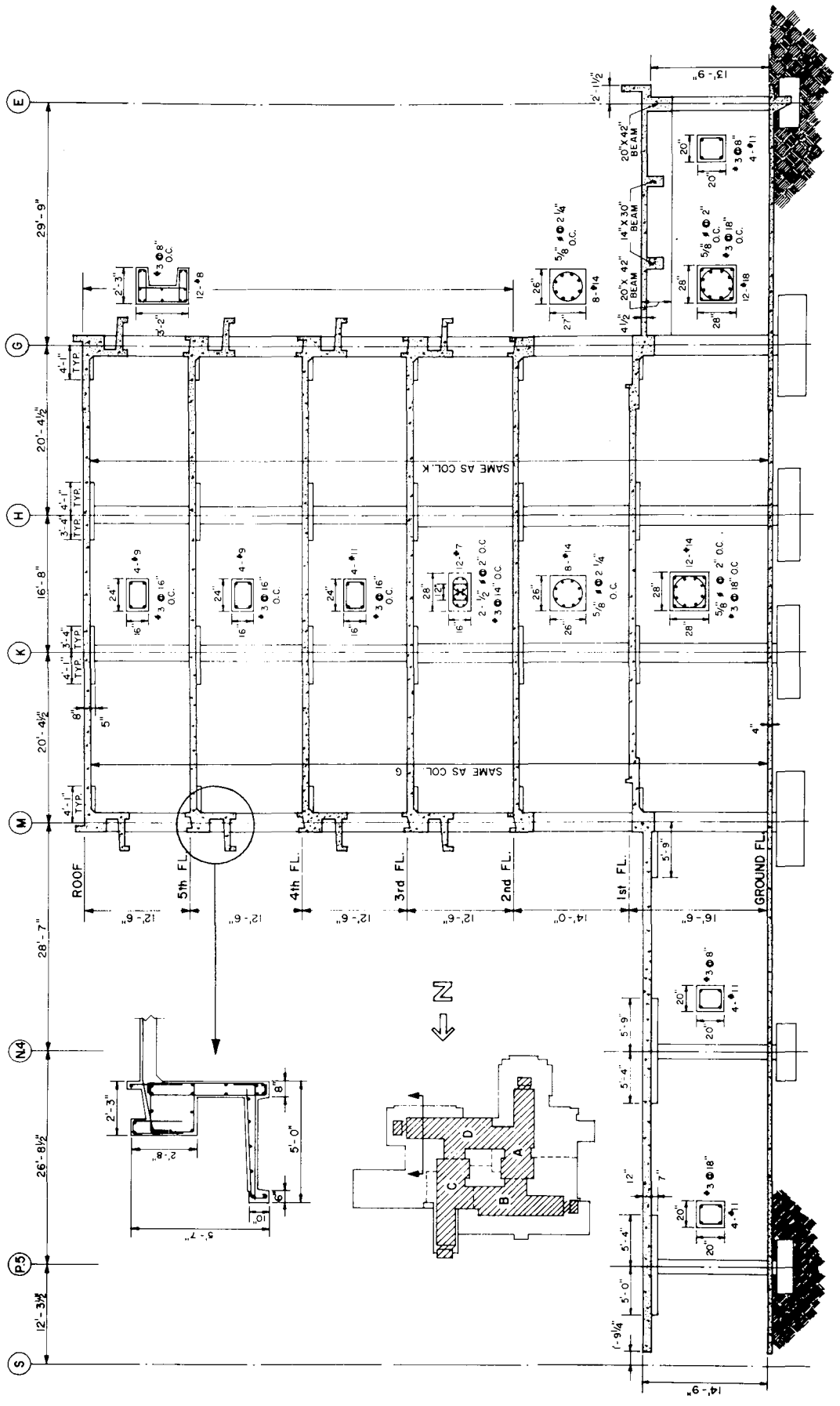

FIG. 2.12 STRUCTURAL DETAILS ALONG FRAME 28, WING D

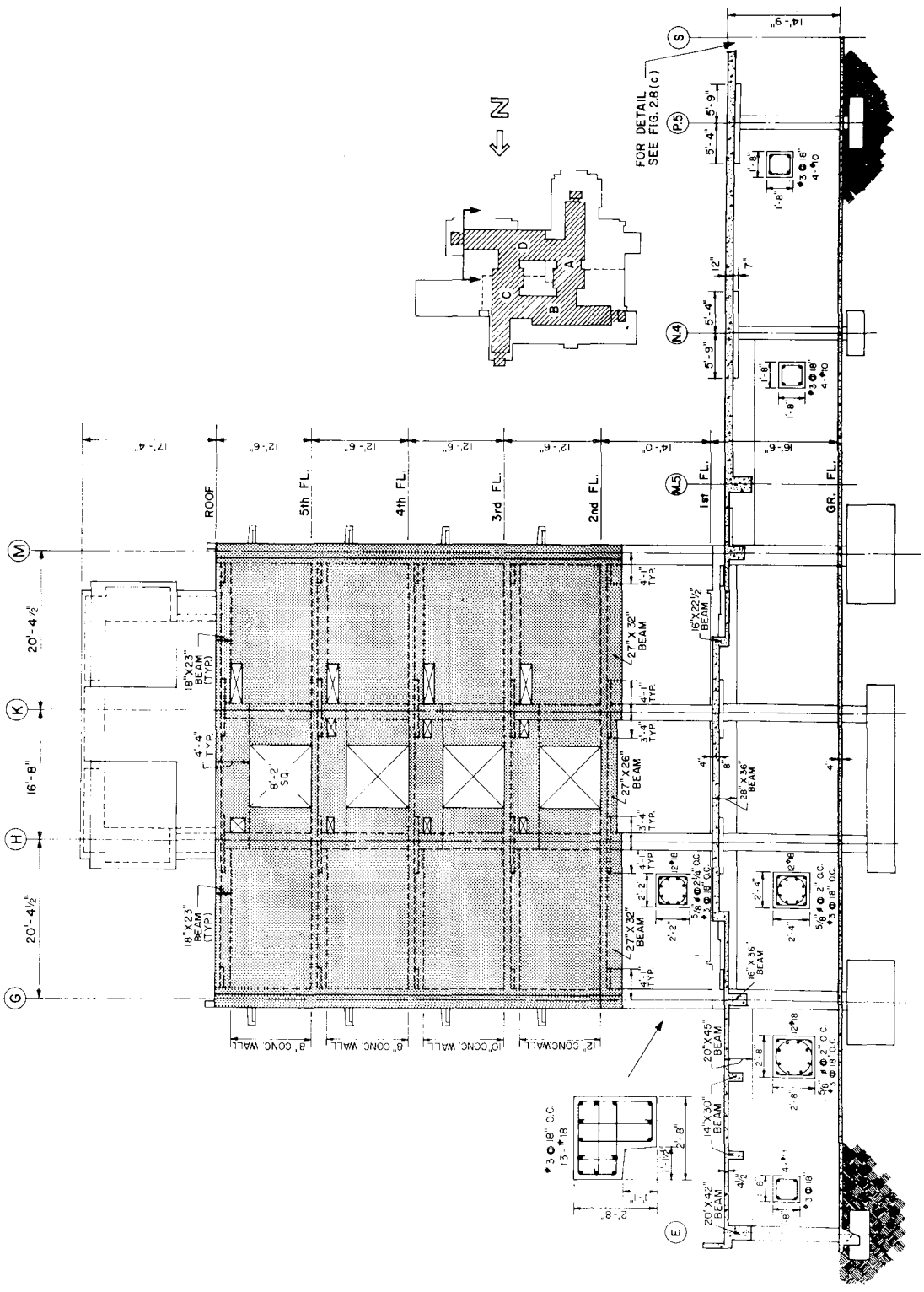

FIG. 2.13 STRUCTURAL DETAILS ALONG FRAME 29, WING D

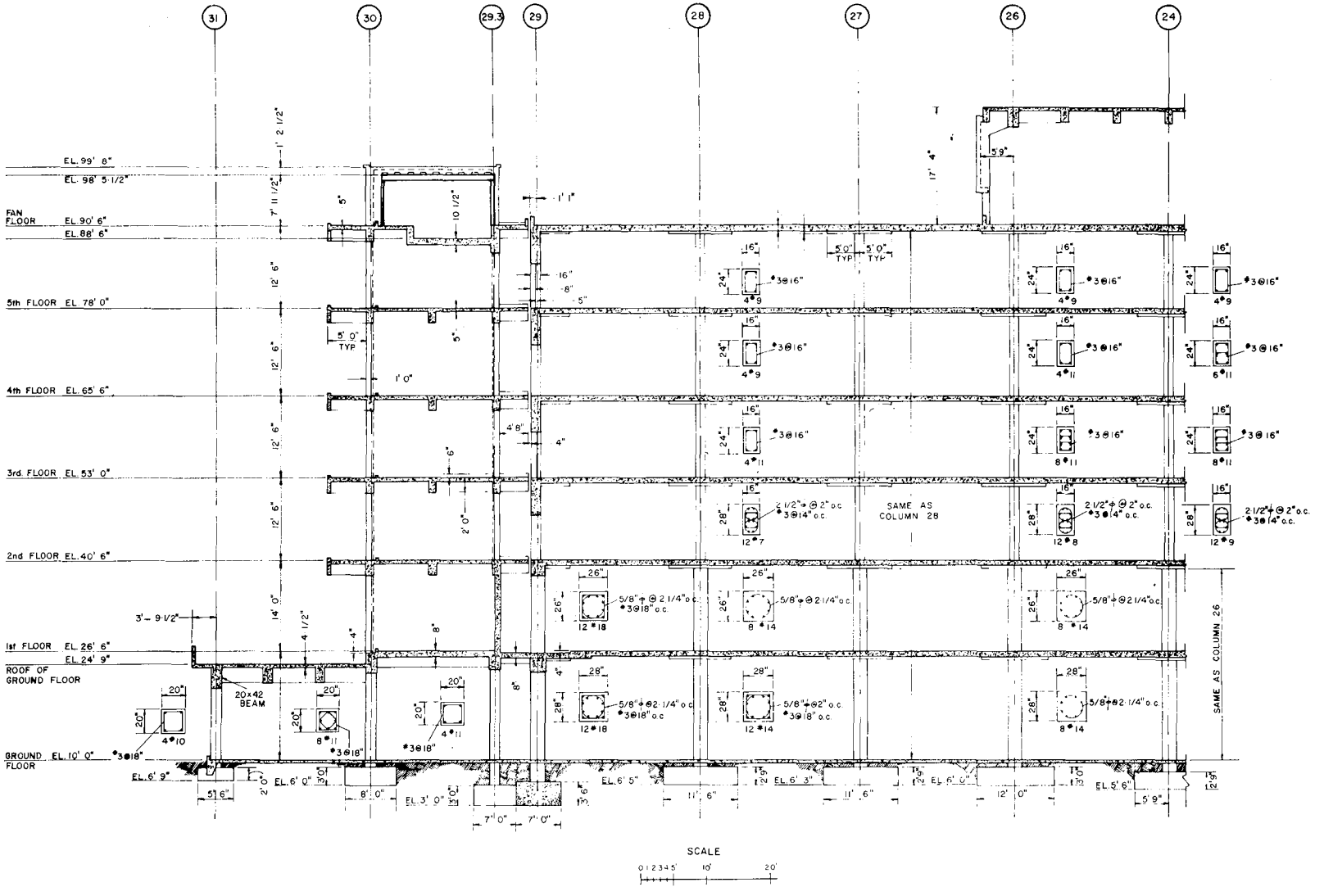

FIG. 2.14 STRUCTURAL DETAILS OF LONGITUDINAL SECTION THROUGH WING D ALONG FRAME M

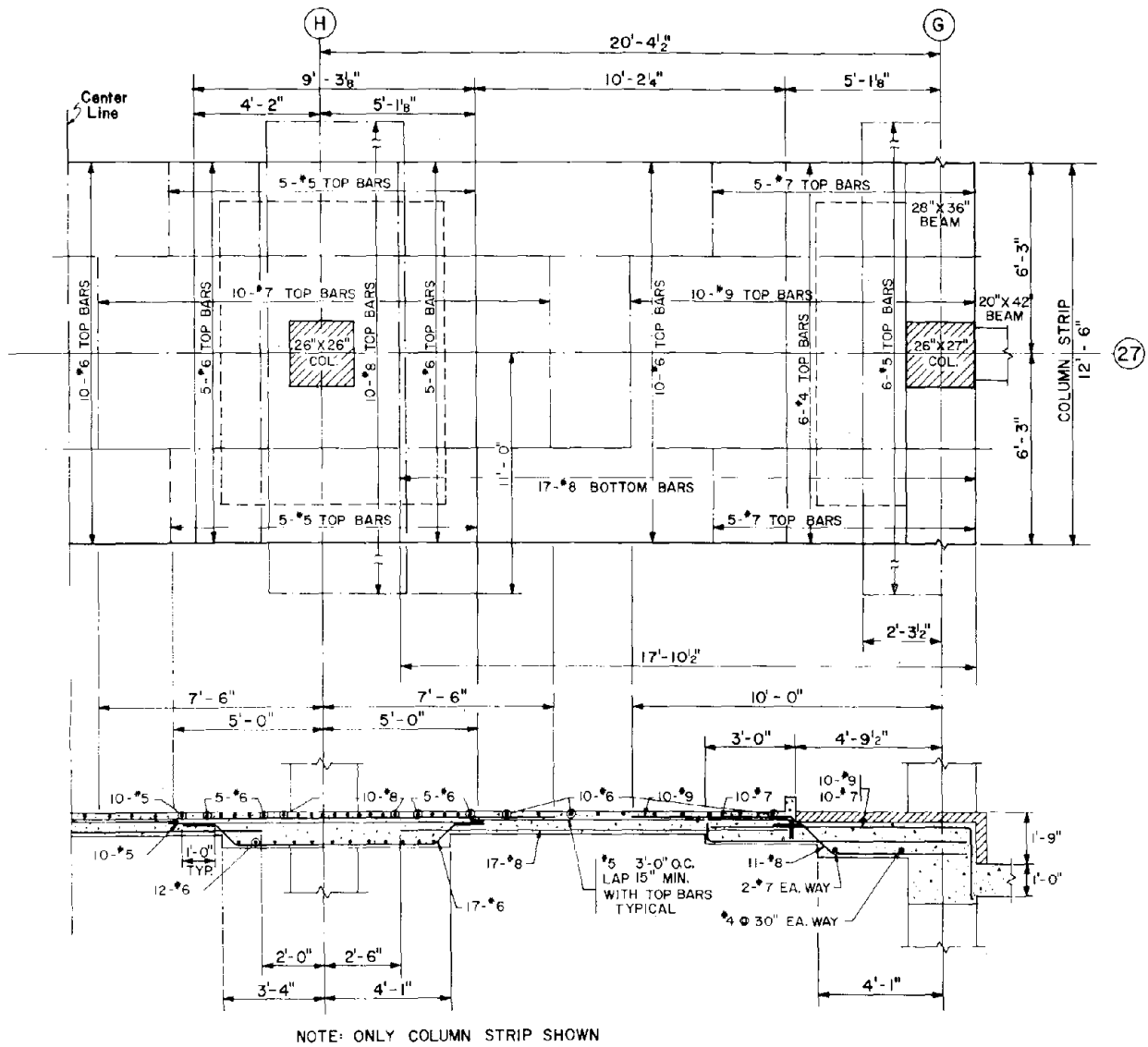

NOTE: ONLY COLUMN STRIP SHOWN

FIG. 2.15 DETAIL OF FIRST FLOOR SLAB REINFORCEMENT

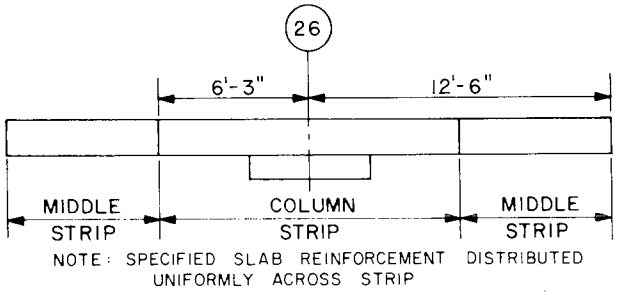

(a) DISTRIBUTION OF SLAB REINFORCEMENT

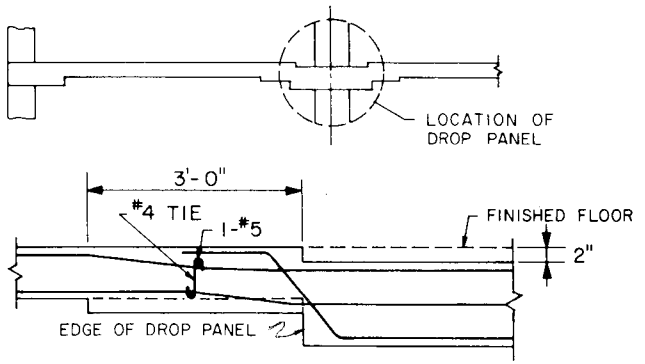

(b) DETAIL AT FLOOR DEPRESSION
TYPICAL ABOVE 2nd FLOOR

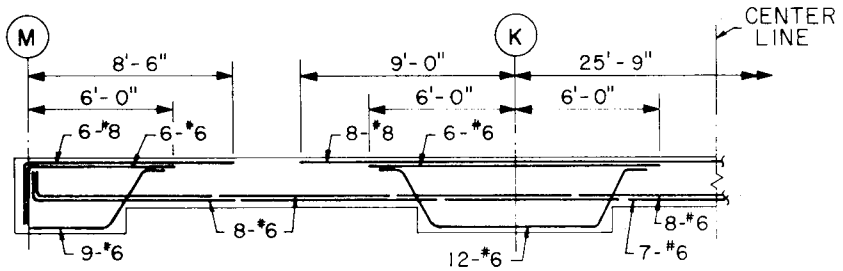

COLUMN STRIP

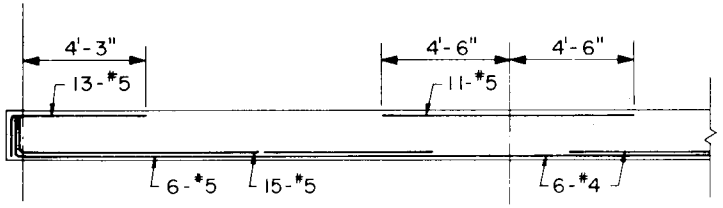

MIDDLE STRIP

(c) 2nd FLOOR

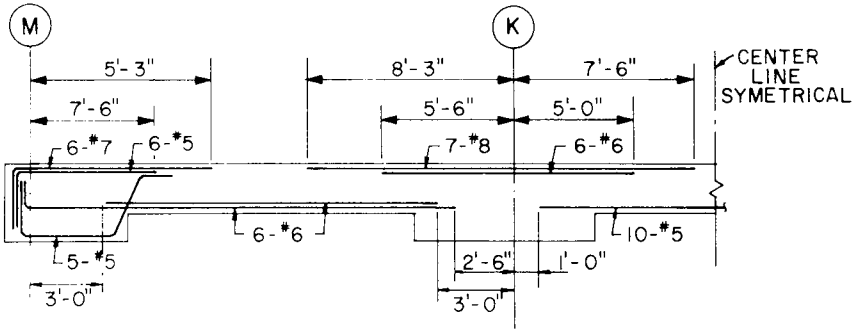

COLUMN STRIP

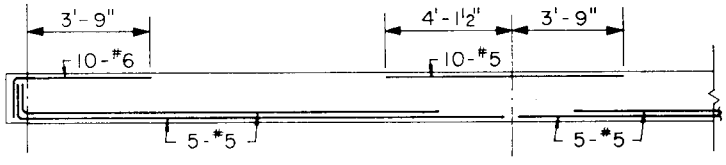

MIDDLE STRIP

(d) TYPICAL UPPER FLOOR

FIG. 2.16 TYPICAL SLAB REINFORCEMENTS - SECOND AND UPPER FLOORS

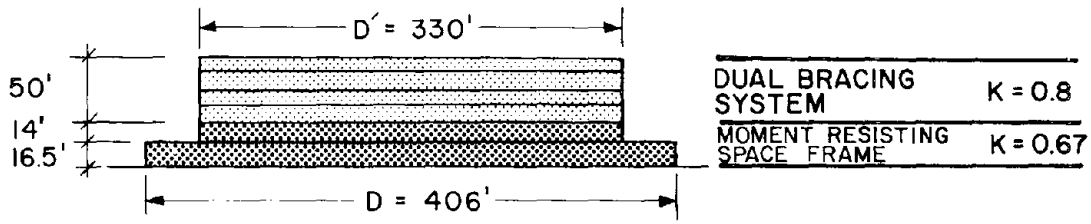

(a) IDEALIZATION OF STRUCTURE USED FOR EVALUATING EQUIVALENT STATIC LATERAL FORCES (N-S SECTION SHOWN, E-W SECTION SIMILAR)

(i) SINCE $\frac{D'}{D} = \frac{330}{406} = 0.81 > 0.75$ NEGLECT SETBACK AT FIRST FLOOR

(ii) CONSIDER THE CHANGE IN LATERAL STIFFNESS AT 2nd FLOOR A SETBACK FOR PURPOSES OF DETERMINING LATERAL FORCES

(iii) LATERAL FORCE COEFFICIENTS FOR ROOF - 2nd FLOOR

$$T = 0.05\frac{H}{\sqrt{D}} = 0.05\frac{50}{\sqrt{330}} = 0.1375 \text{ sec.}$$

$$C = \frac{0.05}{\sqrt[3]{T}} = 0.097$$

$$V = ZCKW = (1.0)(0.097)(0.8)W = 0.0774\,W = V$$

$$J = \frac{0.5}{\sqrt[3]{T^2}} > 1.0 \quad \therefore \quad J = 1.0$$

(iv) LATERAL FORCE COEFFICIENTS FOR 2nd FLOOR-GROUND

$$T = 0.05\,\frac{30.5}{\sqrt{406}} = 0.0756 \text{ sec.}$$

$$C = \frac{0.05}{\sqrt[3]{T}} = 0.1185$$

$$V = (1.0)(0.1185)(0.67)W = 0.08\,W = V$$

$$J = \frac{0.5}{\sqrt[3]{T^2}} > 1.0 \quad \therefore \quad J = 1.0$$

(b) EVALUATION OF DESIGN LATERAL FORCE COEFFICIENTS (N-S DIRECTION; E-W DIRECTION SIMILAR)

FIG. 2.17 MODELING OF MAIN BUILDING FOR DESIGN-EARTHQUAKE LOADING

FIG. 2.18 BUILDING DURING CONSTRUCTION—WING B GROUND FLOOR SLAB FOREGROUND, WINGS A, C, & D BACKGROUND

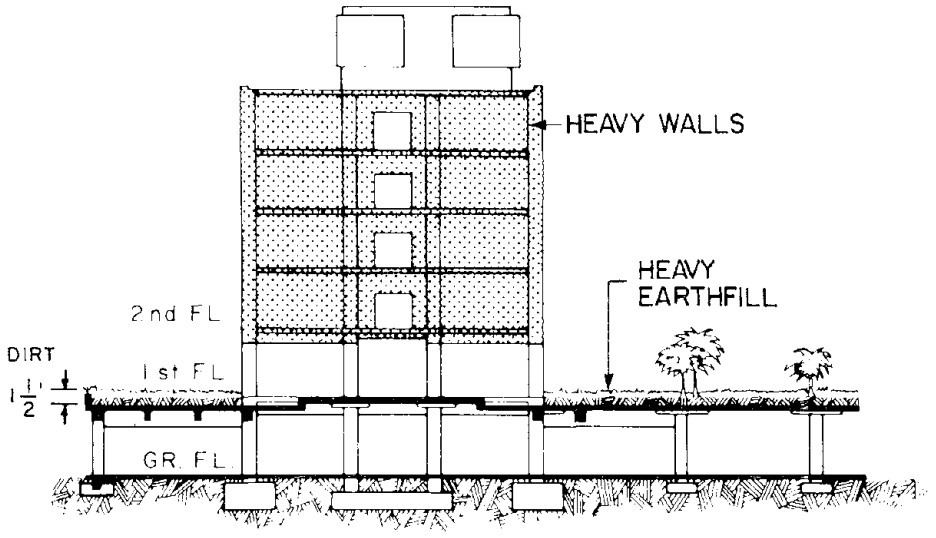

(a) ELEVATION OF OLIVE VIEW MAIN TREATMENT BUILDING ILLUSTRATING PRESENCE OF UNNECESSARY MASSES

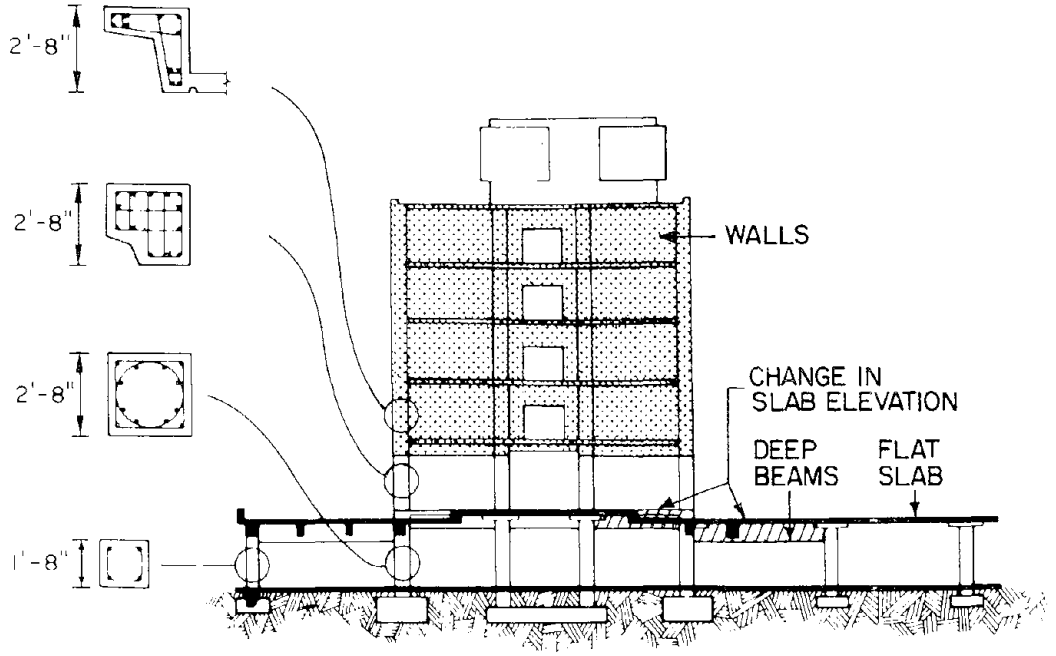

(b) ELEVATION OF OLIVE VIEW MAIN TREATMENT BUILDING ILLUSTRATING DISCONTINUOUS STIFFNESS, STRENGTH, AND DUCTILITY

FIG. 2.19 ILLUSTRATION OF INADEQUATE STRUCTURAL CONCEPTS

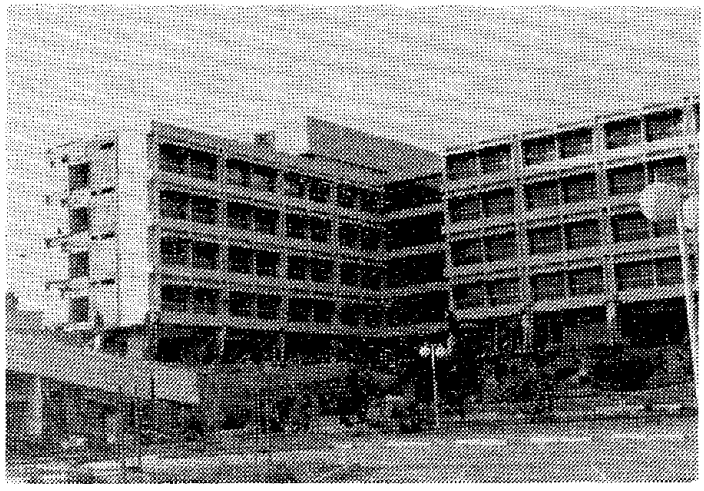

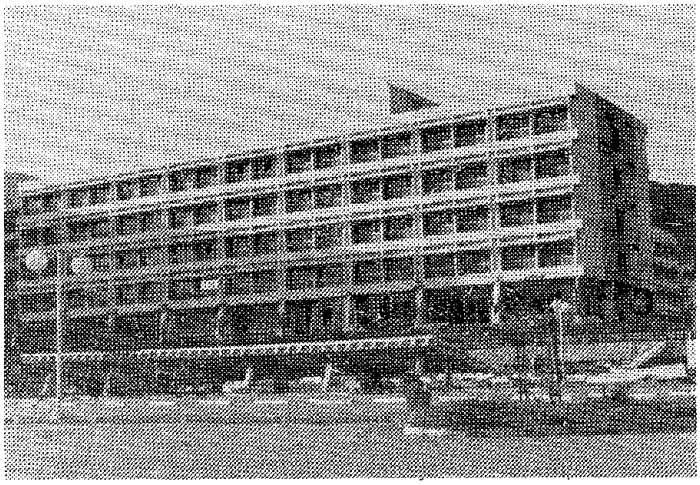

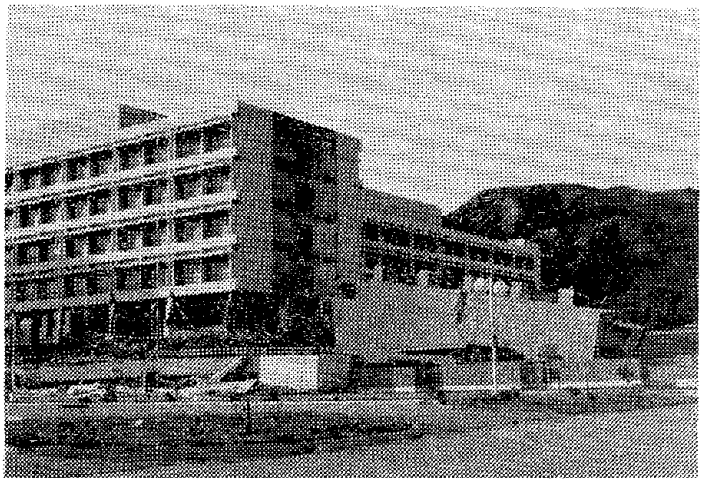

FIG. 3.1 DAMAGE TO MAIN BUILDING
VIEWED FROM SOUTHEAST

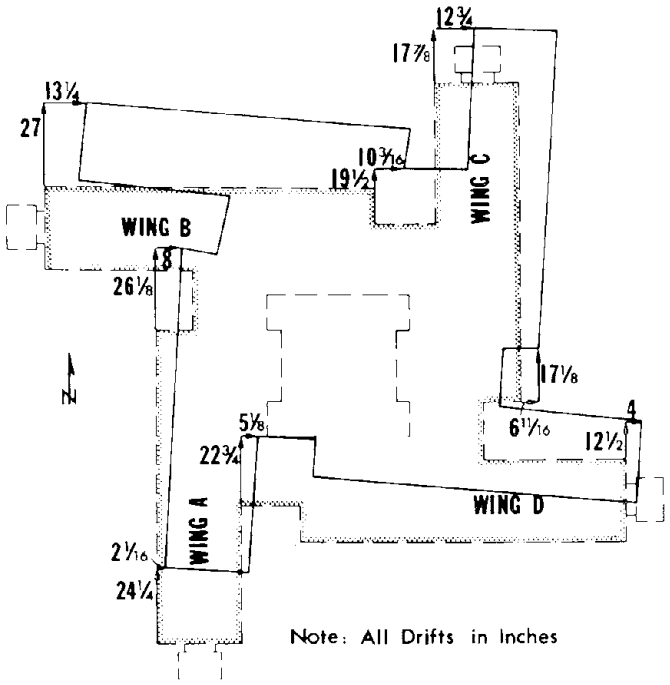

FIG. 3.2 PERMANENT STORY DRIFTS IN FIRST STORY

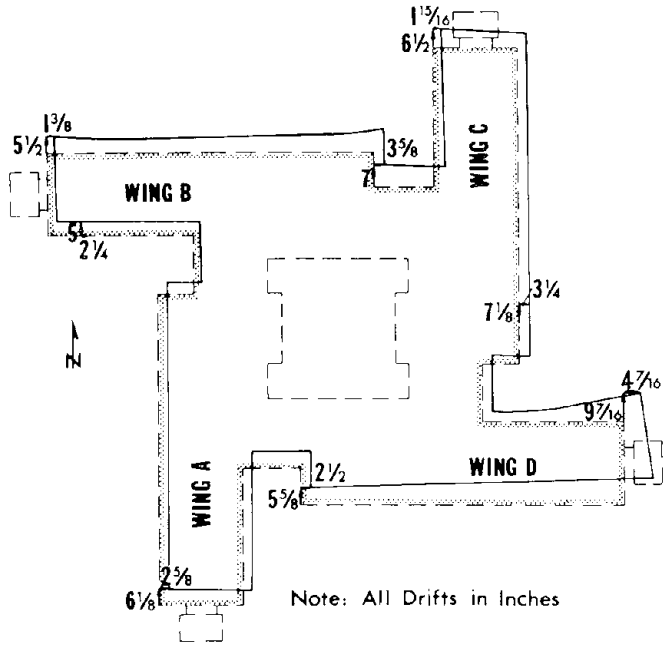

FIG. 3.3 PERMANENT STORY DRIFTS IN GROUND STORY

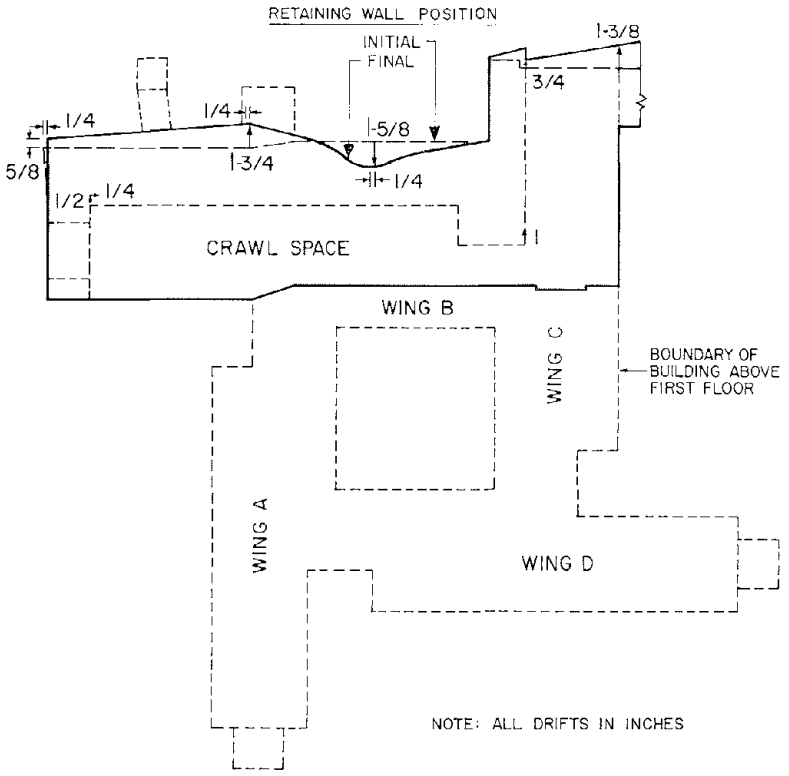

FIG. 3.4 DRIFTS OBSERVED IN CRAWL SPACE

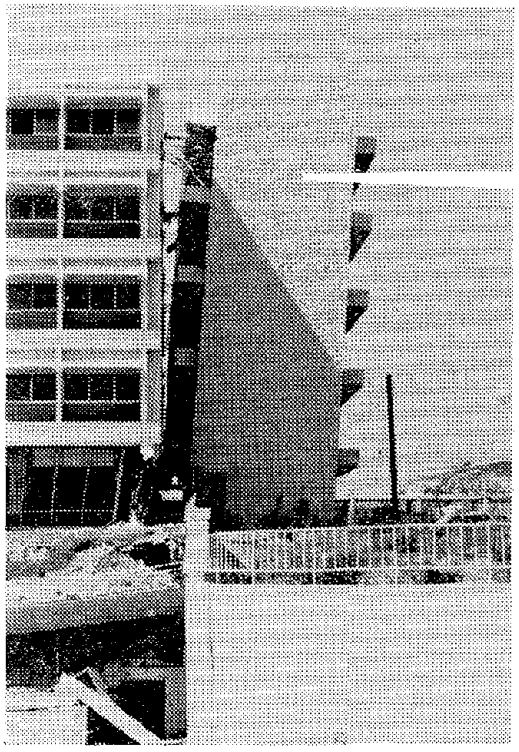

TOWER C

FIG. 3.5 IMPACT OF MAIN BUILDING CAUSED STAIRTOWER C TO TILT TOWARDS NORTH

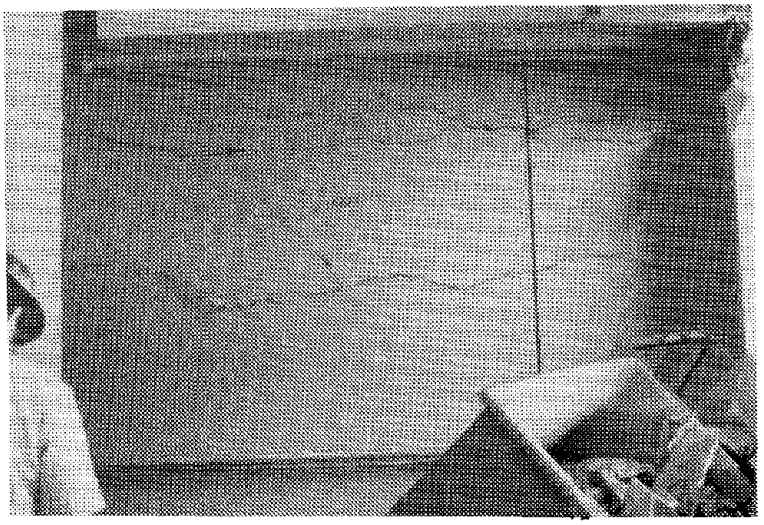

(a) DAMAGE TO NORTH RETAINING WALL BETWEEN COLUMN LINES 26 AND 26.6 ALONG LINE FF

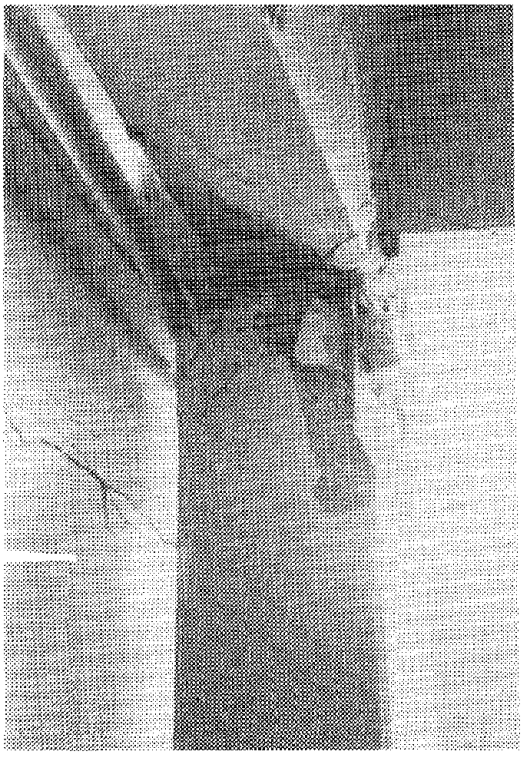

(b) DETAIL OF DAMAGE TO COLUMN FF-26.6 AND ADJACENT RETAINING WALL

FIG. 3.6 DAMAGE AT SEISMIC JOINT DUE TO HAMMERING OF BUILDING AGAINST RETAINING WALL

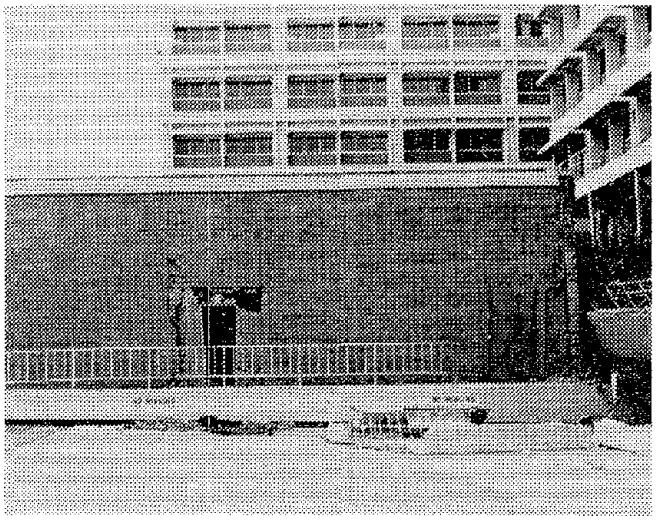

(a) DAMAGE TO MASONARY WALL ON NORTH SIDE OF WAREHOUSE. NOTE COLLAPSED TERRACE CANOPY ON RIGHT HAND SIDE OF PHOTO.

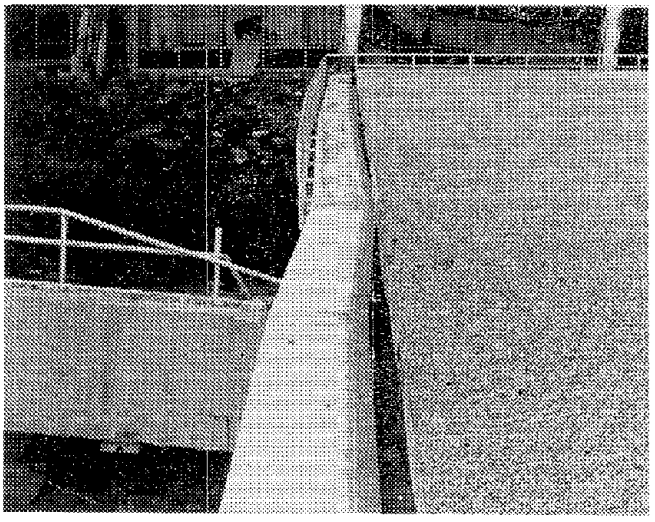

(b) DAMAGE TO SOUTH SIDE OF WAREHOUSE DUE TO IMPACT OF WING D TERRACE

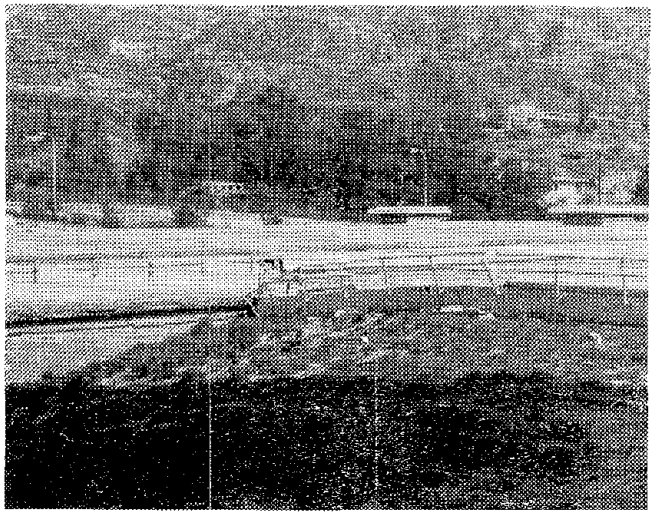

(c) DETAIL OF DAMAGE AT SEISMIC JOINT SEPARATING WING D AND WAREHOUSE. NOTE THAT TERRACE CANOPY HAS DROPPED SEVERAL FEET IN ELEVATION

FIG. 3.7 DAMAGE AT SEISMIC JOINTS DUE TO HAMMERING OF BUILDING AGAINST WAREHOUSE

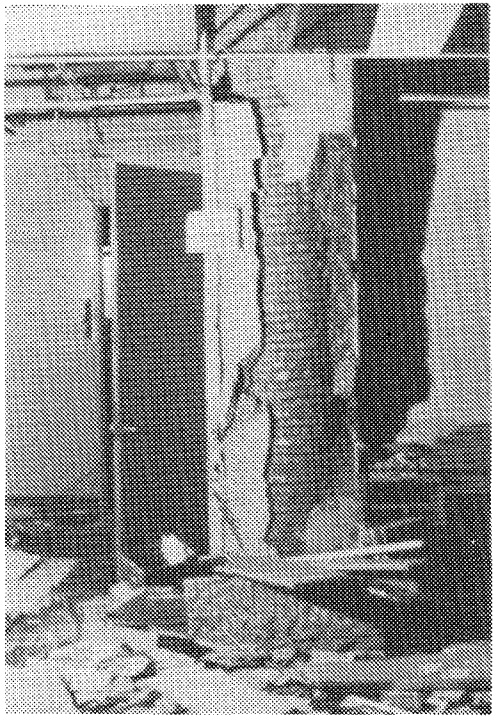

(a) EXTENSIVE SPALLING OF UNCONFINED CONCRETE COVER THROUGHOUT ENTIRE LENGTH OF COLUMN L-16

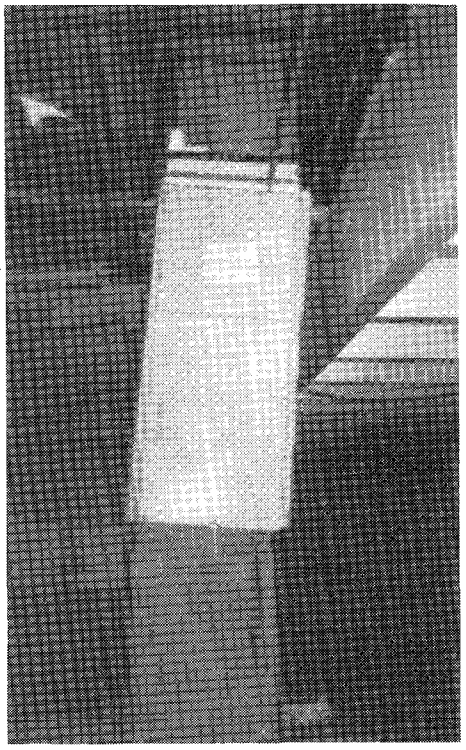

(b) YIELDING AT BOTTOM OF COLUMN H-17. PUNCHING SHEAR FAILURE IN SLAB AT TOP

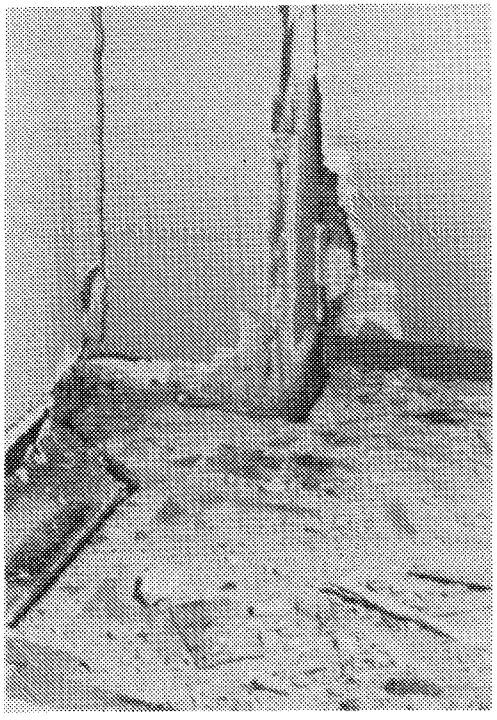

(c) SUBGRADE ROTATION AT COLUMN H-29. LITTLE DISTRESS NOTED IN COLUMN. EXPANSION JOINT OPENED SUBSTANTIALLY

FIG. 3.8 TYPICAL GROUND STORY SPIRAL COLUMN DAMAGE

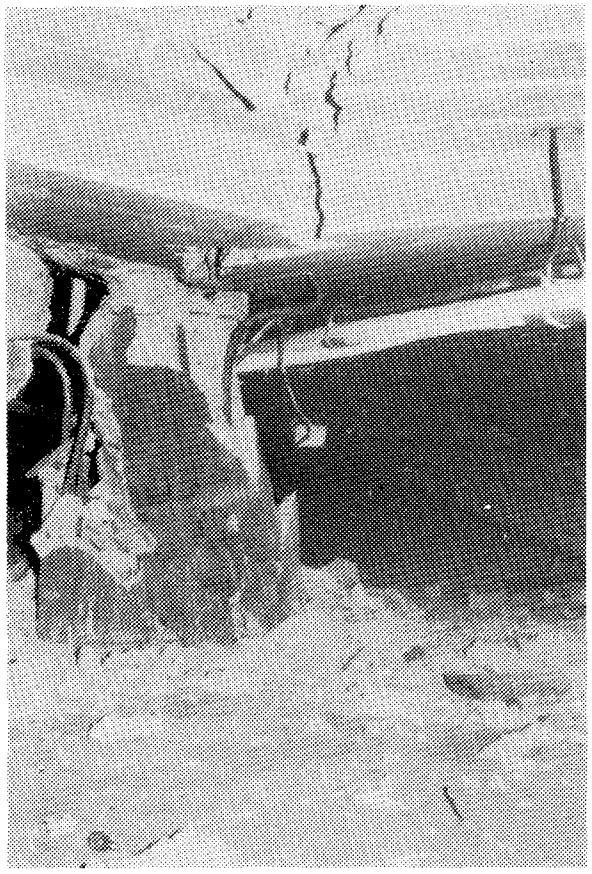

FIG. 3.9 FAILURE OF A TIED COLUMN IN CRAWL SPACE

FIG. 3.10 DAMAGE TO FIRST STORY COLUMN BB-3 ILLUSTRATING SEVERITY OF FIRST STORY DRIFTS AND SUBSIDENCE OF NORTHERN TERRACE CANOPY DUE TO FAILURE OF COLUMNS IN CRAWL SPACE

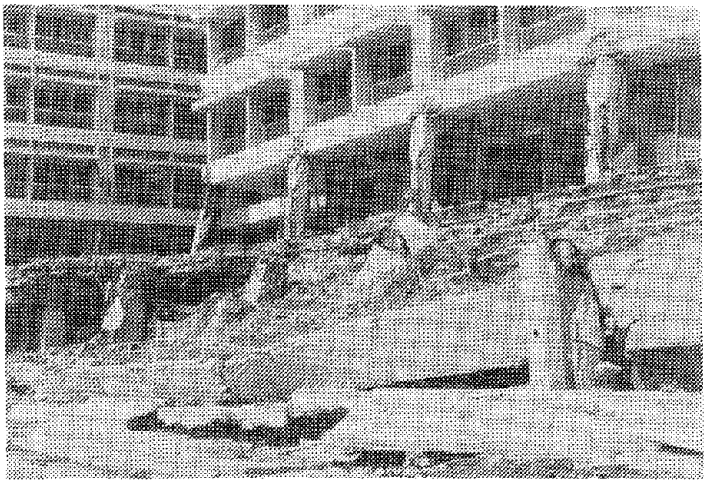

(a) SHEAR FAILURES IN GROUND, FIRST AND SECOND STORY TIED COLUMNS, AND SPALLING IN FIRST STORY SPIRAL COLUMNS AND BEAM-COLUMN JOINTS

(b) DETAIL OF SLAB FAILURE

FIG. 3.11 PUNCHING FAILURE OF UNIT D TERRACE CANOPY

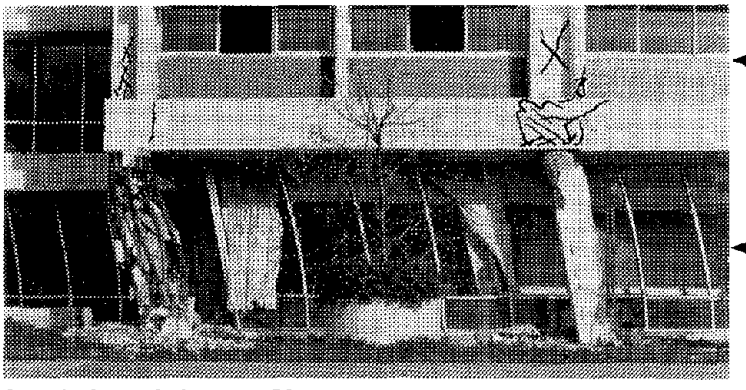

FIG. 3.12 COMPARISON OF DAMAGE TO FIRST STORY TIED AND SPIRAL COLUMNS (UNIT A). NOTE DISTRESS IN BEAM-COLUMN JOINT AND IN SECOND STORY TIED COLUMN

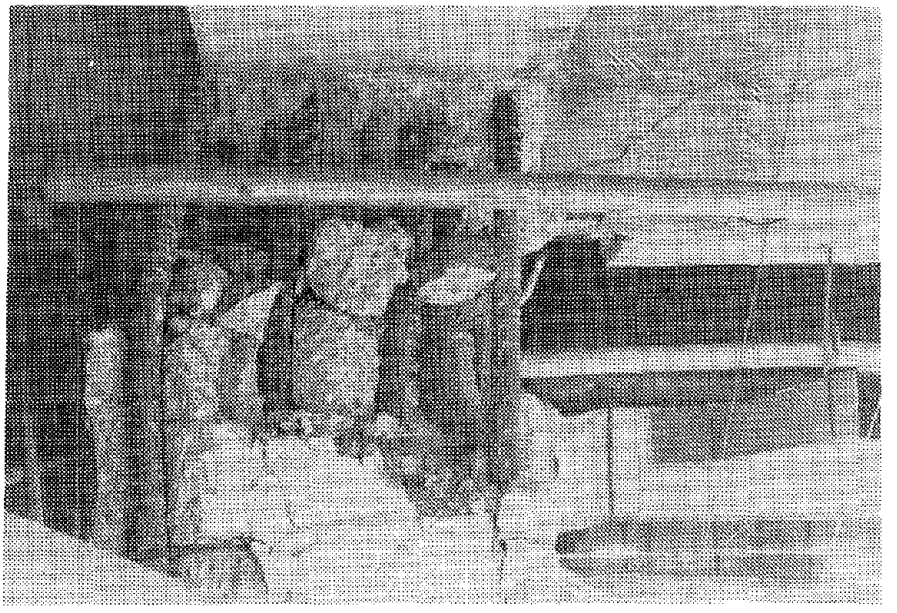

FIG. 3.13 SHEAR FAILURE AT TOP OF GROUND STORY COLUMN M-29 DUE TO TERMINATION OF SPIRALS BELOW LOWEST MEMBER FRAMING INTO COLUMN

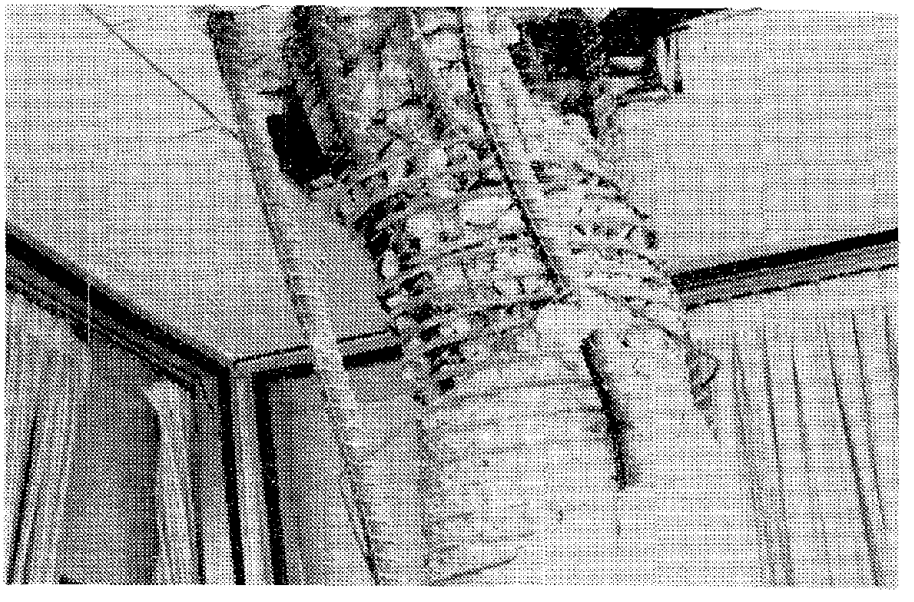

FIG. 3.14 SHEAR FAILURE AT TOP OF FIRST STORY COLUMN Z-18 DUE TO TERMINATION OF SPIRALS OUTSIDE OF BEAM COLUMN JOINT

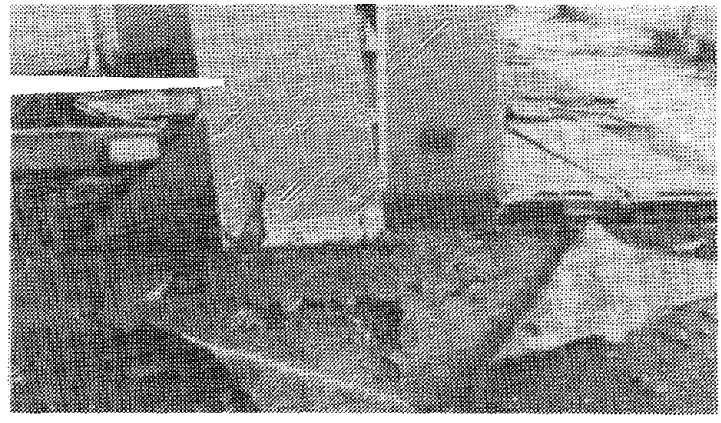

(a) SLAB NEAR COLUMN H-26

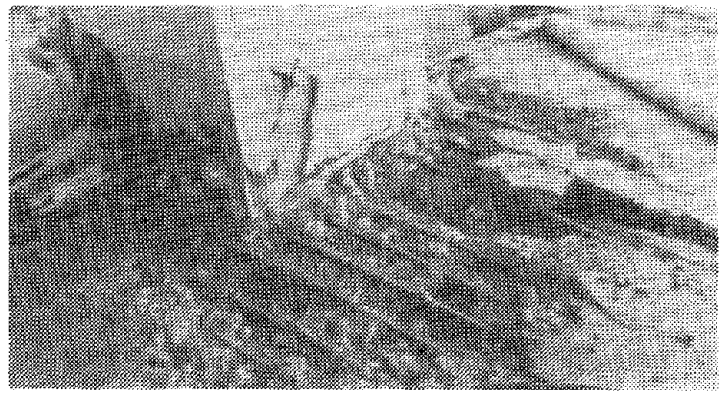

(b) SLAB NEAR COLUMN H-26 AFTER RUBBLE REMOVED

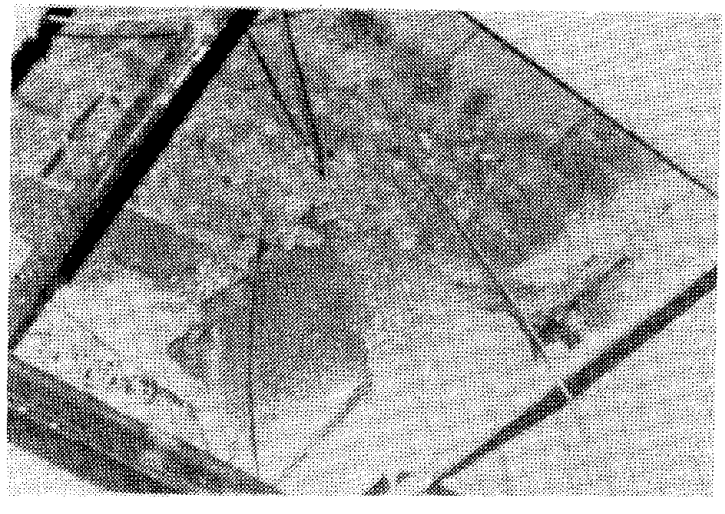

(c) UNDERSIDE OF SLAB NEAR COLUMN L-17

FIG. 3.15 DAMAGE TO FIRST FLOOR SLAB

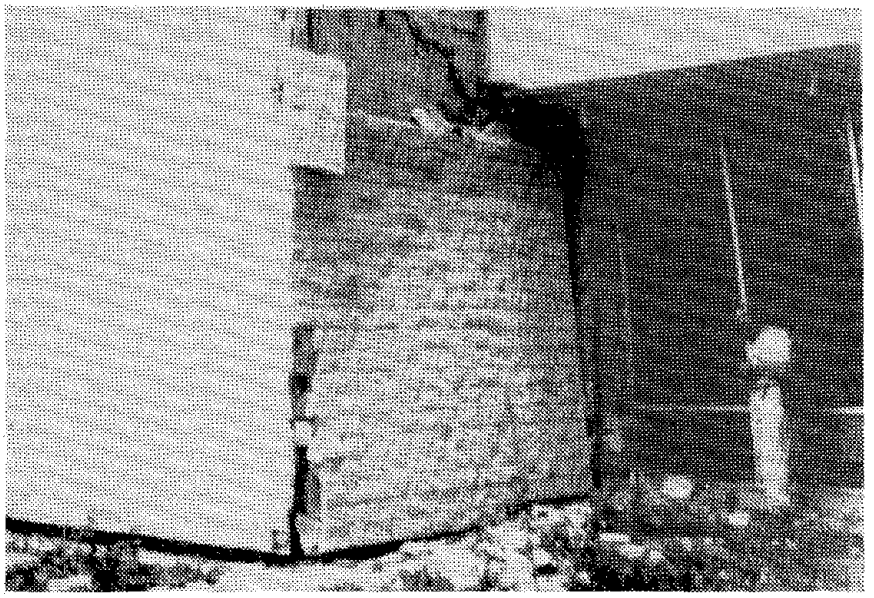

FIG. 3.16 DAMAGE IN FIRST STORY ELEVATOR SHAFT WALL NEAR P-19

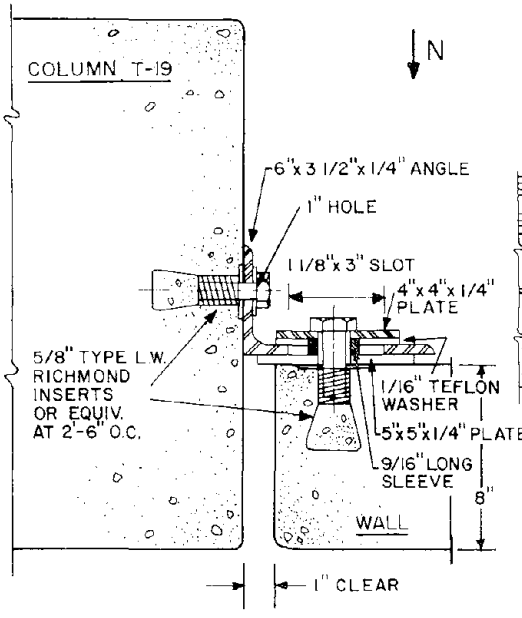

FIG. 3.17 DETAIL OF CONNECTION OF ELEVATOR SHAFT WALLS TO FIRST STORY COLUMNS

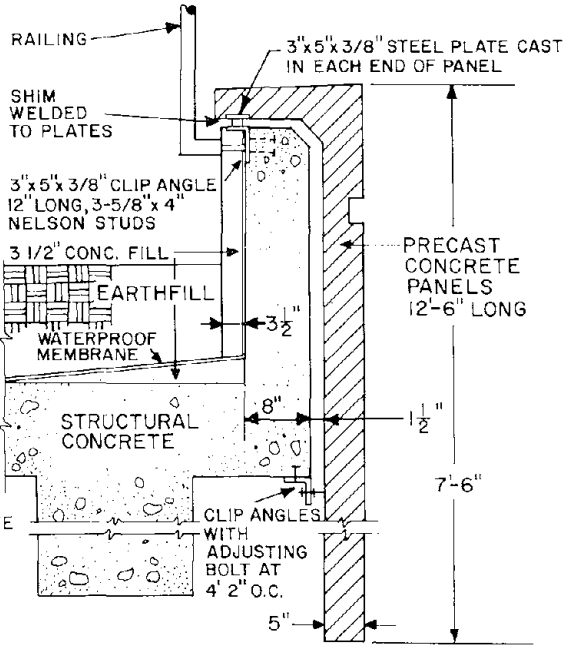

FIG. 3.18 DETAIL OF CONNECTION OF PRECAST PANELS TO TERRACE CANOPY PARAPET

FIG. 3.19 DETAILS OF DAMAGE TO PRECAST PANELS

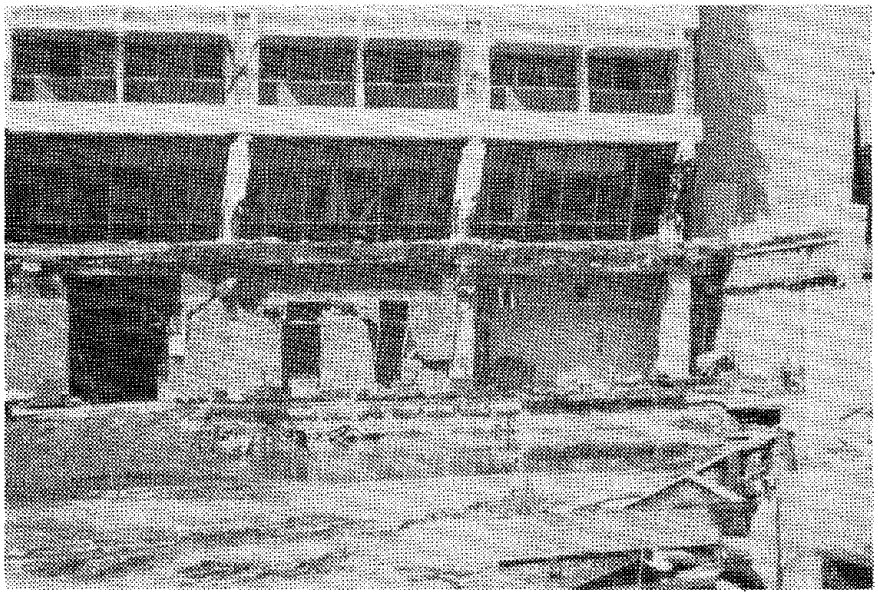

FIG. 3.20 DETAIL OF DAMAGE TO WING C AFTER REMOVAL OF COLLAPSED TERRACE CANOPY SHOWING DISTRIBUTION OF DAMAGE TO LOWER THREE STORIES. NOTE DAMAGE TO NONSTRUCTURAL MASONRY PARTITIONS IN GROUND STORY

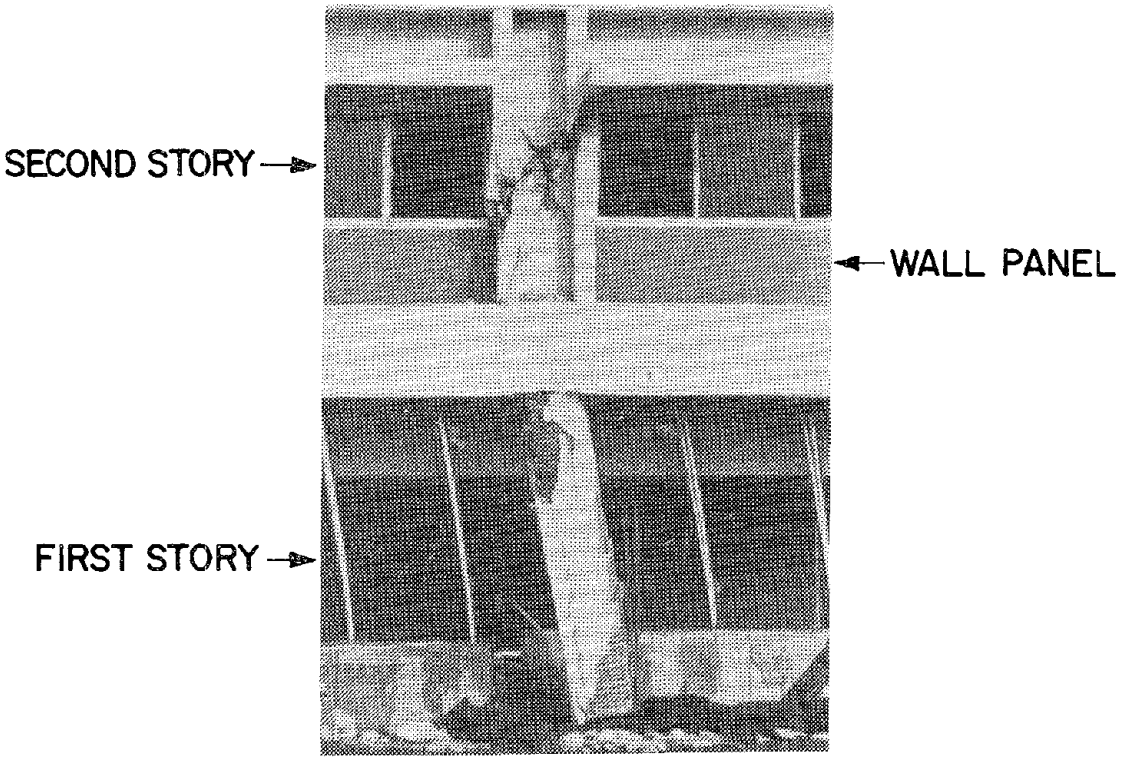

FIG. 3.21 COMPARISON OF DAMAGE TO FIRST STORY SPIRAL COLUMNS AND SECOND STORY TIED COLUMNS IN UNIT A (J-7). NOTE SEVERE NONSTRUCTURAL DAMAGE.

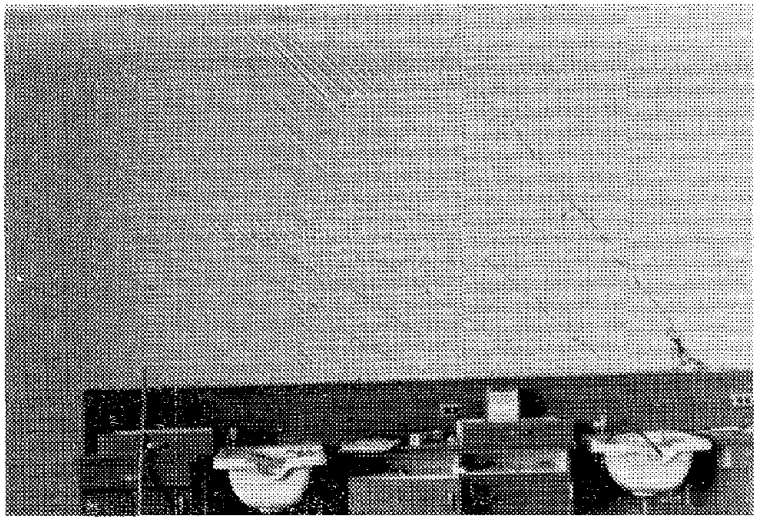

FIG. 3.22 CRACKING IN PLASTER COVERING STRUCTURAL WALL J-L-12 IN SECOND STORY

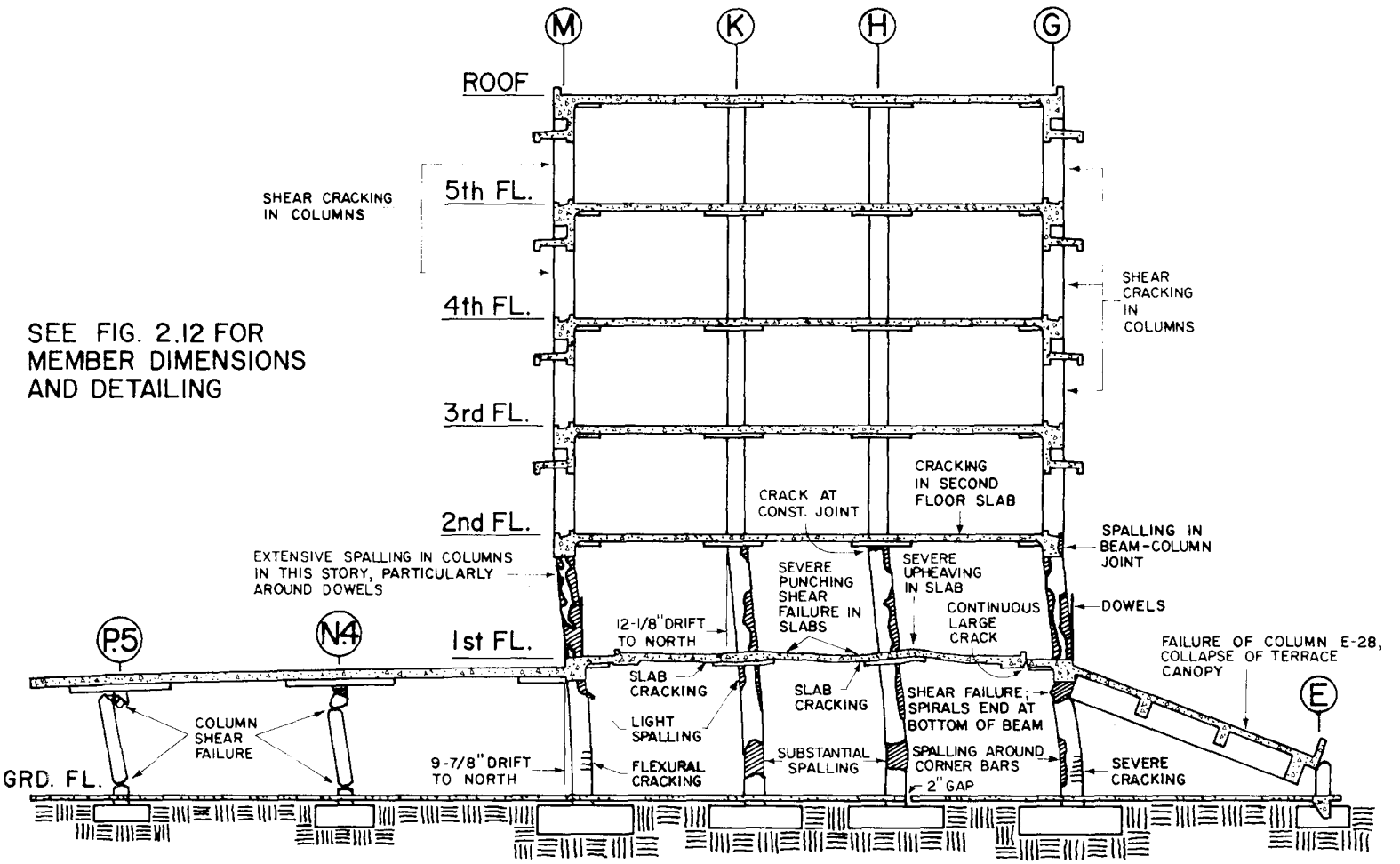

FIG. 3.23 SCHEMATIC DIAGRAM OF DAMAGE TO FRAME 28

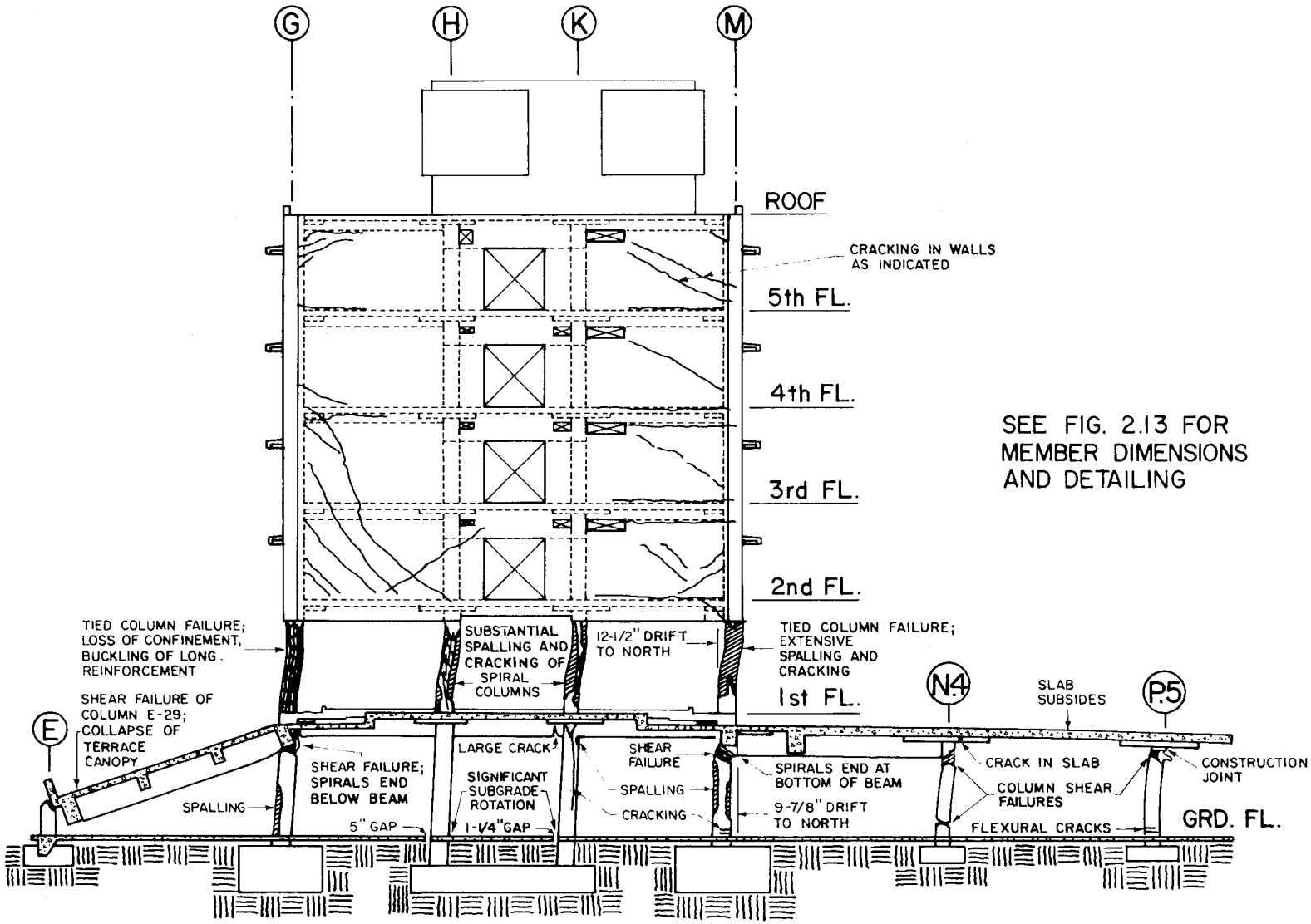

FIG. 3.24 SCHEMATIC DIAGRAM OF DAMAGE TO FRAME 29

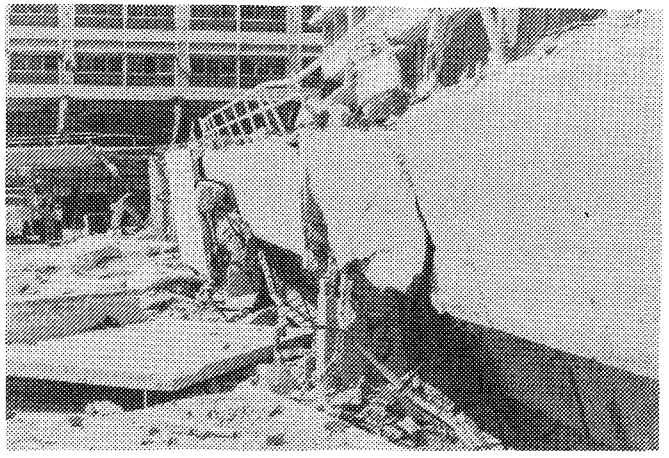

FIG. 3.25 BRITTLE SHEAR FAILURE OF TIED COLUMNS SUPPORTING SOUTHERN EDGE OF TERRACE CANOPY (COLUMN E-27 IN FOREGROUND

FIG. 3.26 SHEAR FAILURE AT BOTTOM OF TIED COLUMN P-27

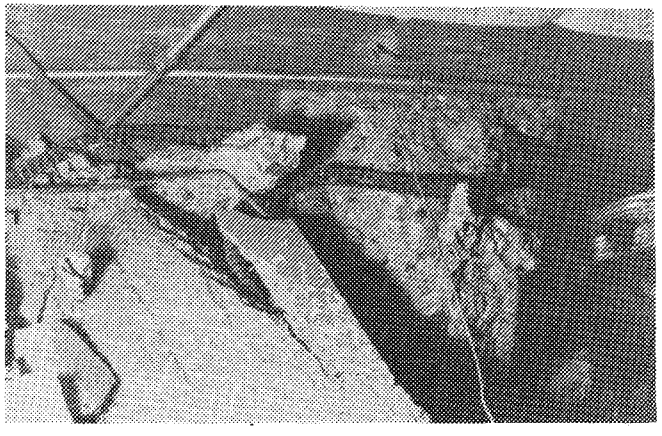

FIG. 3.27 SHEAR FAILURE AT TOP TIED COLUMN P-27

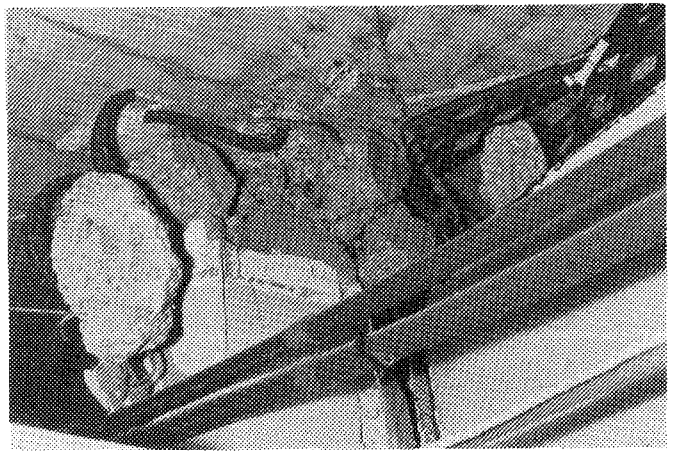

FIG. 3.28 SHEAR FAILURE AT TOP OF COLUMN P-16 SUPPORTING COURTYARD

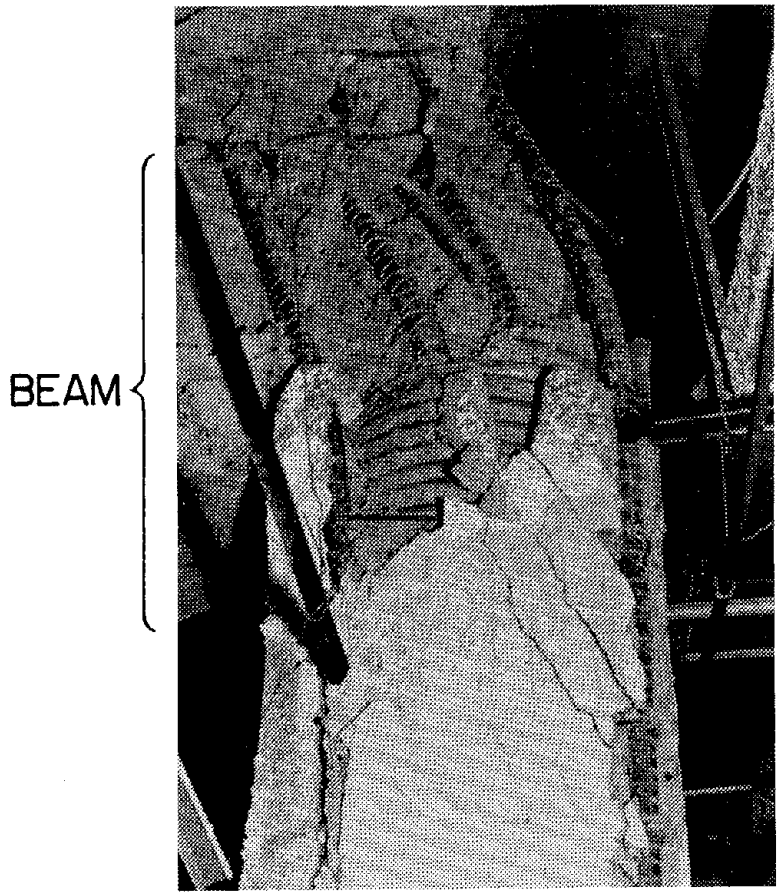

FIG. 3.29 JOINT FAILURE IN GROUND STORY COLUMN G-27. NOTE THAT SPIRALS TERMINATE BELOW DEEP BEAM FRAMING INTO COLUMN FROM TERRACE CANOPY ON LEFT

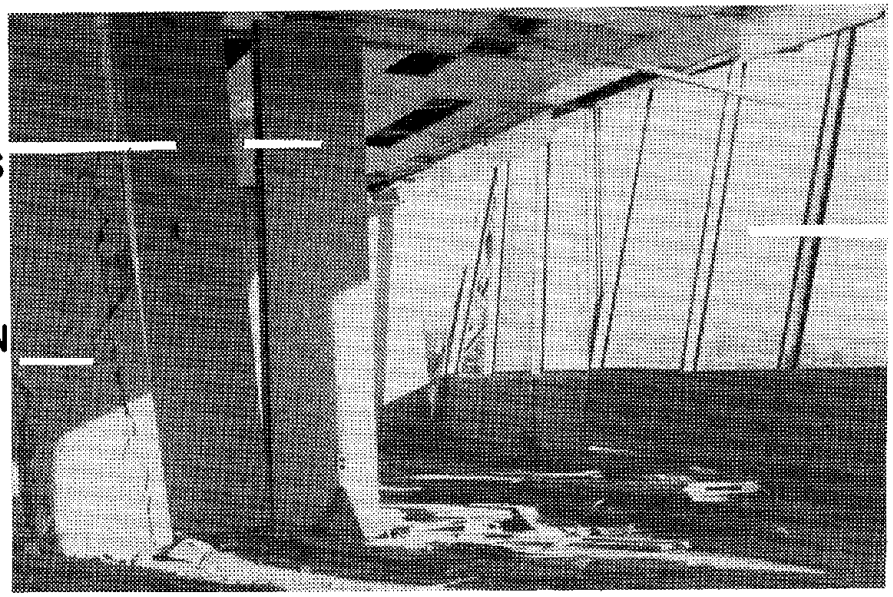

FIG. 3.30 GENERAL VIEW OF FIRST STORY DAMAGE AT H-27

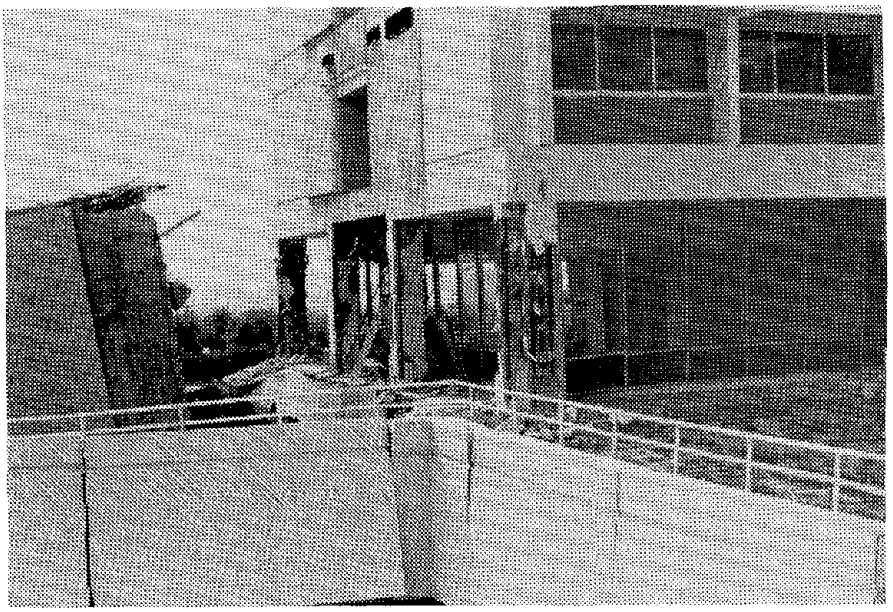

(a) GENERAL VIEW OF FRAME 29-FIRST STORY

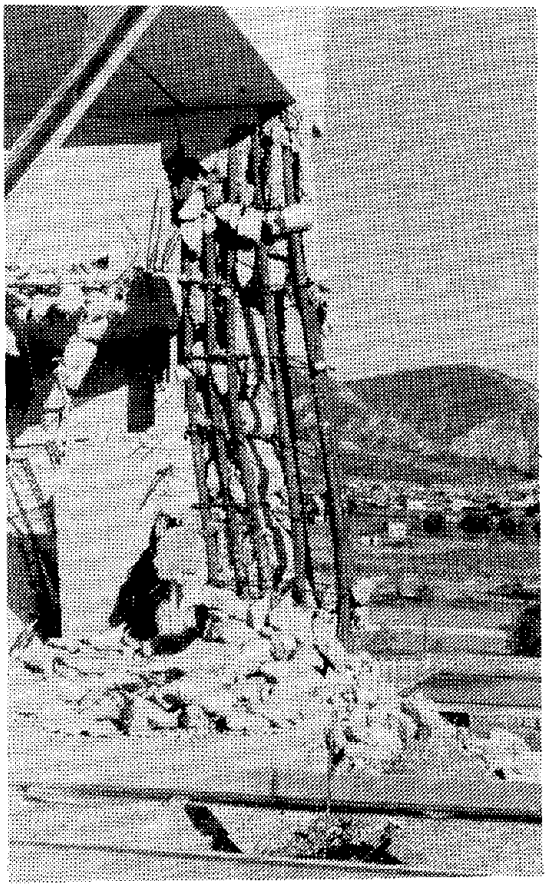

(b) DETAIL OF DAMAGE TO G-29

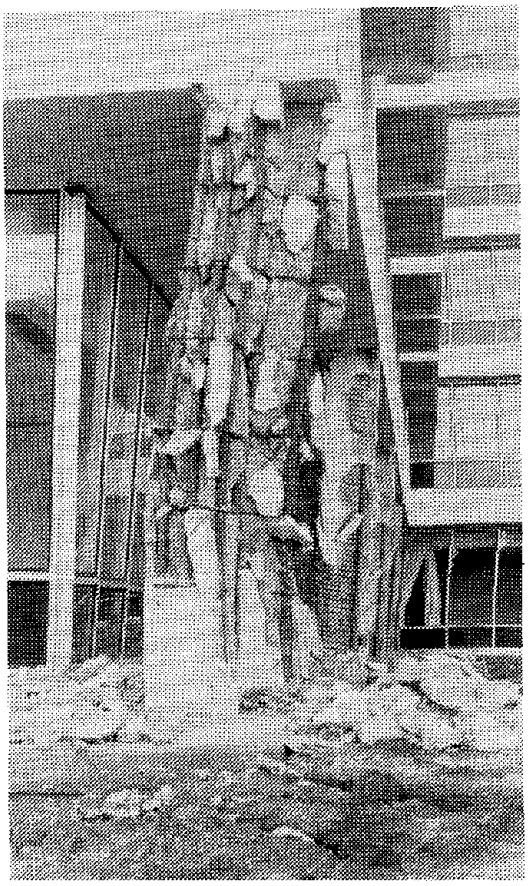

(c) DETAIL OF DAMAGE TO M-29

FIG. 3.31 STRUCTURAL DAMAGE TO FRAME 29 IN FIRST STORY

(a) COLUMN G-17 (b) COLUMN N-16 (c) COLUMN H-22 (d) COLUMN H-28

FIG. 3.32 TYPICAL FIRST FLOOR COLUMN DAMAGE

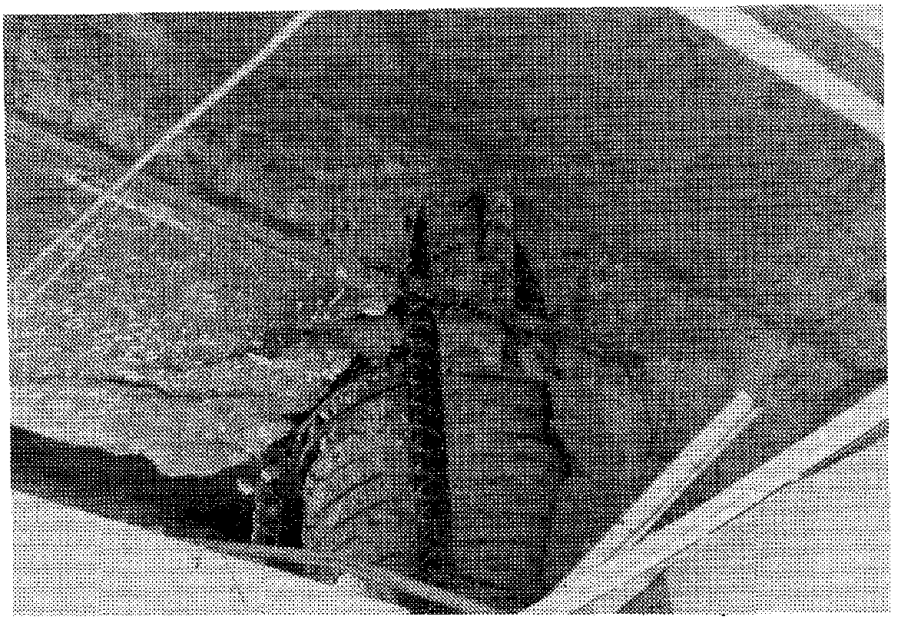

FIG. 3.33 SHEAR FAILURE OF JOINT AT TOP OF FIRST STORY SPIRAL COLUMN L-17. SPIRALS TERMINATE AT BOTTOM OF BEAM FRAMING INTO COLUMN FROM ONLY ONE SIDE

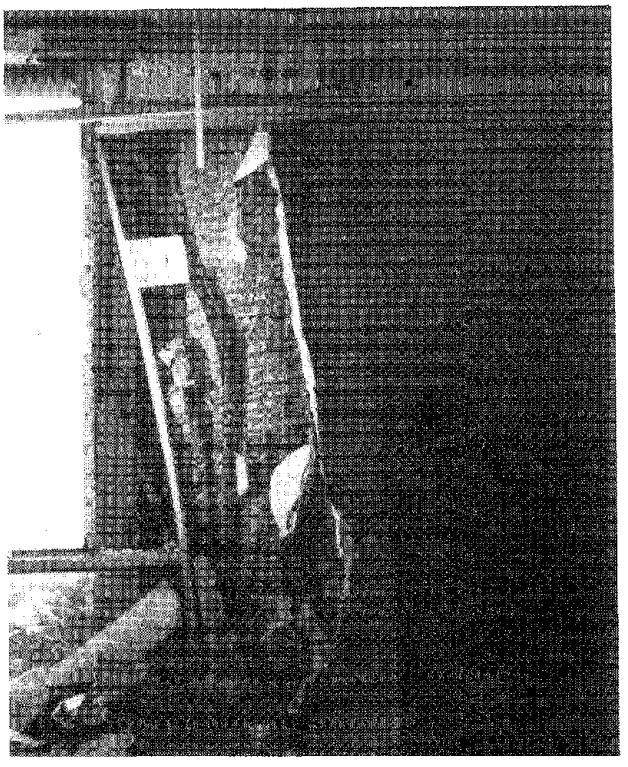

FIG. 3.34 FAILURE OF MECHANICAL CLAMPING DEVICE IN COLUMN

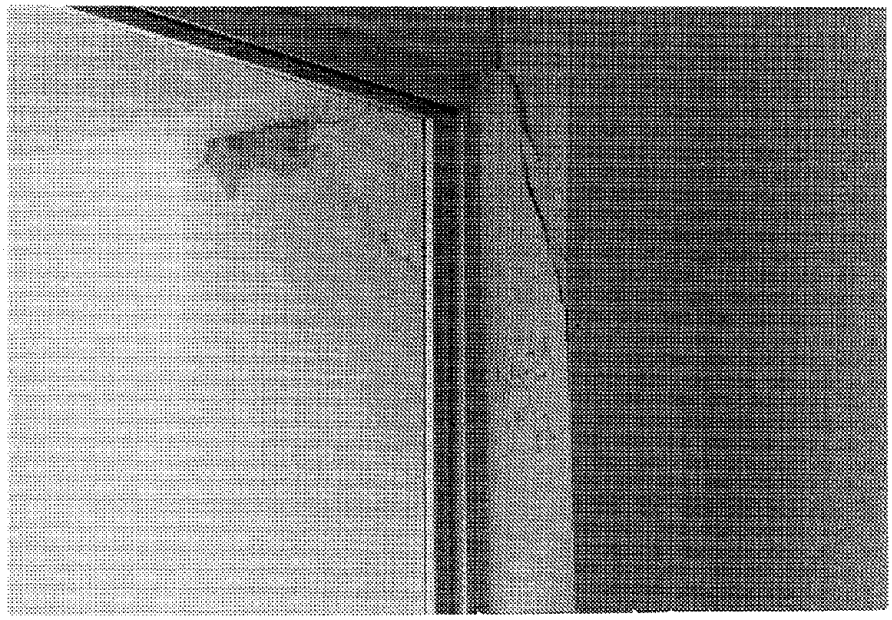

FIG. 3.35 CRACKING IN COLUMN M-29 IN THIRD STORY. COLUMN MONOLITHIC WITH STRUCTURAL WALL

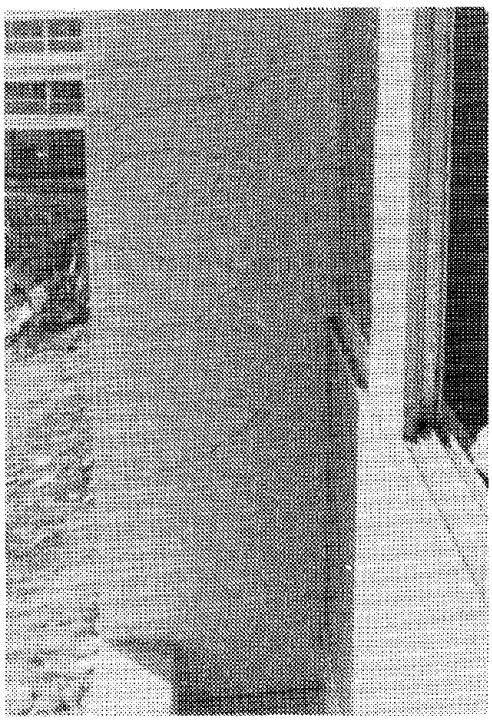

(a) EAST FACE OF COLUMN-28, SECOND STORY

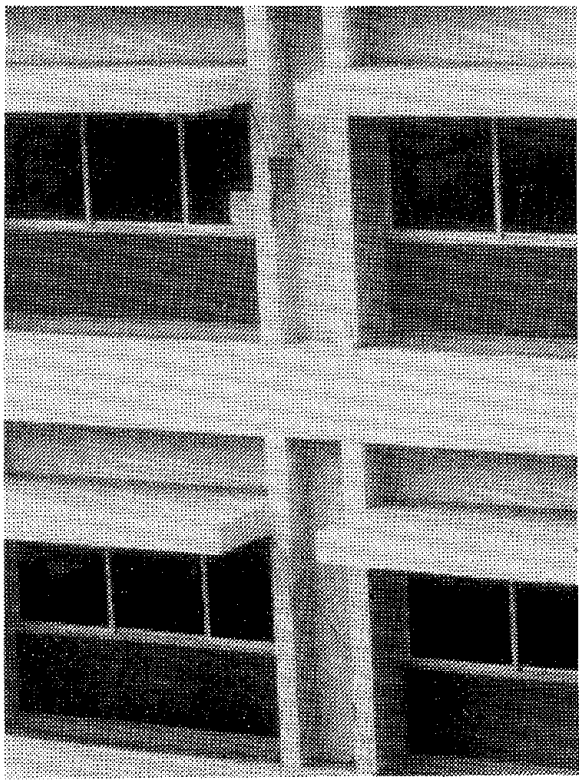

(b) NORTH FACE OF COLUMN-28, FOURTH AND FIFTH STORIES

FIG. 3.36 DETAILS OF DAMAGE TO EXTERIOR CHANNEL COLUMNS

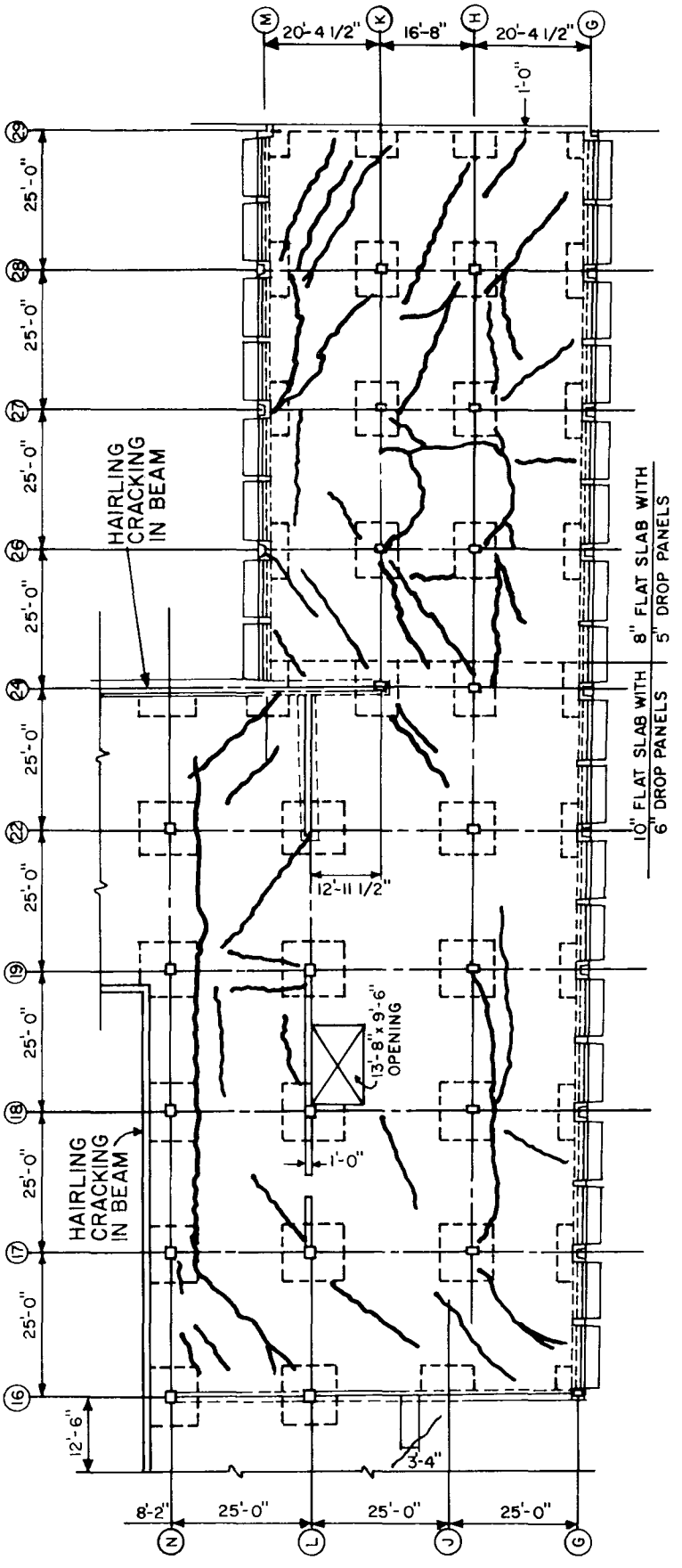

FIG. 3.37 CRACKING PATTERN OBSERVED AT TOP SURFACE OF SECOND FLOOR SLAB, WING D

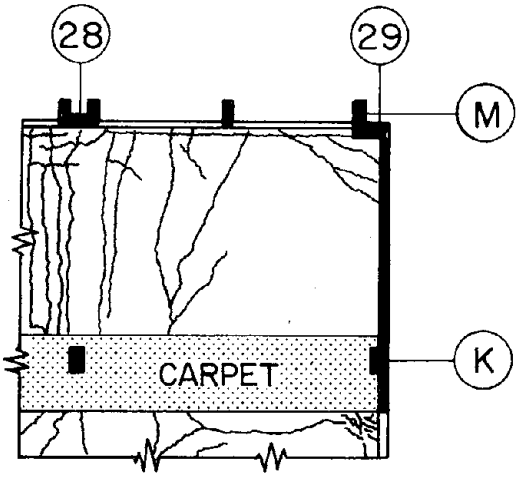

FIG. 3.38 CRACKING PATTERN OBSERVED AT TOP SURFACE OF FOURTH FLOOR SLAB, WING D

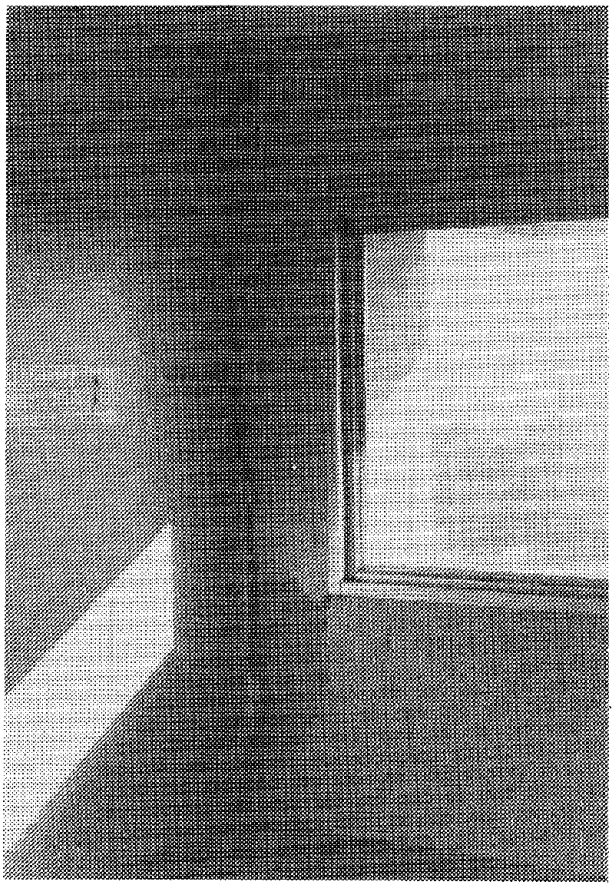

FIG. 3.39 DAMAGE TO PARTITIONS AT CONNECTIONS WITH STRUCTURAL ELEMENTS

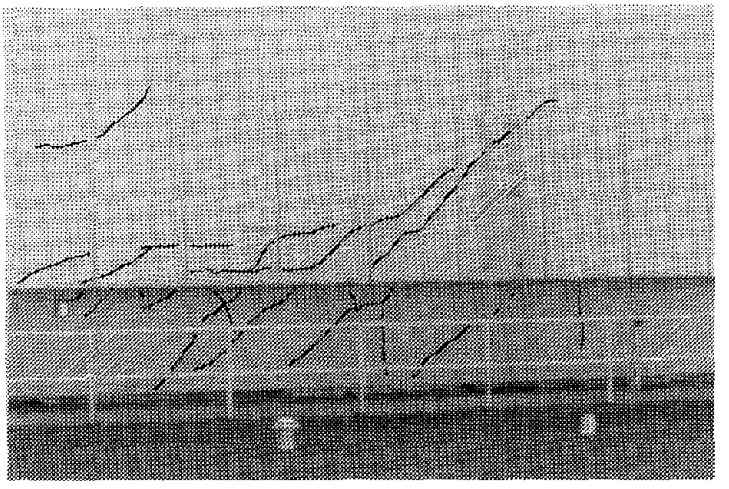

FIG. 3.40 CRACKING PATTERN IN NORTHWALL OF PENTHOUSE D BETWEEN COLUMN L-22 AND L-19

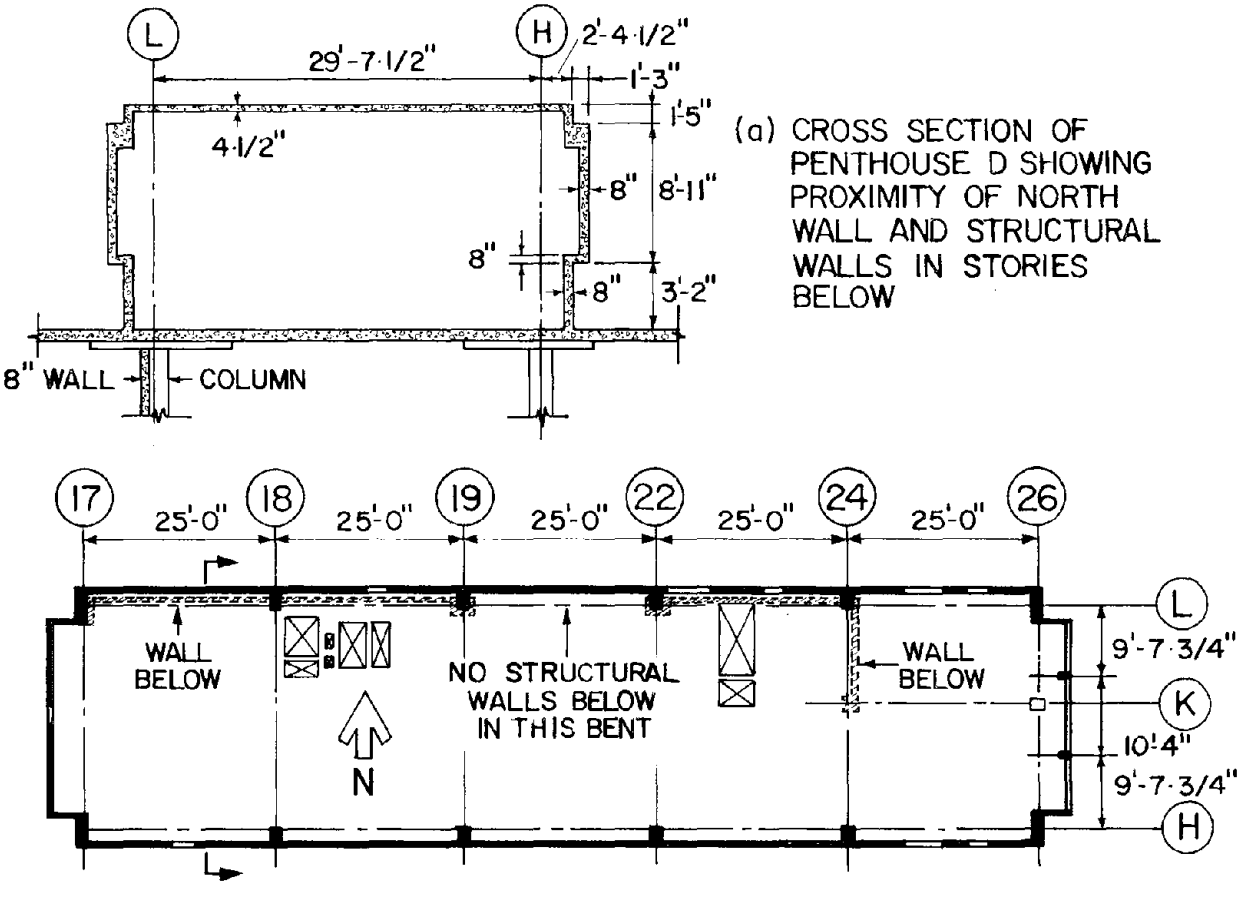

(b) FLOOR PLAN OF PENTHOUSE D

FIG. 3.41 DETAILS OF UNIT D PENTHOUSE

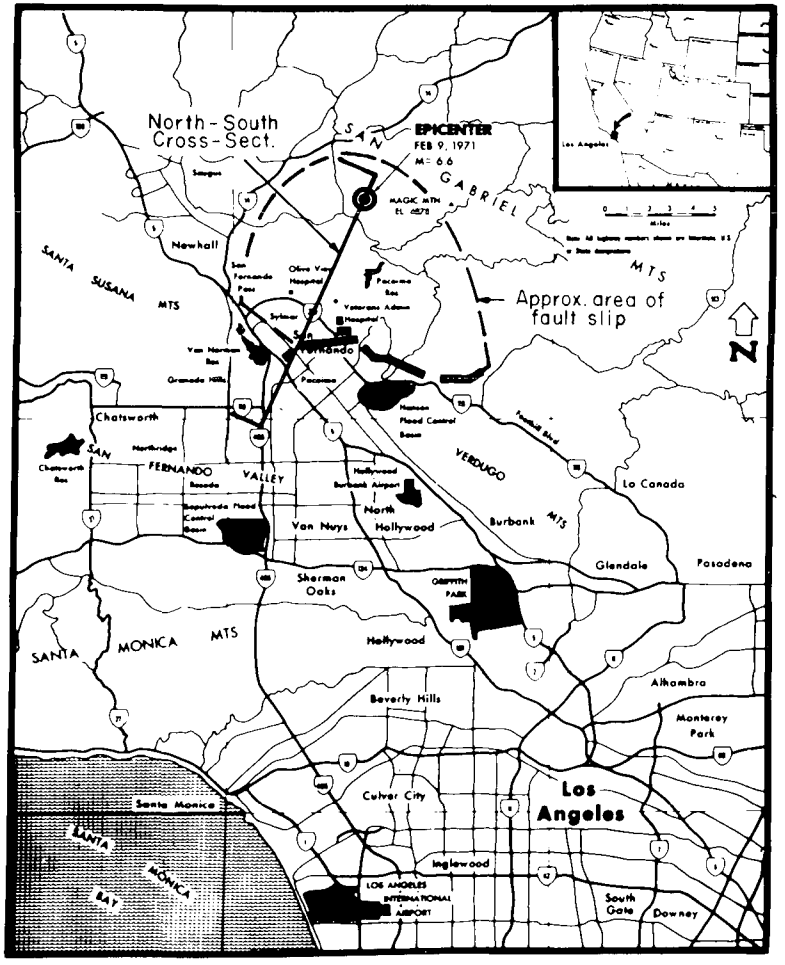

Heavy black lines show the approximate locations of the zone of surface faulting.

FIG. 4.1 THE SAN FERNANDO FAULT ZONE

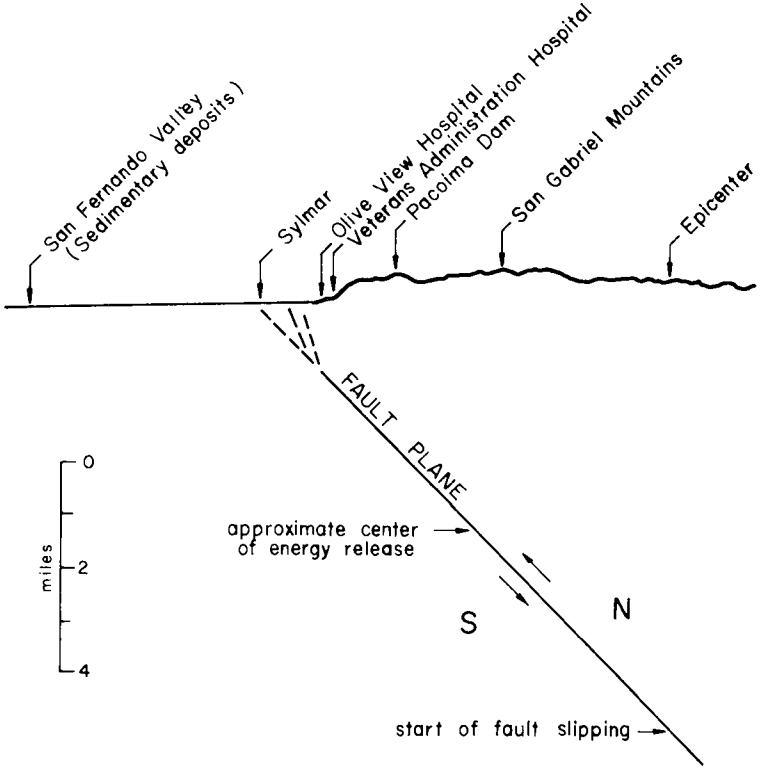

FIG. 4.2 SCHEMATIC N-S CROSS-SECTION SHOWING INFERRED FAULTING.

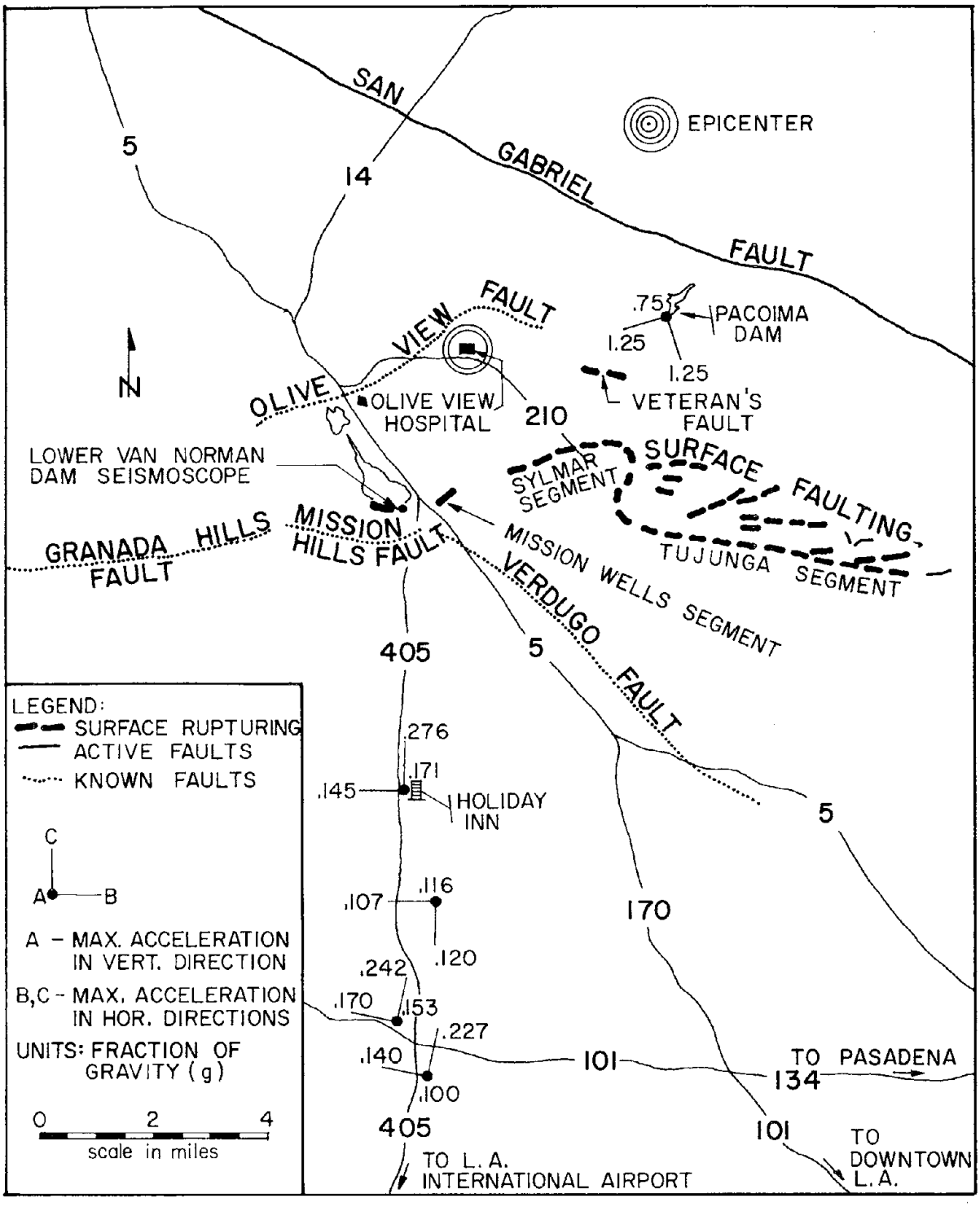

FIG. 4.3 LOCATION OF KNOWN FAULTS, SURFACE RUPTURING AND MAXIMUM RECORDED ACCELERATIONS IN THE VICINITY OF THE OLIVE VIEW HOSPITAL.

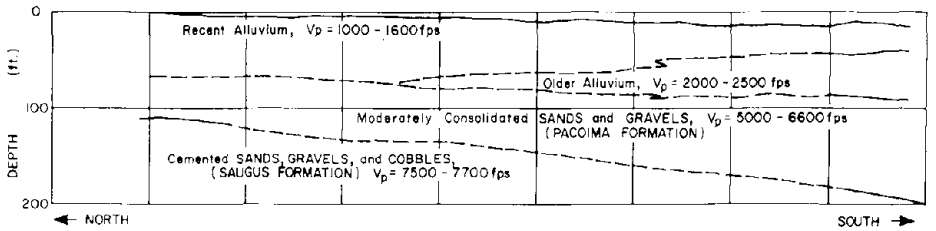

(a) TRAVERSE TAKEN WEST OF MAIN BUILDING

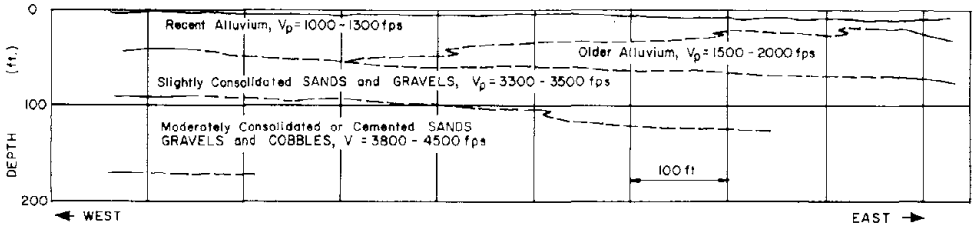

(b) TRAVERSE TAKEN SOUTH OF MAIN BUILDING

FIG. 4.4 INTERPRETED SOIL PROFILES FROM SEISMIC REFRACTION SURVEYS TAKEN FROM REF. 4.7

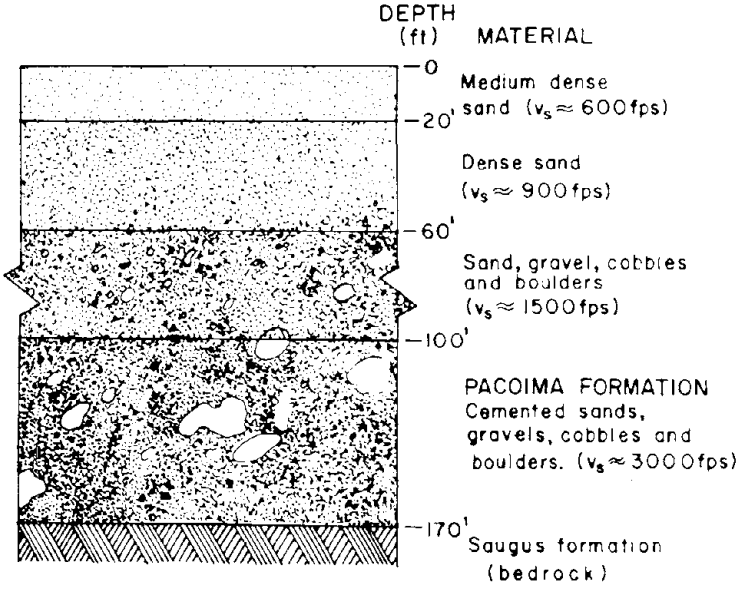

FIG. 4.5 IDEALIZED SOIL PROFILE FOR OLIVE VIEW SITE

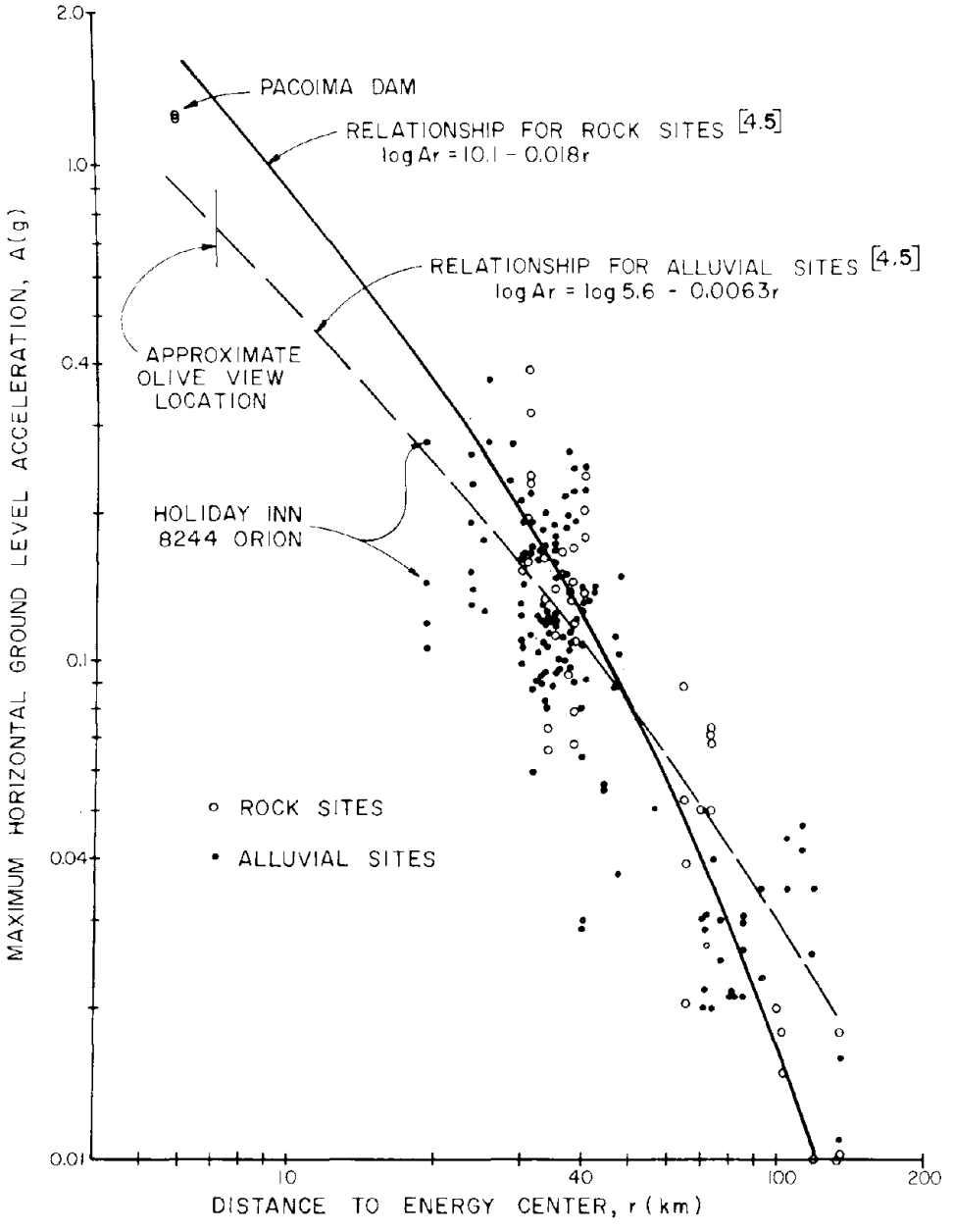

FIG. 4.6 RELATIONSHIP BETWEEN MAXIMUM RECORDED HORIZONTAL ACCELERATION AND DISTANCE TO CENTER OF ENERGY RELEASE

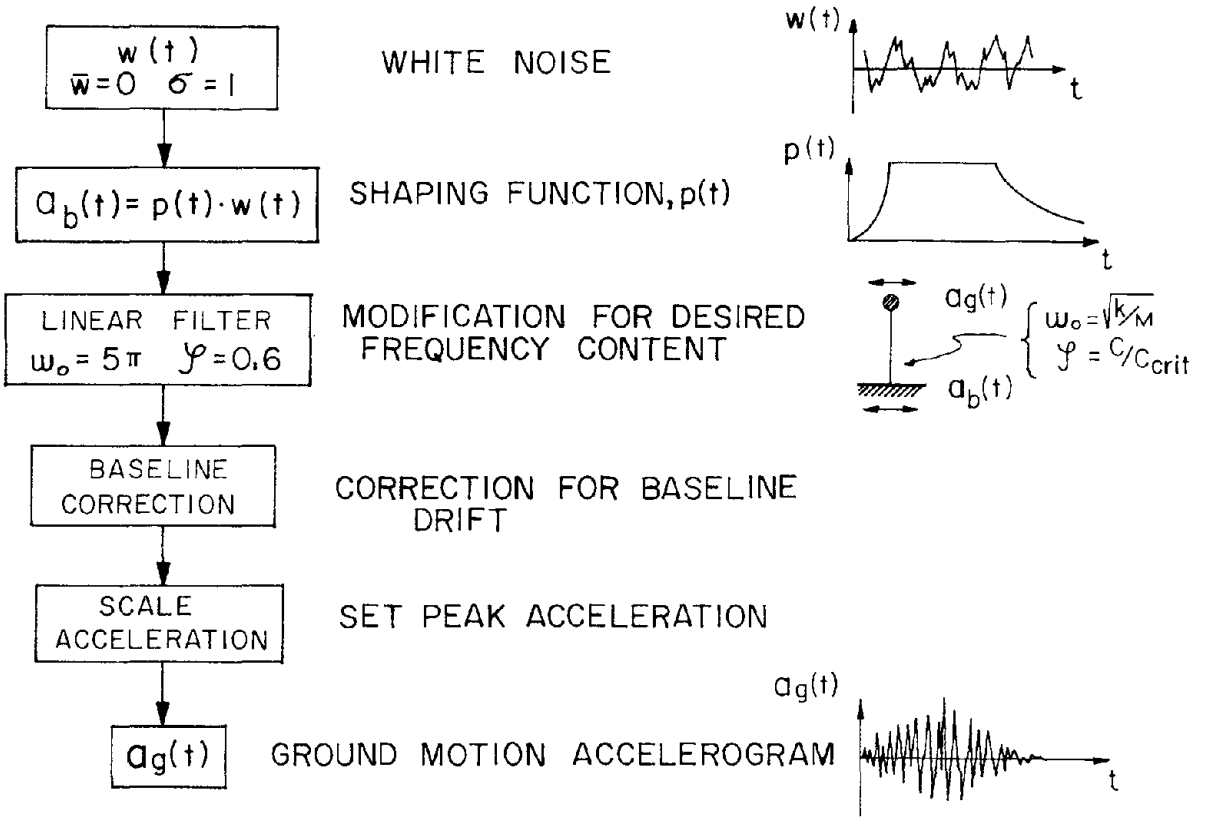

FIG. 4.7 SCHEMATIC OF METHOD FOR GENERATING ARTIFICIAL EARTHQUAKE GROUND MOTIONS

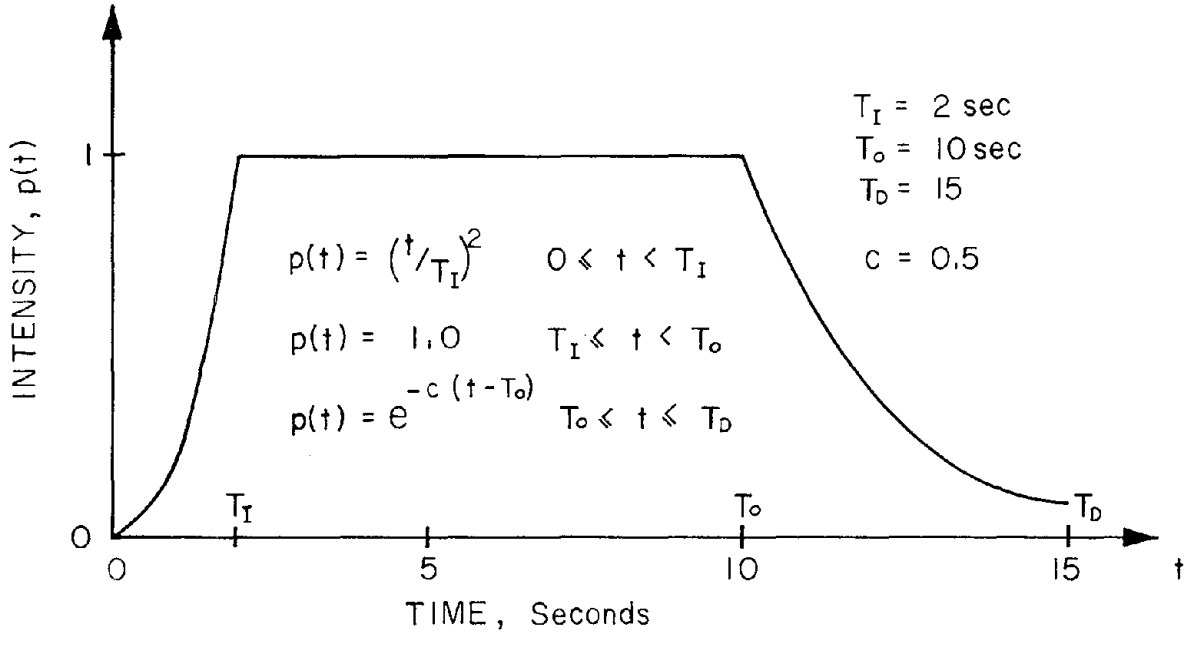

FIG. 4.8 SHAPING FUNCTION USED FOR OLIVE VIEW SITE

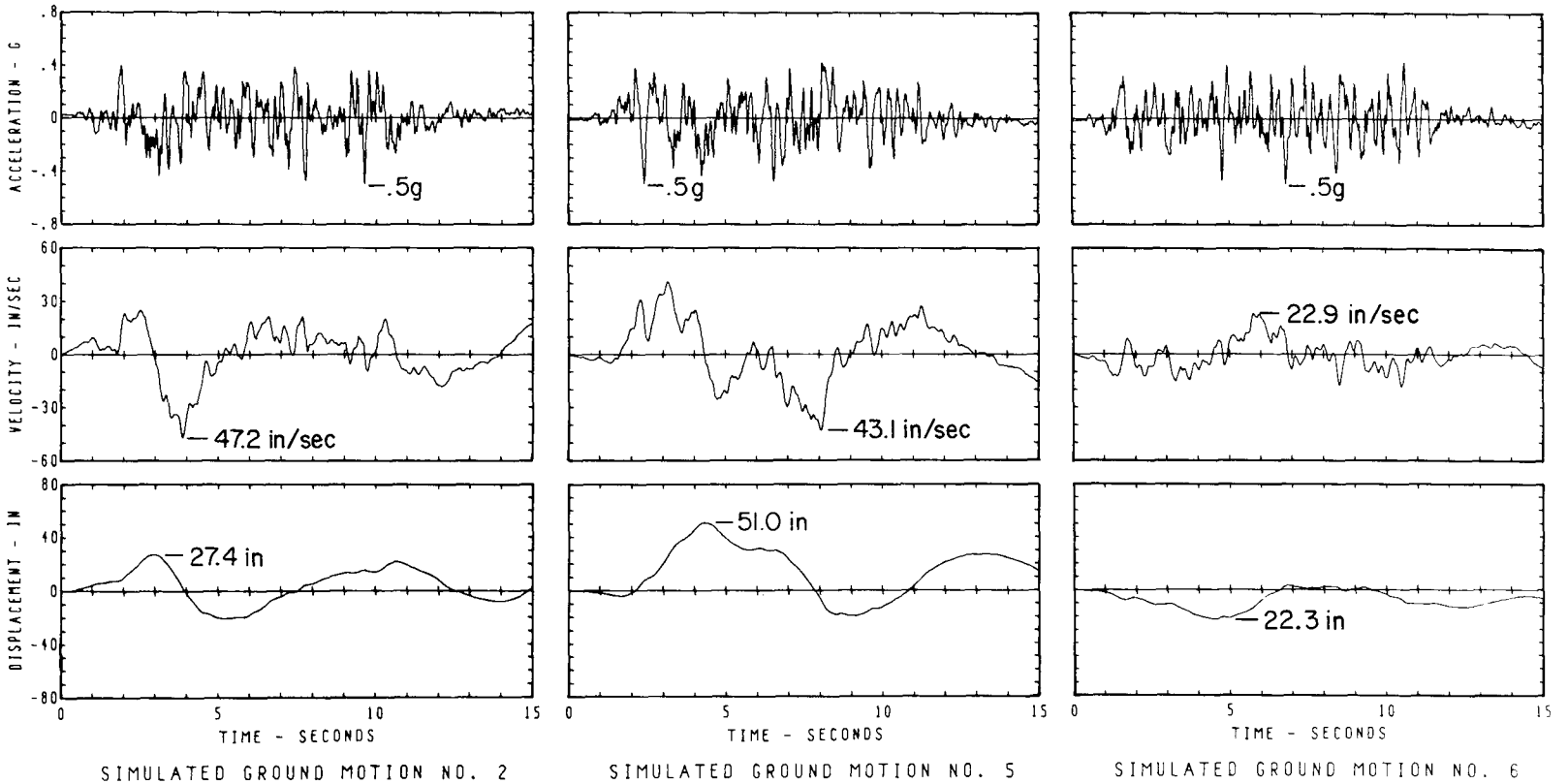

FIG. 4.9 TYPICAL SIMULATED GROUND MOTION TIME HISTORIES

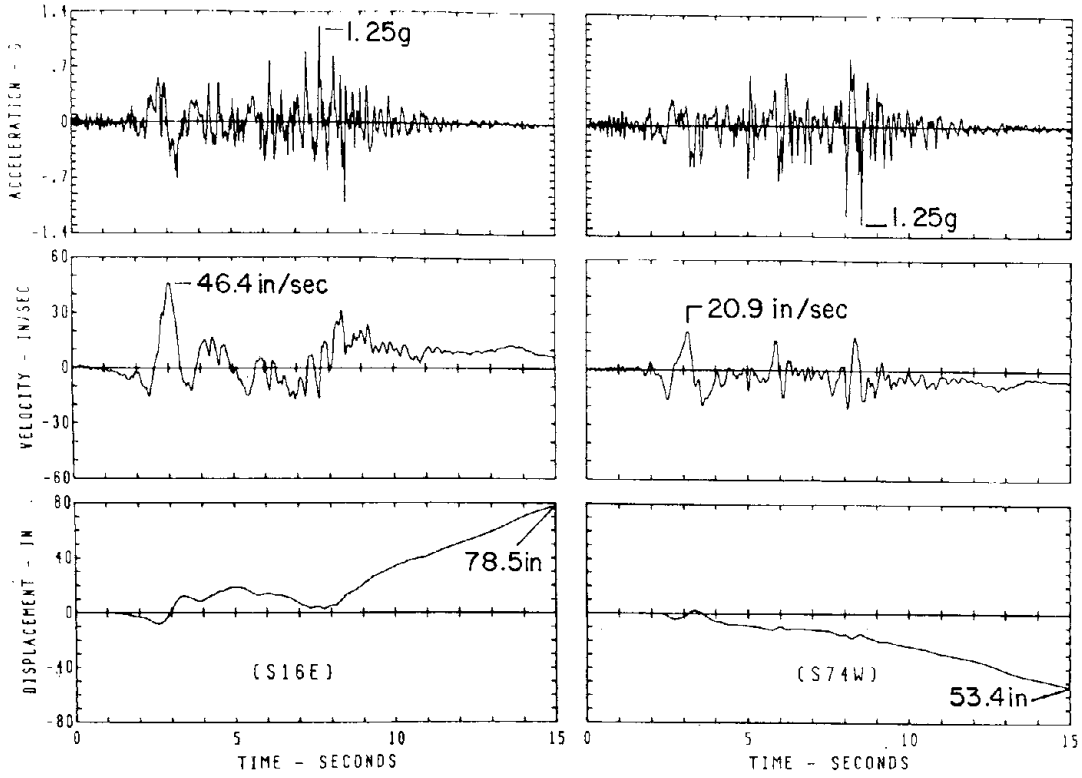

PACOIMA DAM RECORD

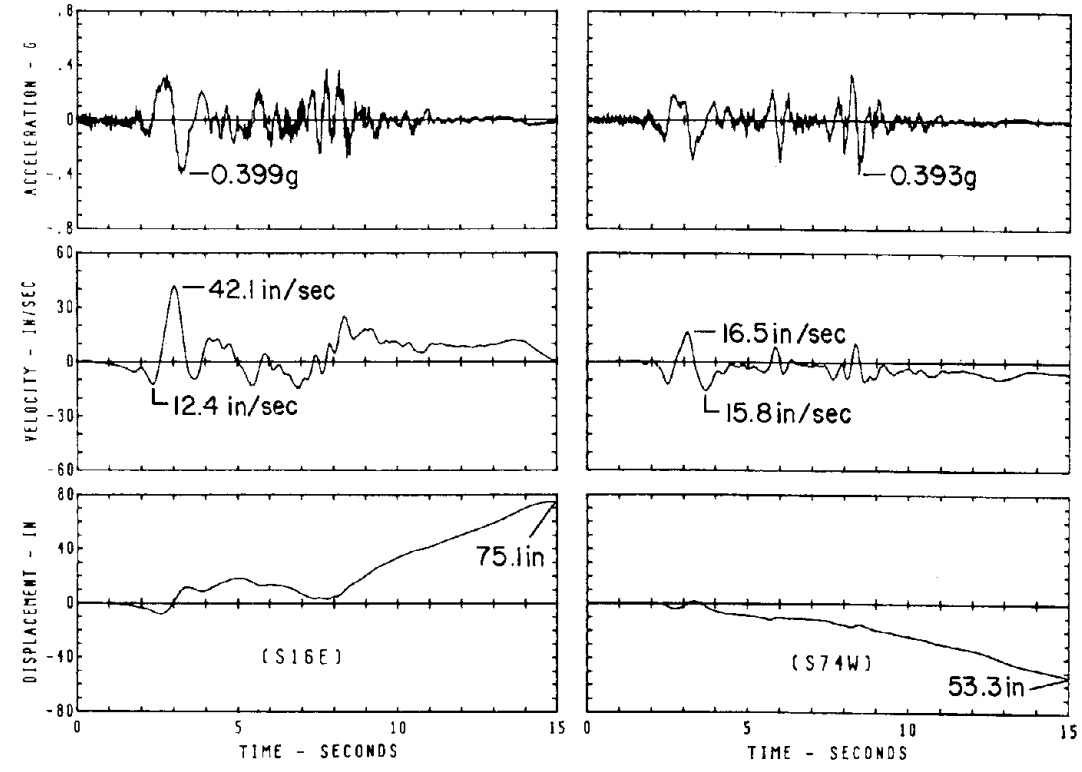

COMPUTED PACOIMA ROCK MOTION (REF. 4.20)

FIG. 4.10 GROUND MOTIONS FOR PACOIMA DAM SITE

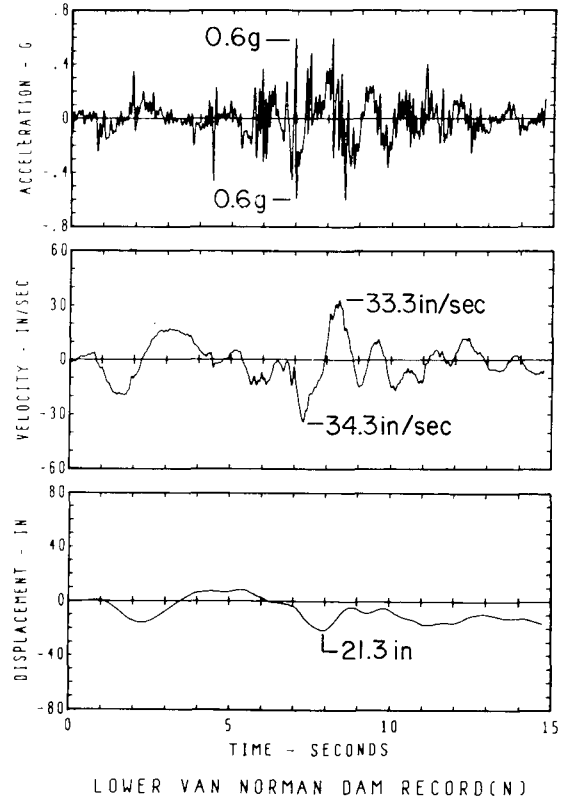

FIG. 4.11 GROUND MOTION DERIVED FROM SEISMOSCOPE RECORD AT THE ABUTMENT TO THE LOWER VAN NORMAN DAM (REF. 4.26)

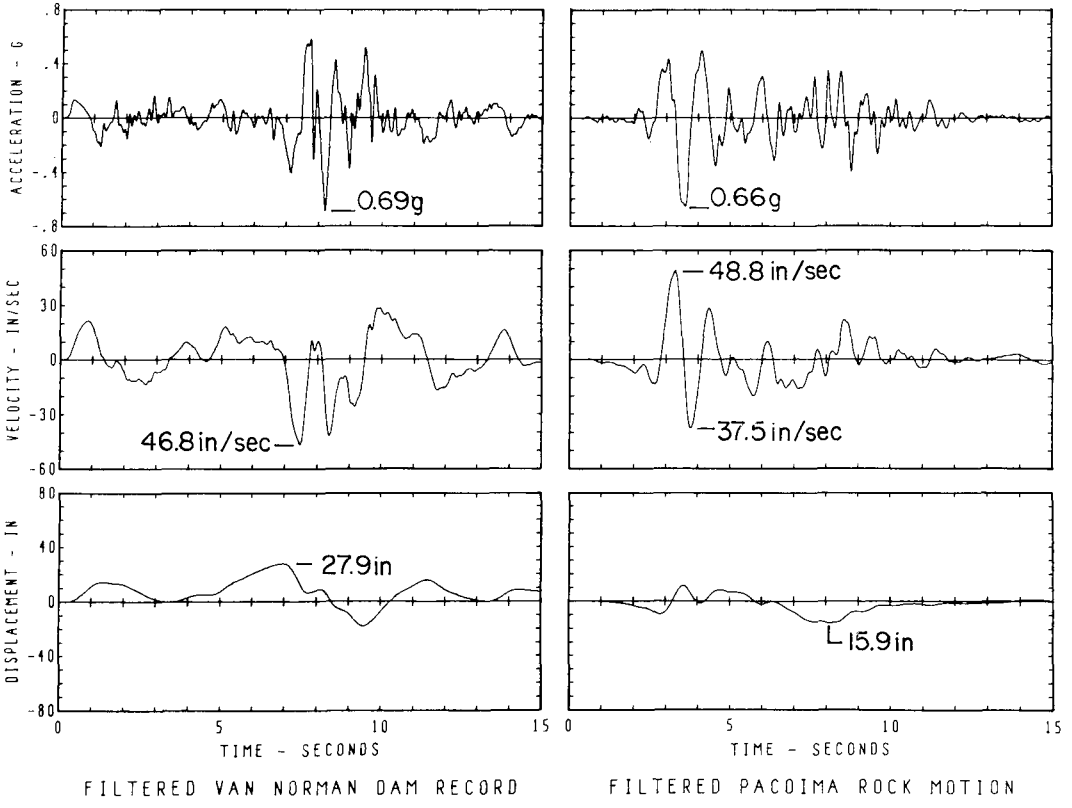

FIG. 4.12 FILTERED GROUND MOTION RECORDS DERIVED ASSUMMING HORIZONTAL SHEAR WAVE PROPAGATION THROUGH SOIL UNDERLYING OLIVE VIEW SITE (REF. 4.9)

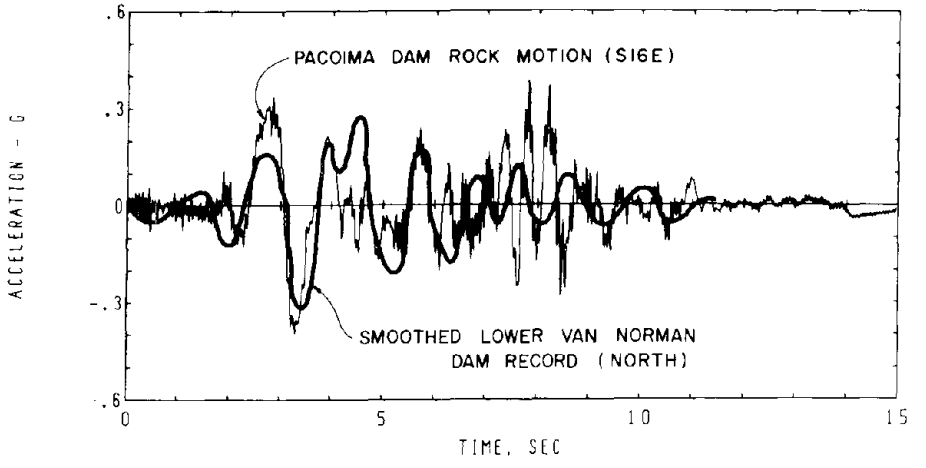

FIG. 4.13 COMPARISON OF CALCULATED PACOIMA ROCK MOTION AND LOWER VAN NORMAN DAM RECORD (SMOOTHED FOR CLARITY)

	GROUND MOTION	ACCELERATION -g-	VELOCITY -in/sec-	DISPLACEMENT -in-	SPECTRAL INTENSITY -ft- (1)
RECORDED	Pacoima Dam				
	-S16E-	1.25	46.4	78.5	N.A.
	-S74W-	1.25	20.9	53.4	6.22
SIMU-LATED	2	0.50	47.2	27.4	8.43
	5	0.50	43.1	51.0	8.15
	6	0.50	22.9	22.3	6.50
DERIVED	Pacoima Rock				
	-S16E-	0.399	42.1	75.1	10.61
	-S74W-	0.393	16.5	53.3	N.A.
	Lower Van Norman Dam N-S	0.600	34.3	21.3	11.51
FILTERED	Pacoima Rock -S16E-	0.658	48.8	15.9	16.96
	Lower Van Norman Dam	0.693	46.8	27.9	14.01

(1) 5% Damping , based on definition by Housner [4.23]

FIG. 4.14 SUMMARY OF PEAK GROUND MOTION VALUES

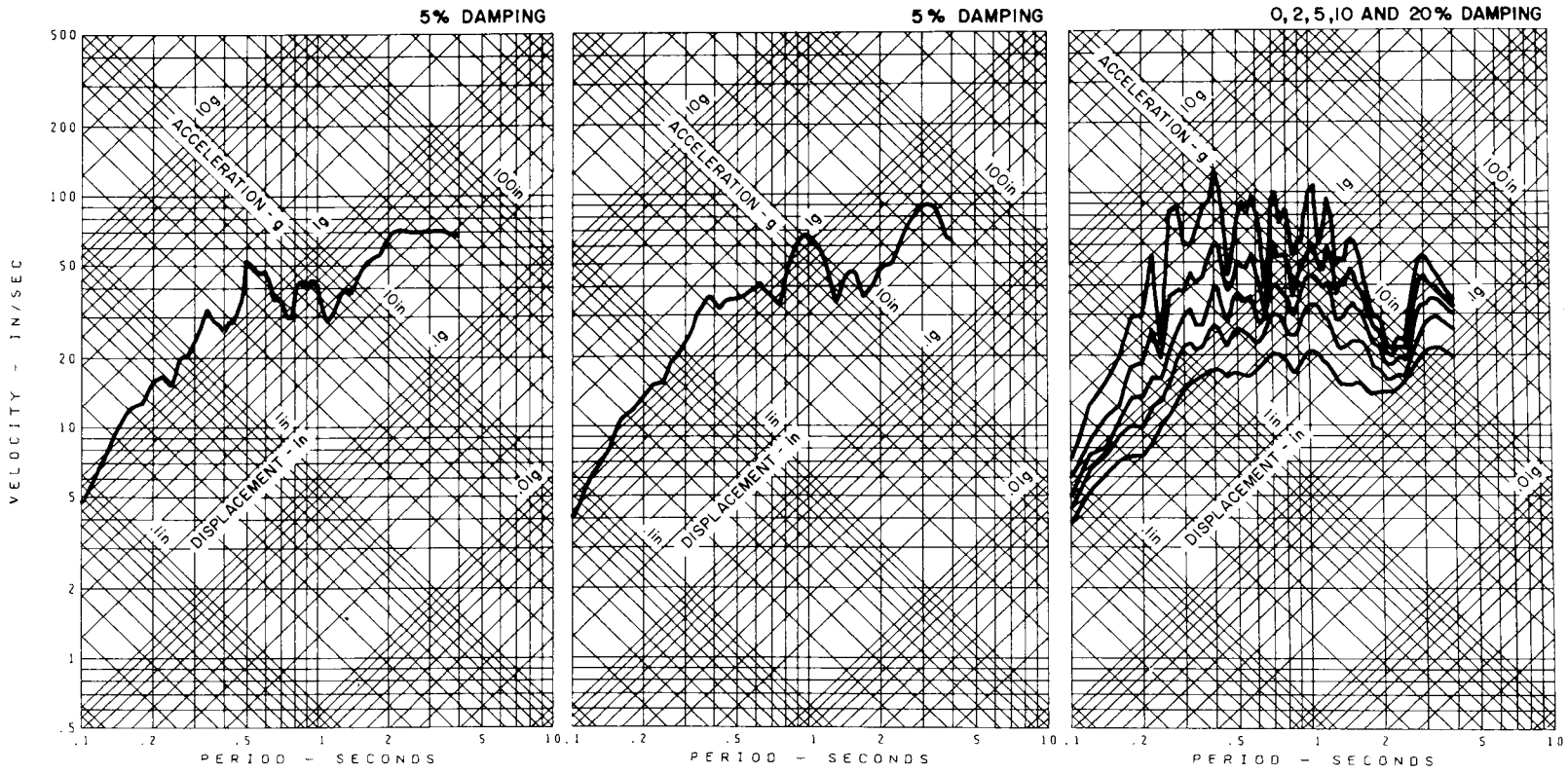

FIG. 4.15 TYPICAL TRIPARTITE RESPONSE SPECTRA FOR SIMULATED GROUND MOTIONS

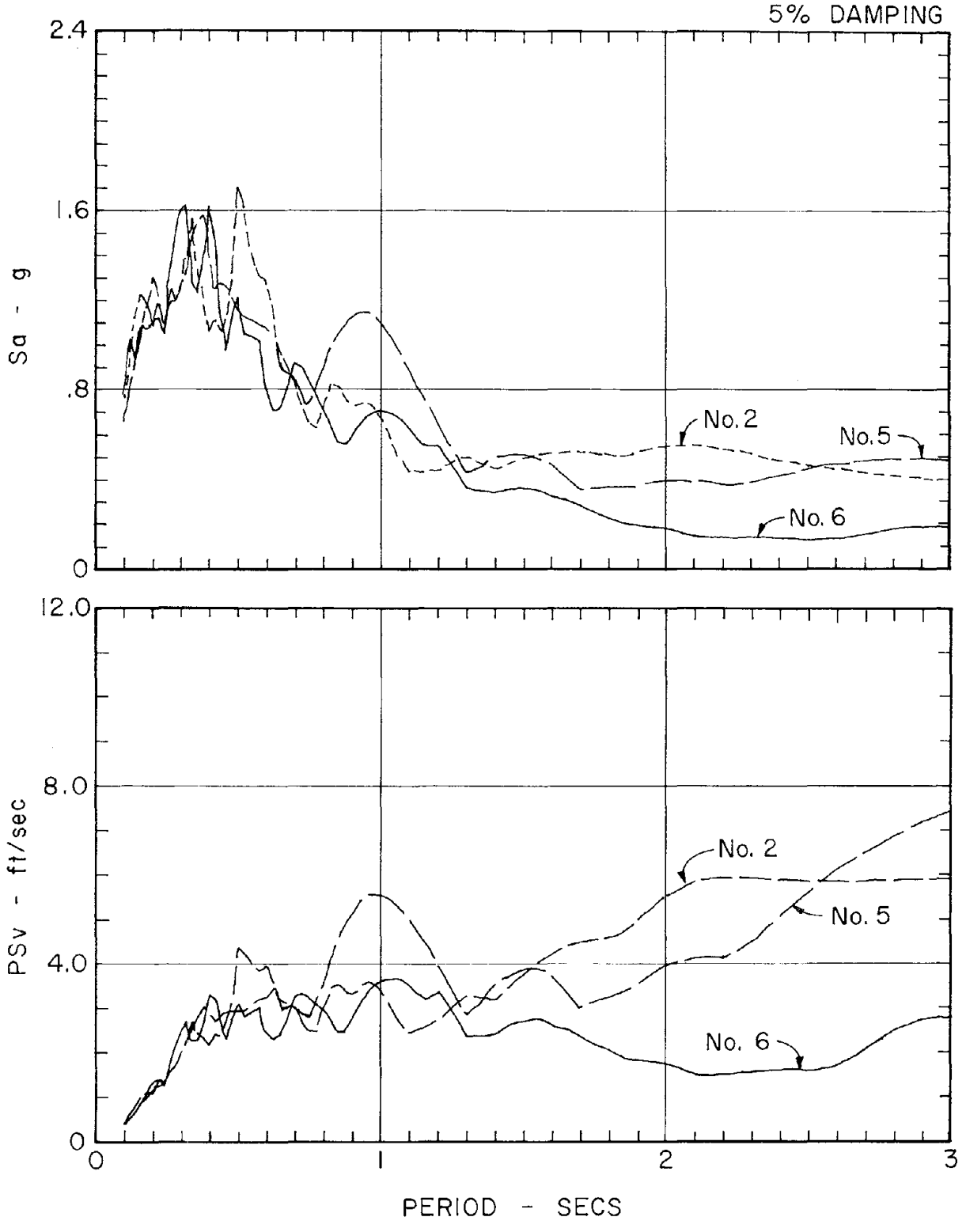

FIG. 4.16 COMPARISON OF RESPONSE SPECTRA FOR SIMULATED GROUND MOTION RECORDS

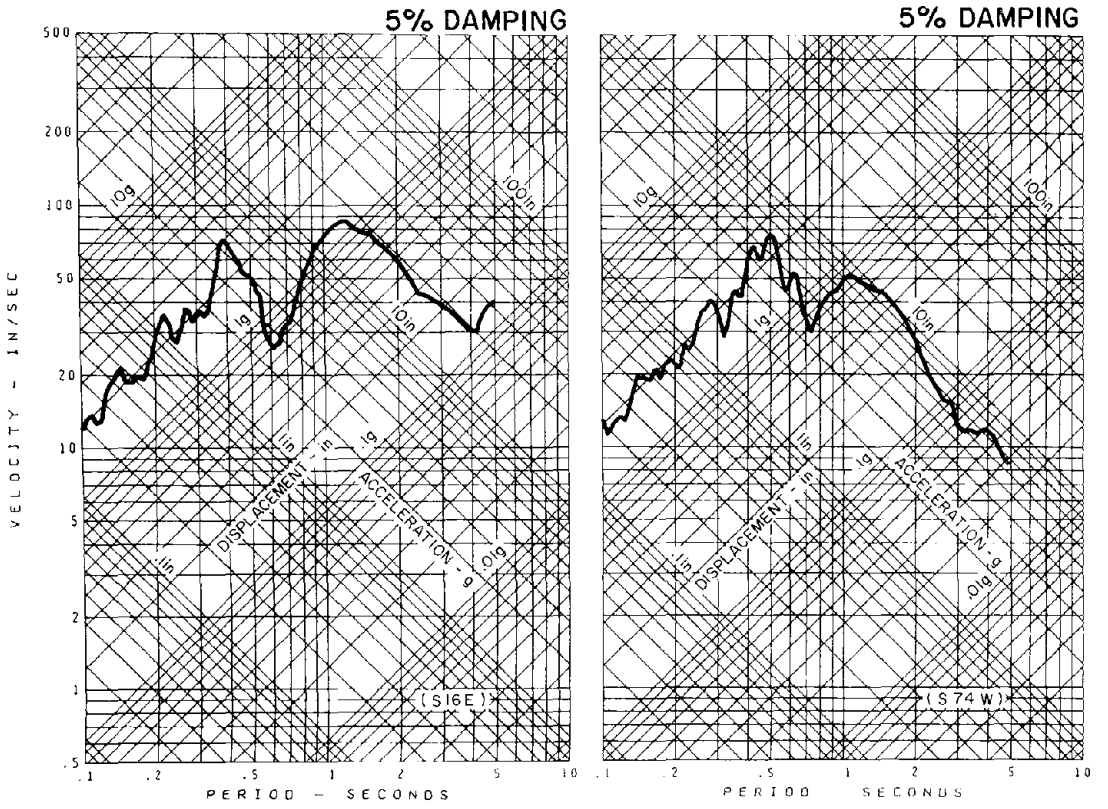

PACOIMA DAM RECORD

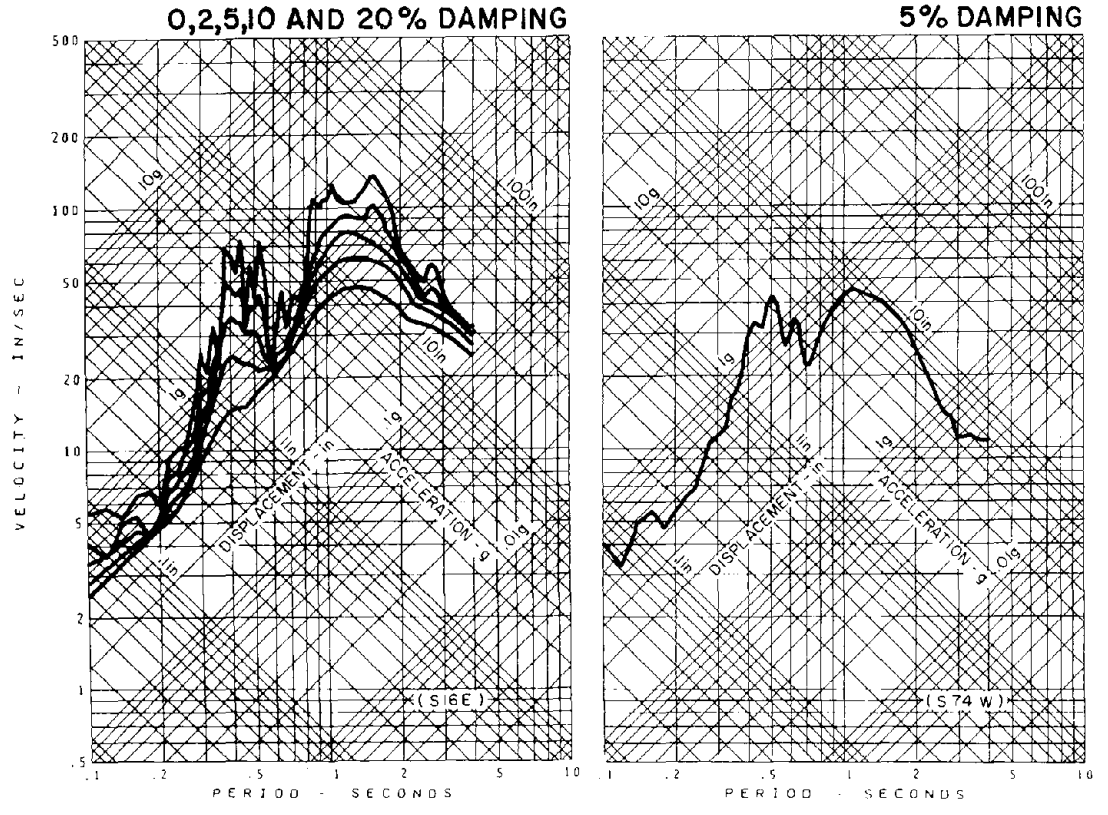

COMPUTED PACOIMA ROCK MOTION (REF. 4.20)

FIG. 4.17 TRIPATITE RESPONSE SPECTRA FOR PACOIMA DAM SITE

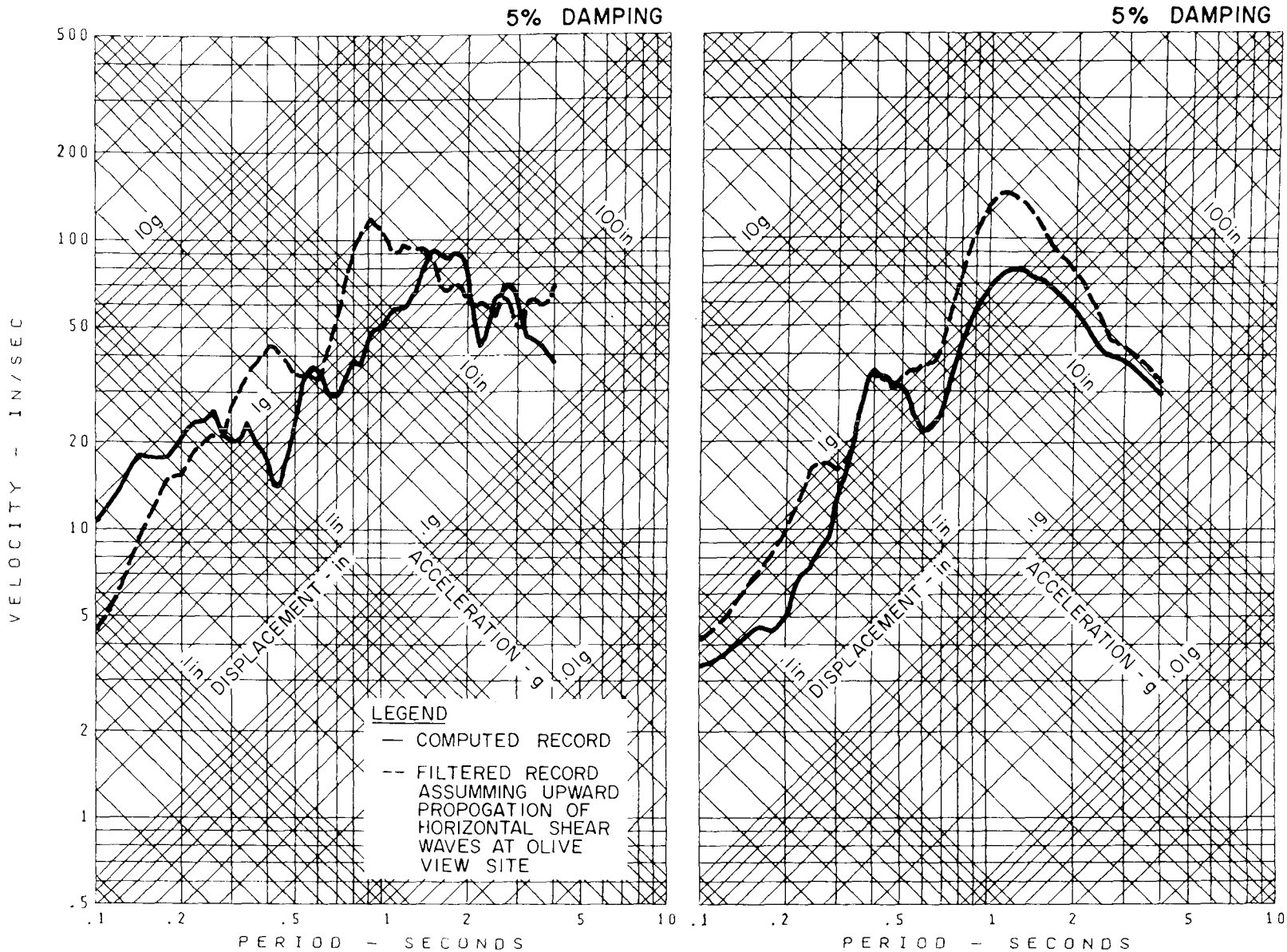

VAN NORMAN DAM RECORD
(N - S)

COMPUTED PACOIMA ROCK MOTION
(S16E)

FIG. 4.18 COMPARISON OF TRIPARTITE RESPONSE SPECTRA FOR FILTERED AND ORIGINAL VERSIONS OF DERIVED GROUND MOTIONS

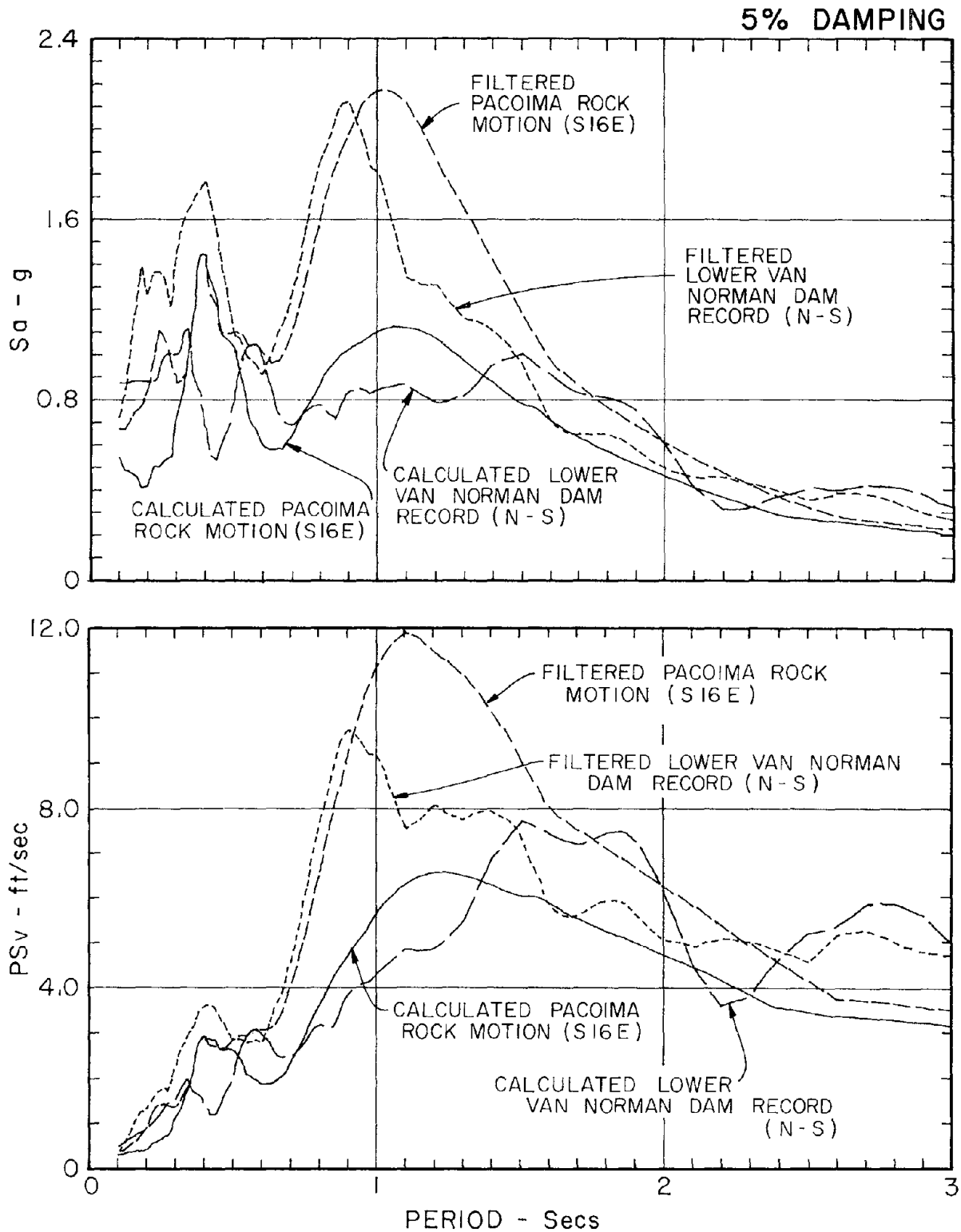

FIG. 4.19 COMPARISON OF RESPONSE SPECTRA FOR CALCULATED GROUND MOTION RECORDS

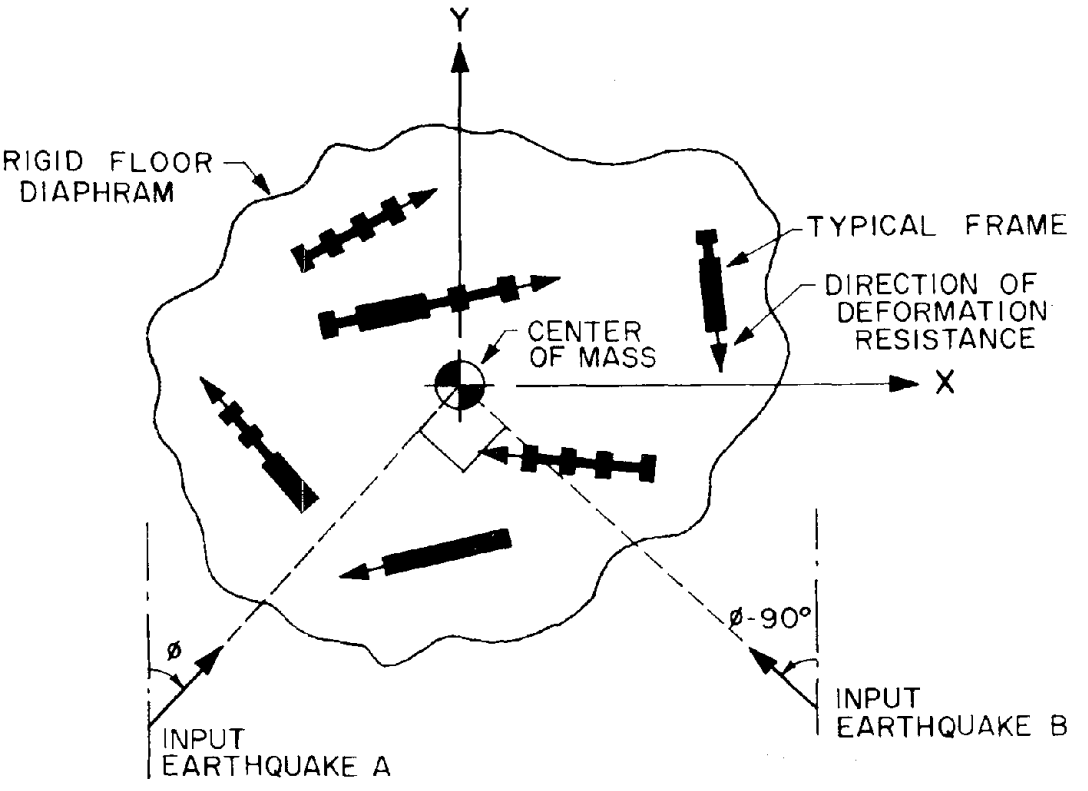

(a) PLAN VIEW OF TYPICAL BUILDING MODEL

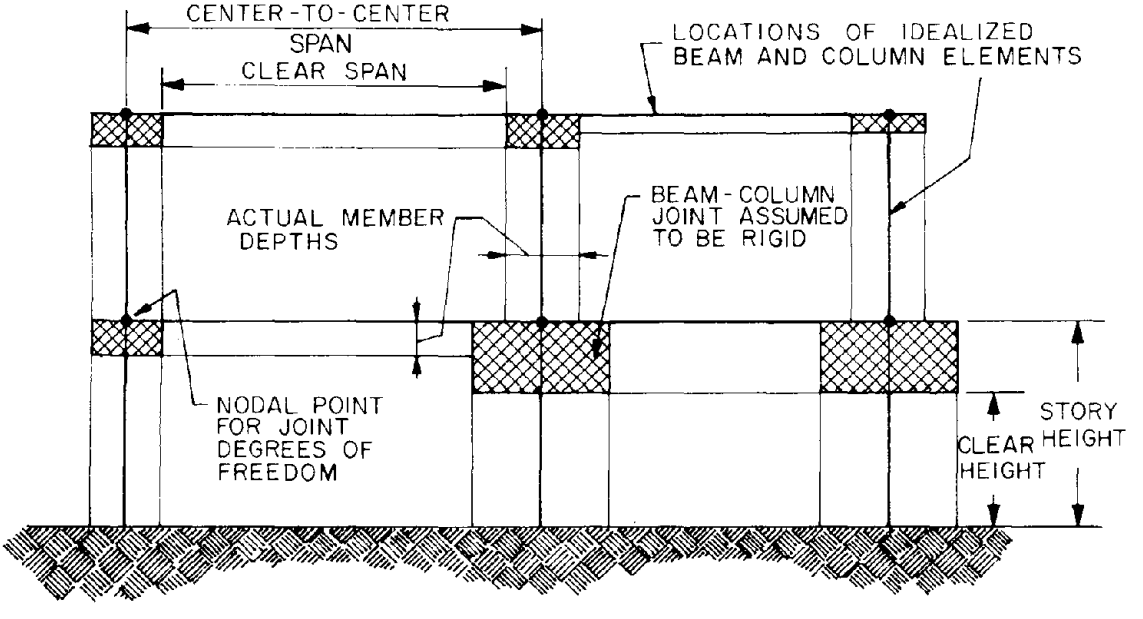

(b) DEFINITION OF FRAME GEOMETRY

FIG. 5.1 MODELING ASSUMPTIONS FOR TABS

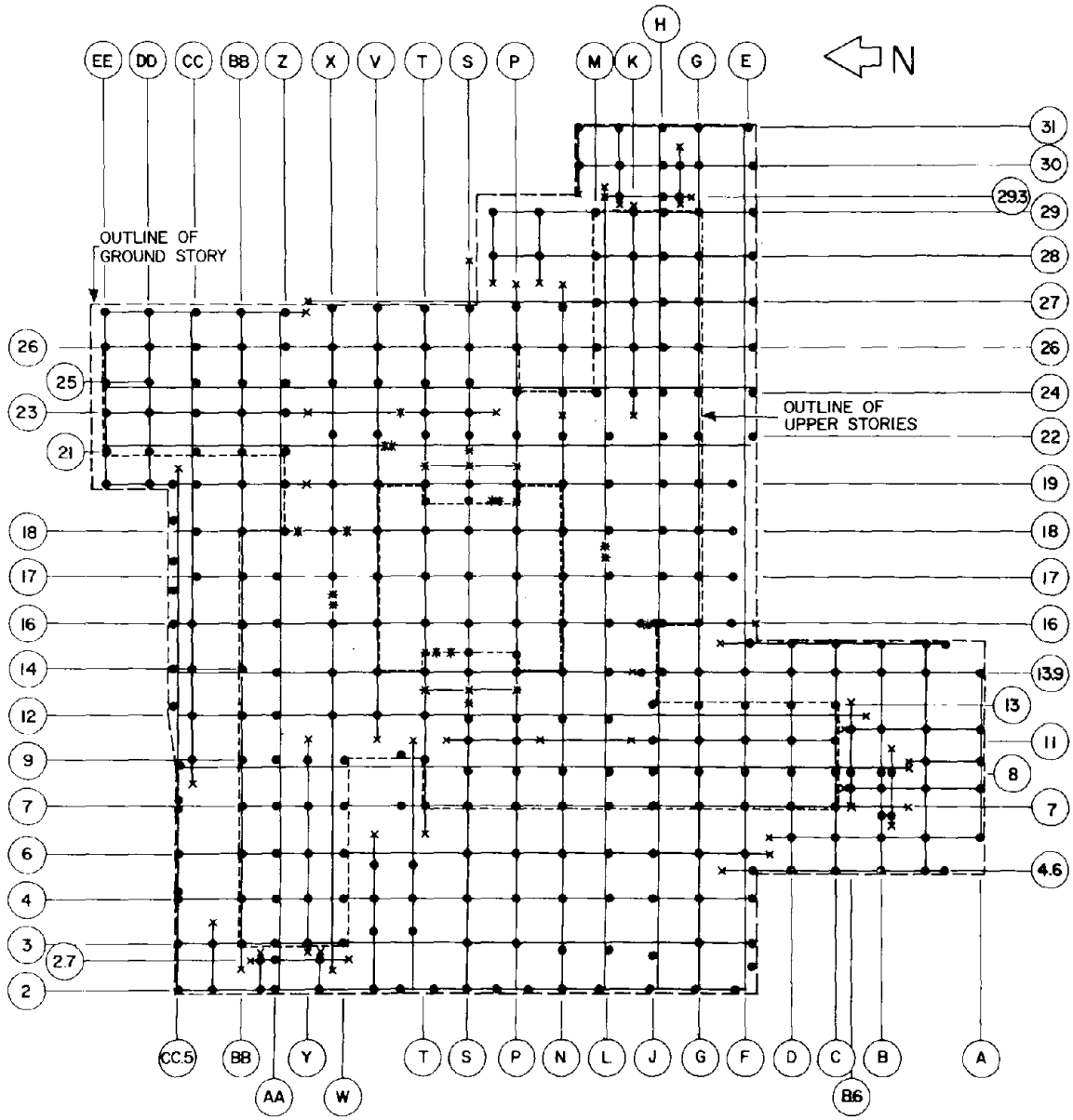

FIG. 5.2 FRAMES USED FOR THREE-DIMENSIONAL MODEL

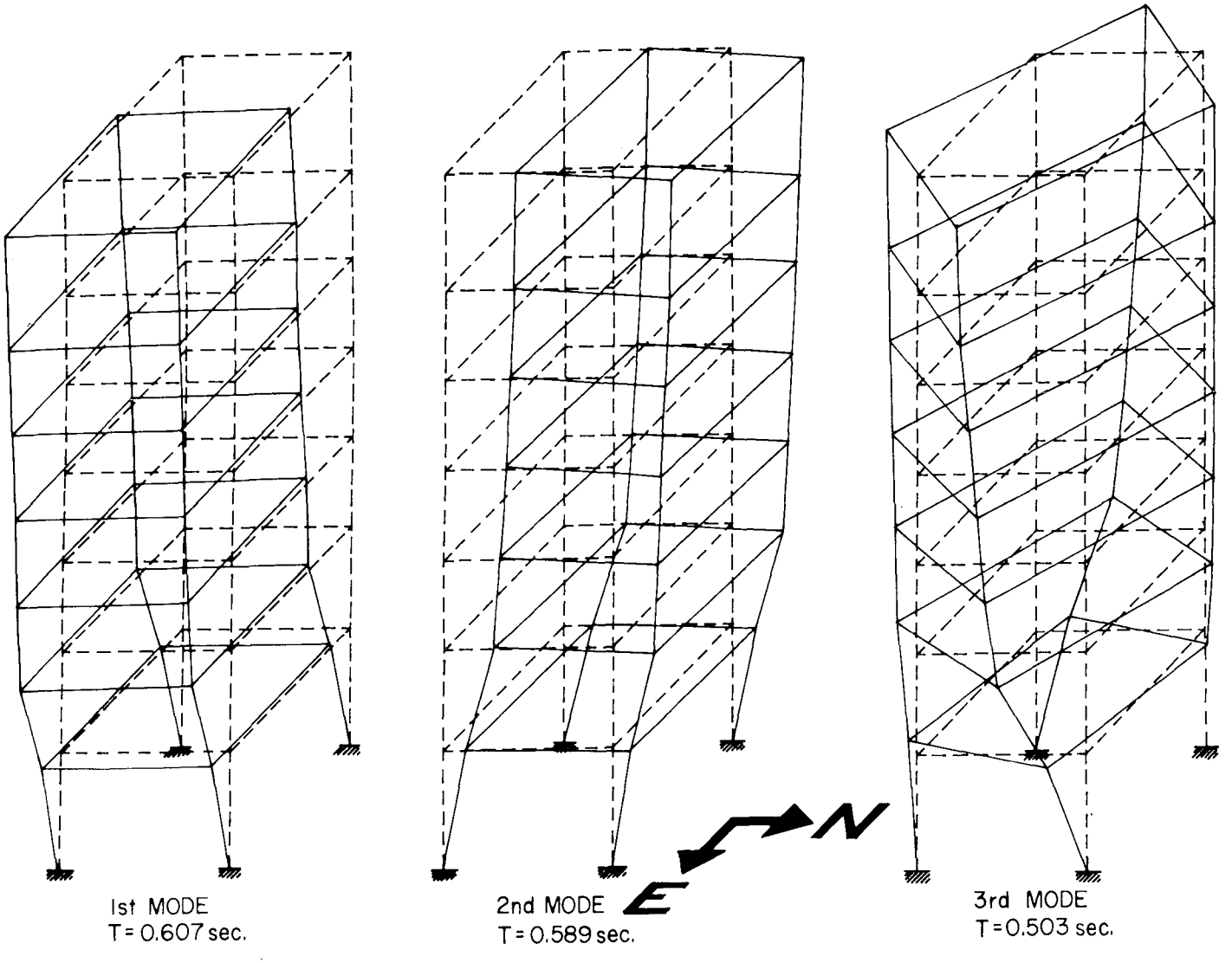

FIG. 5.3 SCHEMATIC REPRESENTATION OF 3-DIMENSIONAL MODE SHAPES

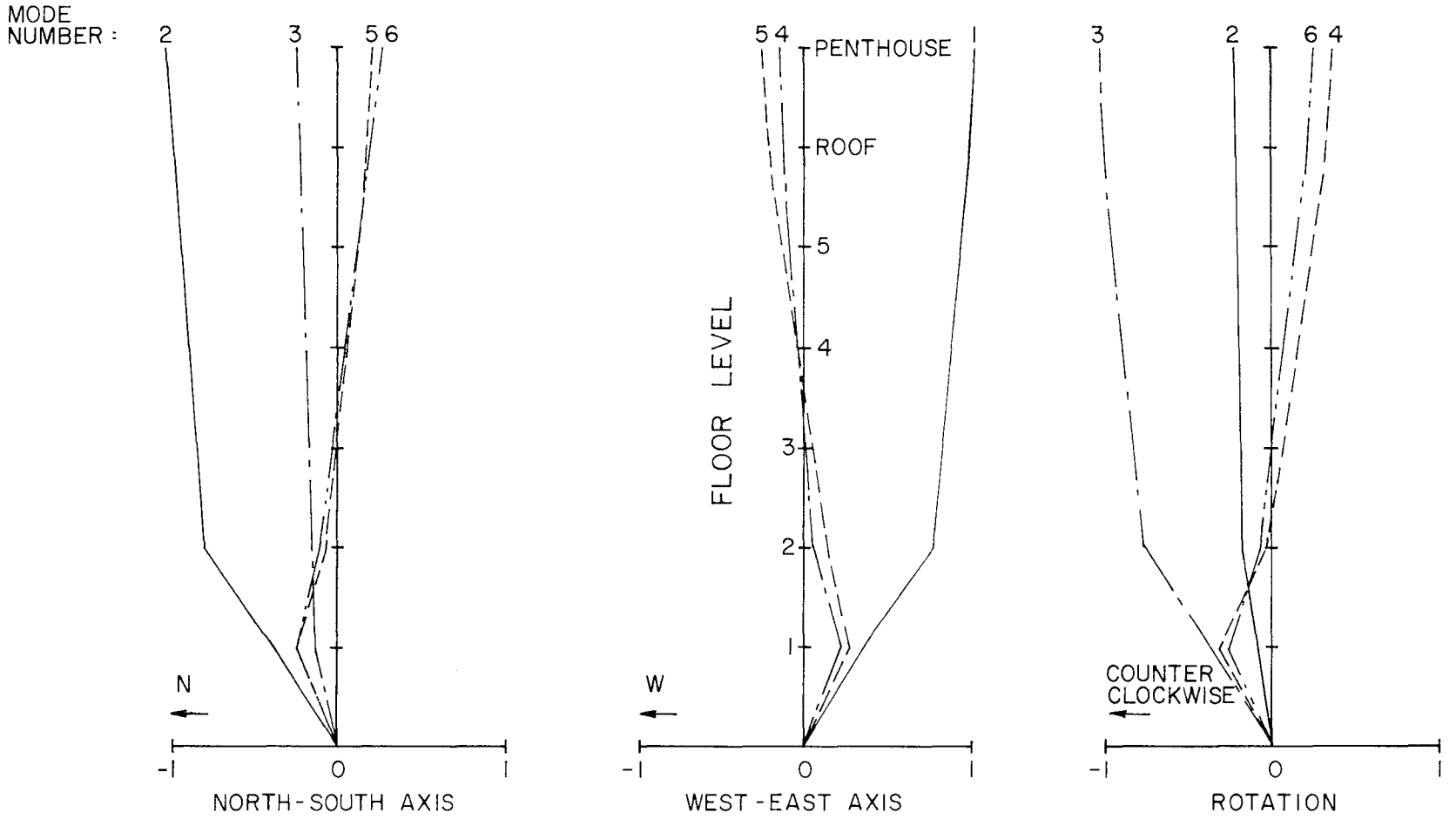

FIG. 5.4 NORMALIZED COMPONENTS OF THE 3-DIMENSIONAL MODE SHAPES

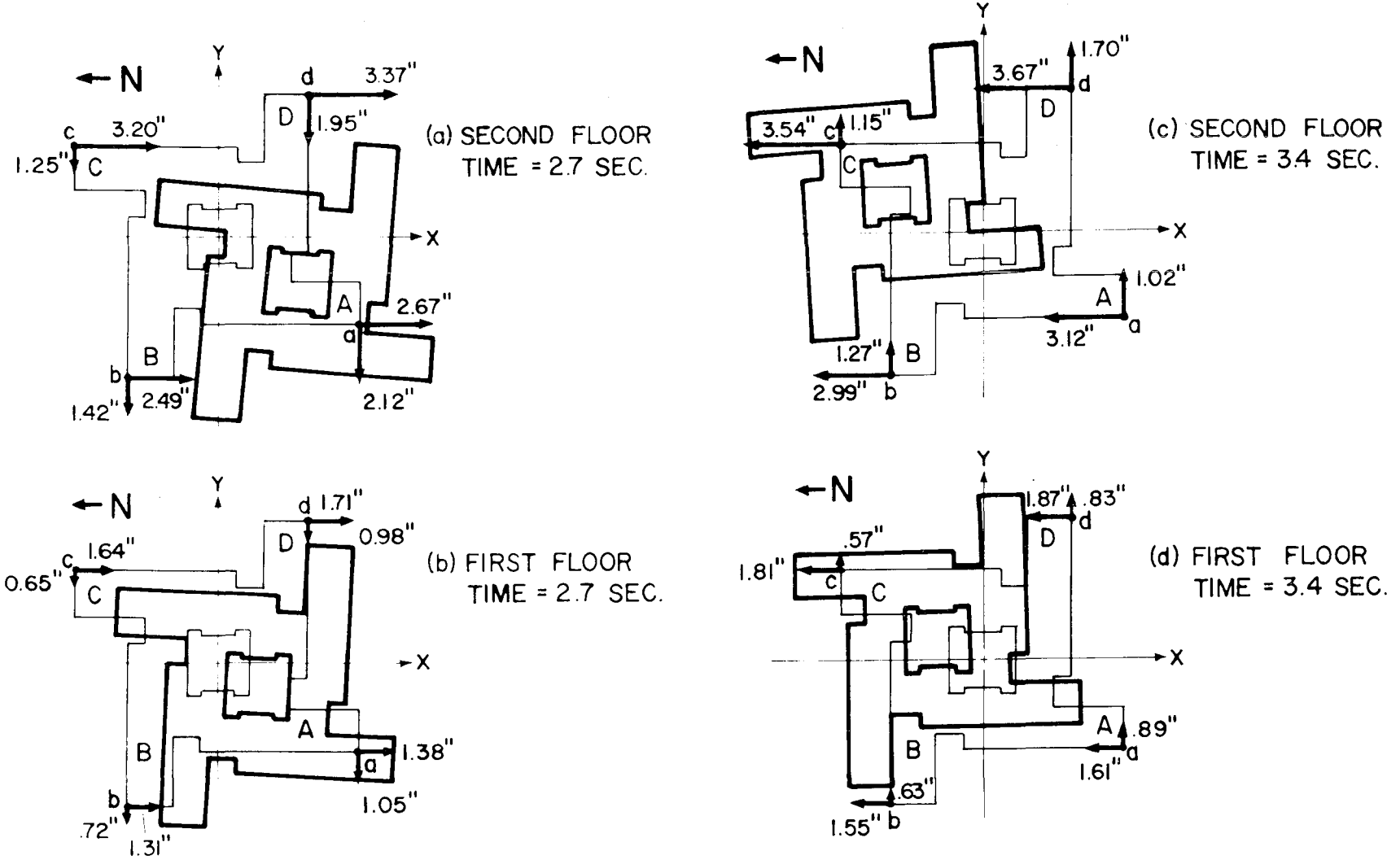

FIG. 5.7 MAXIMUM DISPLACEMENTS OF THE FIRST AND SECOND FLOORS

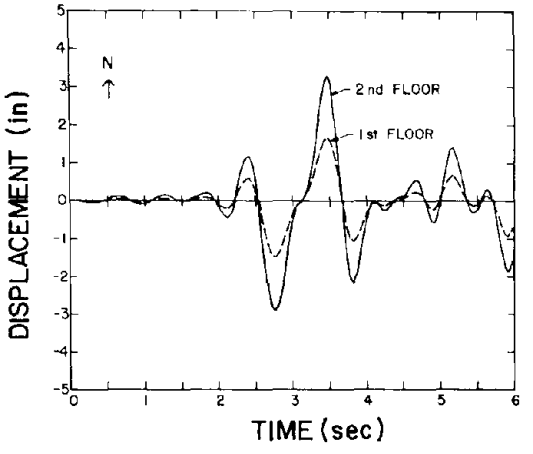

(a) NORTH-SOUTH DISPLACEMENT DUE TO BOTH COMPONENTS

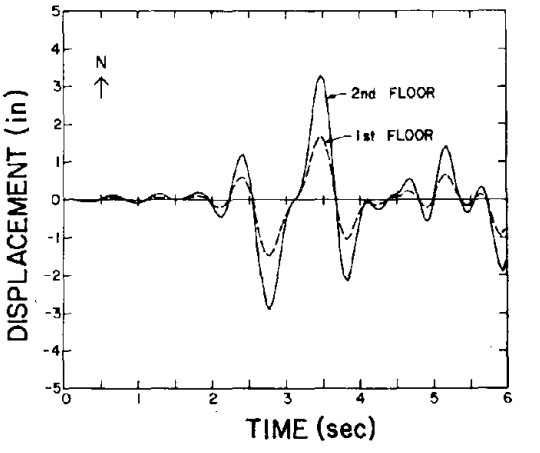

(b) NORTH-SOUTH DISPLACEMENT DUE TO N-S COMPONENT

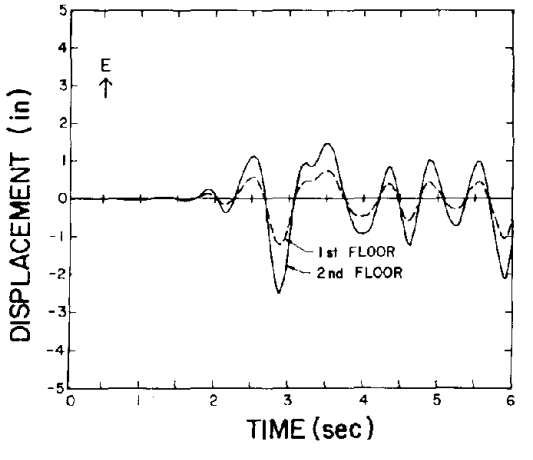

(c) EAST-WEST DISPLACEMENT DUE TO BOTH COMPONENTS

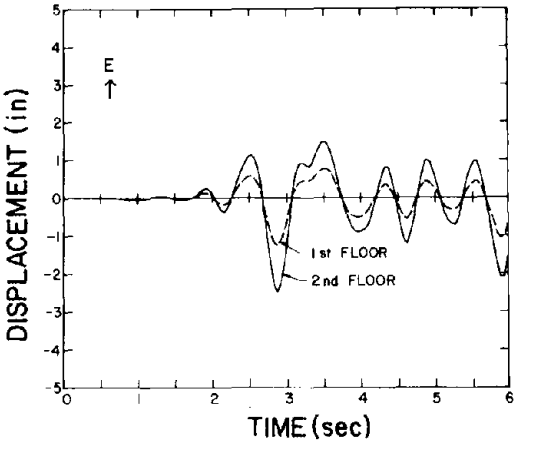

(d) EAST-WEST DISPLACEMENT DUE TO E-W COMPONENT

FIG. 5.8 TIME HISTORIES OF FLOOR DISPLACEMENTS AT THE CENTERS OF MASS DUE TO THE TWO COMPONENTS OF GROUND MOTION

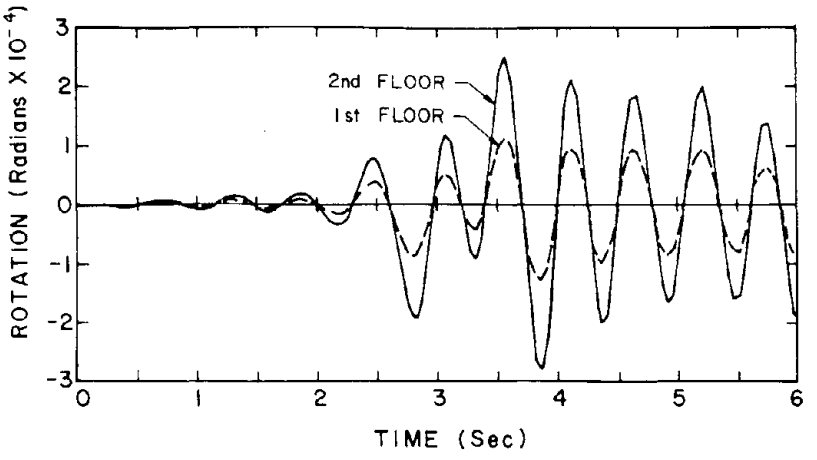

(a) ROTATIONS DUE TO BOTH COMPONENTS

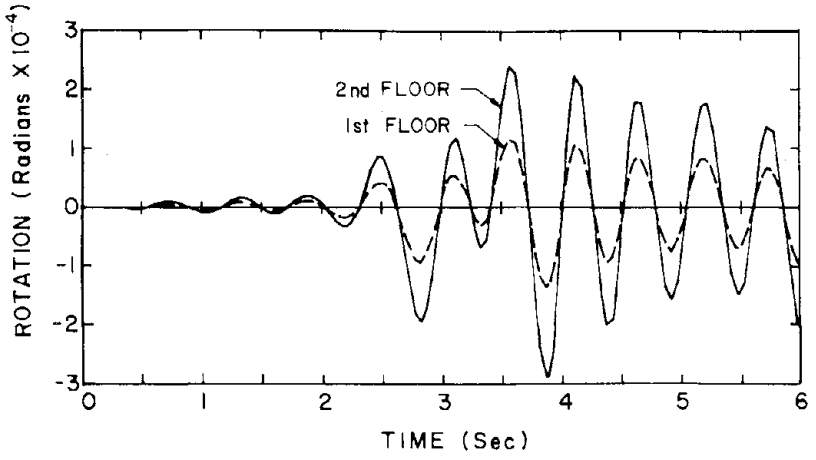

(b) ROTATIONS DUE TO NORTH-SOUTH COMPONENT

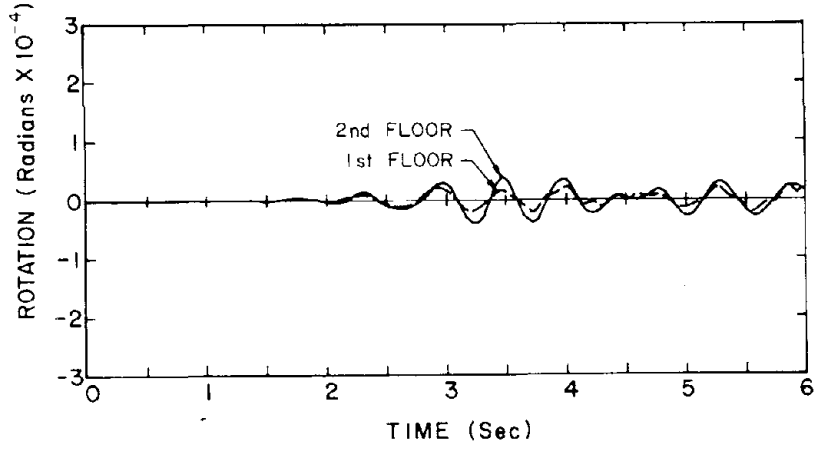

(c) ROTATIONS DUE TO EAST-WEST COMPONENT

FIG. 5.9 TIME HISTORIES OF FLOOR ROTATIONS AT THE CENTERS OF MASS DUE TO THE TWO COMPONENTS OF GROUND MOTION

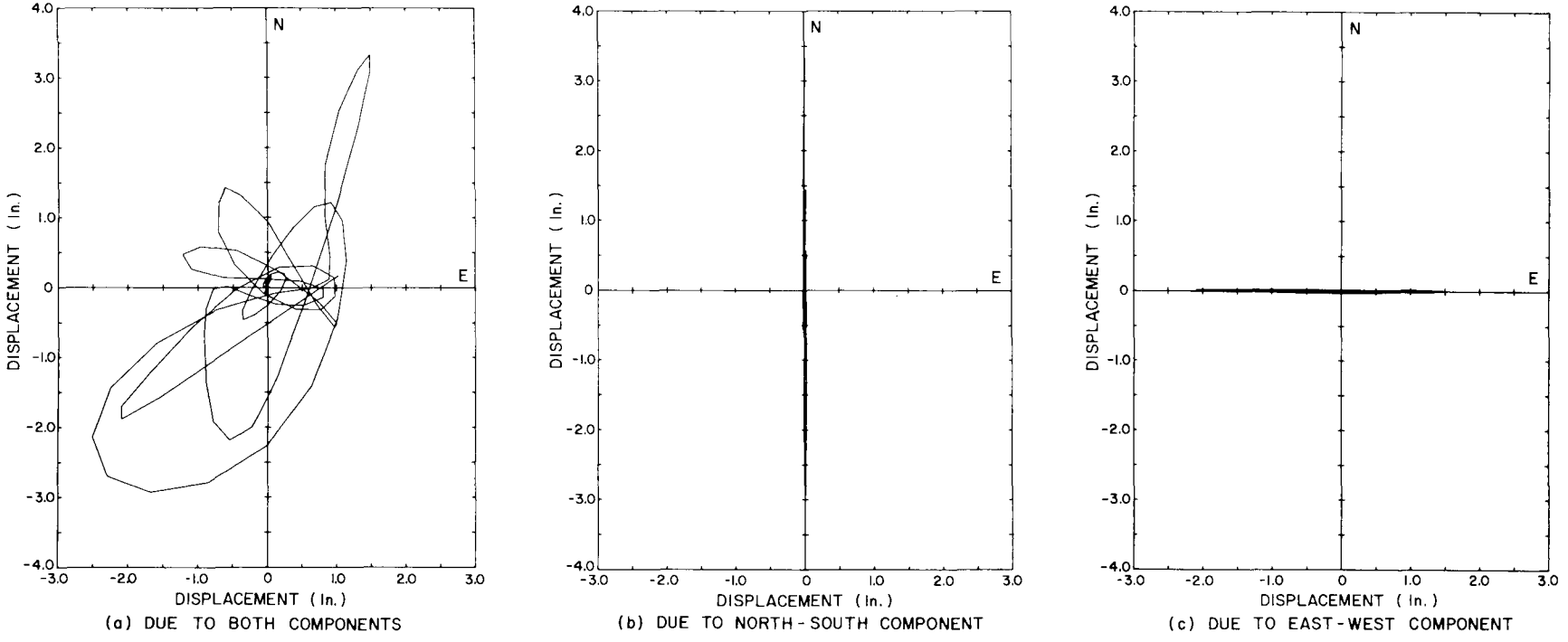

(a) DUE TO BOTH COMPONENTS (b) DUE TO NORTH-SOUTH COMPONENT (c) DUE TO EAST-WEST COMPONENT

FIG. 5.10 BIAXIAL DISPLACEMENT OF SECOND FLOOR CENTER OF MASS

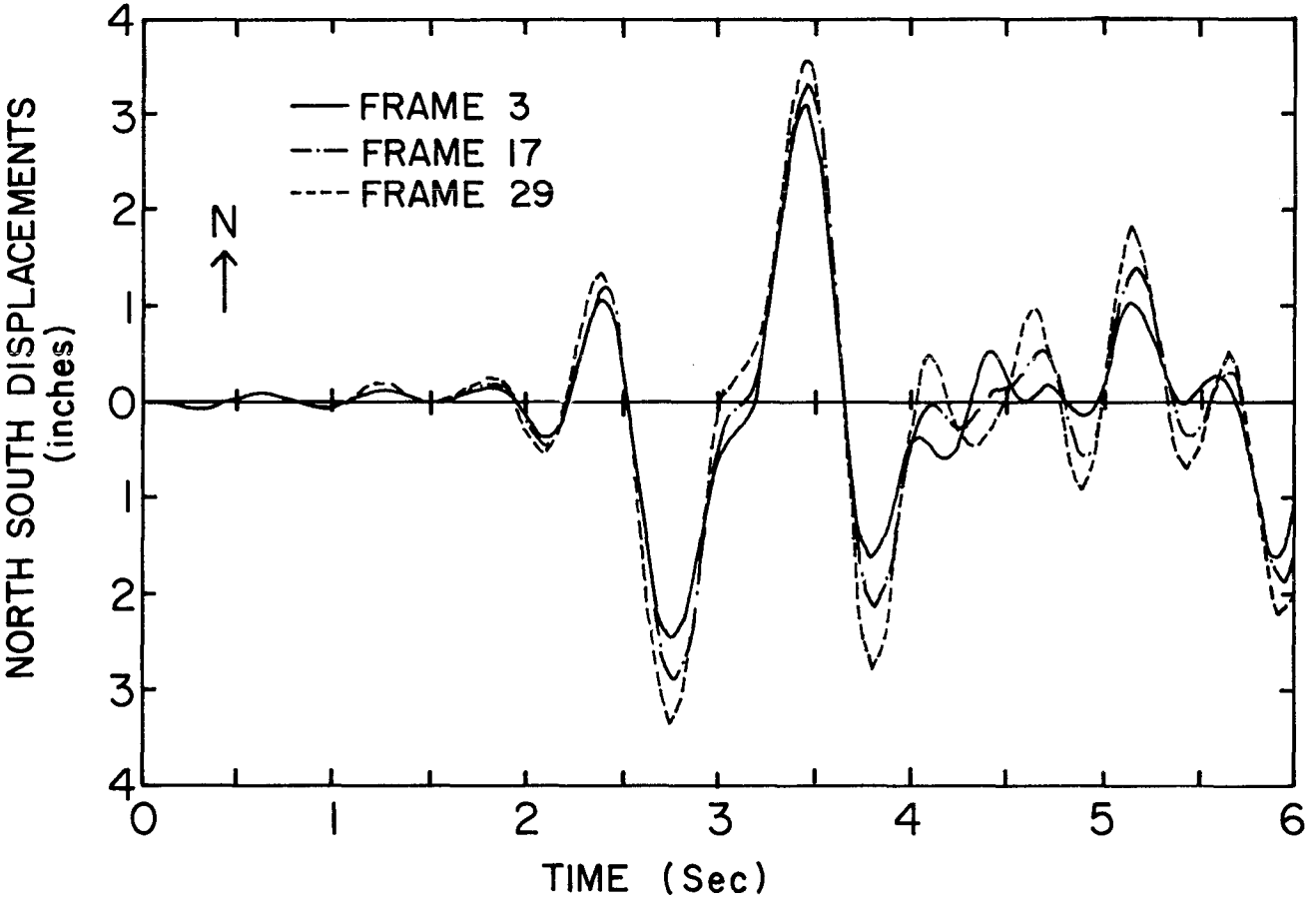

FIG. 5.11 TIME HISTORY OF SECOND FLOOR DISPLACEMENTS OF FRAMES 3, 17, AND 29 (DUE TO THE N-S COMPONENT OF THE GROUND MOTION)

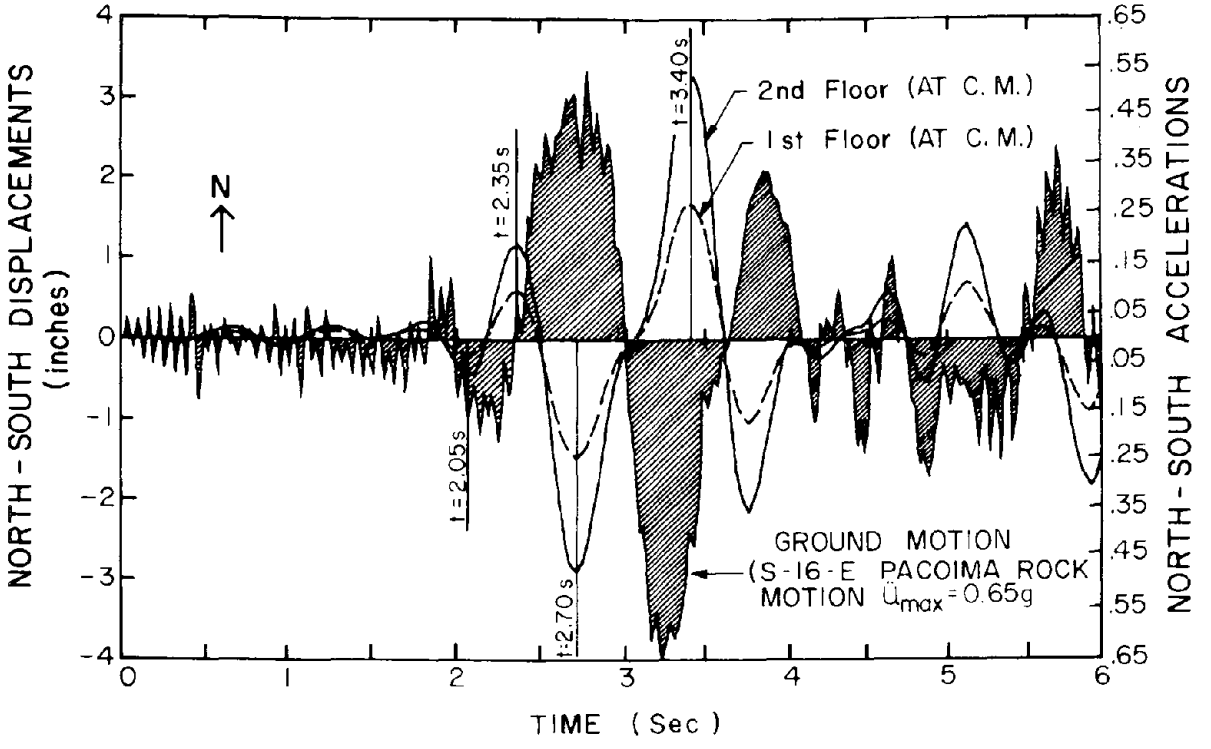

FIG. 5.12 NORTH-SOUTH RESPONSES OF TOTAL STRUCTURE MODEL TO THE NORTH-SOUTH COMPONENT OF GROUND MOTION

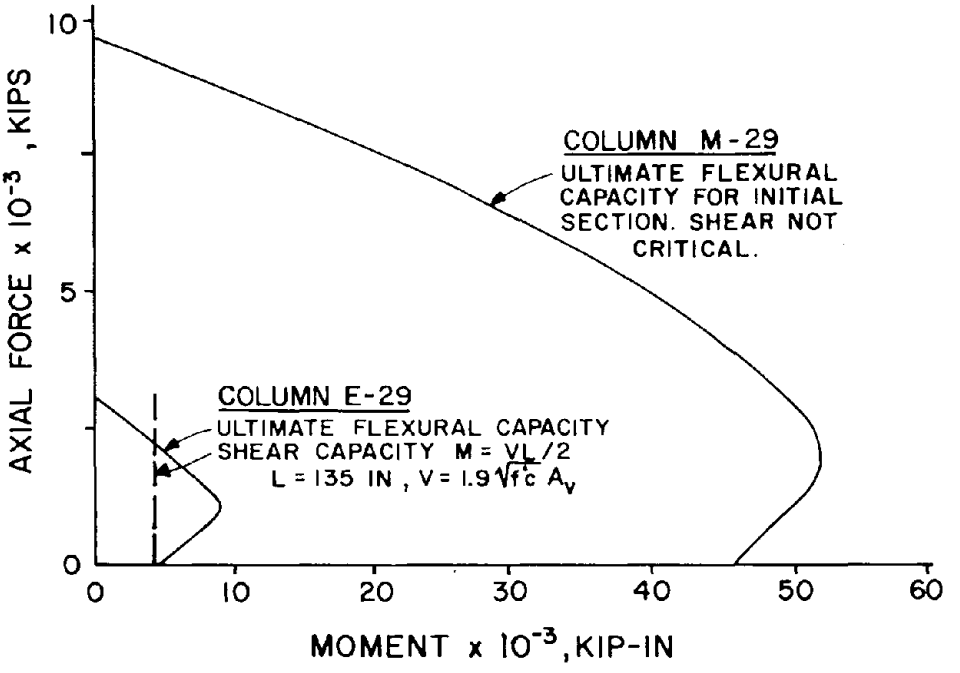

FIG. 5.13 INTERACTION CURVES FOR GROUND STORY COLUMNS E-29 AND M-29

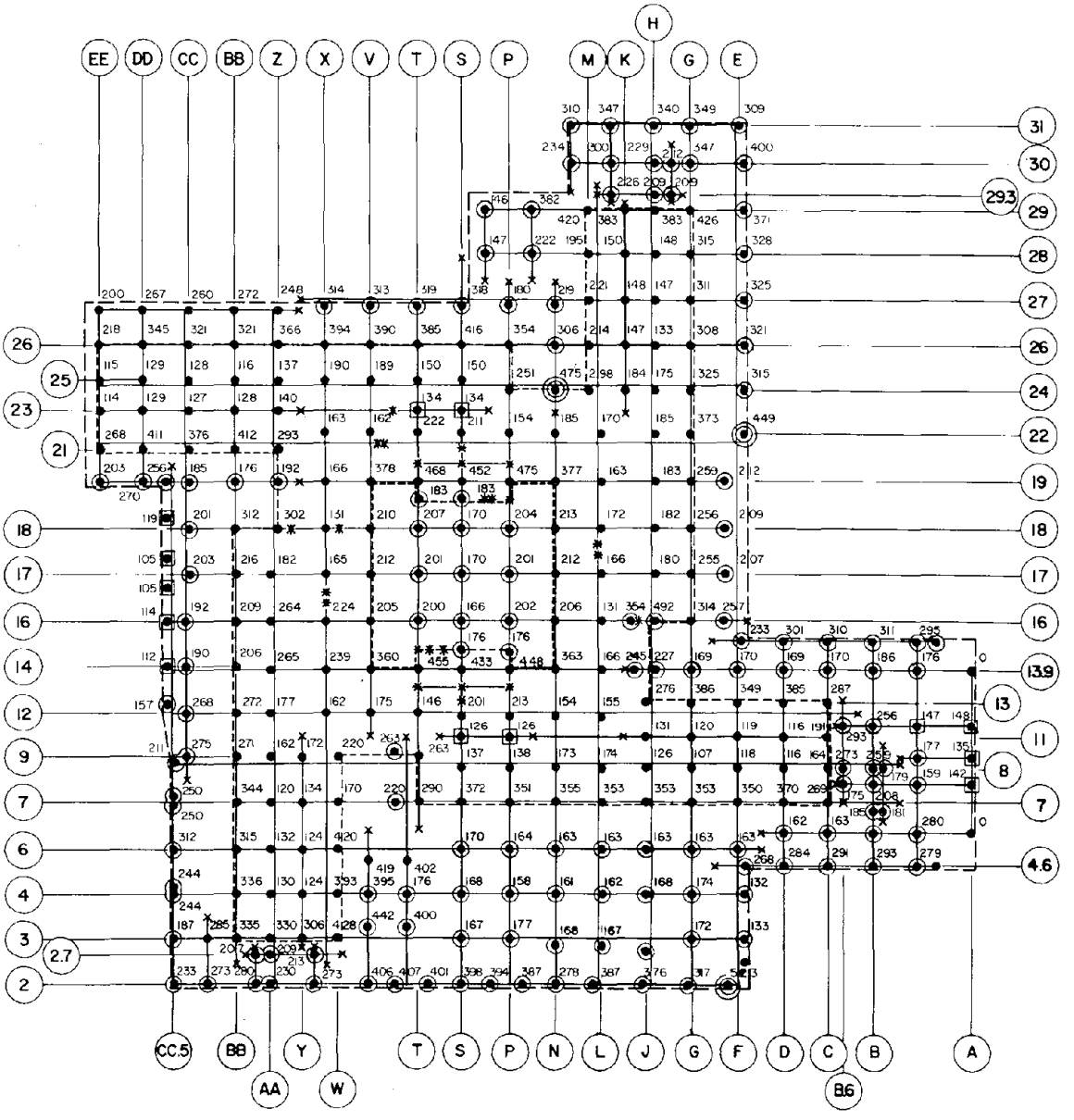

Legend

(a) The numbers indicate the elastic shear stress (psi) in the columns at t = 2.30 sec.

(b) Assuming the tied columns had a maximum shear capacity of 155 psi, the tied columns marked as indicated below failed during the model's displacement peak at: t = 2.05 sec., ◎; t = 2.35 sec., ◉; and t = 2.70 sec., ⊙.

FIG. 5.14a SHEAR STRESSES AND FAILURES IN GROUND STORY COLUMNS DUE TO NORTH-SOUTH DISPLACEMENT OF THE MODEL

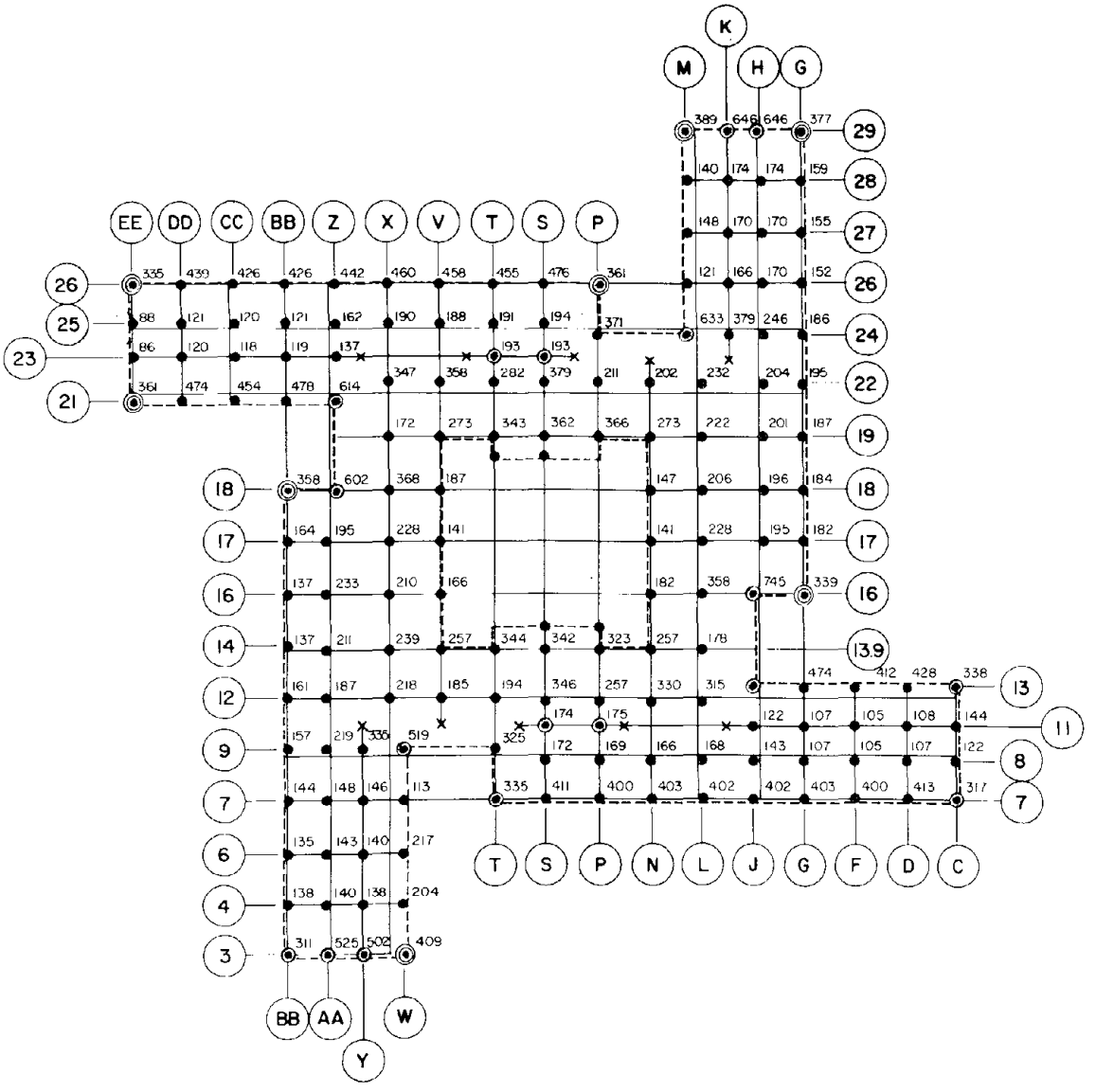

Legend

(a) The numbers indicate the elastic shear stress (psi) in the columns at t = 2.30 sec.

(b) Assuming the tied columns had a maximum shear capacity of 155 psi, the tied columns marked as indicated below failed during the model's displacement excursions which peak at: t = 2.05 sec., ◎; and t = 2.30 sec., ⊙.

FIG. 5.14b SHEAR STRESSES AND FAILURES IN FIRST STORY COLUMNS DUE TO NORTH-SOUTH DISPLACEMENTS OF THE MODEL

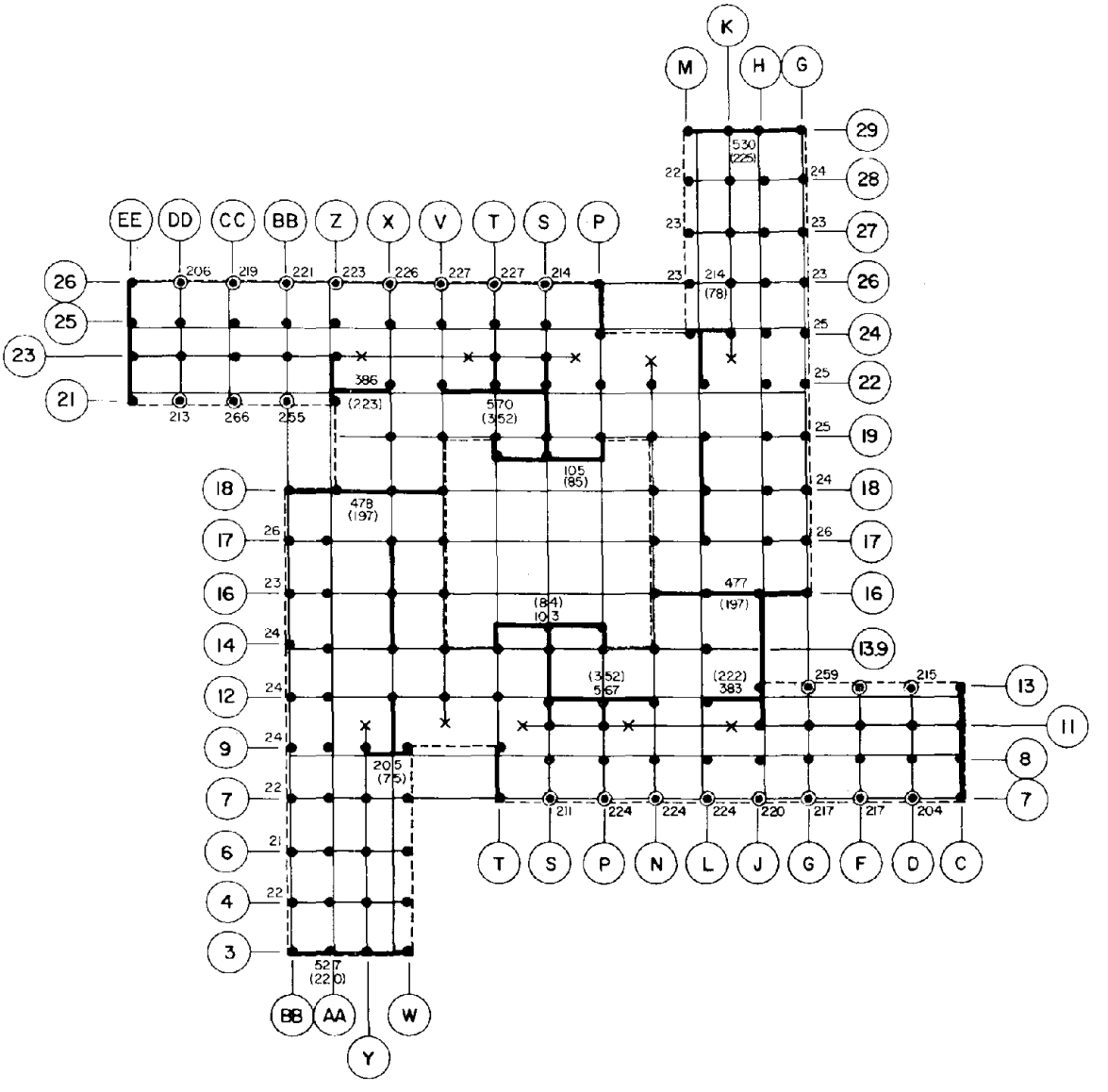

Legend

(a) The numbers indicate the elastic shear stresses in the third story channel columns and second and third (in parenthesis) story shear walls at t = 2.30 sec.

(b) Assuming the channel columns had a maximum shear capacity of 135 psi the channel columns marked as indicated below failed during the model's displacement excursion which peaks at: t = 2.30 sec.◉

FIG. 5.15 SHEAR STRESSES AND FAILURES IN UPPER STORY CHANNEL COLUMNS AND SHEAR WALLS DUE TO NORTH-SOUTH DISPLACEMENTS OF THE MODEL

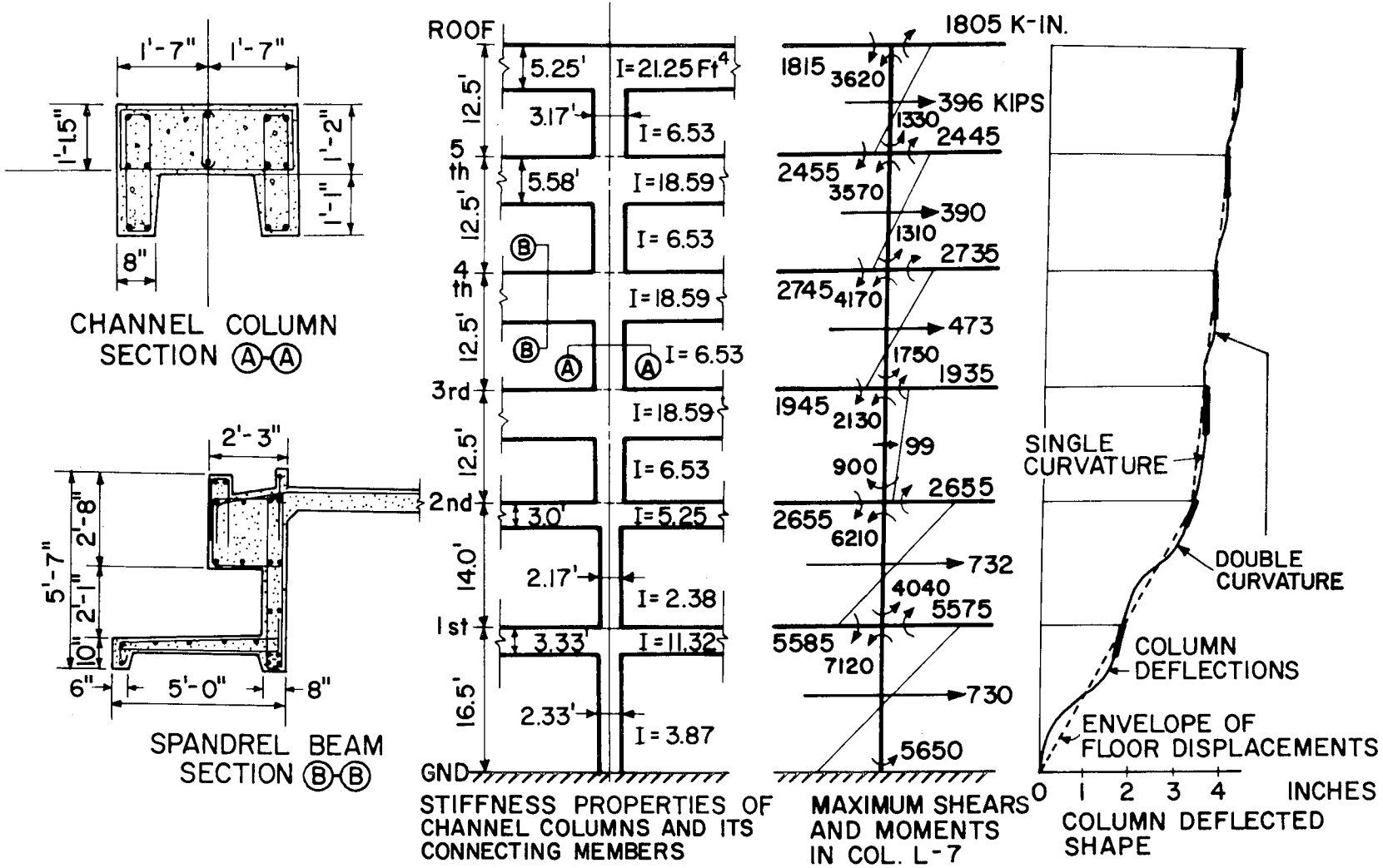

FIG. 5.16 STIFFNESS PROPERTIES, MAXIMUM SHEAR FORCES, MOMENTS, AND DEFLECTED SHAPES OF A ROW OF CHANNEL COLUMNS

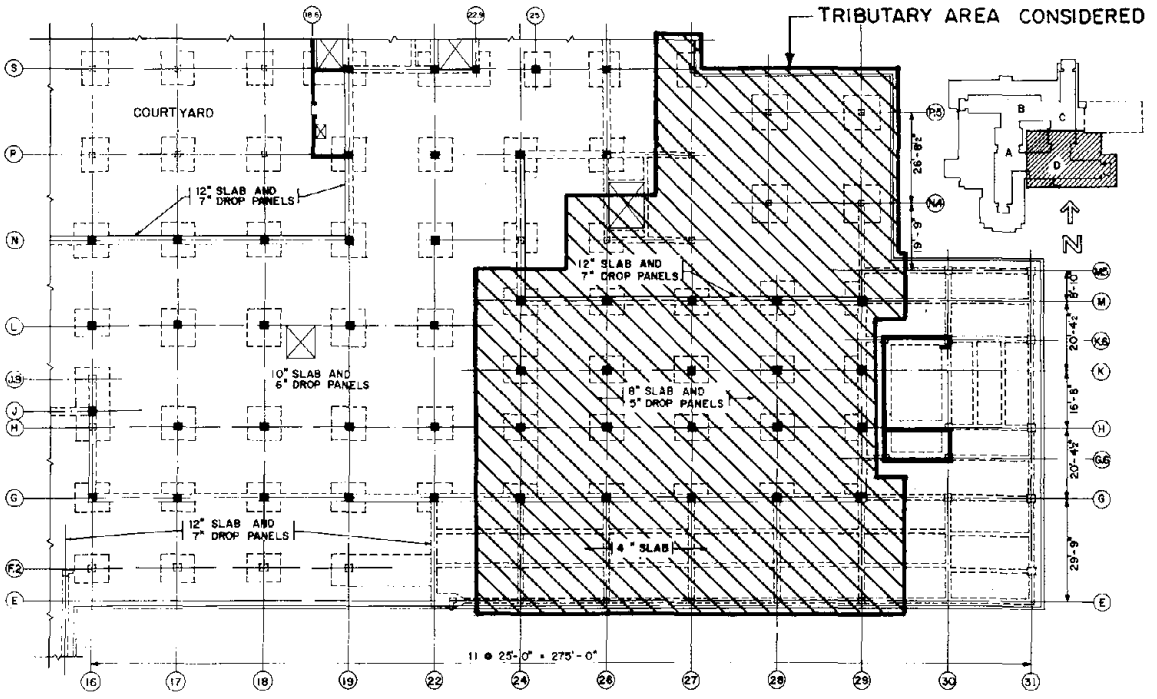

(a) FIRST FLOOR AND BELOW

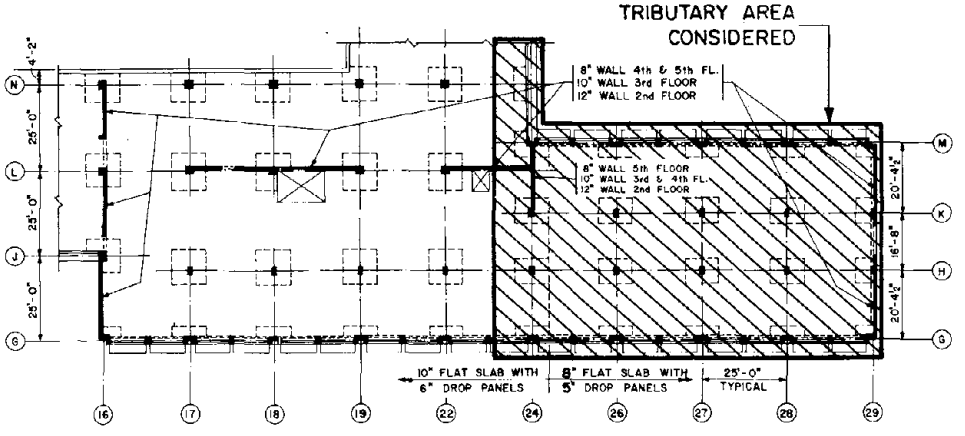

(b) ABOVE FIRST FLOOR

FIG. 5.17 PORTION OF WING D MODELED FOR TWO-DIMENSIONAL ELASTIC ANALYSIS

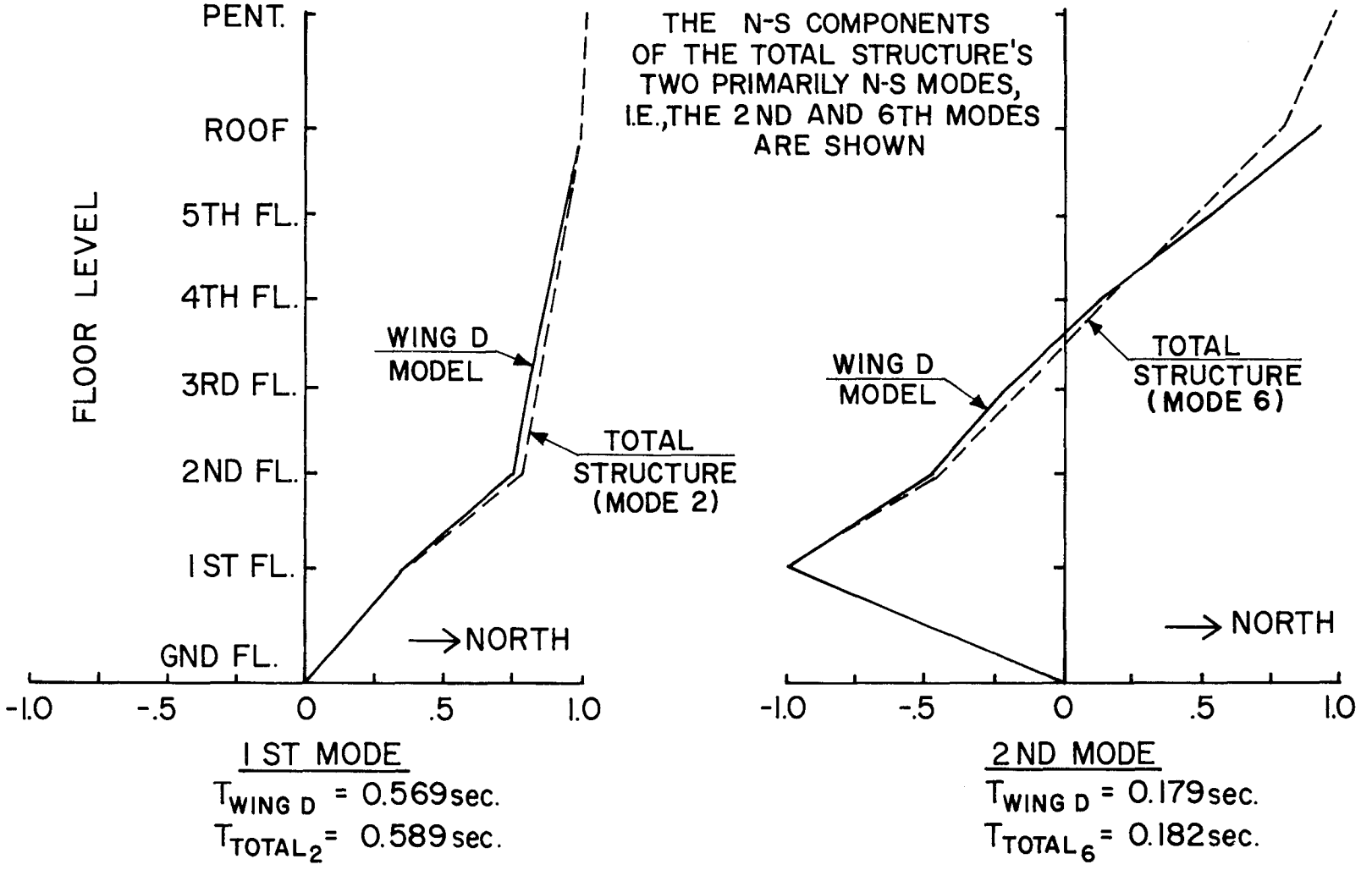

FIG. 5.18 MODE SHAPES AND PERIODS FOR WING D AND TOTAL STRUCTURE MODELS

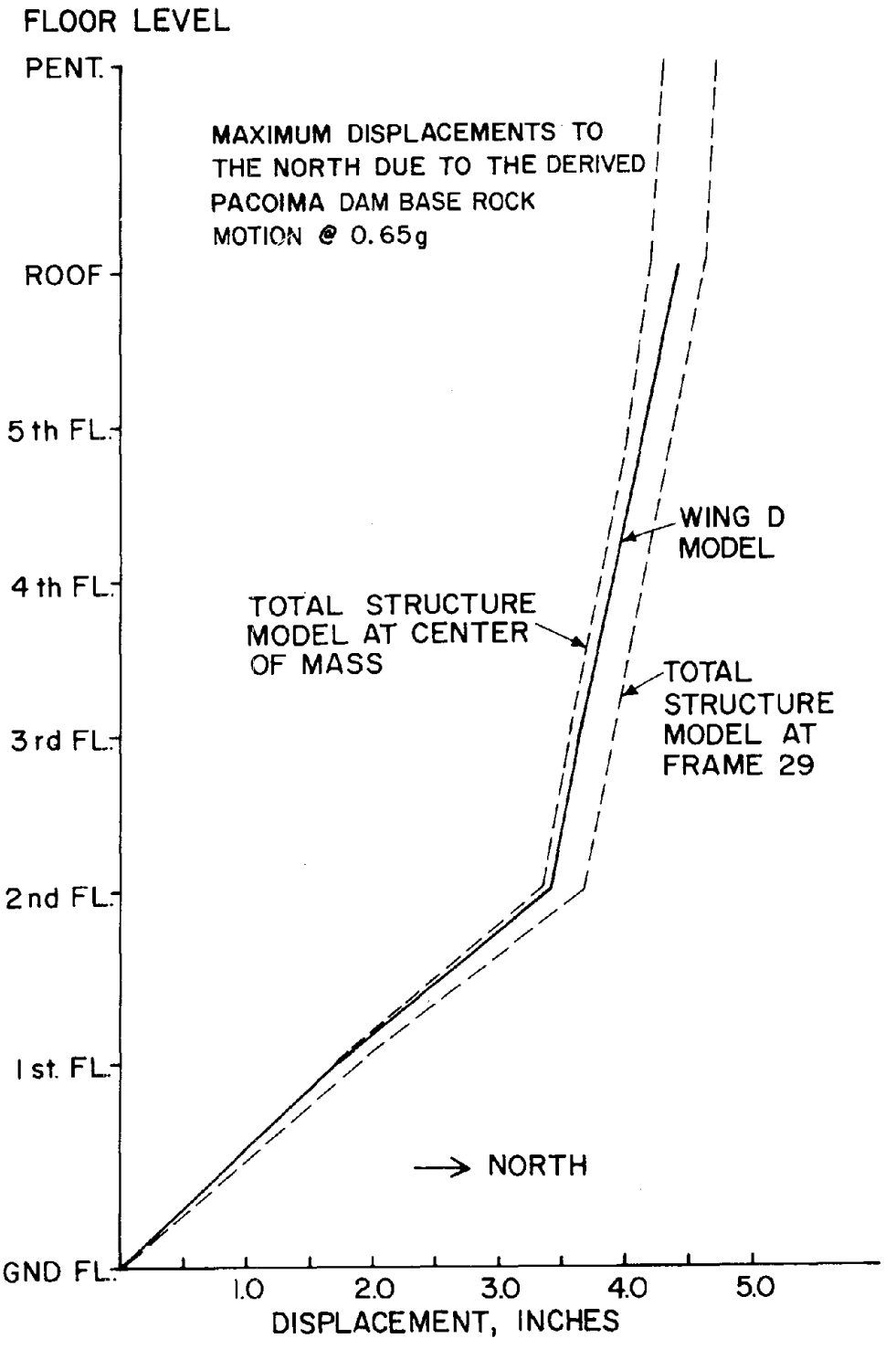

FIG. 5.19 ENVELOPES OF MAXIMUM FLOOR DISPLACEMENTS

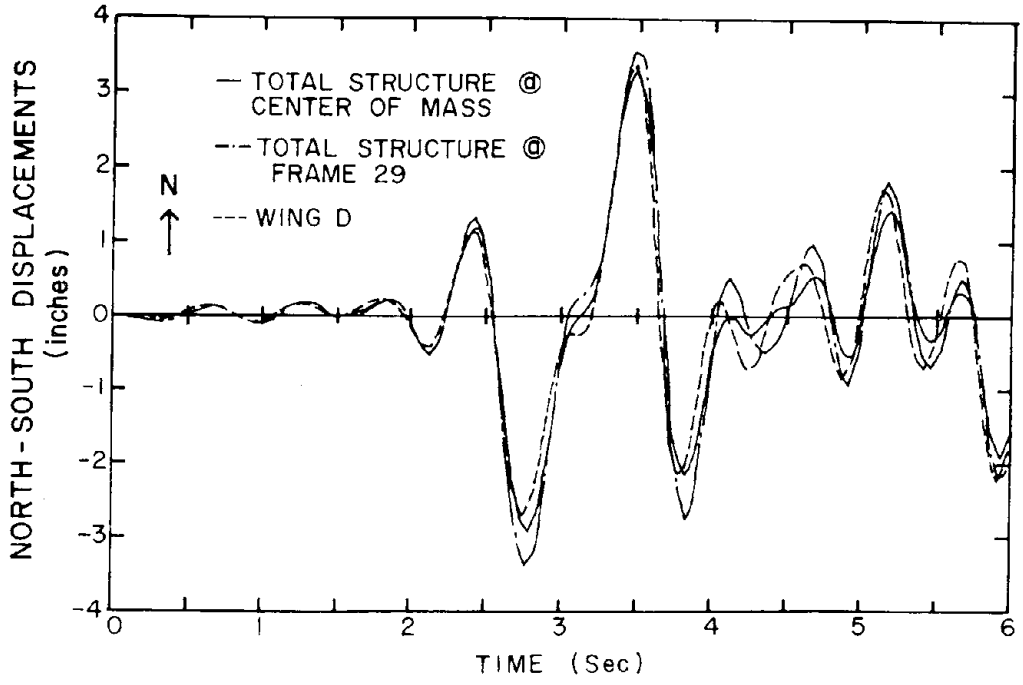

(a) SECOND FLOOR DISPLACEMENTS

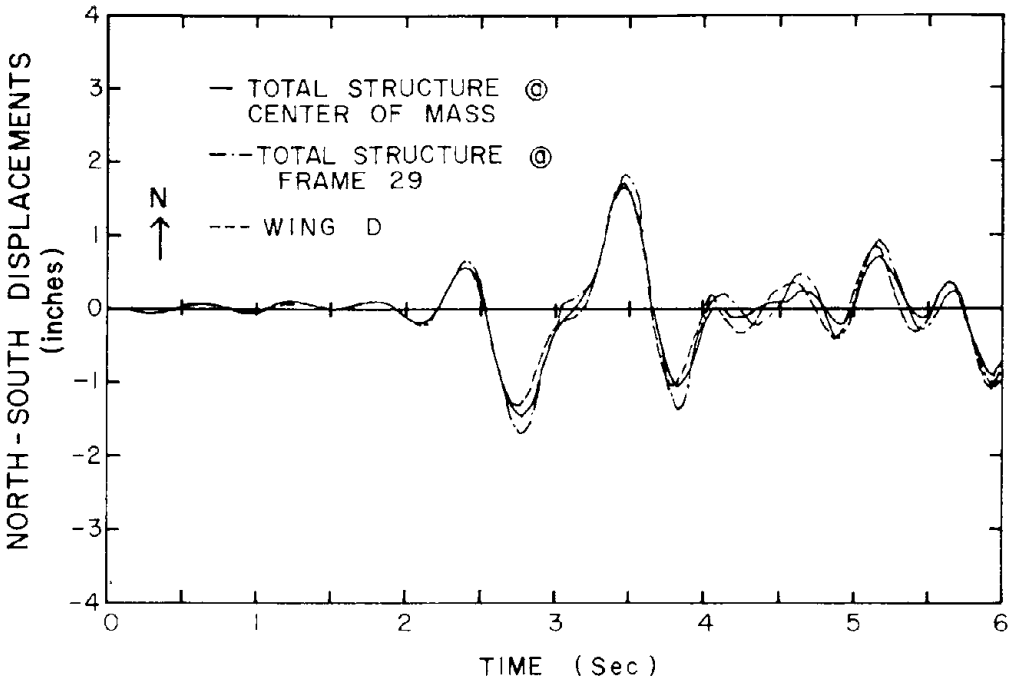

(b) FIRST FLOOR DISPLACEMENTS

FIG. 5.20 TIME HISTORIES FLOOR DISPLACEMENTS OF THE WING D AND TOTAL STRUCTURE MODELS DUE TO S-16°-E COMPONENT OF DERIVED PACOIMA DAM BASE ROCK MOTION

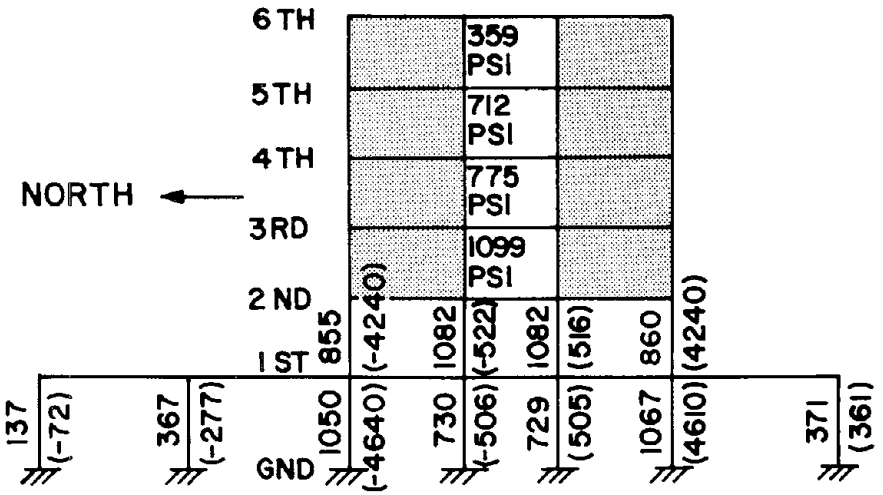

(a) WING D MODEL

(a) MOST OF THESE FORCES OCCURRED AT T=3.40 sec.
(b) AXIAL FORCES ARE IN PARENTHESIS
(c) NEGATIVE AXIAL FORCE INDICATES COMPRESSION
(d) GRAVITY LOADS ARE NOT INCLUDED
(e) SHEAR STRESSES ARE THE AVERAGE OVER THE ENTIRE WALL
(f) ALL OTHER UNITS ARE KIPS

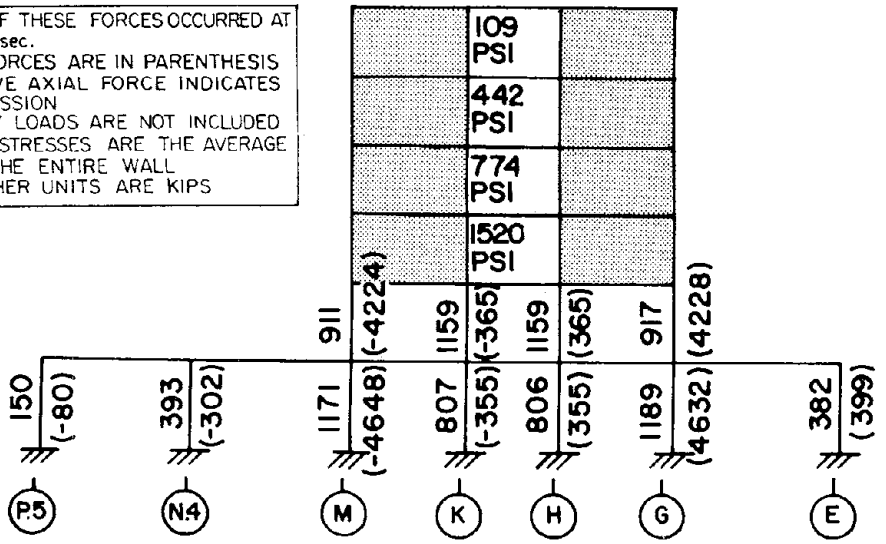

(b) TOTAL STRUCTURE MODEL

FIG. 5.21 MAXIMUM ELASTIC SHEAR AND AXIAL FORCES IN COLUMNS OF FRAME 29

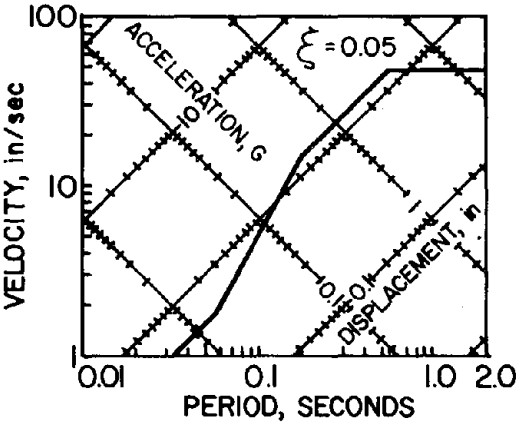

(a) SMOOTHED RESPONSE SPECTRUM FOR 0.5g PEAK GROUND ACCELERATION

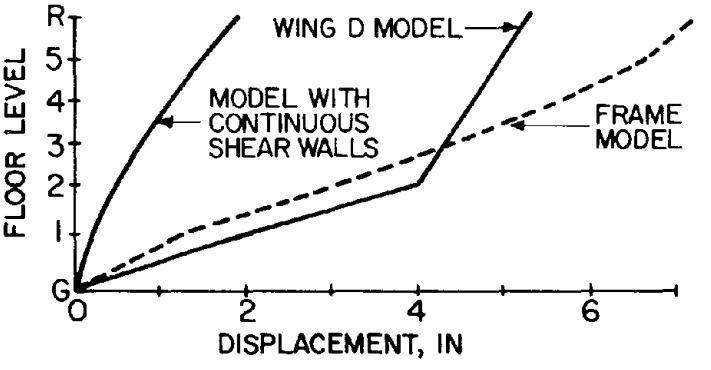

(b) ENVELOPES OF RMS DISPLACEMENTS

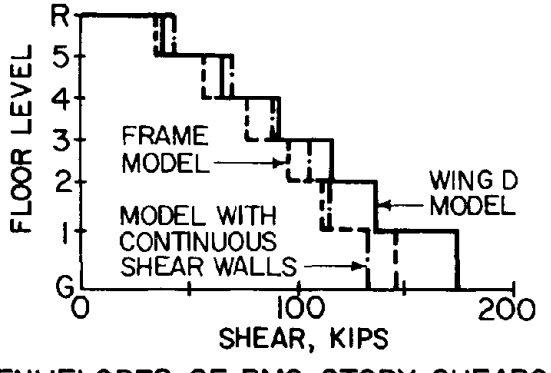

(c) ENVELOPES OF RMS STORY SHEARS

FIG. 5.22 COMPARISON OF ELASTIC RESPONSE OF DIFFERENT STRUCTURAL SYSTEMS FOR WING D-SMOOTHED RESPONSE SPECTRUM

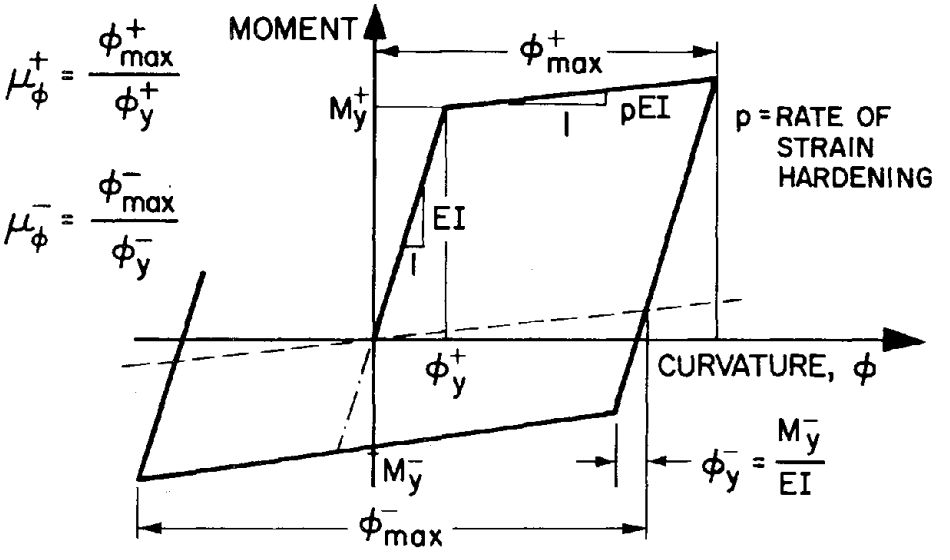

FIG. 6.1 DEFINITION OF CYCLIC DUCTILITY FACTOR, μ_ϕ

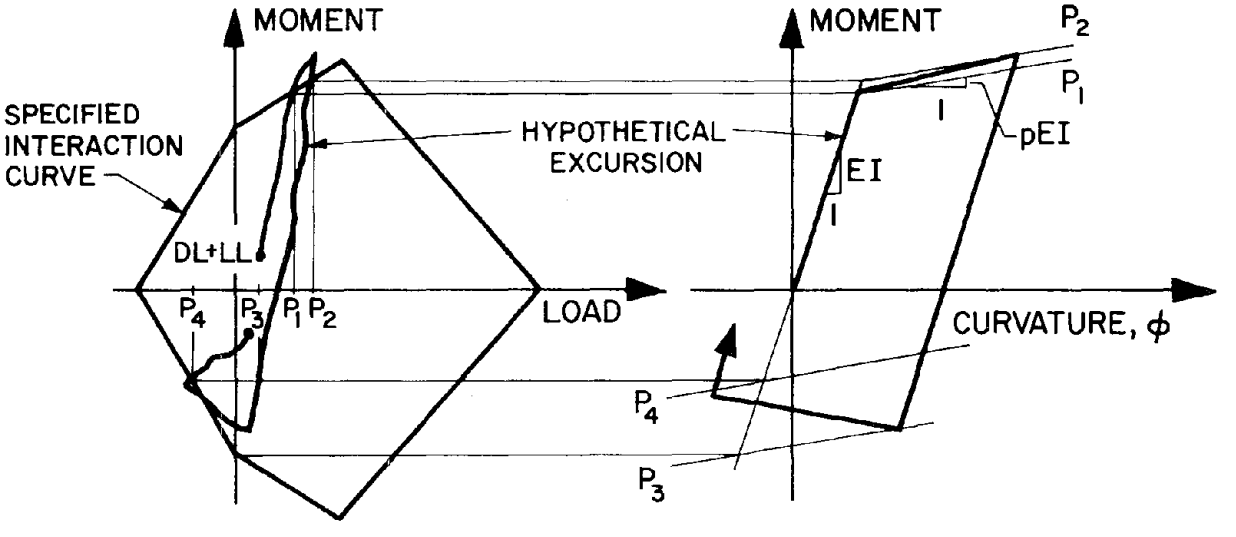

FIG. 6.2 SCHEMATIC REPRESENTATION OF AXIAL LOAD-BENDING MOMENT INTERACTION FOR COLUMNS

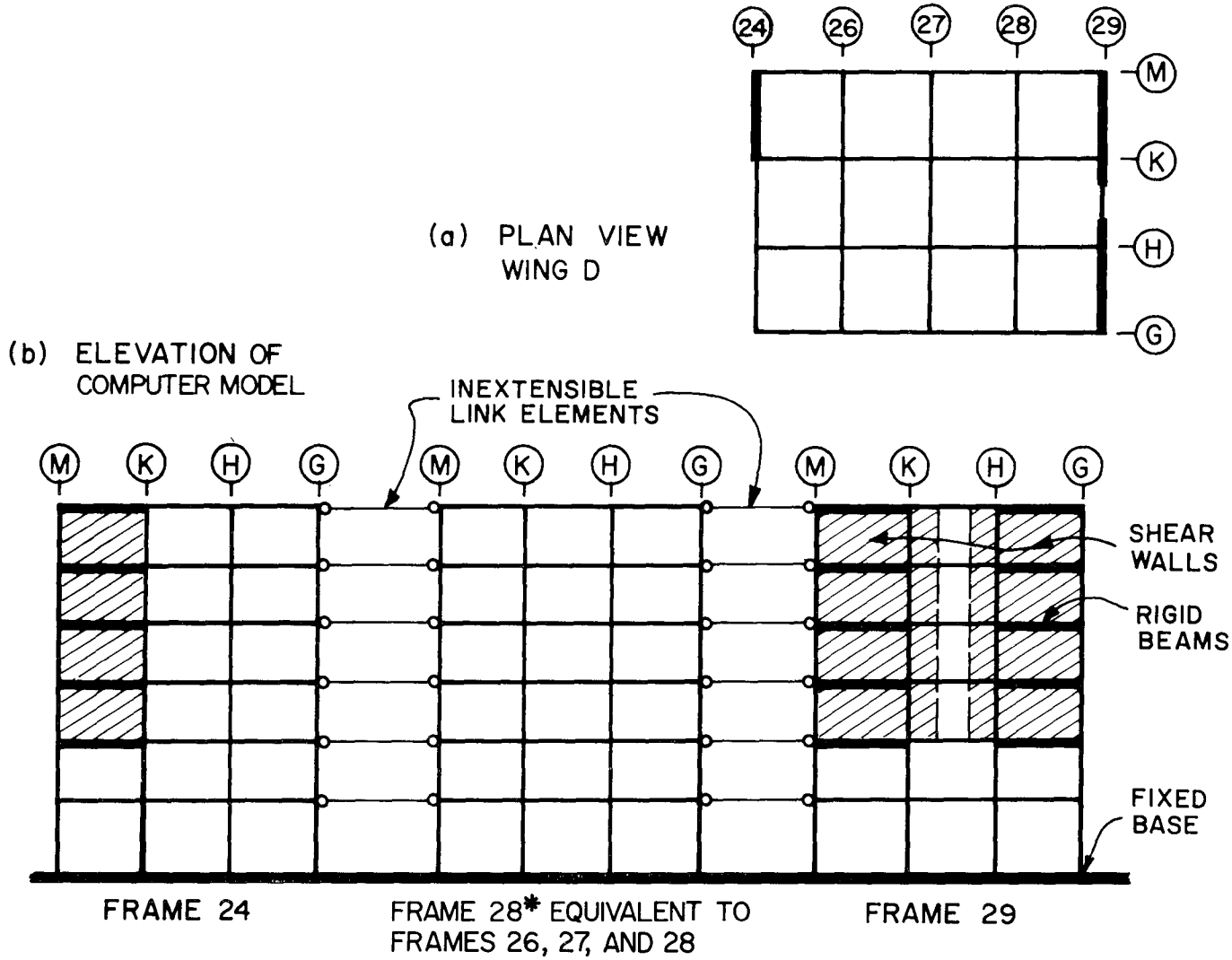

FIG. 6.3 SCHEMATIC REPRESENTATION OF MODELING USED IN NONLINEAR ANALYSIS

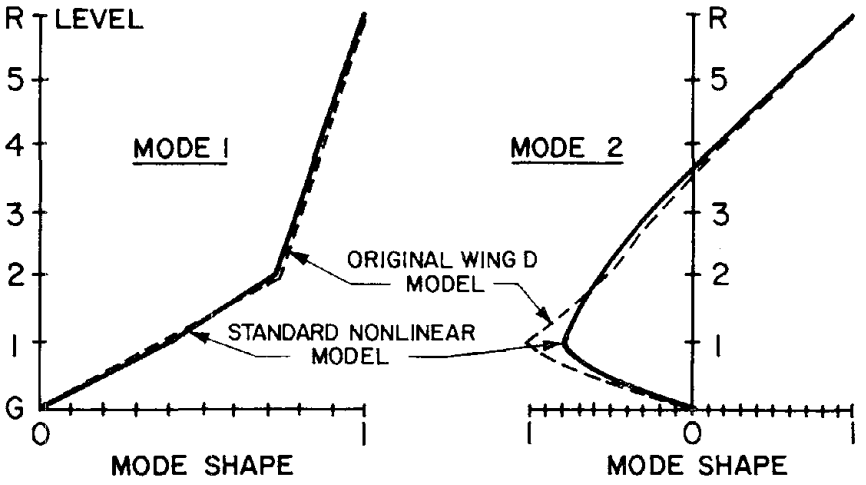

FIG. 6.4 COMPARISON OF NORMALIZED MODE SHAPES FOR ORIGINAL WING D MODEL AND THE STANDARD MODEL USED IN THE NONLINEAR ANALYSIS

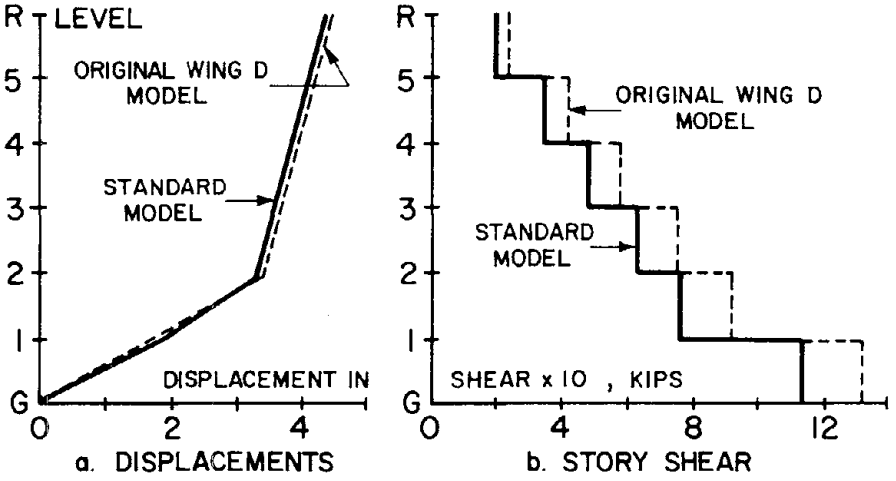

FIG. 6.5 COMPARISON OF ELASTIC RESPONSES OF ORIGINAL AND STANDARD NONLINEAR MODELS OF WING D SUBJECTED TO THE S-16°-E DERIVED PACOIMA DAM BASE ROCK RECORD (0.65g)

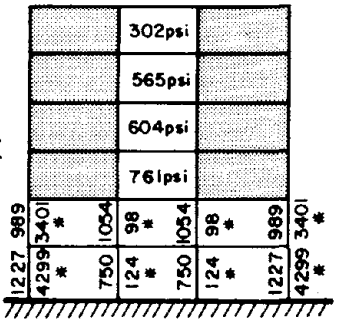

FIG. 6.6 MAXIMUM ELASTIC SHEAR AND AXIAL FORCES IN COLUMNS IN FRAME 29 FOR STANDARD NONLINEAR MODEL; S-16°-E DERIVED PACOIMA DAM BASE ROCK RECORD (0.65g); SHEAR STRESSES IN WALLS

NOTE: UNITS IN KIPS; AXIAL FORCES WITH STAR

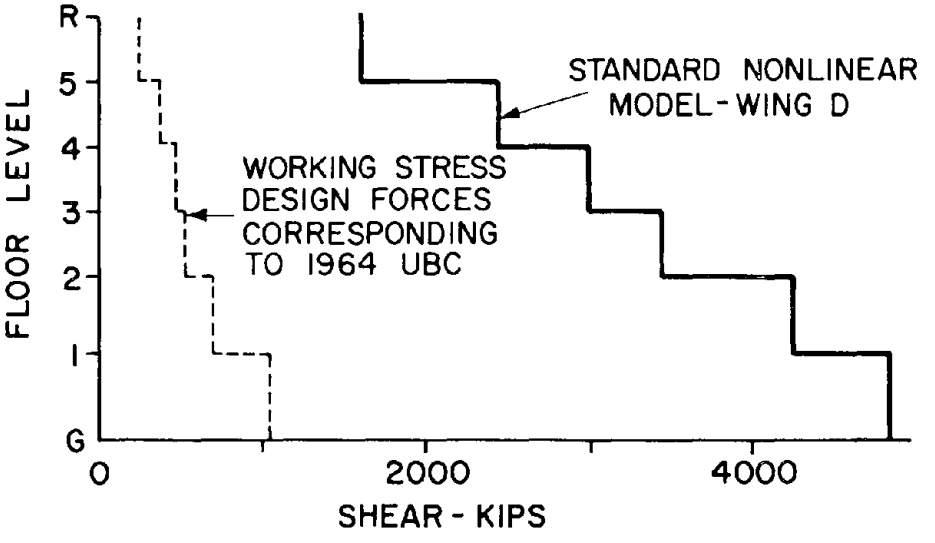

FIG. 6.7 ENVELOPE OF STORY SHEARS FOR STANDARD NONLINEAR MODEL RESULTING FROM SIMULATED RECORD NO. 6 COMPARED TO STATIC DESIGN SHEARS

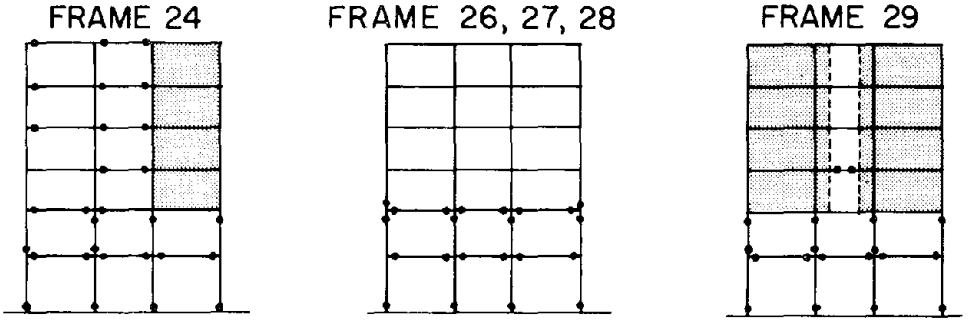

FIG. 6.8 LOCATIONS OF PLASTIC HINGING IN STANDARD NONLINEAR MODEL FOR SIMULATED RECORD NO. 6

FIG. 6.9 FORMATION OF PANEL COLLAPSE MECHANISM

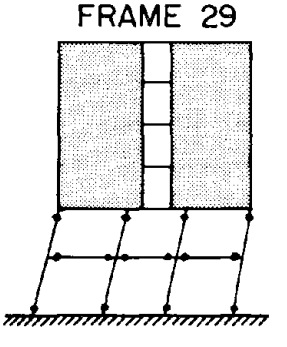

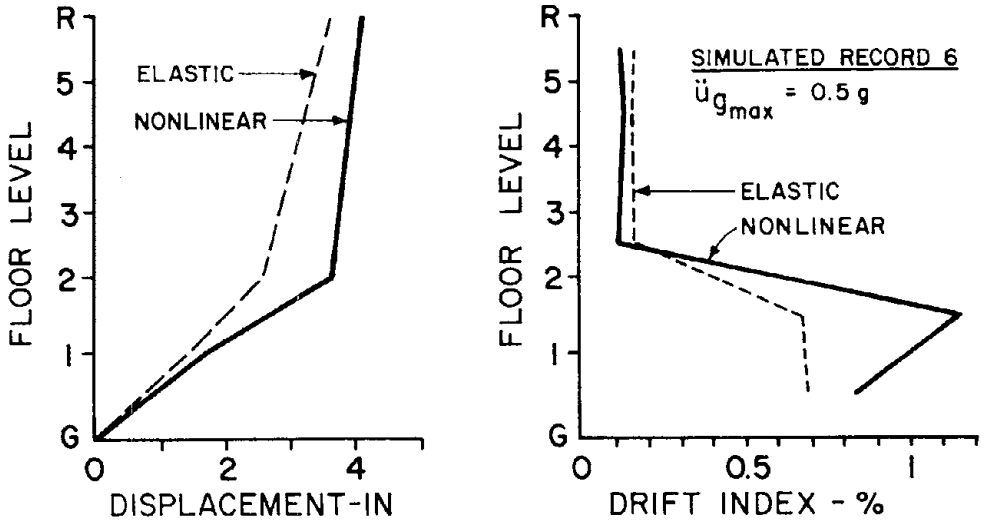

(a) MAXIMUM DISPLACEMENTS (b) MAXIMUM DRIFTS

FIG. 6.10 COMPARISON OF ENVELOPES OF MAXIMUM LATERAL FLOOR DISPLACEMENTS AND STORY DRIFTS OBTAINED IN ELASTIC AND NONLINEAR ANALYSES OF THE STANDARD NONLINEAR WING D MODEL

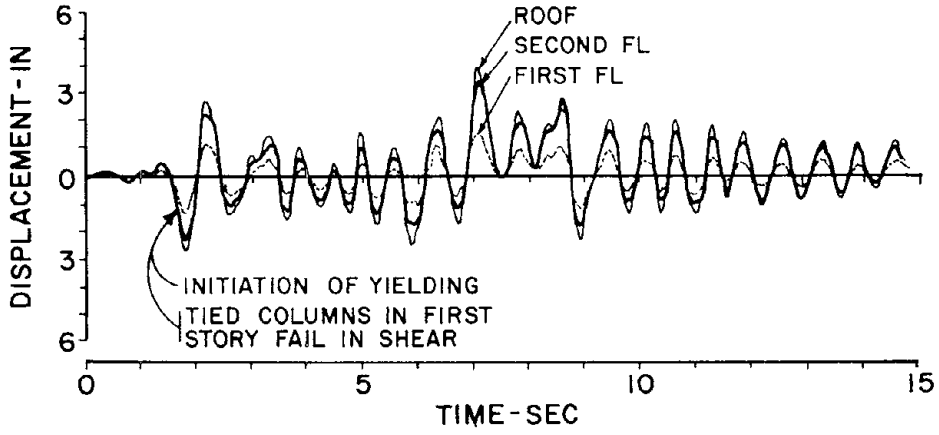

FIG. 6.11 DISPLACEMENT RESPONSE TO SIMULATED GROUND MOTION

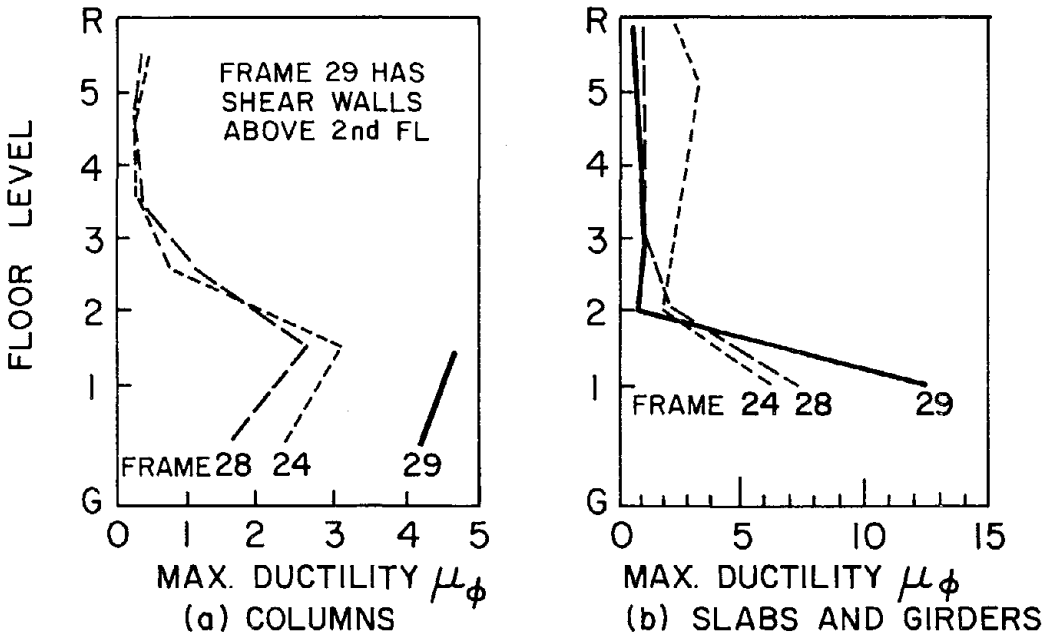

FIG. 6.12 ENVELOPES OF MAXIMUM CYCLIC CURVATURE DUCTILITY FACTORS FOR COLUMNS, GIRDERS AND SLABS FOR THE STANDARD NONLINEAR WING D MODEL SUBJECTED TO THE SIMULATED RECORD NO. 6

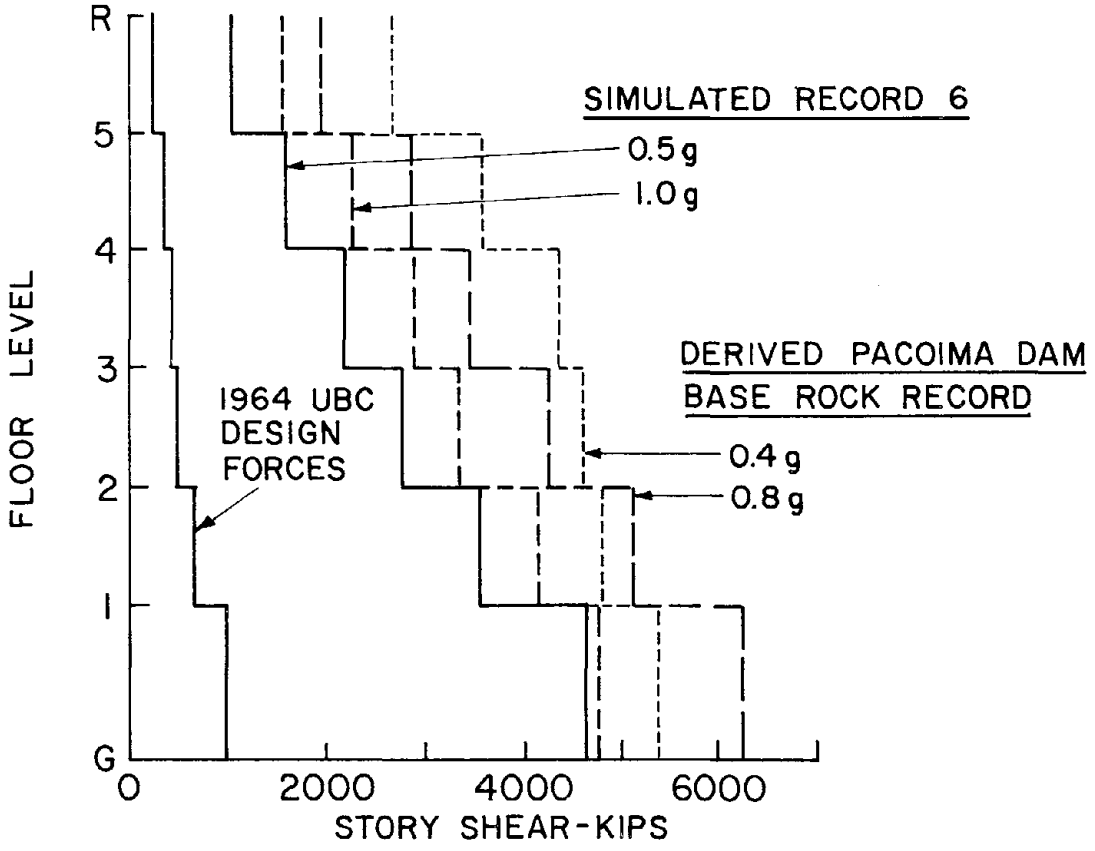

FIG. 6.13 ENVELOPES OF MAXIMUM STORY SHEARS FOR STANDARD NONLINEAR MODEL TO DIFFERENT GROUND MOTIONS

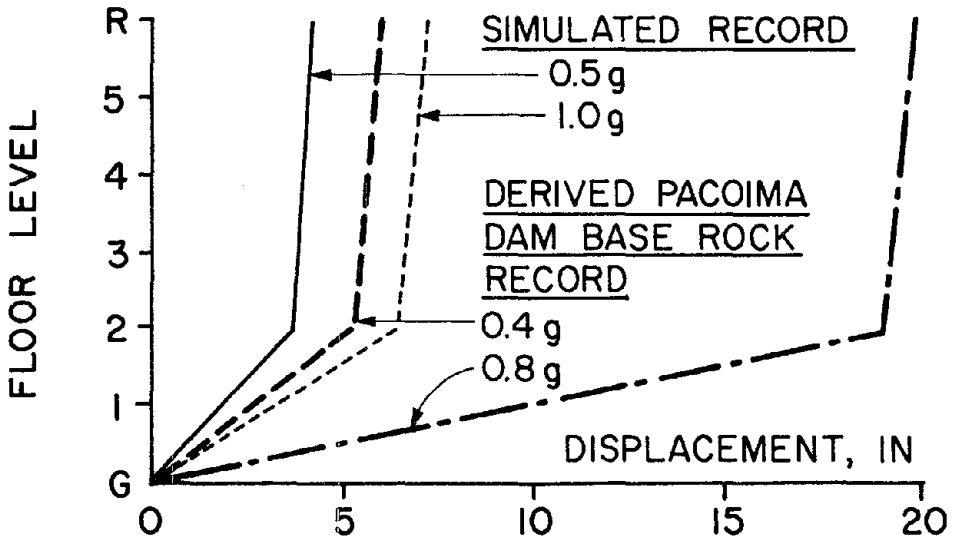

FIG. 6.14 COMPARISON OF MAXIMUM FLOOR DISPLACEMENTS FOR DIFFERENT GROUND MOTION RECORDS – STANDARD NONLINEAR MODEL

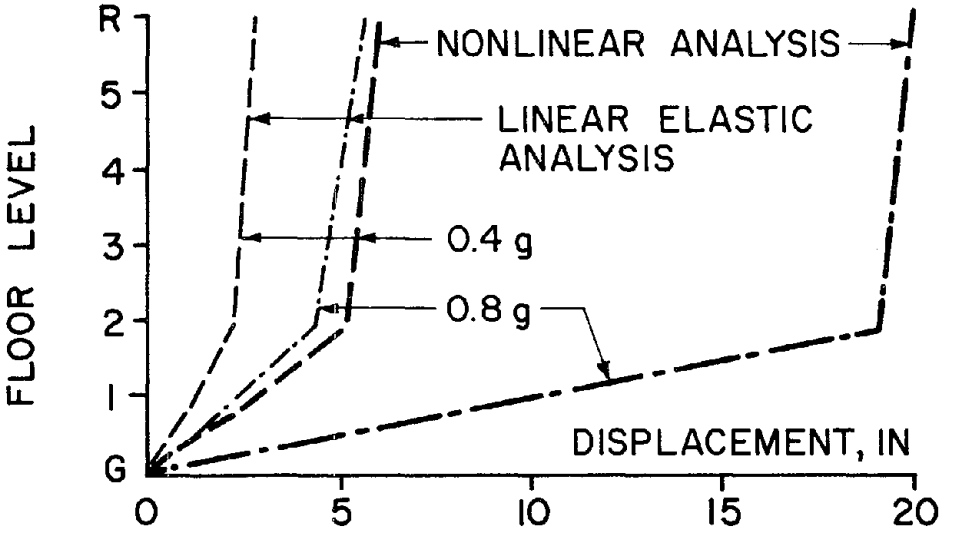

FIG. 6.15 COMPARISON OF LINEAR ELASTIC AND NONLINEAR RESPONSES TO THE DERIVED PACOIMA DAM BASE ROCK RECORD

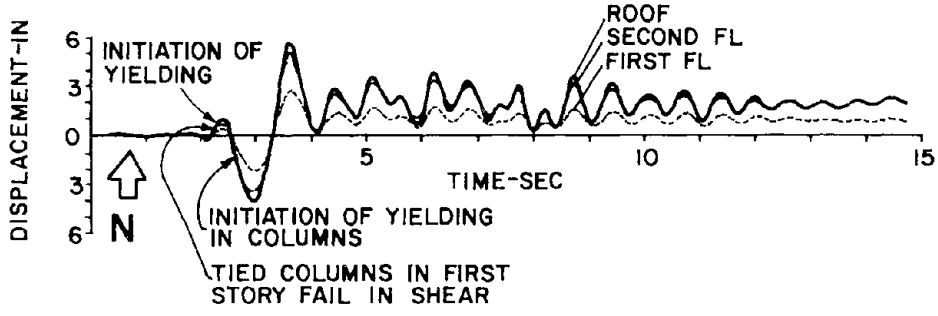

FIG. 6.16 DISPLACEMENT RESPONSE TO DERIVED PACOIMA DAM BASE ROCK MOTION (0.4g)

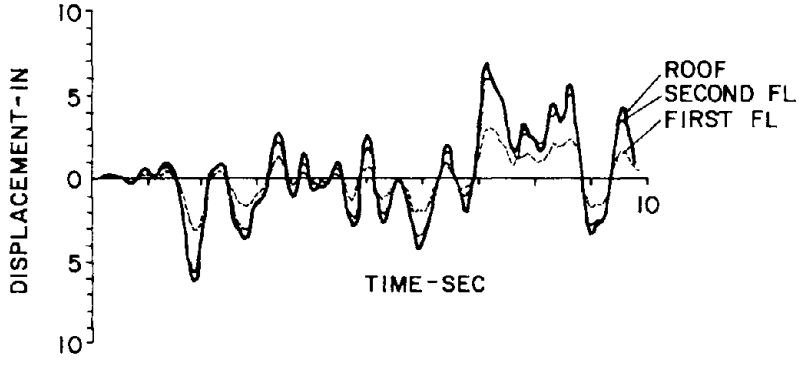

FIG. 6.17 DISPLACEMENT RESPONSE TO AMPLIFIED SIMULATED GROUND MOTION (1.0g)

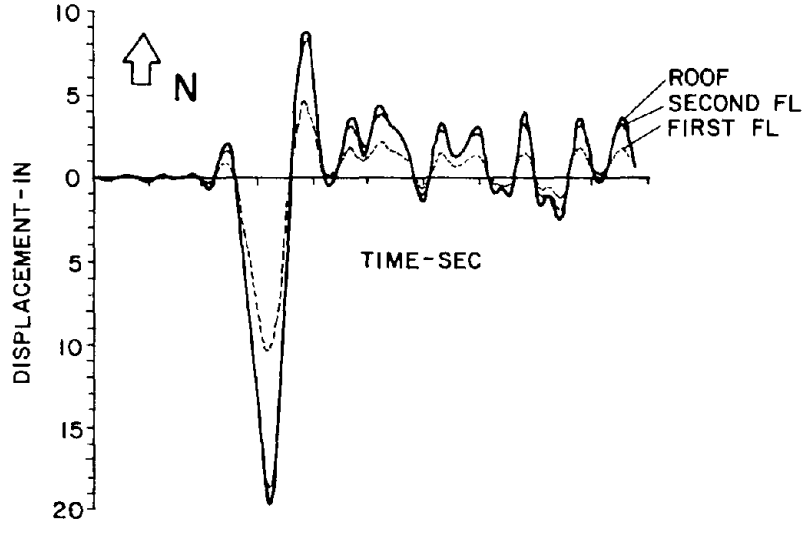

FIG. 6.18 DISPLACEMENT RESPONSE TO AMPLIFIED DERIVED PACOIMA DAM BASE ROCK MOTION (0.8g)

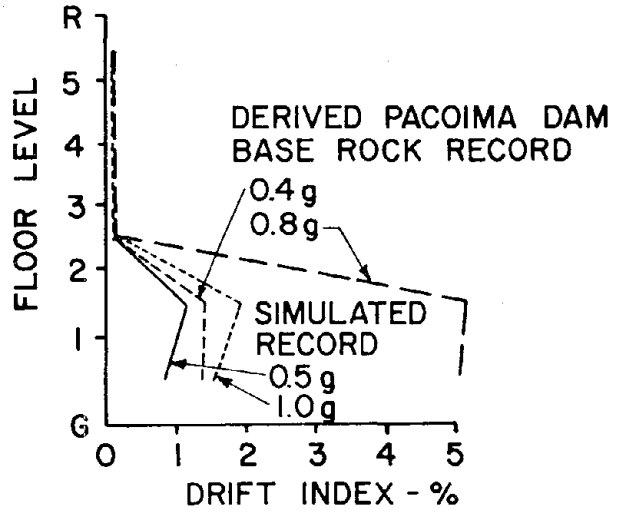

FIG. 6.19 COMPARISON OF MAXIMUM INELASTIC STORY DRIFT INDICES FOR DIFFERENT GROUND MOTION RECORDS

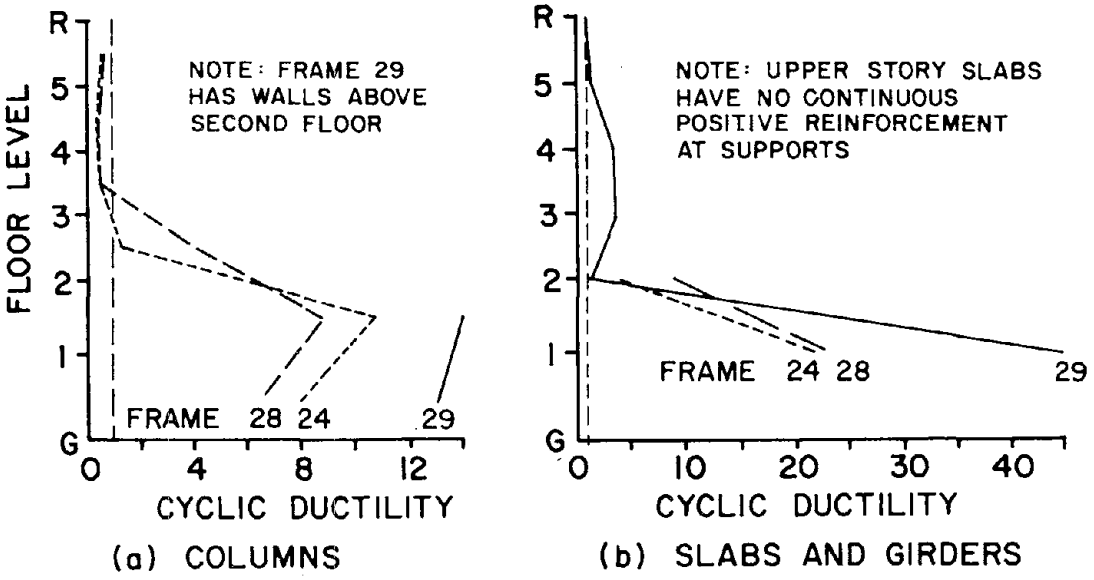

FIG. 6.20 ENVELOPES OF MAXIMUM CYCLIC CURVATURE DUCTILITY FACTORS FOR AMPLIFIED SIMULATED RECORD NO. 6

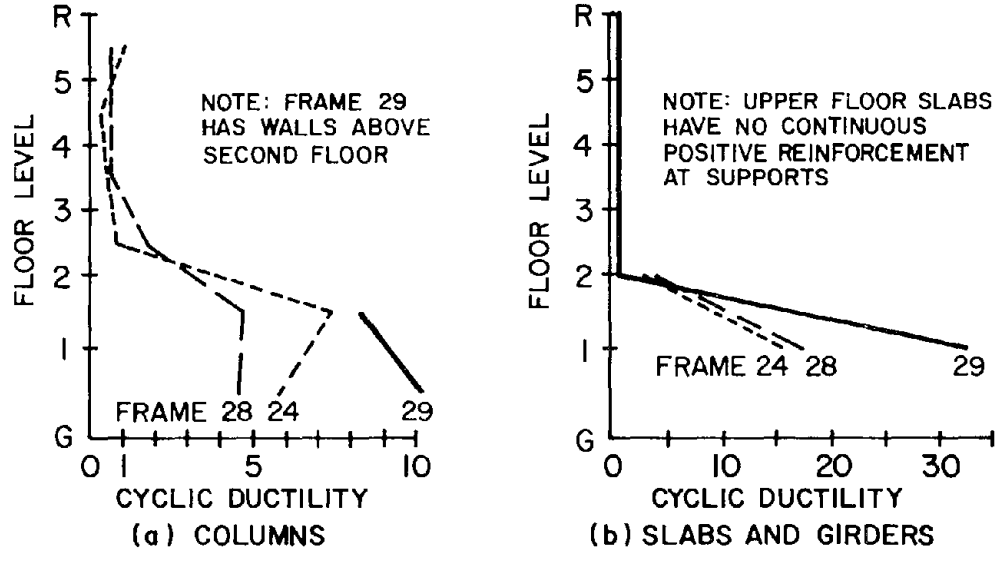

FIG. 6.21 ENVELOPES OF MAXIMUM CYCLIC CURVATURE DUCTILITY FACTORS FOR DERIVED PACOIMA DAM BASE ROCK RECORD (0.4g)

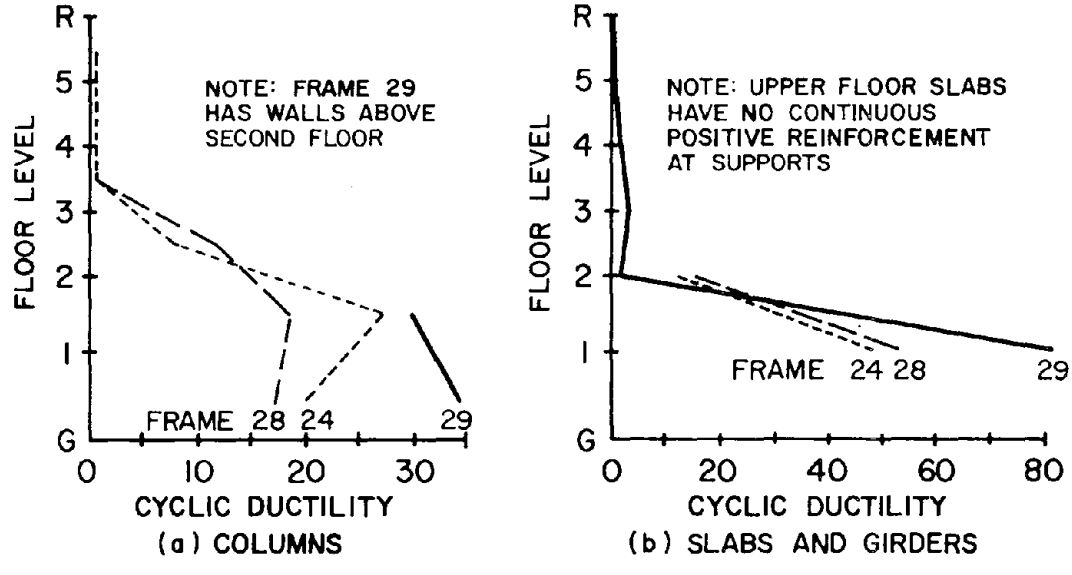

FIG. 6.22 ENVELOPES OF MAXIMUM CYCLIC CURVATURE DUCTILITY FACTORS FOR AMPLIFIED DERIVED PACOIMA DAM BASE ROCK RECORD (0.80g)

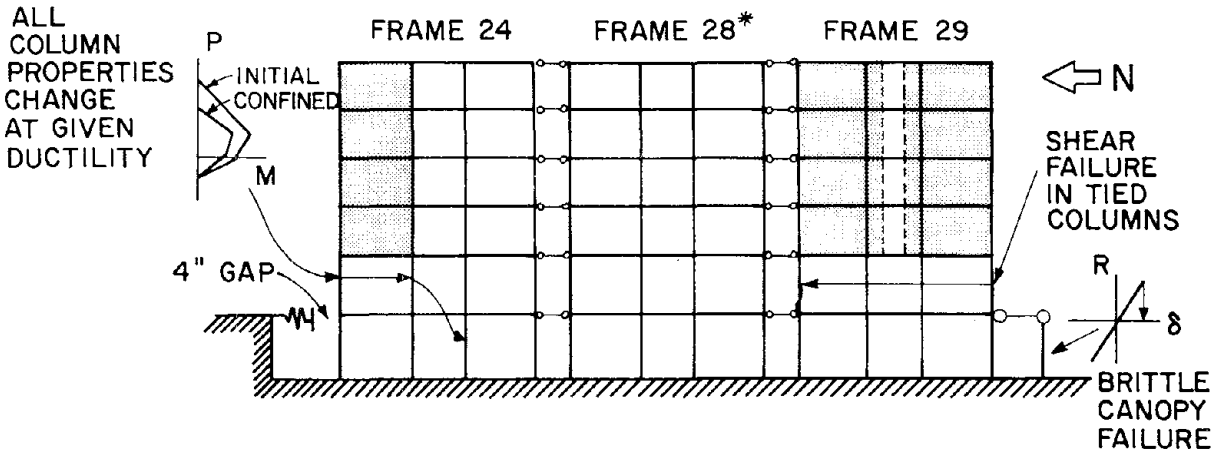

FIG. 6.23 SCHEMATIC REPRESENTATION OF FAILURE MODEL

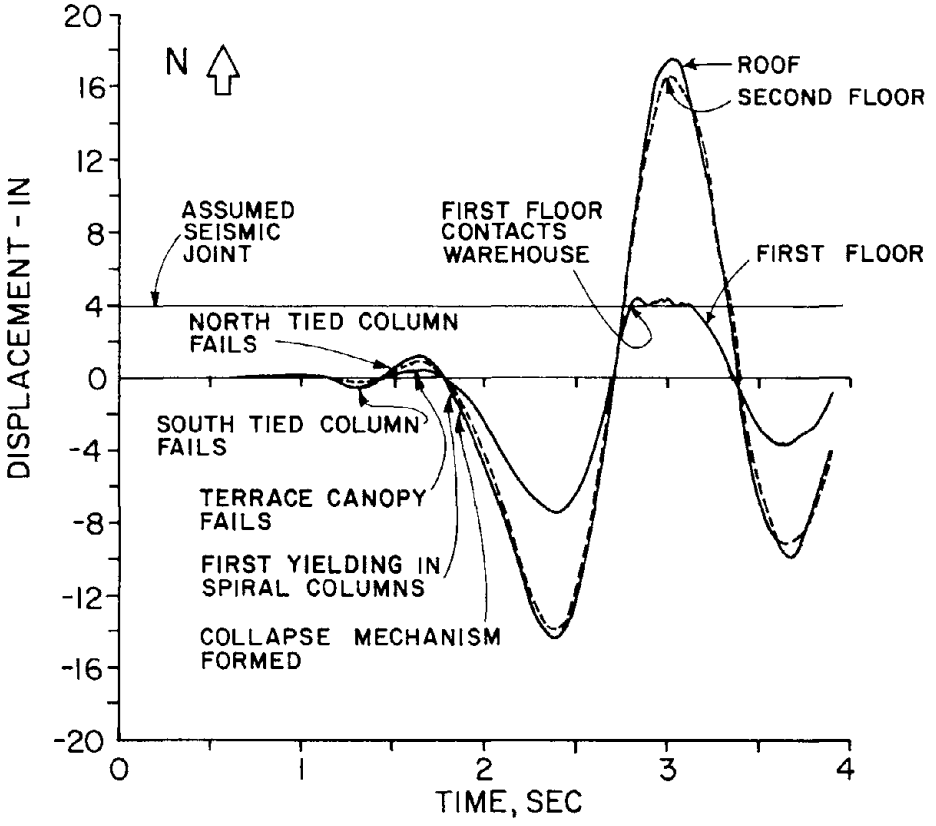

FIG. 6.24 RESPONSE HISTORY FOR FAILURE MODEL SUBJECTED TO FILTERED PACOIMA DAM BASE ROCK RECORD

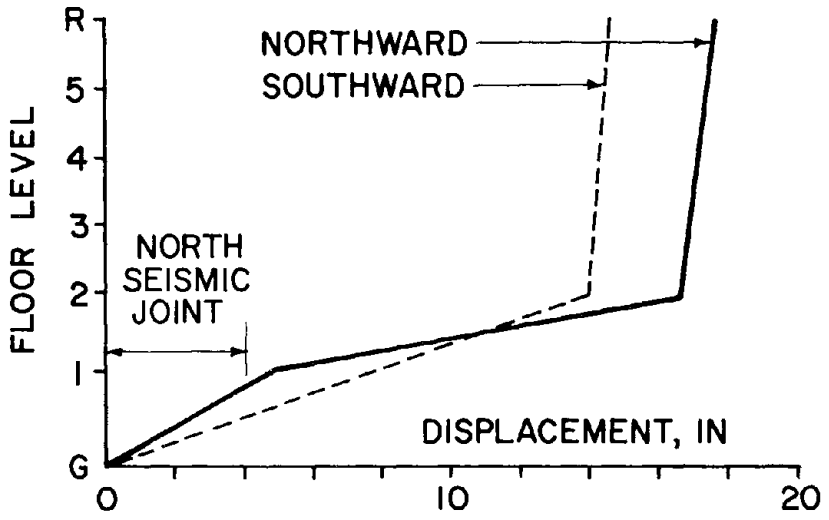

FIG. 6.25 ENVELOPES OF MAXIMUM NORTH AND SOUTH DISPLACEMENTS FOR FAILURE MODEL SUBJECTED TO FILTERED PACOIMA DAM BASE ROCK RECORD

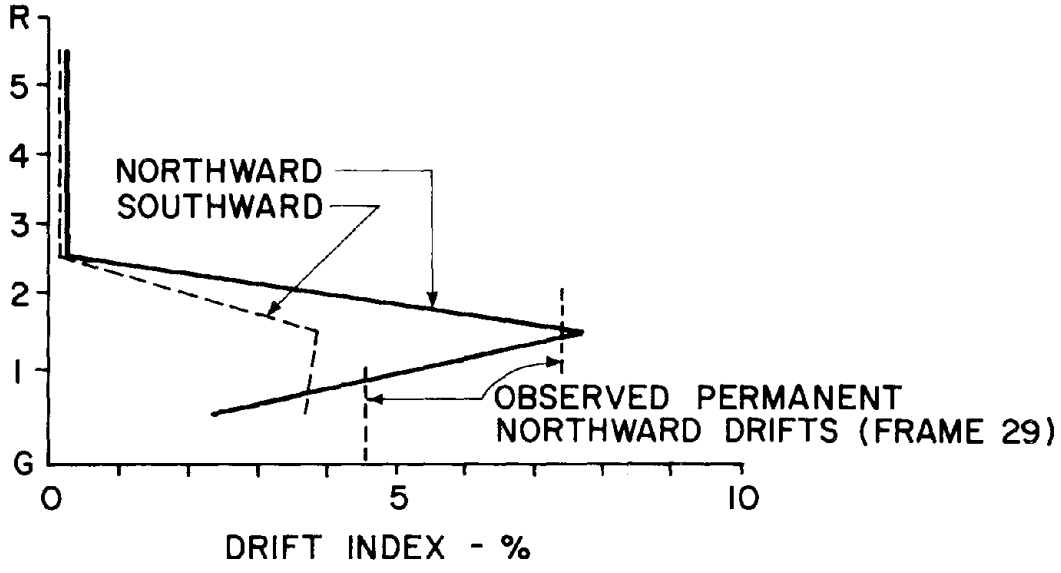

FIG. 6.26 ENVELOPES OF MAXIMUM NORTH AND SOUTH DRIFTS FOR FAILURE MODEL DUE TO FILTERED PACOIMA DAM BASE ROCK RECORD COMPARED WITH OBSERVED PERMANENT DRIFTS

APPENDIX A

EARTHQUAKE REGULATIONS IN THE 1965 LOS ANGELES COUNTY BUILDING LAWS

[2.1]

Sec. 2314. (a) **General.** Every building or structure and every portion thereof shall be designed and constructed to resist stresses produced by lateral forces as provided in this Section. Stresses shall be calculated as the effect of a force applied horizontally at each floor or roof level above the foundation. The force shall be assumed to come from any horizontal direction.

K = Numerical coefficient as set forth in Table No. 23-H.

Σwh = Summation of the products of all "w_x" "h_x" for the building.

M = Overturning moment at the base of the building or structure.

N = Total number of stories above exterior grade.

T = Fundamental period of vibration of the building or structure in seconds in the direction under consideration.

V = Total lateral load or shear at the base.

W = Total dead load.

EXCEPTION: "W" shall be equal to the total dead load plus 25 per cent of the floor live load in storage and warehouse occupancies.

W_p = The weight of a part or portion of a structure.

w_x = That portion of "w" which is located at or is assigned to the level designated as "x."

Z = numerical coefficient equal to one.

(d) **Minimum Earthquake Forces for Buildings. 1. Total lateral force and distribution of lateral force.** Every building shall be designed and constructed to withstand minimum total lateral seismic forces assumed to act nonconcurrently in the direction of each of the main axes of the building in accordance with the following formula:

$$V = ZKCW$$

The value of "K" shall be not less than that set forth in Table No. 23 H. The value of "C" shall be determined in accordance with the following formula:

$$C = \frac{0.05}{\sqrt[3]{T}}$$

EXCEPTIONS: 1. "C" = 0.10 for all one-story and two-story buildings.

2. The product "KC" shall be not less than 0.12 or more than 0.25 for elevated tanks on four or more cross-braced legs.

"T" is the fundamental period of vibration of the structure in seconds in the direction considered. Properly substantiated technical data for establishing the period "T" for the contemplated structure may be submitted. In the absence of such data, the value of "T" shall be determined by the following formula:

$$T = \frac{0.05\,H}{\sqrt{D}}$$

(b) **Definitions.** The following definitions apply only to the provisions of this Section.

SPACE FRAME is a three-dimensional structural system composed of interconnected members, other than shear or bearing walls, laterally supported so as to function as a complete self-contained unit with or without the aid of horizontal diaphragms or floor bracing systems.

SPACE FRAME—VERTICAL LOAD-CARRYING is a space frame designed to carry all vertical loads.

SPACE FRAME—MOMENT RESISTING is a vertical load-carrying space frame in which the members and joints are capable of resisting design lateral forces by bending moments. This system may or may not be enclosed by or adjoined by more rigid elements which would tend to prevent the space frame from resisting lateral forces.

BOX SYSTEM is a structural system without a complete vertical load-carrying space frame. In this system the required lateral forces are resisted by shear walls as hereinafter defined.

SHEAR WALL is a wall designed to resist lateral forces parallel to the wall. Braced frames subjected primarily to axial stresses shall be considered as shear walls for the purpose of this definition.

(c) **Symbols and Notations.** The following symbols and notations apply only to the provisions of this Section.

C = Numerical coefficient for base shear as specified in Section 2314 (d) 1.

C_p = Numerical coefficient as specified in Section 2314 (d) 2 and as set forth in Table No. 23-I.

D = The dimension of the building in feet in a direction parallel to the applied forces.

F_a = Allowable axial stress.

f_a = Computed axial stress.

F_b = Allowable bending stress.

f_b = Computed bending stress.

F_p = Lateral forces on the part of the structure and in the direction under consideration.

F_x = Lateral forces applied to a level designated as "x."

H = The height of the main portion of the building in feet above the base.

h_x = Height in feet above the base to the level designated as "x."

J = Numerical coefficient for base moment as specified in Section 2314 (h).

EXCEPTIONS: 1. "T" = 0.10 N in all buildings in which the lateral resisting system consists of a moment-resisting space frame which resists 100 per cent of the required lateral forces and which frame is not enclosed by or adjoined by more rigid elements which would tend to prevent the frame from resisting lateral forces. For the purpose of computing "C" the value of "T" need not be less than 0.10 seconds.

2. The period "T" for elevated tanks or towers with four or more legs, cross braced, shall be computed by an acceptable method.

The total lateral force "V" shall be distributed over the height of the building in accordance with the following formula:

$$F_x = \frac{V\,w_x\,h_x}{\Sigma wh}$$

EXCEPTIONS: 1. One-story and two-story buildings shall have uniform distribution.

2. Where the height to depth ratio of a lateral force resisting system is equal to or greater than five to one, 10 per cent of the total force "V" shall be considered as concentrated at the top story. The remaining 90 per cent shall be distributed as provided for in the above formula.

At each level designated as "x," the force "F_x" shall be applied over the area of the building in accordance with the mass distribution on that level.

2. Lateral force on parts or portions of buildings or other structures. Parts or portions of buildings or structures and their anchorage shall be designed for lateral forces in accordance with the following formula:

$$F_p = ZC_pW_p$$

The values of "C_p" are set forth in Table No. 23-I. The distribution of these forces shall be according to the gravity loads pertaining thereto.

3. **Pile foundations.** Individual pile or caisson footings of every building or structure shall be so interconnected by ties each of which can carry by tension and compression a horizontal force equal to 10 per cent of the larger pile cap loading unless it can be demonstrated that equivalent restraint can be provided by other approved methods.

[**EXCEPTION:** Ties may be omitted for belled footings having a height not exceeding six feet (6') nor twice the diameter of the bell and for piles supporting one-story buildings of lightweight Type IV-N Construction.]

(e) **Distribution of Horizontal Shear.** Total shear in any horizontal plane shall be distributed to the various resisting elements in proportion to their rigidities considering the rigidity of the horizontal bracing system or diaphragm as well as the rigidities of the vertical resisting elements.

(f) **Drift.** Lateral deflections or drift of a story relative to its adjacent stories shall be considered in accordance with accepted engineering practice.

(g) **Horizontal Torsional Moments.** Provisions shall be made for the increase in shear resulting from the horizontal torsion due to an eccentricity between the center of mass and the center of rigidity. Negative torsional shears shall be neglected. In addition, where the vertical resisting elements depend on diaphragm action for shear distribution at any level, the shear resisting elements shall be capable of resisting

TABLE NO. 23-H—HORIZONTAL FORCE FACTOR "K" FOR BUILDINGS OR OTHER STRUCTURES[1]

TYPE OR ARRANGEMENT OF RESISTING ELEMENTS	VALUE OF K
All building framing systems except as hereinafter classified	1.00
Buildings with a box system as specified in Section 2314 (b)	1.33
Buildings with a complete horizontal bracing system capable of resisting all lateral forces, which system includes a moment resisting space frame, which when assumed to act independently is capable of resisting a minimum of 25 per cent of the total required lateral force.	0.80
Buildings with a moment resisting space frame which when assumed to act independently of any other more rigid elements is capable of resisting 100 per cent of the total required lateral forces in the frame alone.	0.67
Elevated tanks supported with four or more cross-braced columns and not supported by a building	3.00[2]
Structures other than buildings and other than those set forth in Table No. 23-I.	1.50

[1]Where wind load as set forth in Section 2307 would produce higher stresses, this load shall be used in lieu of the loads resulting from earthquake forces.

[2]The tower shall be designed for an accidental torsion of five per cent as set forth in Section 2314 (g). Elevated tanks which are supported by buildings or do not conform to type or arrangement of supporting elements as described above shall be designed in accordance with Section 2314 (d) 2 using "C_p" .2.

coefficients at the base of the tower determined by considering the tower as either a separate building for its own height or as part of the over-all structure. The resulting total shear from the tower shall be applied at the top of the lower part of the building which shall be otherwise considered separately for its own height.

(j) **Structural Frame.** Buildings more than 13 stories or one hundred and sixty feet (160') in height shall have a complete moment resisting space frame capable of resisting not less than 25 per cent of the required seismic load for the structure as a whole. The frame shall be made of a ductile material or a ductile combination of materials. The necessary ductility shall be considered to be provided by a steel frame with moment resistant connections or by other systems proved by tests and studies to provide equivalent energy absorption.

TABLE NO. 23-I—HORIZONTAL FORCE FACTOR "C_p" FOR PARTS OR PORTIONS OF BUILDINGS OR OTHER STRUCTURES

PART OR PORTION OF BUILDINGS	DIRECTION OF FORCE	VALUE OF C_p
Exterior bearing and nonbearing walls, interior bearing and nonbearing walls which extend three-fourths of the height of the room, and masonry and concrete fences over six feet (6') in height.[1]	Normal to flat surface	0.2
Cantilever parapet and other cantilever walls, except retaining walls.	Normal to flat surface	1.00
Exterior and interior ornamentations and appendages.	Any direction	1.00
When connected to or a part of a building: towers, tanks, towers and tanks plus contents, chimneys, smokestacks, and penthouses.	Any direction	0.20[2]
When resting on the ground, tank plus effective mass of its contents.	Any direction	0.10
Floors and roofs acting as diaphragms.[3]	Any direction	0.10

[1]In no case shall horizontal force be less than 10 pounds per square foot. See Section 2312 (b) for limitations on deflection.

[2]When "H/D" of any building is equal to or greater than five to one, increase value by 50 per cent.

[3]Floors and roofs acting as diaphragms shall be designed for a minimum value of "C_p" of 10 per cent applied to loads tributary from that story unless a greater value of "C_p" is required by the basic seismic formula $V = ZKCW$.

a torsional moment assumed to be equivalent to the story shear acting with an eccentricity of not less than five per cent of the maximum building dimension at that level.

(h) **Overturning.** Every building or structure shall be designed to resist the overturning effects caused by the wind forces and related requirements specified in Section 2307, or the earthquake forces specified in this Section, whichever governs.

EXCEPTION: The axial loads from earthquake force on vertical elements and footings in every building or structure may be modified in accordance with the following provisions:

1. The overturning moment "M" at the base of the building or structure shall be determined in accordance with the following formula:

$$M = J \Sigma F_x h_x$$

WHERE:

$$J = \frac{0.5}{\sqrt[3]{T^2}}$$

The required value of "J" shall be not less than 0.33 nor more than 1.00.

"J" shall be 1 for elevated tanks supported with four or more cross-braced legs.

2. The overturning moment "M_x" at any level designated as "x" shall be determined in accordance with the following formula:

$$M_x = \frac{H - h_x}{H} M$$

At any level the overturning moments shall be distributed to the various resisting elements in the same proportion as the distribution of the shears in the resisting system. Where other vertical members are provided which are capable of partially resisting the overturning moments, a redistribution may be made to these members if framing members of sufficient strength and stiffness to transmit the required loads are provided.

Where a vertical resisting element is discontinuous, the overturning moment carried by the lowest story of that element shall be carried down as loads to the foundation.

(i) **Set-Backs.** Buildings having set-backs wherein the plan dimension of the tower in each direction is at least 75 per cent of the corresponding plan dimension of the lower part may be considered as a uniform building without set-backs for the purpose of determining seismic forces.

For other conditions of set-backs the tower shall be designed as a separate building using the larger of the seismic

(k) **Design Requirements.** 1. **Combined axial and bending stresses in columns forming a part of a space frame.** Maximum allowable extreme fiber stress in columns at intersection of columns with floor beams or girders for combined axial and bending stresses shall be the allowable bending stress for the material used. Within the center one-half of the unsupported length of the column, the combined axial and bending stresses shall be such that

$$\frac{f_a}{F_a} + \frac{f_b}{F_b}$$

is equal to or less than 1.

When stresses are due to a combination of vertical and lateral loads, the allowable unit stresses may be increased as specified in Section 2303.

2. **Building separations.** All portions of structures shall be designed and constructed to act as an integral unit in resisting horizontal forces unless separated structurally by a distance sufficient to avoid contact under deflection from seismic action or wind forces. [Structural separations of at least one inch (1"), plus one-half inch ("½") for each ten feet (10') of height above twenty feet (20') are considered adequate to meet the requirements of this paragraph.]

3. **Minor alterations.** Minor structural alterations may be made in existing buildings and other structures, but the resistance to lateral forces shall be not less than that before such alterations were made, unless the building as altered meets the requirements of this Section of the Code.

4. **Unreinforced masonry.** All elements within the structure which are of masonry or concrete and which resist seismic forces or movement shall be reinforced so as to qualify as reinforced masonry or concrete as specified in Chapters 24 and 26.

5. **Combined vertical and horizontal forces.** In computing the effect of seismic force in combination with vertical loads, gravity load stresses induced in members by dead load plus design live load, except roof live load, shall be considered.

APPENDIX B - EVALUATION OF MEMBER PROPERTIES

B.1 INTRODUCTION

The methods used to determine the properties of the various types of members encountered in the facility are examined in this appendix. This includes evaluation of the properties essential to both the elastic and nonlinear computer analyses. Because of the large number of members contained in the building, tabulation of all member properties is not possible. Consequently, numerical values will generally be limited to a single quantitative example for each member type.

B.2 COLUMN PROPERTIES

To specify the elastic sectional stiffness of a column element, its axial area, A, shear area, A_v, and moment of intertia, I, had to be calculated. The elastic properties of the initial sections were calculated using the following equations:

$$A = A_g + (n-1)A_s \tag{B.1a}$$

$$A_v = \frac{5}{6} A_g \tag{B.1b}$$

$$I = I_g + (n-1) \sum_{i=1}^{NB} A_{s_i} d_i^2 \tag{B.1c}$$

where

A_g = gross concrete area, sq. in.;

A_s = total area of longitudinal reinforcement, sq. in.;

d_i = distance of reinforcement i to neutral axis, in.;

I_g = moment of inertia of gross concrete section, $in.^4$;

$n = E_{steel}/E_{concrete}$; and

NB = number of longitudinal reinforcing bars.

For the nonlinear analyses, evaluation of the necessary input data was more complex due to the member's nonlinear material characteristics and the alteration of their cross-sections due to spalling. The computer program, *RCCOLA*, discussed in detail in Reference 6.2, was used to perform the required calculations. This program calculates the moment required to maintain equilibrium at a section given the section geometry, the material properties, the axial load, and the maximum compressive concrete strain. The principal assumptions are that the neutral axis is perpendicular to an axis of symmetry of the section, plane sections remain plane, and stresses are uniquely determined by the monotonic constitutive relationships specified for the various materials.

The program accepts general piecewise linear concrete stress-strain relationships. In this investigation the stress-strain relationship suggested by Park and Kent [B.1] was assumed for tied columns, and for spiral columns the relationship by Blume, et al. [B.2] was assumed. For both of these idealizations, the stress-strain relationship is a function of the amount and location of the transverse reinforcement.

For the longitudinal steel reinforcement, an elasto-perfectly plastic stress-strain relationship is assumed up to initiation of strain-hardening. A cubic strain-hardening law is then assumed. Wherever possible, parameters for these relationships were taken from the material properties discussed in Chapter 2.

Once an axial load, P, and a maximum concrete strain is specified, an iterative procedure, illustrated in Fig. B.1, is followed by the computer program until the internally resisted axial force equals the specified external load, i.e.

$$P = \int_A \sigma \, dA \qquad (B.2)$$

where σ is the material stress distribution based on the given steel and concrete stress-strain relationships. The strain distribution is determined by geometry from the specified maximum concrete strain and the assumed location of the neutral axis. When the location of the neutral axis corresponding to the maximum concrete strain

and to the applied axial load is correctly determined, the resisting moment, M, is evaluated by:

$$M = \int_A y \, \sigma \, dA \tag{B.3}$$

where y is the distance of the area, dA, from the plastic centroid. Thus, by specifying a sequence of maximum concrete strains, the moment-average curvature relationship can be constructed for a section at a constant axial load by noting that the average curvature, ϕ, is related to the maximum concrete strain, ε_c, by:

$$\phi = \frac{\varepsilon_c}{kd} \tag{B.4}$$

where kd is the distance from the compression face of the section to the neutral axis (see Fig. B.1).

When the maximum concrete strain exceeds the value which would initiate spalling, this computational method must be modified if it is to account realistically for the changes in the cross-sectional geometry resulting from spalling of the concrete cover and buckling of any unconfined longitudinal reinforcement.

Two alternate methods are used to incorporate these effects in the computer program. In the first, the calculations are based on the initial section until the spalling strain is reached; then, the entire cover and any unconfined reinforcement is assumed ineffective, and further calculations are based on the confined section alone. This idealization generally gives a conservative indication of the post-spalling behavior of sections. In the second method, the concrete in the cover and core are considered separately (see Fig. B.1) and different stress-strain relationships are assumed for each. Spalling can be accounted for explicitly using this method by specifying that the unconfined cover can sustain no stress for strains larger than that necessary to initiate spalling. However, this procedure is not as computationally efficient as the former.

The data generated for the moment-curvature relationships can alternatively be presented in the form of interaction curves in order to clarify the influence of axial loads, P, on the bending resistance,

M, of a column. By connecting points with the same maximum concrete compressive strains in a P and M plane, conventional interaction diagrams are obtained.

A member may not be able to develop the full flexural capacity indicated by the previous computational procedures due to insufficient shear strength. It is important, particularly in aseismic design, to avoid brittle shear failure modes. To help assess the possibility of a shear failure, the computer program calculates the shear strength of column members according to current ACI code requirements [B.3] or according to the empirical relationship obtained by Faradji Capon and Diaz de Cossio [B.4] for circular columns with spiral reinforcement. For example, the ACI code gives the permissible shear force, V_u, at a section in compression as:

$$V_u = b_w d \left(\frac{f_y A_v}{b_w s} + v_c \right) \qquad (B.5)$$

where the nominal concrete shear stress, v_c, is taken as the minimum of

$$v_c = 1.9\sqrt{f'_c} + 2500\, \rho_w \frac{V_u d}{M_m} \qquad (B.6a)$$

or

$$v_c = 3.5 \sqrt{f'_c} \sqrt{1 + 0.002\, N_u/A_g} \qquad (B.6b)$$

and in which

A_g = gross area of section, sq. in.;

A_s = area of longitudinal reinforcement, sq. in.;

A_v = area of shear reinforcement within a distance s along the member, sq. in.;

b_w = web width, or diameter of circular sections, in.;

d = distance from extreme compression fiber to centroid of tension reinforcement (for circular sections, d need not be less than distance from extreme compression fiber to centroid of longitudinal reinforcement on opposite half of member), in.;

f'_c = specified concrete compressive strength, psi;

f_y = yield stress of shear reinforcement, psi;

h = overall thickness of member, in.;

M_m = $M_u - N_u (4h-d)/8$;

M_u = applied moment at section, in.-lb;

N_u = axial load applied normal to the cross-section occurring simultaneously with V_u (compression positive), lb.;

s = spacing of shear reinforcement in a direction parallel to the longitudinal reinforcement, in.; and

ρ_w = $A_s/(b_w d)$.

Alternatively, the permissible shear force may be predicted for circular members with compressive loads using the relationship presented in Reference B.4

$$V_u = A_g \left[1.9\sqrt{f'_c} + 2500\rho \frac{V_u D}{M_u}\right]\left(1 + 0.04 \frac{N_u}{V_u}\right) + \frac{f_y A_v D}{s} \quad \text{(B.}$$

in which all terms are as defined previously, except that D is the diameter of the section, $\rho = A_{ST}/A_g$, and A_{ST} is the total area of longitudinal reinforcement. Appropriate equations may be found in codes to consider members with tensile axial loads [B.3].

Rather than using the shear capacity directly, it is helpful to compute the end moment, M_s, in an antisymmetrically loaded column with a constant shear distribution and an effective length, L, corresponding to the development of the ultimate shear force, i.e. $M_s = V_u L/2$. Envelopes of the shear capacity for a column for various axial loads and effective lengths may be directly compared with the flexural capacity interaction curves to determine the adequacy of the shear reinforcement. Further remarks regarding this type of computation may be found in Reference 6.2.

Curvature ductility has been extensively used as an index of the ability of a section to sustain inelastic deformation. This factor is generally defined as the ratio of the maximum curvature that can be developed at a section to the curvature indicating yielding at that section, ϕ_y. Once the moment-average curvature relationships are known, the ductility factors can easily be determined for given concrete strains and axial loads. Where there

are many layers of reinforcement or where spalling occurs, moment-average curvature relationships may deviate substantially from an ideal elasto-perfectly plastic shape. In such cases this definition of ductility is not directly related to the energy absorption capacity of the section. Consequently, in these cases an "equivalent" ductility factor, μ_{equiv}, may be useful:

$$\mu_{equiv} = \frac{A_{M\phi}}{M_y \phi_y} + \frac{1}{2} \qquad (B.8)$$

in which $A_{M\phi}$ is the area under the moment-curvature plot; M_y is the moment at first yield of reinforcement (in tension or compression); and ϕ_y is the curvature corresponding to M_y. Ductility factors obtained in this manner may then be used to interpret the results of the inelastic dynamic analyses in order to assess the adequacy of the design.

To illustrate the methods used to determine the column properties for the analyses of the main building, and to briefly examine the nonlinear behavior of reinforced concrete members, two sections used in Wing D were selected for detailed presentation. These sections are a typical spirally reinforced column found in the first story and a tied column representative of those that failed in the ground story.

B.2.1 Spiral Column Example

The first column to be considered, shown in Fig. B.2, is a 26-in. square, spirally reinforced column having eight No. 14 bars arranged in a circular pattern for longitudinal reinforcement and 5/8-in. diameter spirals spaced at 2.25-in. intervals.

The assumed properties of the longitudinal reinforcement, shown in Fig. B.2(b) were based on laboratory tests of No. 14 bars taken from the building after the earthquake and from mill test records [2.9]. Idealized concrete stress-strain relationships based on the recommendations of Reference B.2 were used for the analysis of this spiral column. These relationships were based on the detailing of the member and an estimated concrete compressive strength of 6.67 ksi.

The confined concrete was assumed to sustain an ultimate compressive strain of 2.5 percent. The stress-strain curve assumed for the unconfined cover was the same as that for the confined core up to a strain of 0.0035 in./in., above this level, the concrete cover was assumed to have spalled; consequently, it was unable to sustain stress. The effect of spalling was considered explicity in all of the calculations performed for this example.

To compute the initial section properties to be used in the elastic analyses, Eq. B.1 was used assuming a modulus of elasticity of 3540 ksi for the concrete. Thus, for this column:

$$n = E_s/E_c = 29000/3540 = 8.2;$$

$$A = (26)^2 + (8.2 - 1)(8)(2.25) = 806 \text{ in.}^2;$$

$$A_v = 5(26)^2/6 = 563 \text{ in.}^2; \text{ and}$$

$$I = 26(26)^3/12 + (8.2 - 1)(4)(2.25)(9.24^2 + 3.82^2) = 44,559 \text{ in.}^4$$

Moment-curvature relationships generated for this section under different axial loads are shown in Fig. B.3. A number of observations can be made regarding these results. The curves clearly do not have an ideal elasto-plastic shape as assumed in the non-linear dynamic analyses, and there were significant differences between the shapes of the curves for various axial loads. The initial cracked stiffness of the section, measured as the initial slope of the M-ϕ curves, increased with increasing axial loads. A substantial increase in moment capacity after the first yielding of the reinforcement is observed since the reinforcement is not concentrated at the extreme tension and compression faces. With the onset of spalling, however, the strength of the section drops, especially in the case of high axial loads, and only after substantial strain-hardening does the section regain its initial strength. The effect of spalling is particularly significant for this type of cross-section due to the large fraction of the initial area taken by the unconfined cover.

The variation of the post-yield flexural capacity is also clearly illustrated by plotting the ratio of the moment corresponding

to a particular post-elastic state (e.g., spalling) to the yield moment for various axial loads. This ratio, $O_{M_y} = M/M_y$, will be described as an over-strength ratio, although values less than unity can occur. The yield moment used in this definition is taken as the minimum moment necessary to yield any of the reinforcement in either tension or compression. Curves of over-strength ratios are shown in Fig. B.4 corresponding to the critical moment values for (1) the minimum post-yield strength, (2) the strength at the onset of spalling (i.e. $\varepsilon_c = 0.0035$ in./in.), (3) the minimum strength developed after the onset of spalling, and (4) the maximum strength developed by the section.

The behavior of this section is significantly different for loads above and below about 40 percent of the balanced load ($P_b \simeq$ 1450 kips). Above this load intensity, the maximum bending strength is developed at the onset of spalling. This value is generally just larger than the yield moment except for very high axial loads. The flexural capacity decreases substantially (see the shaded portion of Fig. B.4) after spalling starts. The strength generally reaches its minimum at a concrete strain of 0.005 in./in. and increases to about the initial yield level as the strain is increased to 2.5 percent (although not quite to the strength present at spalling). This type of behavior is exemplified by the M-ϕ curve in Fig. B.3 for P = 3000 kips.

For axial forces less than about 40 percent of the balanced load, the strength of the section at the onset of spalling was considerably higher than the initial yield moment, as seen in Figs. B.3 and B.4. Furthermore, the severity of the strength reduction that occurred after spalling decreased with decreasing axial load. The strength of the section at a strain of 2.5 percent was generally significantly greater than the moment present when spalling initiated; this strength corresponded to the maximum flexural capacity of the section for these lower axial loads (Fig. B.4). The effect of spalling decreased with decreasing axial loads since smaller portions of the section were generally in compression and, therefore, subject

to spalling. The behavior of the section at low axial loads is exemplified by the M-ϕ curve shown in Fig. B.3 for zero axial force.

The effect of spalling can also be seen by inspecting the axial load-bending moment interaction curves shown in Fig. B.5 for maximum compressive concrete strains of 0.002, 0.0035, 0.005, and 0.025 in./in. These curves indicate that there was a significant increase in the strength of the section as the maximum concrete compressive strain increased from 0.002 in./in. to 0.0035 in./in. After spalling occurred at a strain of 0.0035 in./in., however, the flexural capacity of the section dropped significantly. At a strain of 0.005 in./in., the strengths were generally the lowest developed after spalling occurred and these were similar to those obtained at a strain of only 0.002 in./in. Generally, it was not until the maximum strain approached 2.5 percent that the flexural capacities of members with compressive axial loads regained their initial maximum values.

Since the moment-curvature relationships computed for the section (Fig. B.3) are not elasto-perfectly plastic in shape, the equivalent curvature ductility factor, defined by Eq. B.8 should be a more useful index of the maximum energy absorption capacity of the section than ϕ_{max}/ϕ_y. Plots of equivalent curvature ductility factors, corresponding to the concrete strains used for the interaction curves, are also shown in Fig. B.5. These curves indicate that the ductility capacity of the section was reduced appreciably by the presence of compressive axial forces. This phenomenon is illustrated by the moment-curvature relationships (Fig. B.3) which show that the maximum curvatures also decrease with increasing axial load.

For axial forces above the balanced point, Fig. B.6 shows that the equivalent curvature ductility factors were somewhat smaller than the conventional yield ductility values (i.e. $\mu_\phi = \phi/\phi_y$) due to the large reduction of the moment capacity that occurred after spalling. The equivalent ductility capacities, however, were much greater than the conventional values for tensile axial loads due to the large increase in the post-yield moment resulting from the substantial strain-hardening that occurred in this case.

It is interesting to note that while the maximum curvature and curvature ductility capacities at a given concrete strain generally decreased with increasing axial load, the actual energy absorption did not always follow this trend. Figure B.7 shows that the energy absorption capacity increased slightly as the axial load increased from zero to about 40 percent of the balanced load. For example, the area under the moment-curvature plots for axial loads of +1000 kips and zero load were both nearly 35 kip-in./in., while the ratios of ϕ_{max} to ϕ_y were 9.9 and 17.1, respectively. This fact is due to the difference in the moment capacities of the sections.

The input for the nonlinear dynamic analyses must be extracted from this information. It is clear from the preceding dicussions that modeling of the mechanical characteristics must take into account the extent of the potential inelastic deformations that may occur in a member since current analytical models are much simpler than the actual behavior. The damage in the building provided a good estimate of the severity of yielding at various locations. In many cases, however, these values had to be readjusted to reconcile differences in the assumed and calculated response. The rate of strain-hardening assumed in the analyses was 0.03 on the basis of average values calculated for several columns at the axial loads developed under gravity loading. As discussed in Chapter 6, two sets of yield levels were selected; one, representing the mechanical properties prior to spalling; the other, based on the confined core, representing severe inelastic distress. The idealized interaction curves selected for the example spiral column are superimposed in Fig. B.8 with the interaction curves computed for maximum concrete compressive strains of 0.0035 and 0.01 in./in. It is clear from this figure that the idealized shape of the interaction curves used in the analyses differ from the actual curves by substantial amounts at some axial load intensities. The idealized curves were selected to have about the same average post-elastic moment as the actual member for the range of loads anticipated during the seismic response. For example, the post-yielding portions of the M-ϕ curves (Fig. B.3) indicate that the section strengthens significantly before spalling; the idealized

interaction curve was therefore located between the actual curves for first yielding and spalling. The curve corresponding to the post-spalling behavior was similarly selected. The difficulties of representing the complex nonlinear behavior of reinforced concrete members by bilinear hysteretic mechanical models controlled by simple interaction curves is clearly demonstrated by this example.

The example spiral column was able to develop its flexural capacity without shear failure during the earthquake due to the presence of closely spaced spiral reinforcement. It is interesting to compare the flexural capacity of this member with its shear capacity as indicated by various code recommendations. For a clear span length of 156 in. the end moments corresponding to the development of the shear capacity under double curvature (the point of inflection at midheight) is shown in Fig. B.9. Curves corresponding to just the confined core have been computed according to the recommendations of ACI 318-71 [B.3], the ductile moment-resisting space frame provisions of the 1973 edition of the UBC [2.5] for seismic zones and the empirical recommendations of Reference B.4. While the curves corresponding to these recommendations indicate that the shear capacity of this member would clearly be expected to exceed its ultimate flexural capacity at all axial load intensities, there are substantial differences in the shear strengths predicted by the different recommendations.

The ductile moment-resisting space frame (D.M.-R.S.F.) provisions of the UBC and the ACI code use the same method to compute the nominal shear stress carried by the concrete. For circular sections, computation of the contribution of the transverse reinforcement to the shear strength and the effective shear area is based on the ACI recommendation (Eq. B.5) of an equivalent rectangular section with a width equal to the diameter of the section and an effective depth not less than the distance from the extreme compression face to the centroid of the longitudinal reinforcement in the opposite half of the member. The UBC (D.M.-R.S.F.) bases the contribution of concrete to the shear strength on the area of the confined core (to the

outside of the hoops); this contribution should be disregarded for axial loads less than 0.12 $f'_c A_g$. The UBC bases the contribution of spiral transverse reinforcement on the diameter of the confined section, but only two-thirds of the area of the spirals should be considered effective in this case. For the spiral column considered in this example, the differences in these definitions result in substantially lower predictions of shear strength by the UBC than by the ACI code. Also, it is clear that the major contribution to the shear capacity comes from the transverse reinforcement and the concrete contributes relatively little strength at low axial loads. The experimentally derived relationship given in Reference B.4 for compressive axial loads indicates shear strengths even higher than those predicted using code equations.

At zero axial load, the effective length of the column would have to be less than 7 ft before shear would control its behavior, even if the contribution of the concrete is disregarded (based on the ACI provisions). The large differences between these shear capacity curves indicate the need for experimental and analytical investigations of the shear capacity of members subjected to axial load, bending moments and shear forces.

B.2.2 Tied Column Example

Although the spiral columns used in the building exhibited very substantial inelastic energy absorption and dissipation capacities, the tied columns generally failed in shear, resulting in the collapse of many parts of the building. To clarify the reasons for the different behavior observed for the tied and spiral columns in the building, an idealized cross-section exemplifying the building's tied columns is also investigated.

The tied column considered as the basis of this example was a 20-in. square column having four No. 10 bars for longitudinal reinforcement and No. 3 hoops spaced at 18-in. intervals as shown in Fig. B.10. This ground story column was located at the intersection of column lines P.5 and 29. The design engineers specified minimum

strengths of 60 ksi for the longitudinal reinforcement, 40 ksi for the transverse hoops, and 5 ksi for the concrete. Tests of the materials conducted after the earthquake indicated that the actual strengths were significantly higher: 68 ksi for the No. 10 bars, 45 ksi for the No. 3 ties, and 6.67 ksi for the concrete. The constitutive relations used for the concrete and reinforcement in the subsequent analyses are shown in Fig. B.10. The relationships for concrete were based on the idealized relations presented in Reference B.1. Spalling was explicitly considered for these analyses.

The transverse reinforcement in this column was proportioned in accordance with the minimum provisions of the 1964 edition of the UBC [2.2]; i.e., No. 3 lateral ties, spaced at not more than 16 longitudinal bar diameters, 48 tie diameters, or the smallest dimension of the column. This detailing fails to satisfy the special provisions for seismic design contained in ACI 318-71 [B.3] or the 1973 edition of the UBC [2.5].

The mechanical characteristics of the column as designed will be examined in this section. A discussion of the behavior of the column that would have resulted had current ACI minimum requirements for ductile moment-resisting frames been met will be presented in Appendix C.

To compute the initial section properties for use in the elastic analyses of the building, Eq. B.1 was used assuming a modulus of elasticity equal to 3540 ksi for the concrete. Thus, for this tied column:

$$n = E_s/E_c = 29{,}000/3549 = 8.2$$

$$A = (20)^2 + (8.2 - 1)(4)(1.27) = 437 \text{ in.}^2;$$

$$A_v = 5(20)^2/6 = 333 \text{ in.}^2; \text{ and}$$

$$I = 20(20)^3/12 + (8.2 - 1)(4)(1.27)(7.8)^2 = 15{,}559 \text{ in.}^4.$$

Since the ties used in this column were spaced so far apart, practically no transverse confinement was provided for the concrete

core. Thus, the concrete stress-strain relationship assumed for the entire section was based on Reference B.1, except that the stress corresponding to strains greater than 0.0035 in./in. was taken as zero, and the longitudinal reinforcement was assumed to buckle whenever the compressive strain in the adjacent concrete exceeded 0.0035 in./in. For these assumptions, the initiation of spalling at a maximum concrete strain of 0.0035 in./in. resulted in an immediate loss of load carrying capacity. The column, however, was able to sustain significant inelastic deformations before spalling occurred when the axial forces were lower than the balanced load (provided that the shear forces were also low). This can be seen from the moment-curvature relationships presented in Fig. B.11 for different axial load intensities.

While there are many similarities between these M-ϕ curves and those shown in Fig. B.3 for the spiral column, a number of significant differences should be mentioned. Since the only longitudinal reinforcement present in the tied section was located near the extreme tension and compression faces, the flexural stiffness of the section decreased considerably with the first yielding of the reinforcement. Below the balanced load, the moment-curvature relationships for this section could adequately be represented by elasto-plastic idealizations, although those for the spirally reinforced column could not. For axial loads close to or greater than the balanced load ($P \approx 1100$ K), the ultimate moment capacity of the tied column occurred when yielding developed in the compression reinforcement and the moment capacity decreased rapidly thereafter (Fig. B.11). The axial load-bending moment interaction curves shown in Fig. B.12 also clearly show the significant loss in axial load and moment capacity that occurred after compression yielding (indicated by the ultimate capacity curve), but before spalling at these higher axial loads. There was insufficient transverse reinforcement provided to confine the concrere core of the tied column. Once spalling initiated, an immediate flexural failure could result at any axial load intensity.

Prediction of the section's mechanical characteristics on the basis

of the minimum specified material properties, rather than on the basis of its actual properties, resulted in a significant underestimation of the moment capacity. This can be seen in Figs. B.11 and B.12. The maximum curvatures developed for the different material properties were similar, however, as can be seen in Fig. B.11. This is also shown by the plots of maximum equivalent curvature ductilities shown in Fig. B.13. These ductility curves again indicate that at low axial load intensities the section was capable of developing signficicant inelastic flexural deformations before spalling occurred.

The transverse reinforcement provided in the column was insufficient for developing high shear forces, and, consequently, the column could have failed prematurely in shear. The actual column in the building was restrained at the top and bottom by much stiffer and stronger elements. The moments corresponding to shear failures in such a member are shown in Fig. B.12 for various axial loads and member lengths. Methods for computing these shear capacity-axial load interaction curves are based on Eqs. B.5 and B.6. For the given transverse reinforcement and specified material properties, Fig. B.12 indicates that the member had to be more than 14 ft long to avoid a shear failure. Since the actual moment capacity was underestimated by using the specified properties, even higher shear forces could have been developed, requiring a clear span greater than 18 ft to avoid shear failure. The clear span length of the actual member was less than 13 ft and its axial load was about 25 percent of the balanced load. Consequently, these curves indicate that such a column would likely fail in shear, before yielding, as observed in the actual column.

To avoid premature shear failures, the results presented in this section clearly show the need for considering realistic, or even maximum, values for the material properties, rather than the minimum specified strengths, in determining the maximum moments and shear that may act on a member. It is also apparent that it is necessary to estimate realistically a member's boundary conditions and axial

loading, since the shear capacity is very sensitive to the shear span and axial forces.

B.3 STRUCTURAL WALL PROPERTIES

Because of the simple, rectangular framing configuration assumed by the computer programs used in this investigation, it was not possible to model the walls in the upper four stories in a completely realistic manner. Each of the structural walls in the upper four stories were modeled by a series of two or more columns (colinear with the columns in the bottom of the two stories) connected within the width of the wall by rigid beams (Fig. 5.2). The properties of the equivalent columns were selected so that the framework representing the wall had lateral stiffness characteristics similar to those of the actual wall [5.2]. While this method is not exact, it permitted the highly overstressed columns that supported these walls to be realistically modeled. Since there was little evidence of yielding in the walls, they were treated as completely elastic elements.

B.3.1 Determination of Stiffness Parameters

The elastic stiffness parameters, i.e. the moment of inertia, I_c, and the axial area, A_c, of the columns in the equivalent frame were calculated using the equations illustrated in Fig. B.14. The beams connecting the columns in the walls were assumed to be rigid. The walls were considered as linear-elastic elements even in the nonlinear dynamic analyses.

To illustrate the modeling techniques used in the analyses, numerical values obtained for the second story wall located along frame line 18 between column lines BB and Z [i.e. Wall 18-BB-Z, see Fig. 2.1 and B.15(a)] will be presented. This wall was part of a series of walls located along frame line 18; note that it was connected to these other walls by tie beams. A detailed cross section of this isolated wall is shown in Fig. B.15(b). The columns in the equivalent frame were assumed to coincide with the column lines so that they were continuous with the columns in the bottom two stories. Additional fictitious column lines were added to the model to idealize the adjacent walls attached to this wall by the tie beams [see Fib. 5.2(b)].

Wall Parameters (Second Story Wall 18-BB-Z)

$$h = 12.5 \text{ ft}$$

$$a = 25.0 \text{ ft}$$

$$A_s = 1.0\left(25.0 + \frac{19 - 7.5}{12}\right) + \frac{(11)(21)}{144} = 27.6 \text{ ft}^2$$

$$I_s = 2510 \text{ ft}^4$$

Equivalent Column Parameters (derived according to Fig. B.14)

$$I_c \cong \left(2/I_s + 72/(A_s h^2)\right)^{-1}$$

$$= \left(2/2510 + 72/(27.9\ (12.5)^2)\right)^{-1} = 57.2 \text{ ft}^4$$

$$A_c \cong (2/a)^2\ (I_s/2 - I_c)$$

$$= \left(4/(25)^2\right)\ (2510/2 - 57.2) = 7.67 \text{ ft}^2$$

B.3.2 Shear Stress Capacity of Walls

The shear stress capacity of the walls in the building can be estimated using Kokusho's equations [B.5] for the unit cracking shear stress, τ_{crack}, and the maximum shear stress, τ_{max}, where:

$$\tau_{crack} = 0.085\ f'_c \qquad \text{(B.9a)}$$

$$\tau_{max} = 0.138\ f'_c + 0.5\ \rho_w f_y \qquad \text{(B.9b)}$$

in which f'_c is the compressive strength of concrete, psi; f_y is the yield stress of horizontal reinforcement, psi; and ρ_w is the horizontal reinforcement ratio.

On the basis of tests of specimens taken from the building, the strength of the specified 3000 psi concrete was assumed to be 5040 psi and the yield stress of the Grade 40 reinforcement was assumed to 51.0 ksi. For the walls used in the building, cracking would be initiated at a shear stress of 429 psi, and the maximum shear stresses that the walls could resist are given in Table B.1. It should be noted that these values are higher than those obtained using current ACI code recommendations. For example, the nominal ultimate shear stresses in the top two stories should be about $3.32\sqrt{f'_c}$ according to

the ACI recommendations [B.3] whereas the values in Table B.1 are about 10.8 $\sqrt{f'_c}$.

TABLE B.1 WALL REINFORCEMENT AND MAXIMUM SHEAR STRESS

Story	Wall Thickness	Horizontal Steel Reinforcement	Steel Ratio $\rho_w = A_s/A_w$	$0.138f'_c$ (psi)	$0.5\rho_w f_y$ (psi)	τ_{max} (psi)
5th, 4th	8 inch	#4 @ 18" o.c. each face	0.00278	696	71	767
3rd	10 inch	#4 @ 15" o.c. each face	0.00267	696	68	764
2nd	12 inch	#4 @ 12" o.c. each face	0.00278	696	71	767

B.4 FLAT SLAB PROPERTIES

Two different approaches for modeling the slab behavior were employed to obtain refined values for the effective sectional stiffnesses of the equivalent beams used in the nonlinear dynamic analyses. Both methods were based on finite element idealizations of the flat slabs encountered in frames 24 and 28. The analyses were performed with computer programs SAP [B.6] and PB-LCCT [B.7]. Equivalent numerical results were obtained using these programs. The effect of the reinforcement on the slab's stiffness was disregarded in the analyses.

The first approach consisted of modeling the slab for an isolated frame and imposing unit deformations at each of the joint's degrees of freedom in turn, while restraining the other degrees of freedom. In this manner, the stiffness coefficients for the slab were determined. The slab idealization used for this approach, shown in Fig. B.16, consisted of a three-bay, 25-ft wide strip of slab including the edge beams, drop panels, and rigid column-slab joints. The edges where the slab was isolated from the adjacent frames were constrained so that they could not rotate about an axis

parallel to the frame axis. This boundary condition represented the continuity of the slab with similar adjacent frames undergoing the same displacements. The slab was considered inextensible in its own plane.

Accordingly, the stiffness coefficients for the degrees of freedom shown in Fig. B.16 were computed. Because of the structural symmetry of the model, only the reactions of one-half of the system need be investigated. The stiffness coefficients obtained for frame 28 are shown in Eq. B.10.

$$\begin{Bmatrix} R_1 \\ M_1 \\ R_2 \\ M_2 \end{Bmatrix} = \left[\begin{array}{cccc|cccc} 56.6 & 6450. & -65.5 & 5400. & 9.6 & -462. & -0.6 & 42. \\ 6450. & 952000 & -7130. & 441000. & 720. & -33800. & -42. & 2800. \\ -65.5 & -7130. & 155. & 1230. & -98.7 & 7090. & 9.6 & -722. \\ 5400. & 441000. & 1230. & 1670000. & -7090. & 391000. & 463. & -338. \end{array}\right] \begin{Bmatrix} \Delta_1 \\ \Theta_1 \\ \Delta_2 \\ \Theta_2 \\ \Delta_3 \\ \Theta_3 \\ \Delta_4 \\ \Theta_4 \end{Bmatrix} \quad \text{(B.10)}$$

It is interesting to note from Eq. B.10 that substantial reactions develop at joints not immediately adjacent to a displaced node. This is further clarified in Fig. B.16 which shows the reactions resulting from a unit rotation of the degree of freedom at the exterior joint. Although the adjacent joint degrees of freedom were fixed, the slab allows stresses to be transferred beyond the adjacent fixed supports. If the beam analogy were correct, the stiffness coefficients in Eq. B.10 to the right of the solid line would be zero. This is clearly not the case, however. Several attempts were made to establish appropriate values for the moments of inertia of the equivalent beams. While it is possible to obtain approximate values suitable for design by matching only some of the stiffness coefficients (e.g., the rotational terms), a more general solution requires elaborate trial-and-error or least squares techniques. Because of the problems inherent in this approach, no definitive determination was reached and another method was subsequently used.

These problems clearly illustrate the complex nature of flat slab behavior, even in the elastic range, and the need for further research in this area.

To resolve this problem an alternative approach was followed which permitted an explicit determination of the desired properties. By recognizing that the midspan between column lines H and K was a line of structural symmetry and of antisymmetry for displacements under lateral loading of the structure, only one-quarter of the slab considered in the previous discussion need be analyzed (i.e. the shaded portion in Fig. B.16). The finite element idealization used for this model is shown in Fig. B.17. To obtain the desired slab behavior, the required boundary conditions were continuous roller supports along the discontinuous midspan between lines H and K and a constraint that tangents to the slab perpendicular to the frame axis remain horizontal along the two discontinuous edges of the slab parallel to the frame axis.

If only rotational joint degrees of freedom are considered in this case, the rotation of the slab joints, $\{\theta\}$, can be calculated for a set of assumed applied moments, $\{m\}$. The stiffness of an equivalent beam system is given by:

$$\begin{Bmatrix} M_1 \\ M_2 \end{Bmatrix} = E \begin{bmatrix} \frac{4I_1}{L_1} & \frac{2I_1}{L_1} \\ \frac{4I_1}{L_1} & \left(\frac{4I_1}{L_1} + \frac{3I_2}{L_2}\right) \end{bmatrix} \begin{Bmatrix} \theta_1 \\ \theta_2 \end{Bmatrix} \qquad \text{(B.11a)}$$

or

$$\{m\} = [K] \{\theta\} \qquad \text{(B.11b)}$$

where the terms are as defined in Fig. B.17. Since $\{m\}$ and $\{\theta\}$ are known from the finite element analyses, the moments of inertia for the equivalent beams can be solved by rewriting Eq. B.11 in the form:

$$\begin{Bmatrix} M_1 \\ M_2 \end{Bmatrix} = E \begin{bmatrix} \left(\frac{4\theta_1}{L_1} + \frac{2\theta_2}{L_1}\right) & 0 \\ \left(\frac{2\theta_1}{L_1} + \frac{4\theta_2}{L_1}\right) & \frac{3\theta_2}{L_2} \end{bmatrix} \begin{Bmatrix} I_1 \\ I_2 \end{Bmatrix} \qquad \text{(B.12a)}$$

or

$$\{m\} = [A]\{I\} \qquad \text{(B.12b)}$$

and solving for the required moments of inertia:

$$\{I\} = [A]^{-1}\{m\} \qquad \text{(B.13)}$$

The matrix, [A], however, depends on the applied moment distribution. To calculate the ratio of the applied joint moments corresponding to lateral floor deflections in the actual structure, an iterative procedure was used. Computations were based on a two-story, three bay subassemblage incorporating the equivalent beams and the actual columns. The effective moments of inertia of the beam subassemblages were obtained from Eq. B.13 using the results of an initial finite element analysis of the slab subjected to an assumed distribution of moments; those for the column subassemblages were based on values for the actual columns in the building. The columns were considered to be fixed at their far ends. A lateral force was applied to the subassemblage, and the moment distribution corresponding to the assumed equivalent moments of inertia was calculated. These refined joint moments were then applied to the slab in the finite element analysis and new, effective beam stiffnesses were calculated based on Eq. B.13. This process was then repeated until the ratio of applied moments for the finite element analysis matched that calculated for the subassemblage.

Using this method the equivalent moments of inertia of the slabs in frames 26 to 28 were calculated to be 20,940 $in.^4$ for the exterior bays and 19,230 $in.^4$ for the interior bay. For a 13-in. deep

flat slab (i.e. a slab with a uniform thickness equal to the total depth at the drop panel) this corresponds to an effective width of 110 in. The method suggested by Khan and Sbarounis [5.3] for flat slabs without drop panels indicates an effective width of 111 in. in this case, which is in close agreement, if the depth of the slab is taken to be the total depth of the drop panel and slab, and not that of the slab alone.

A similar analysis was conducted for the slabs in frame 24. In this case the slab was unsymmetric with respect to frame line 24 so that the full width of the slab was considered in the analysis. As shown in Fig. 2.5, the depth of the slab changes from 8 in. to 10 in. near frame 24. Strictly speaking it is not possible to isolate this frame from the adjoining ones, since they do not have the same geometrical configuration. However, it is assumed that the errors will be small enough in this case to disregard this effect. Thus, boundary conditions similar to those assumed for frames 26 to 28 are used. By using the iterative procedure just discussed, the equivalent beam moments of inertia for frame 24 were determined to be 36,720 $in.^4$ for the exterior bays and 36,150 $in.^4$ for the interior bay.

The yielding mechanisms that occur in flat slabs are complex and difficult to idealize using the simple models required by the existing computer programs. Because of the intricate placement of reinforcement, as exemplified by Fig. 2.15, and the uncertainty of the loading conditions, it is difficult to ascertain the appropriate yield lines. In addition, divergence from ideal elastic behavior due to cracking and local yielding is likely to occur substantially before the slab's full plastic moment is developed. The presence of large shear deformations which develop during yielding further complicates a completely realistic representation of the mechanical behavior of the slabs used in this building.

In order to establish the yield moments of the equivalent beams used to represent the slab behavior, several assumptions were made. Yield lines were assumed to form across the full width of the slab perpendicular to the frame line. The moment capacities of various

potential critical yield lines were determined using conventional ultimate strength techniques based on the experimentally determined material properties and the slab details (see Figs. 2.15 and 2.16). Since the moments due to gravity loads were generally small in comparison to the moment capacities, a linear moment distribution with reversal was assumed along the equivalent beam member. The equivalent yield moments at the column lines were taken as the minimum moments corresponding to this moment distribution required to form two yield lines across the slab between two column lines. This method is illustrated in Fig. B.18. Additional research is required to improve methods for modeling these types of slabs in the nonlinear range.

B.5 BEAM PROPERTIES

The elastic properties of the beams were based on their gross concrete sectional dimensions. Since axial and shear deformations were disregarded in the analyses, only flexural characteristics were evaluated. As an example of these types of calculations, the third floor coupling beam will be examined. This member was an 18-in. wide by 65-in. deep beam connected at the top on one side to an 8-in. deep slab. The effective overhanging flange formed by the slab was taken to be the minimum of one-twelfth of the span length (16 ft, 8 in./12 $\tilde{=}$ 16.5), six times the slab thickness (6 x 8 in. = 48 in.), or one-half the clear distance to the next beam (25 ft/2 = 12 ft, 6 in.). Thus, the width of the flange was assumed to be 16.5 in. for the purposes of evaluating the effective beam stiffness. The neutral axis relative to the bottom surface of the beam can be found as:

$$\bar{x} = \frac{\sum A_i x_i}{\sum A_i} = \frac{(18x65)(32.5) + (8x16.5)(65-8/2)}{(18x65) + (8x16.5)} = 35.4 \text{ in.} \quad (B.14)$$

in which A_i is the area of a part of the section, x_i is the location of the centroid of this area relative to a fixed datum, and $\bar{x}$ is the location of the neutral axis relative to the fixed datum. The moment of inertia of the section is given by:

$$I = \sum[I_i + A_i(x_i - \bar{x})^2] \qquad (B.15)$$

$$= 18(65)^3/12 + 18(65)(32.5 - 35.4)^2 + 16.5(8)^3/12$$

$$+ 16.5(8)(65 - 8/2 - 35.4)^2 = 508{,}988 \text{ in.}^4$$

in which I and I_i are the moments of inertia of the section and the ith subsection, respectively, and the other terms are as defined in Eq. B.14. Once the moment of inertia of the section is determined, it must be modified using a method similar to that discussed in Section 6.3.1 for columns, so as to conform to the computer program input requirements. To account for the rigid portions of the beam between the nodal points considered in the nonlinear analysis and the actual face of the wall and the difference in Young's modulus of the member and that specified in the program, the moment of inertia must be transformed according to Eq. 6.4:

$$I_{equiv} = \frac{3080 \text{ ksi}}{3540 \text{ ksi}} \left(\frac{200 \text{ in.}}{96 \text{ in.}}\right)^3 508{,}988 \text{ in.}^4 = 4.00 \times 10^6 \text{ in.}^4$$

This procedure is not exact since the carry over factor should also be modified, but this is not possible with the computer programs used. However, the value used was found to be acceptable for these analyses.

The strength of beams at the face of their supports was determined using the computer program described in Section B.2. In this case a zero axial load was specified to represent a beam condition. Moment capacities at intermediate locations in the beam were checked and were generally found not to be critical even with gravity loads imposed. For all beams in the nonlinear analyses, except the coupling beams connecting the shear walls in frame 29, the moment capacity at the support centerlines was taken to be that computed at the face of the supporting columns due to the small ratio of column width to slab span. In the spandrel beams a transformation was necessary because of the large distance between the face of the opening and the assumed column line. The method used is shown in Fig. B.19.

REFERENCES

B.1 Park, R. and Kent, D. M., "Flexural Members with Confined Concrete," Journal of the Structural Division, ASCE, Vol. 97, No. ST7, July 1971.

B.2 Blume, J. A., Newmark, N. M., and Corning, L. H., Design of Multistory Reinforced Concrete Buildings for Earthquake Motions, Portland Cement Association.

B.3 ACI Committee 318, Building Code Requirements for Reinforced Concrete (ACI 318-71), ACI, Detroit, 1971.

B.4 Faradji Capon, M. J. and Diaz de Cossio, R., "Tensión diagonal en miembros de concreto de sección circular," Ingenieria, April 1965 (In Spanish).

B.5 Umemura, H., Earthquake-Resistant Design of Structures, University of Tokyo, Tokyo, 1972.

B.6 Wilson, E. L., et al., "Computer Program for Static and Dynamic Analysis of Linear Structural Systems," Earthquake Engineering Research Center Report No. EERC 72-10, University of California, Berkeley, November 1972.

B.7 Felippa, C. A., "Refined Finite Element Analysis of Linear and Nonlinear Two-dimensional Structures," Structures and Materials Research Report No. UC-SESM 66-2, Department of Civil Engineering, University of California, Berkeley, 1966.

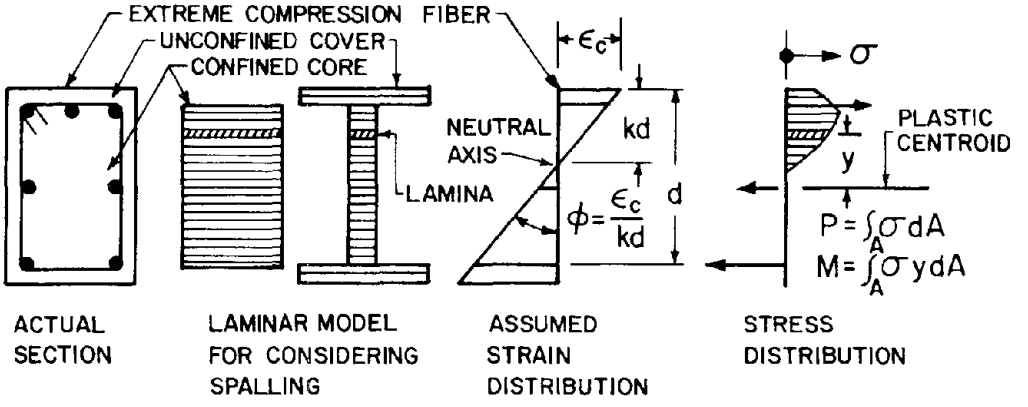

FIG. B.1 CALCULATION OF INTERNAL STRESSES AND FORCES

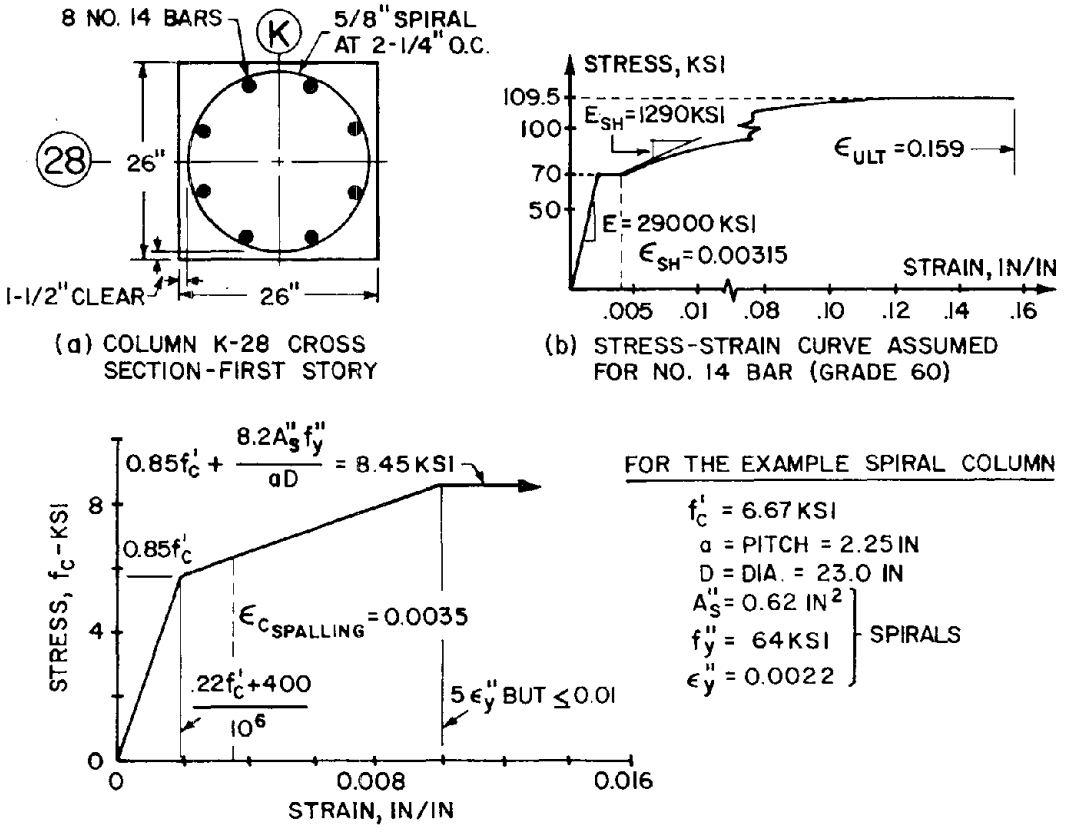

(a) COLUMN K-28 CROSS SECTION-FIRST STORY

(b) STRESS-STRAIN CURVE ASSUMED FOR NO. 14 BAR (GRADE 60)

(c) STRESS-STRAIN CURVE ASSUMED FOR CONCRETE BASED ON REF. B.2

B.2 DESCRIPTION OF FIRST STORY SPIRAL COLUMN K-28

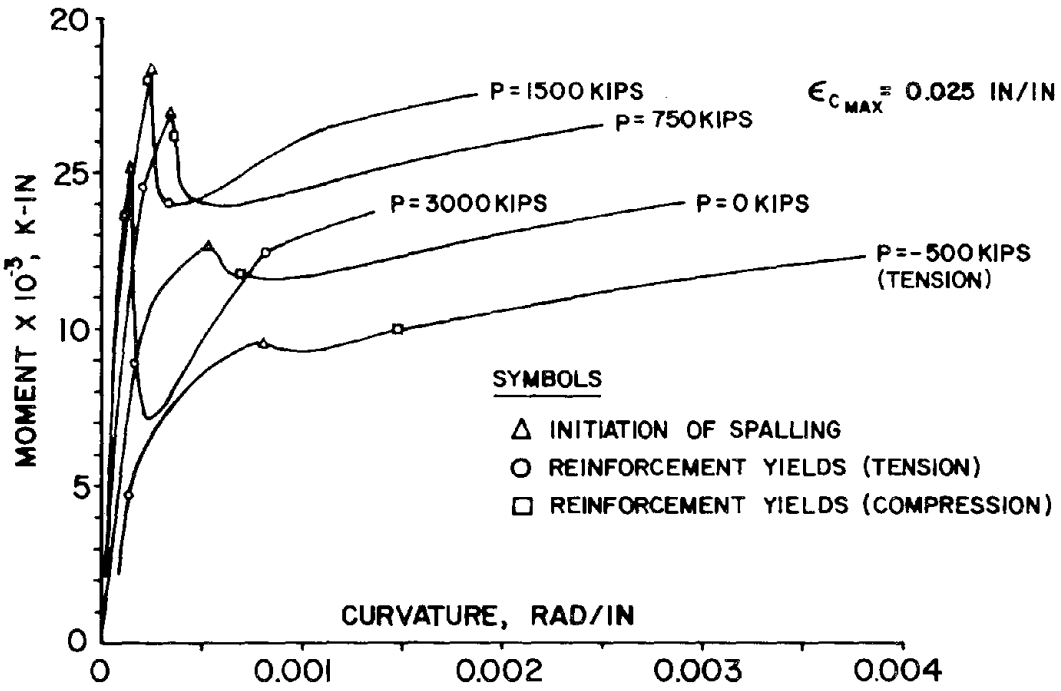

FIG. B.3 MOMENT-CURVATURE RELATIONSHIPS FOR FIRST STORY SPIRAL COLUMN K-28

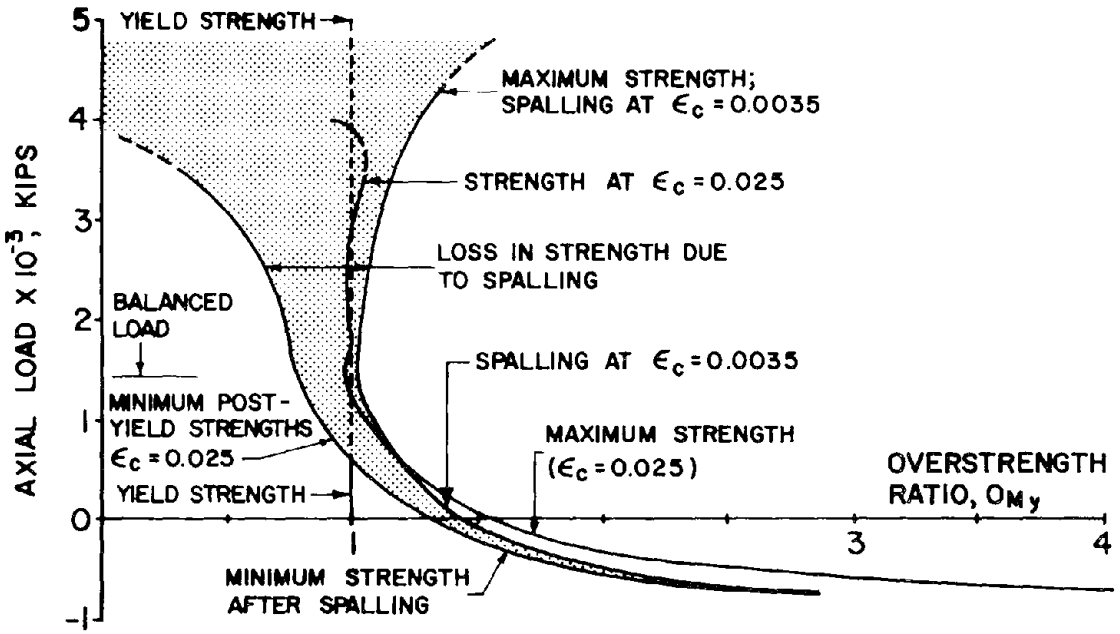

FIG. B.4 OVERSTRENGTH RATIOS FOR FIRST STORY SPIRAL COLUMN K-28

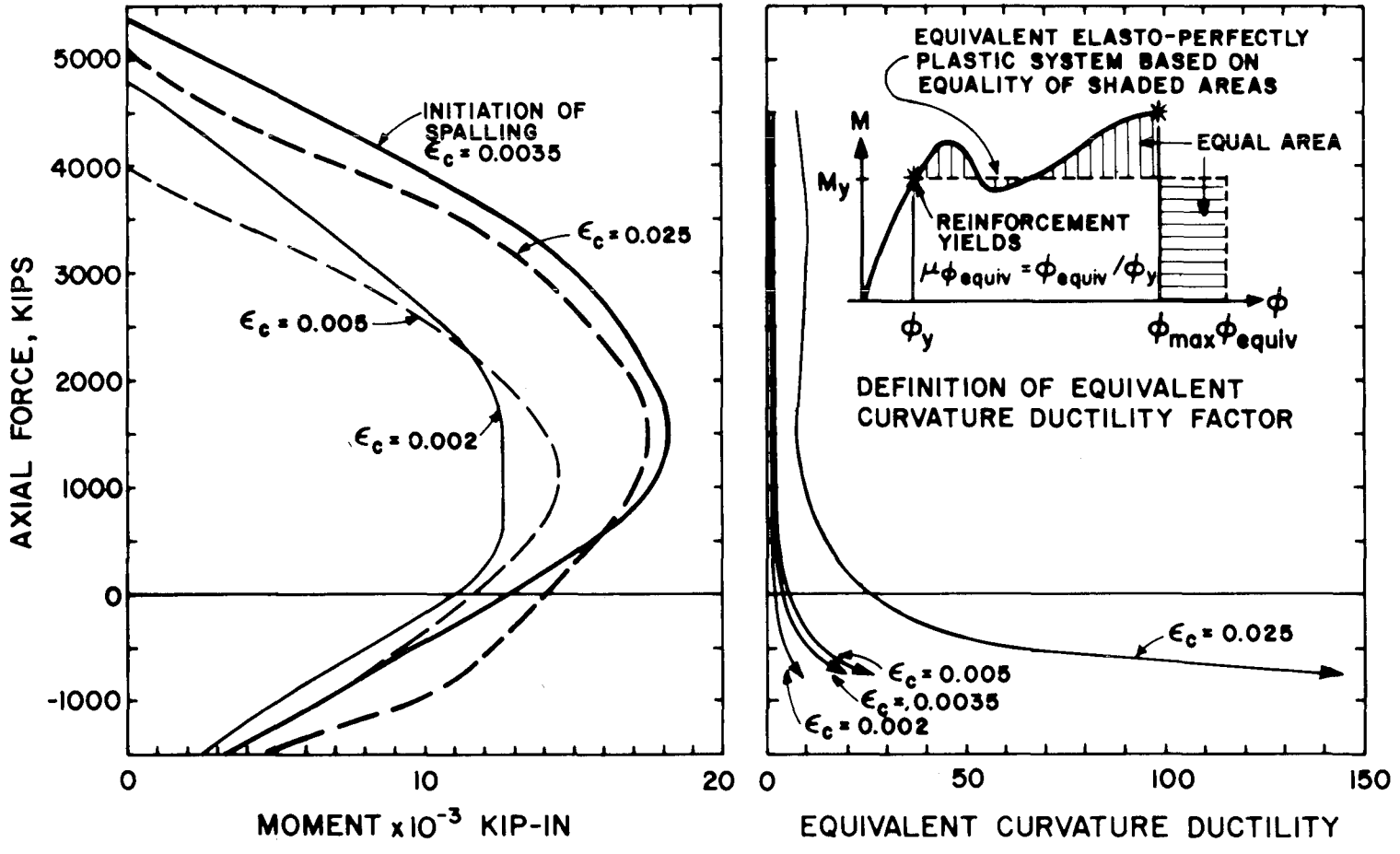

B.5 MOMENT AND CURVATURE DUCTILITY CAPACITIES AS FUNCTION OF AXIAL LOAD — FIRST STORY SPIRAL COLUMN K-28

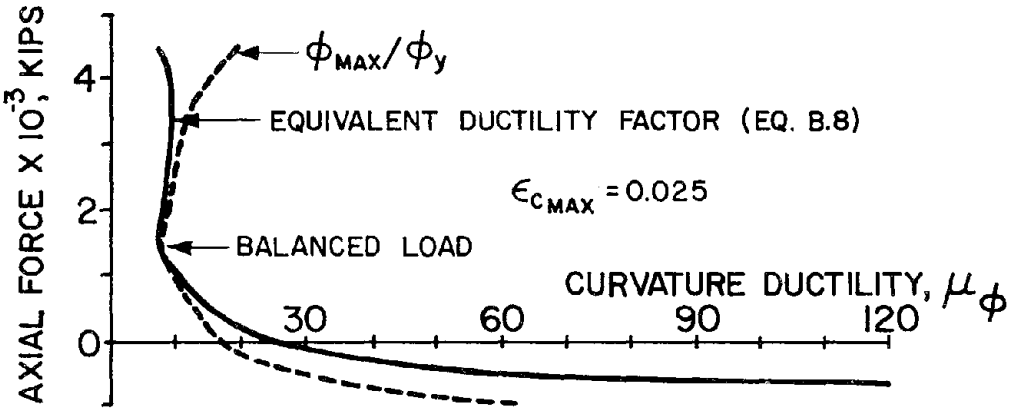

FIG. B.6 COMPARISON OF DUCTILITY FACTORS OBTAINED BY DIFFERENT DEFINITIONS-FIRST STORY SPIRAL COLUMN K-28

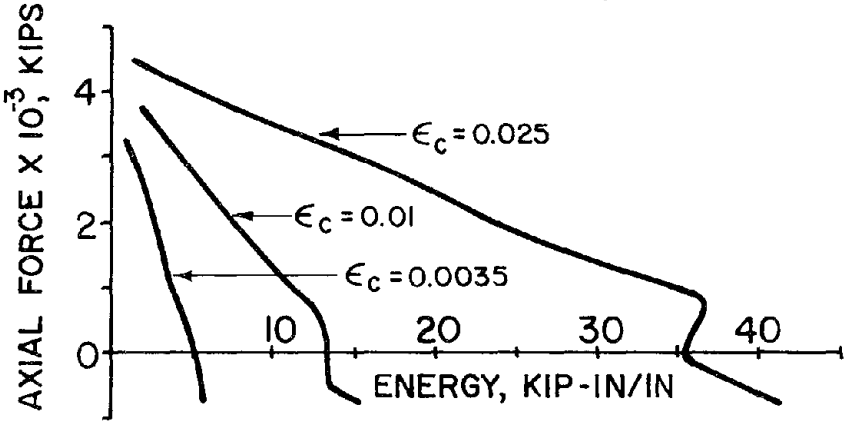

FIG. B.7 ENERGY ABSORPTION CAPACITY-FIRST STORY SPIRAL COLUMN K-28

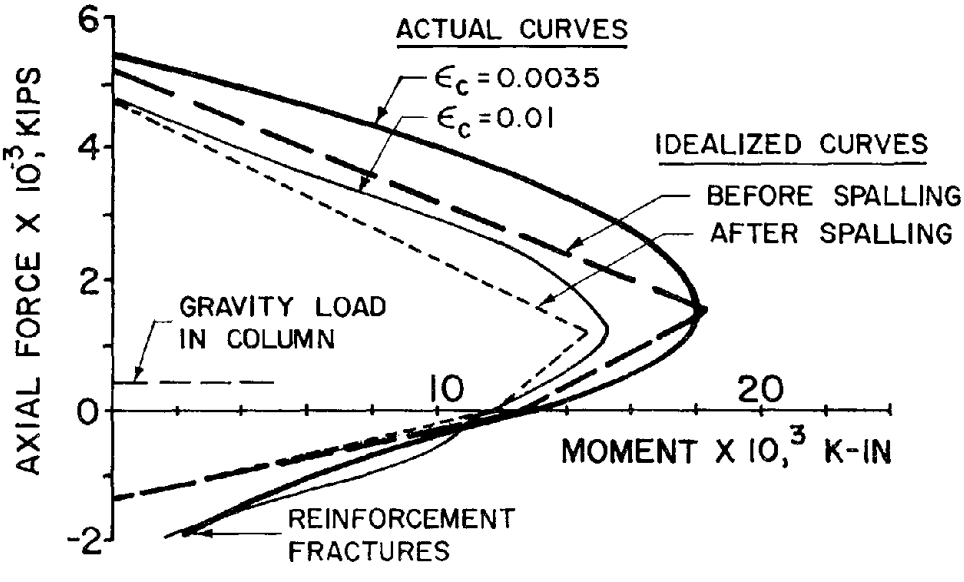

FIG. B.8 COMPARISON OF ACTUAL AND IDEALIZED INTERACTION CURVES FOR FIRST STORY SPIRAL COLUMN K-28

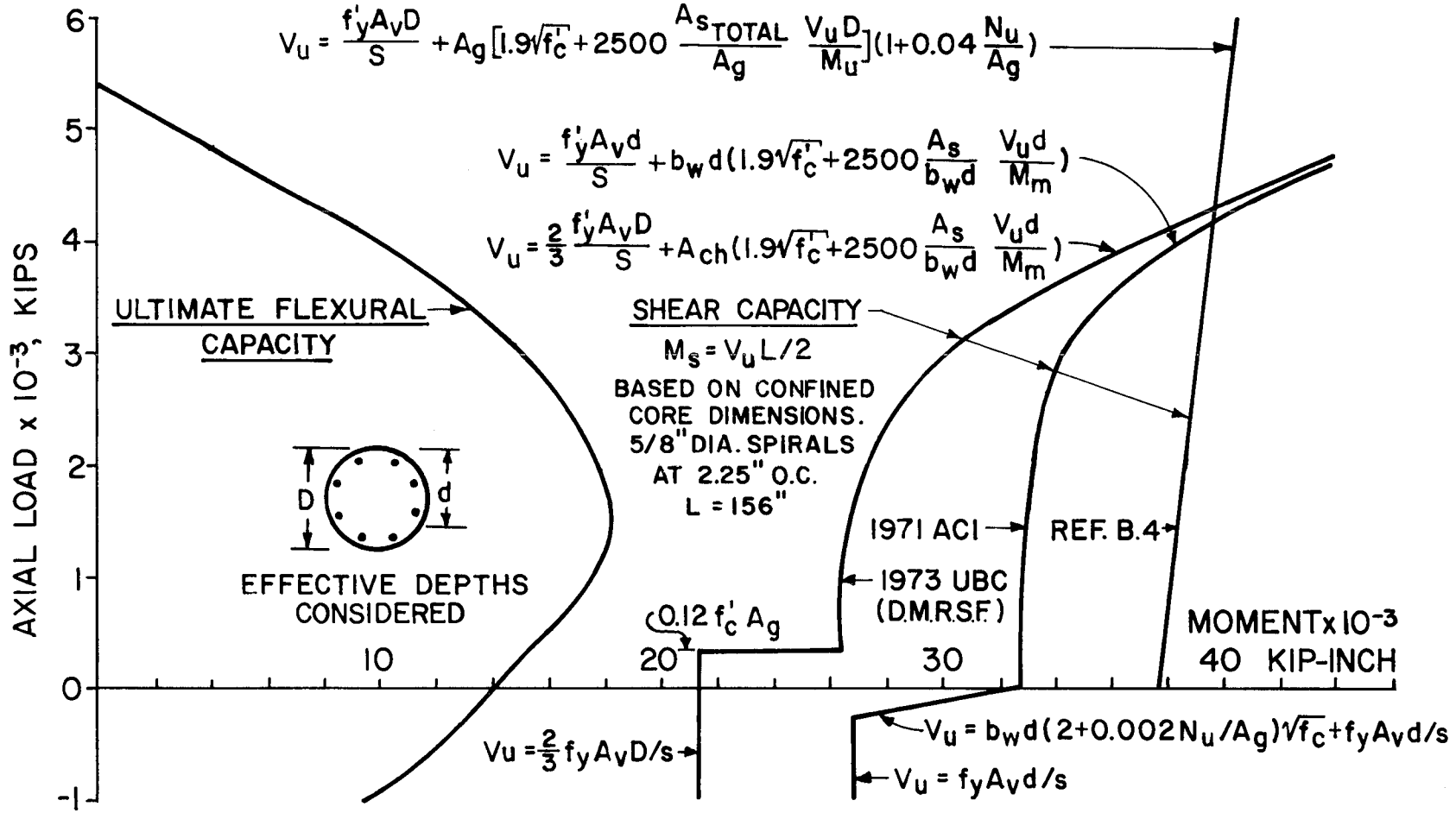

FIG. B.9 COMPARISON OF SHEAR AND FLEXURAL CAPACITIES OF FIRST STORY SPIRAL COLUMN K-28

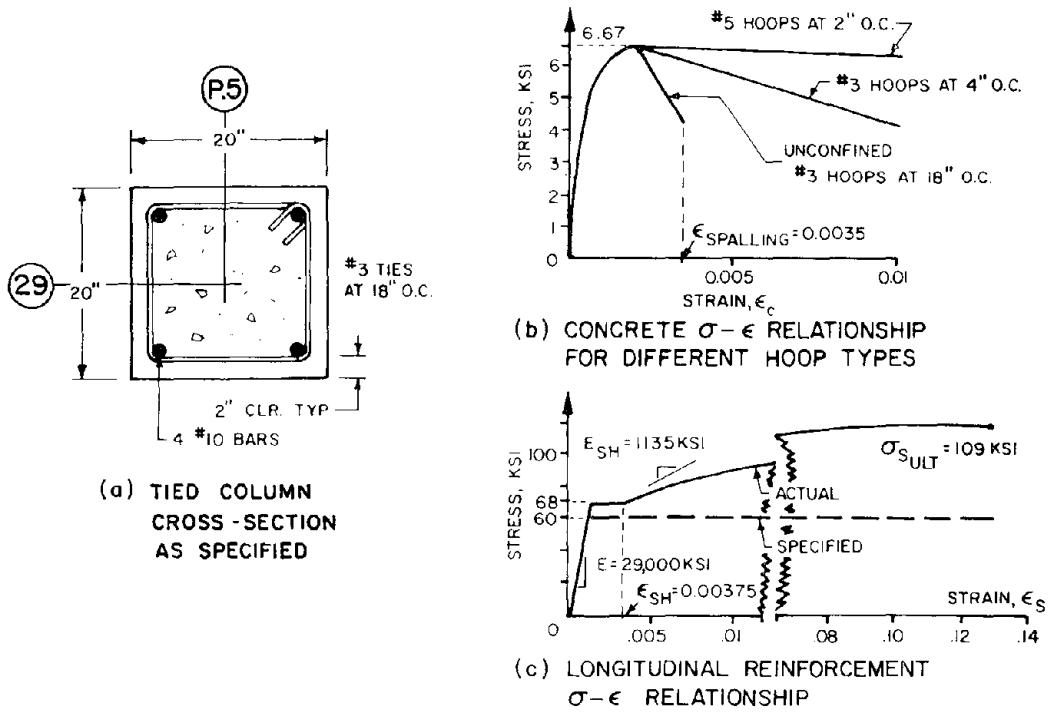

FIG. B.10 DESCRIPTION OF TIED COLUMN EXAMPLE

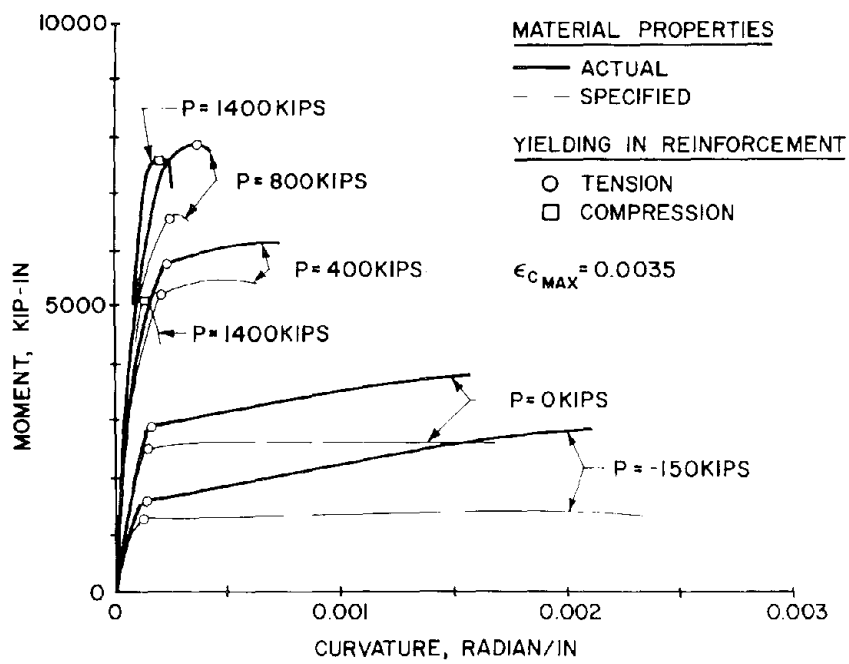

FIG. B.11 MOMENT-CURVATURE RELATIONSHIPS FOR UNCONFINED SECTION-GROUND STORY TIED COLUMN P.5-29

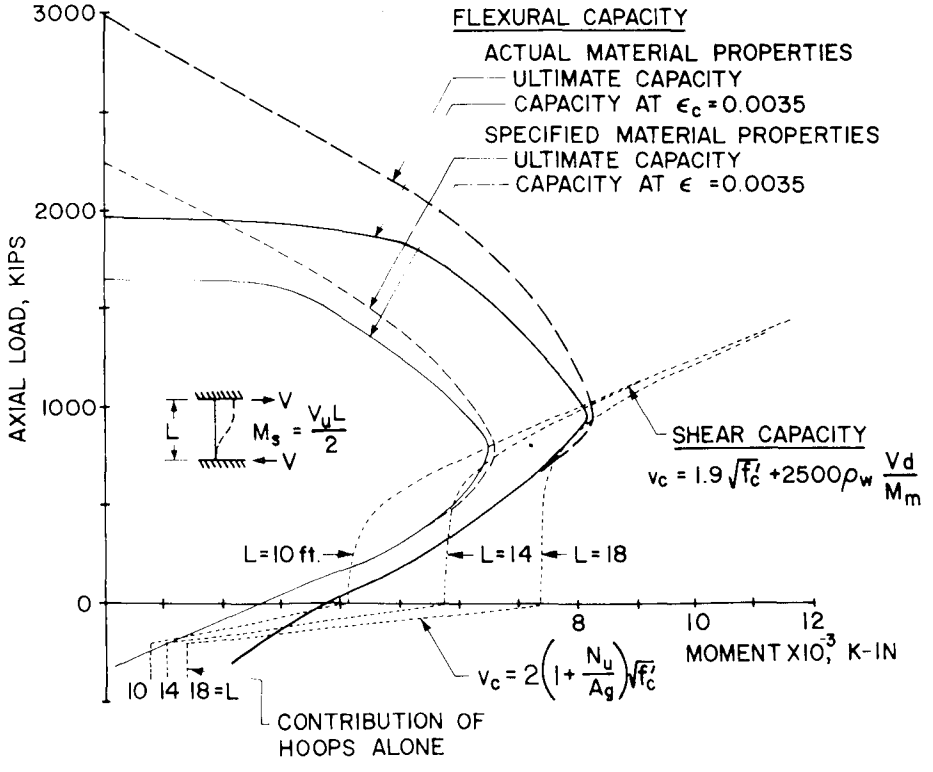

FIG. B.12 INTERACTION CURVES FOR UNCONFINED SECTION-TIED COLUMN EXAMPLE (P.5-29)

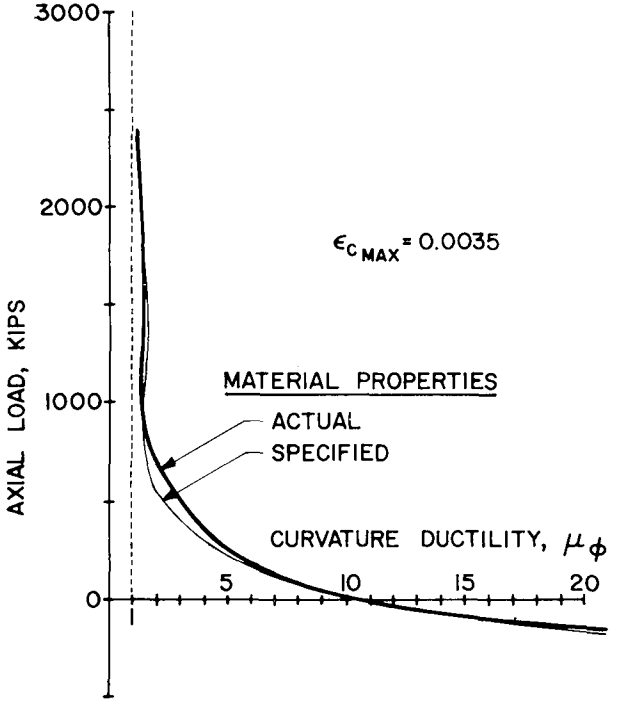

FIG. B.13 EQUIVALENT CURVATURE DUCTILITY FACTORS FOR UNCONFINED SECTION-TIED COLUMN EXAMPLE (P.5-29)

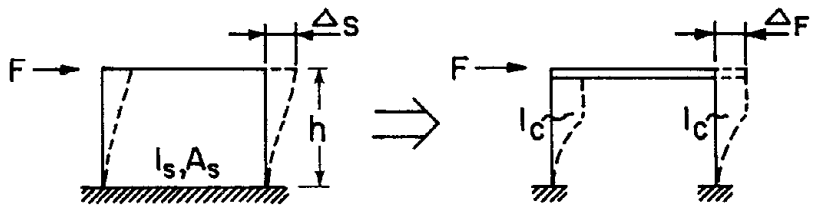

SHEAR WALL EQUIVALENT FRAME

$$\Delta_S = \frac{Fh^3}{12EI_s} + \frac{1.2Fh}{A_sG} \qquad \Delta_F = \frac{Fh^3}{12EI_c} \times \frac{1}{2}$$

$$\Delta_S = \Delta_F \quad \text{ASSUME} \quad G = \frac{E}{2.5}$$

$$\text{THUS:} \quad I_c = \left[\frac{2}{I_s} + \frac{72}{A_s h^2}\right]^{-1}$$

(a) TO OBTAIN EQUAL LATERAL DISPLACEMENTS FOR APPLIED SHEAR FORCES

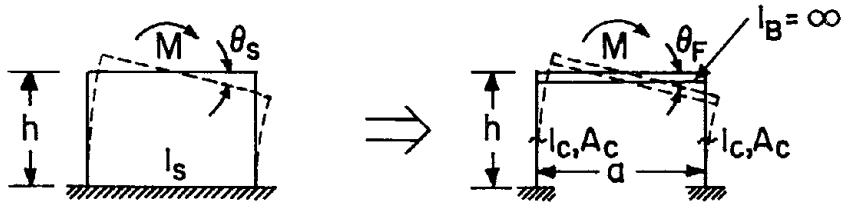

SHEAR WALL EQUIVALENT FRAME

$$\theta_S = \frac{Mh}{EI_s} \qquad \theta_F = \frac{Mh}{2E}\left[I_c + A_c\left(\frac{a}{2}\right)^2\right]^{-1}$$

$$\theta_S = \theta_F$$

$$\text{THUS:} \quad A_c = \left(\frac{2}{a}\right)^2\left(\frac{I_s}{2} - I_c\right)$$

(b) TO OBTAIN EQUAL ROTATIONS FOR APPLIED OVERTURNING MOMENTS

FIG. B.14 CALCULATION OF EQUIVALENT ONE BAY FRAME PARAMETERS FOR SHEAR WALLS

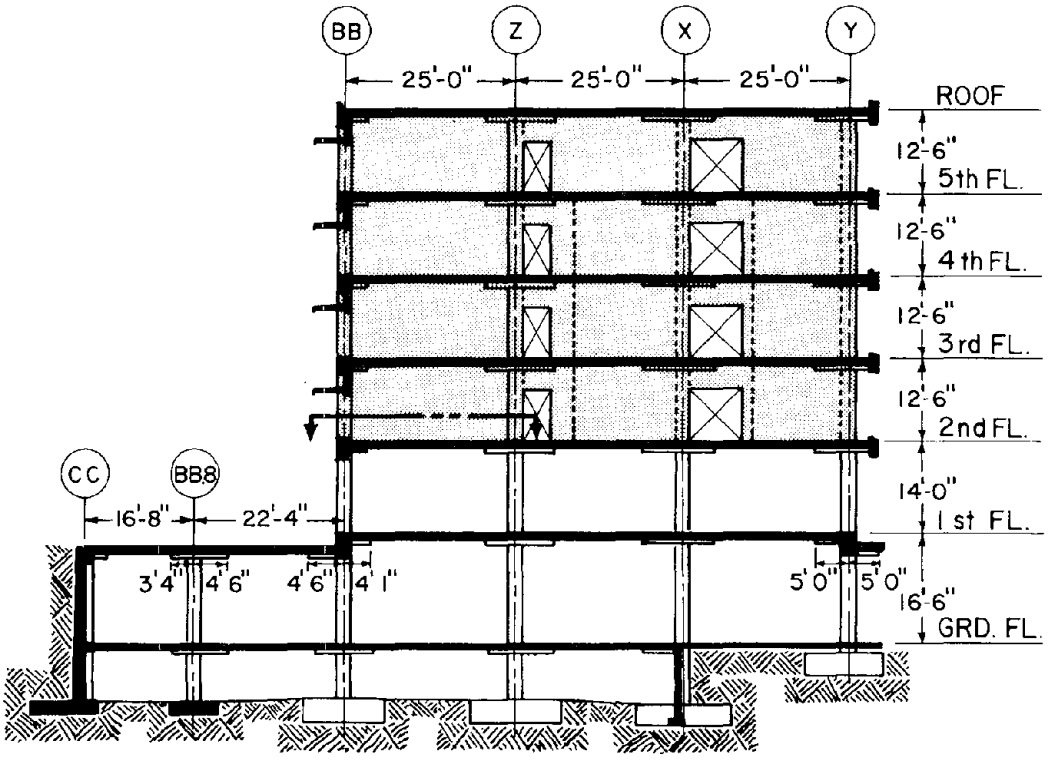

(a) WALL ELEVATION - FRAME 18

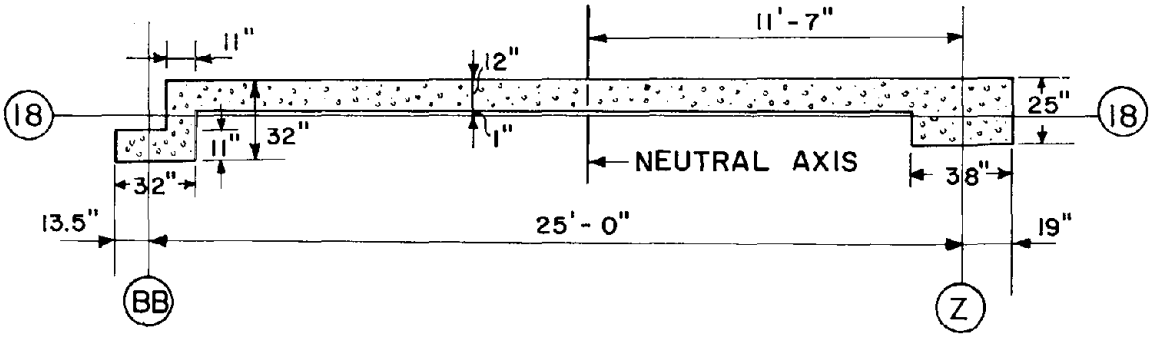

(b) WALL CROSS SECTION

FIG. B.15 SECOND STORY SHEAR WALL 18-(BB-Z) CROSS SECTION

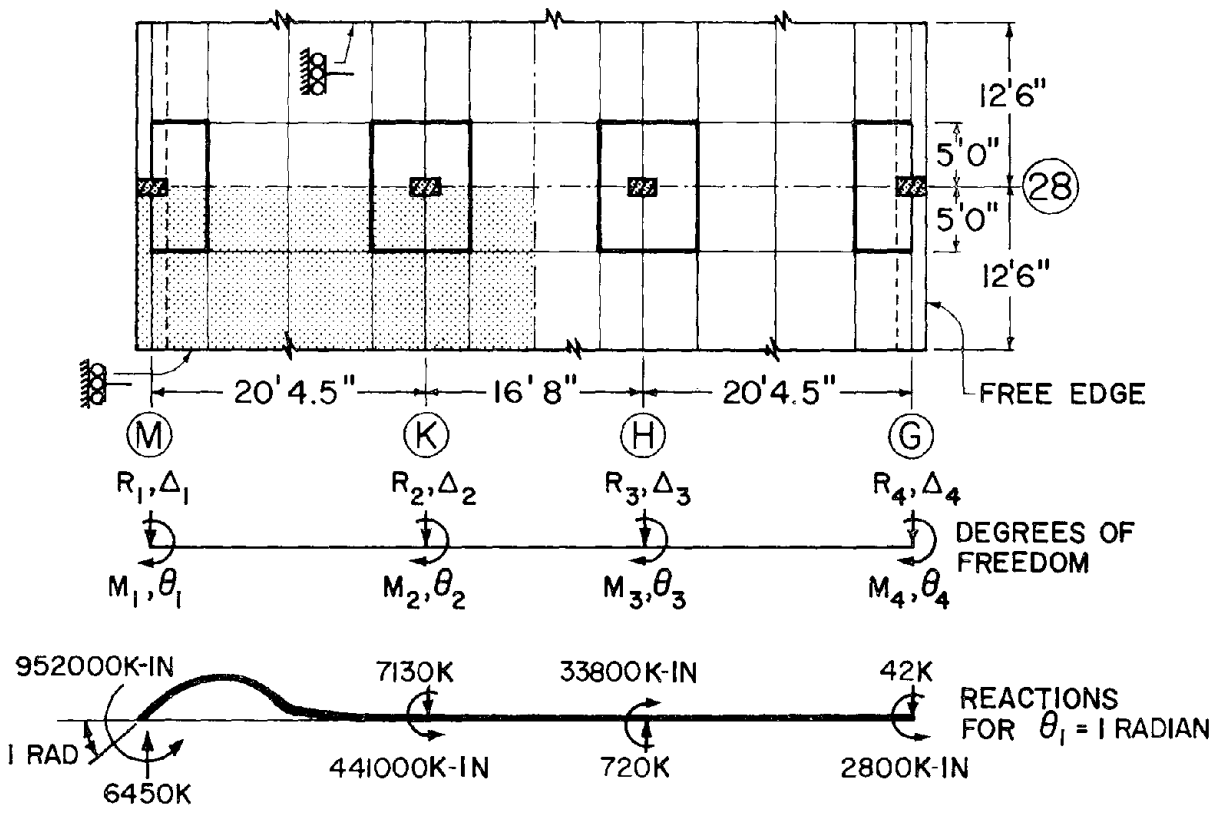

FIG. B.16 FINITE ELEMENT MODEL 1-FRAME 28 SLAB

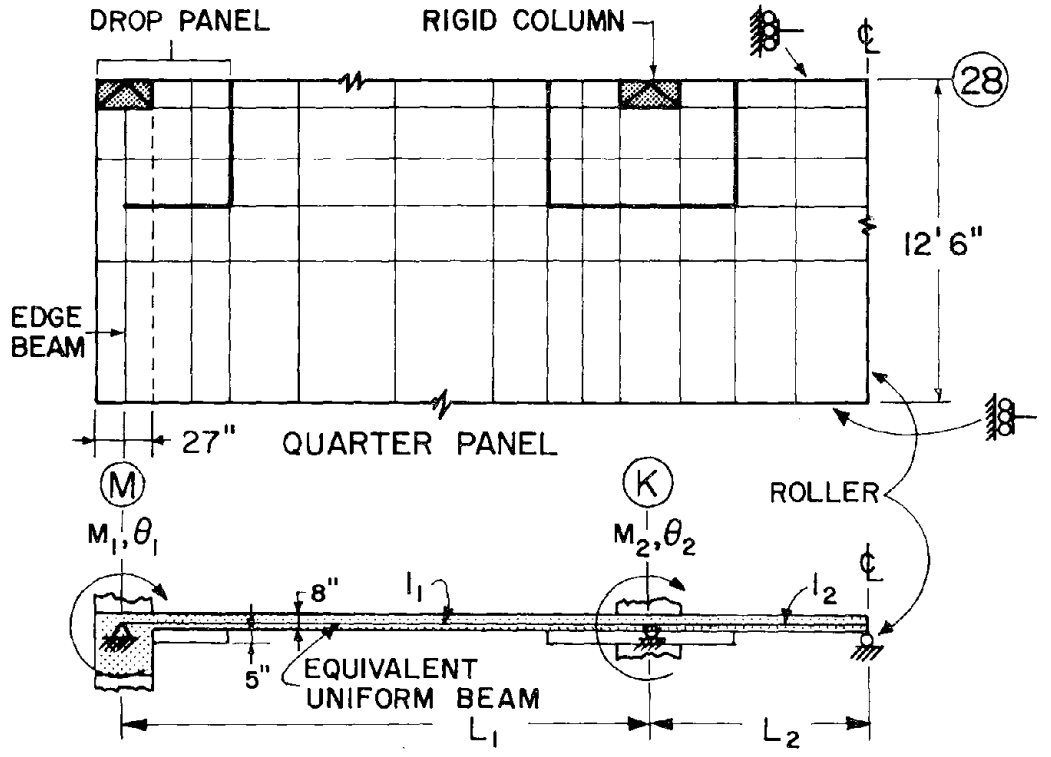

FIG. B.17 FINITE ELEMENT MODEL 2-FRAME 28 SLAB

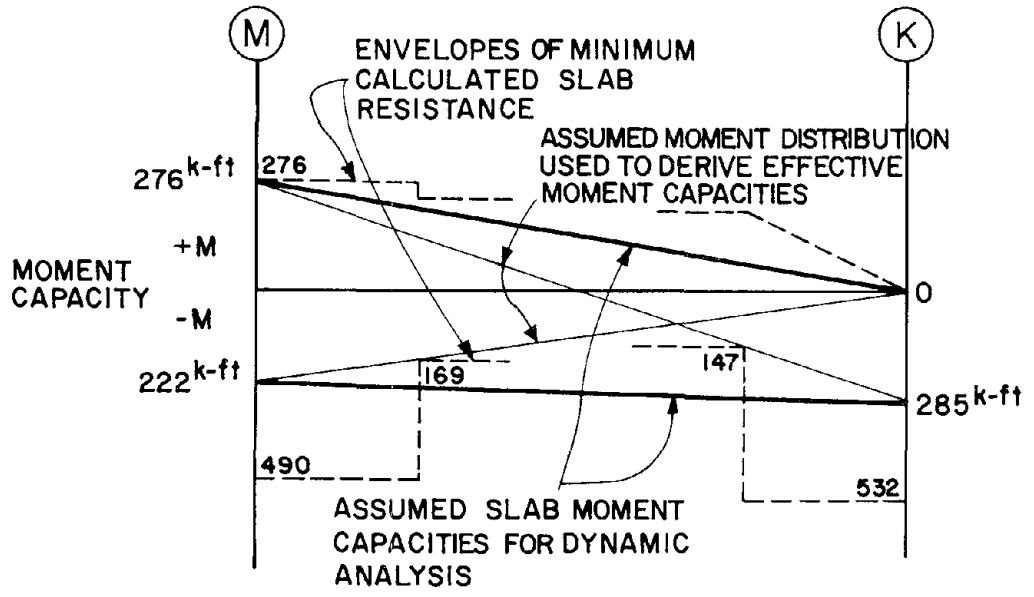

FIG. B.18 CALCULATION OF EFFECTIVE SLAB MOMENT CAPACITIES FOR USE IN NONLINEAR ANALYSES - TYPICAL FLOOR, FRAME 28

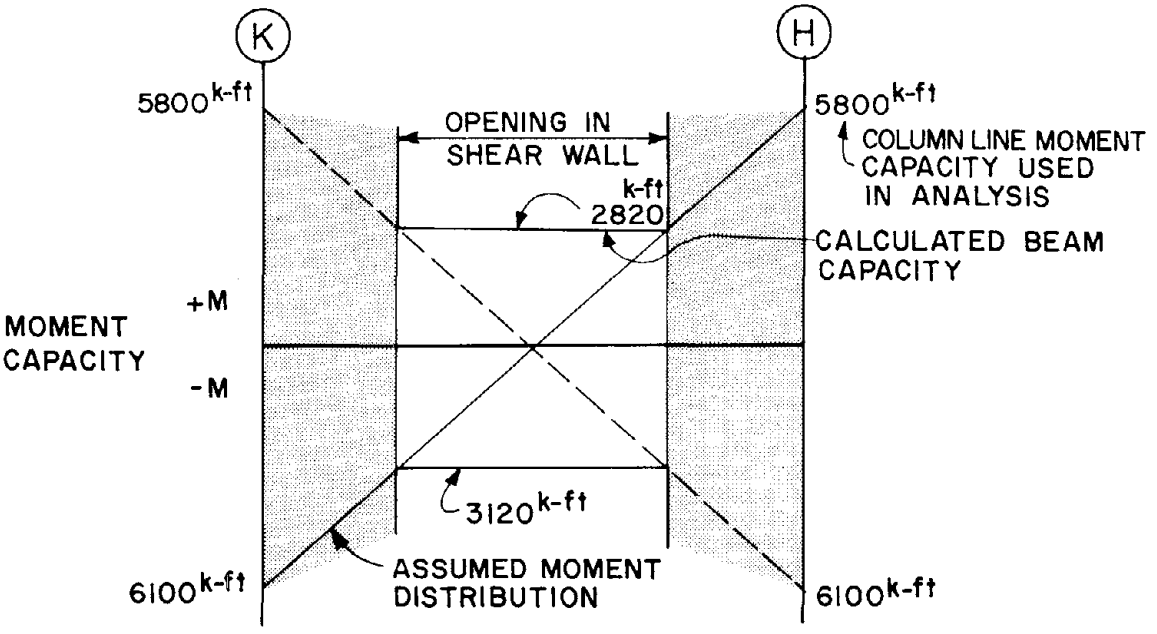

FIG. B.19 CALCULATION OF EFFECTIVE SPANDREL MOMENT CAPACITIES BETWEEN SHEAR WALLS FOR NONLINEAR ANALYSIS - FOURTH FLOOR, FRAME 29

APPENDIX C - EFFECT OF TRANSVERSE REINFORCEMENT ON TIED COLUMN BEHAVIOR

When ductile moment-resisting frames are designed to resist the effects of seismic loading, the ACI [B.3] and UBC [2.5] currently recommend minimum amounts of special transverse reinforcement to be placed at the ends of columns. These amounts are generally far in excess of the amounts of transverse reinforcement used in the tied columns of the main building. To assess the effect that such special transverse reinforcement might have had on the behavior of these tied columns, the mechanical characteristics of the tied column discussed in Section B.2.2 will be re-evaluated for different amounts of transverse reinforcement. The cross-sectional geometry and material properties of this column are shown in Fig. B.10. As previously discussed, the No. 3 hoops at 18-in. intervals met existing nominal tie requirements, but failed to confine the section or to provide sufficient shear so the column could develop its ultimate flexural capacity.

For design axial forces less than 40 percent of the balanced load, the ACI [B.3] currently recommends that columns be detailed according to the special provisions for ductile flexural members. In this case, the minimum size stirrup is No. 3, and the maximum spacing is d/2. At the ends of the member, or wherever inelastic deformations might occur, however, the web reinforcement should not be less than:

$$A_v \frac{d}{s} = 0.15A'_s \text{ or } 0.15A_s \qquad (C.1)$$

whichever is greater, where A'_s and A_s are the areas of the compressive and tensile reinforcement, respectively. Furthermore, the hoop spacing, s, parallel to the direction of the longitudinal reinforcement should not exceed d/4 in these regions. For the tied column considered in this example, No. 3 hoops would be required at no more than $d/4 \cong 4$-in. intervals at the top and bottom of the member according to these ACI provisions.

For columns in which the maximum axial forces may exceed 0.4 of the balanced load, the ACI recommends lateral confinement consisting

of spiral or hoop reinforcement in order to prevent loss of axial strength after spalling. The basis and limitations of the resulting provisions are discussed in the Commentary to Reference B.3. Where rectangular hoops are to be used without supplementary cross ties (as in this example), the bar area required for one leg of the hoop is given by:

$$A_{sh} = \frac{1}{2} \ell_h \rho_s s_h \qquad (C.2)$$

in which ℓ_h is the maximum unsupported length of the rectangular hoop, ρ_s is the ratio of the volume of transverse reinforcement to the total volume of core (measured to the outside of the hoops) and s_h is the hoop spacing. The volumetric ratio, ρ_s, is given by:

$$\rho_s = 0.45\left(\frac{A_g}{A_c} - 1\right)\frac{f'_c}{f_y} \qquad (C.3)$$

but not less than $0.12\, f'_c/f_y$, and A_c is the core area taken to the outside of the transverse reinforcement. The hoop spacing in this case should not exceed 4 in. center-to-center. To satisfy these ACI requirements No. 5 hoops at about 2-in. centers or No. 6 hoops at about 2.75-in. centers would have to be used for the example column based on the actual material characteristics and an assumed strength for the transverse reinforcement of 60 ksi.

The UBC requirements [2.5] differ from the ACI provisions in that equations similar to Eqs. C.2 and C.3 are used to determine the amount of special transverse reinforcement to be provided in critical regions regardless of the axial load. For the case of the tied column example considered in this appendix, application of the UBC recommendations requires at least No. 5 hoops spaced at about 2.75-in. intervals (assuming Grade 60 hoop steel).

On the basis of these code requirements, two bounds were considered for the transverse reinforcement in the critical end regions for the tied column example: (1) No. 3 hoops at 4-in. centers, and (2) No. 5 hoops at 2-in. centers. Both types were assumed to have a yield strength of 60 ksi. The effect of the transverse reinforcement on the concrete stress-strain

relationships was estimated using the empirical relationships presented in Reference B.1; the resulting idealized relationships are shown in Fig. B.10. The first type of hoop corresponds to a Z value (see Reference B.1) of 45.62 and the second, 6.25. The concrete cover outside the hoops was assumed to be unconfined and to spall at a compressive strain of 0.0035 in./in. The confined core was assumed to be able to withstand concrete strains up to 0.01 in./in.

Moment-curvature relationships for the critical region under different axial load intensities, computed as discussed in Section B.2, are shown in Fig. C.1. Plots of bending moment-axial load interaction, energy absoprtion, overstrength ratios, and curvature ductilities derived from these moment-curvature relationships are presented in Figs. C.2 through C.5. The moment-curvature plots (Fig. C.2) are essentially identical to those presented in Fig. B.11 for the unconfined cross-section up to the onset of spalling. The unconfined member was unable to maintain any load capacity once spalling occurred; however, both forms of special transverse reinforcement considered here were successful in delaying this failure.

In fact, for axial forces well below the balanced load, the effect of spalling on the moment capacity was very small [see Figs. C.1(a) and C.2] and the ultimate curvatures developed by the confined sections increased substantially after spalling occurred. At these low axial load intensities, there was little difference between the behavior computed for the different quantities of hoop reinforcement considered here, as reflected in the plots for energy absorption (Fig. C.3), and for overstrength ratios (Fig. C.4). For axial forces less than about 40 percent of the balanced load, a substantial increase in moment capacity was observed between first yielding and spalling (Fig. C.4), and the reduction in strength that accompanied spalling was insufficient to reduce the strength below the initial yield value. Furthermore, this reduction in moment capacity was generally regained at the maximum concrete strain due to strain hardening in the reinforcement.

For axial forces near the balanced load (about 1100 kips), a

significant drop in moment capacity accompanied spalling (Figs. C.1, C.2, and C.4), but the confined sections were generally able to maintain this reduced capacity until the ultimate concrete strain was developed. There was only a small difference in the ability of the different hoop details considered here to maintain the moment capacity of the section after spalling for these axial loads.

Above the balanced load, the moment capacity of the section dropped with the onset of yielding, and spalling resulted in further losses in both moment and axial load capacities (Figs. C.1(b) and C.4]. The interaction curves (Fig. C.2) indicate that neither hoop arrangement was able to maintain the ultimate axial load capacity of the section (as would be expected from the nature of the assumed concrete constitutive equations; Fig. B.10). Prior to the onset of spalling (ε_c = 0.0035 in./in.), the interaction curves (Fig. C.2) were similar regardless of the amount of confinement provided. After the initiation of spalling at these higher axial loads, the moment capacity dropped rapidly. The severity of this strength reduction increased with increasing axial load intensity (Fig. C.4), and the quantity of transverse reinforcement had a substantial effect on the post-spalling behavior of the section. As can be seen in Fig. C.2, and as expected from Fig. B.10(b) the No. 5 hoops spaced at 2-in. intervals were nearly able to provide sufficient confinement to maintain the capacity of the confined section at a constant value as the maximum concrete strains increased from 0.005 to 0.01 in./in., whereas the No. 3 hoop arrangement was unable to do so (see Fig. C.4 also).

The energy absorption capacity of the section in flexure decreased significantly with increasing compressive axial loads, as can be seen in Fig. C.3. The quantity of special transverse reinforcement had little effect on the energy absorption capacity, particularly at low axial loads. A substantial increase in the curvature ductility capacity of the confined sections was observed between the initiation of spalling and the ultimate concrete strain at all axial load intensities, as can be seen in Fig. C.5. The adverse effect of compressive axial loads on ductility can also be seen in this figure. The section was able to develop some ductility at all axial loads. The maximum equivalent

curvature ductilities developed for the different quantities of transverse reinforcement were similar, except at high axial loads where the more heavily confined section achieved greater ductilities. As noted for the spiral column, the equivalent ductility factors were greater than the ratio ϕ_{max}/ϕ_y under low axial loads, and less under large compressive loads.

It is clear from the results presented in this section that transverse reinforcement in critical regions can significantly improve the flexural behavior of tied columns. However, when the expected axial forces are smaller than the section's balanced load and ductile flexural behavior is the primary design objective, it may not be necessary to provide the large quantities of transverse reinforcement required to maintain the axial load capacity of the section after spalling. This has been recognized by the ACI [B.3]. It appears that details conforming to the UBC may be overly conservative at low axial loads, according to the results presented in this section. However, these results do not account for possible buckling of the reinforcement. Determination of the quantities of special transverse reinforcement required to obtain satisfactory performance must await further experimental and analytical investigations.

Although the unconfined member discussed in Section B.2.2 was able to develop significant inelastic deformations at low axial load intensities, it did not have sufficient shear strength to develop its flexural capacity under antisymmetric moment distributions unless the clear span length was very large. The ACI [B.3] and UBC [2.5] contain provisions requiring all members in a D.M.-R.S.F. to have transverse reinforcement sufficient to develop the shears applied at the "formation of plastic hinges in the frame due to the combination of lateral displacement and design gravity loads." The UBC is more specific than the ACI in defining the loading conditions that should be considered, and requires that yield moments be computed without capacity reduction factors and for a maximum reinforcement yield strength 25 percent greater than the specified yield strength. Recognizing the deterioration of concrete shear capacity under shear reversal at low axial loads, the UBC also specifies that computation of shear strength should

be based on the column core area and that permissible concrete shear stress should be considered zero for axial loads less than 0.12 $f'_c A_g$. The maximum hoop spacing in the central portions of the member is d/2 according to either code.

These code provisions are intended to prevent the brittle type of premature shear failure observed in the unconfined column. However, as discussed, there are substantial differences between the ACI and UBC recommendations. To illustrate the effects of some of these differences on the computed shear strengths, the shear capacity of the tied column considered in this example was evaluated assuming that it was reinforced throughout its entire length by the special transverse reinforcement specified for the critical regions. Moments corresponding to the shear capacity of the member for the antisymmetric moment distribution considered in Section B.2 are presented in Figs. C.6 and C.7. For this loading distribution, transverse reinforcement consisting of No. 3 hoops spaced at 4-in. intervals was nearly sufficient to develop the ultimate flexural capacity for a clear span length of 10 ft according to the ACI provisions discussed previously. Figure C.6 indicates that the corresponding length was less than 5 ft for the No. 5 hoops at 2 in.

If the confined core (outside-to-outside dimension of hoops) is used as the basis of all shear stress and strength calculations, and the contribution of the concrete to the shear capacity is disregarded entirely for axial loads less than 0.12 $f'_c A_g$, as recommended by the UBC, the moments corresponding to the effective shear strength decrease significantly (Fig. C.6) from the values computed in conformance with the ACI code provisions. The largest difference between the shear capacity curves corresponding to the UBC and ACI provisions was observed at low axial loads where the contribution of the concrete is disregarded by the UBC. For the columns considered in this example, applications of the UBC provisions resulted in a considerable change in the shear capacity at a load of 0.12 $f'_c A_g$. The abruptness of this transition may not be desirable in view of the uncertainty regarding the actual shear capacity of members subjected to load reversal.

A number of problems were also detected in the application of these code provisions to actual members. Firstly, the ACI [B.3] gives an alternative formula to Eq. B.6 for evaluating the concrete shear stress, i.e.

$$v_c = 2\left(1 + 0.0005 \frac{N_u}{A_g}\right)\sqrt{f'_c} \qquad (C.4)$$

in which the terms are as defined for Eq. B.6. For the member considered in this example, Eq. C.4 results in the linear relationships between shearing moment capacity and axial load shown in Fig. C.7. These were significantly different from the curves obtained using Eq. B.6. Whereas the shearing moment capacity based on Eq. B.6 indicated the possibility of a shear failure for a 10-ft long member reinforced transversely by No. 3 hoops at 4-in. centers, Eq. C.4 suggests that such a member was adequately reinforced.

Moreover, in applying the UBC provision requiring that the shear strength be based on the column core area, it is not entirely clear whether the permissible shear stress should also be based on the confined core dimensions or whether they should be based on the initial section's dimensions. The effect of using initial or core dimensions on the computed shearing moment capacity is indicated in Fig C.7. Note that d_c and A_{ch} in this figure refer to the effective depth and area of the confined core. The shear strengths based on the confined core dimensions were generally, but not always, smaller than those based on the initial section dimensions. When computing the shear strength of the confined core using Eq. B.6, strengths were lower when the ultimate concrete shear stresses were based on the core dimensions than when they were based on the initial section dimensions. The opposite occurred using Eq. C.4, however, since the ultimate concrete shear stress computed from Eq. C.4. was substantially increased for a given compressive axial load by using the confined core area rather than the area of the initial section.

It is clear from these brief discussions that there is considerable uncertainty involved in predicting the shear strength of even simple

members. Of particular concern are the various equations contained in current codes for determining the shear strength of members subjected to axial load which resulted in substantially different strength values. Moreover, uncertainties regarding the appropriate cross-section to be used for shear computations, and regarding the effective contribution of the concrete to the shear resistance after cycles of inelastic reversal, indicate the need for further experimental research in this area. Nonetheless, it is clear from these results that increased ductility and shear capacity resulting from special transverse reinforcement of the type recommended by the ACI [B.3] and UBC [2.5] could have significantly improved the structural behavior of the main building.

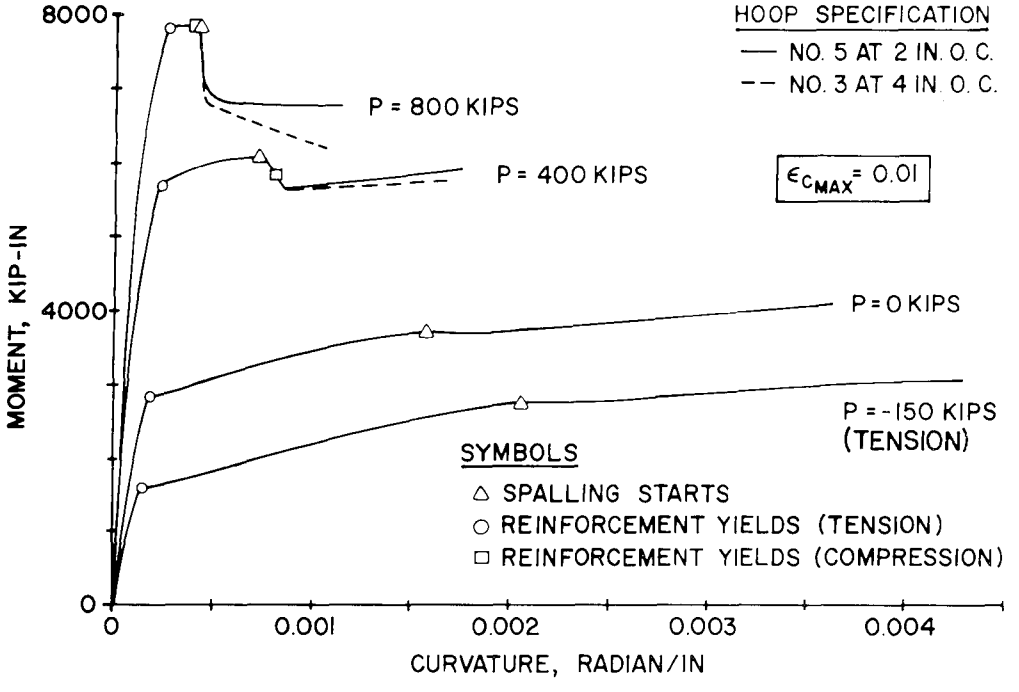

(a) FOR AXIAL LOADS $\leq$ 800 KIPS

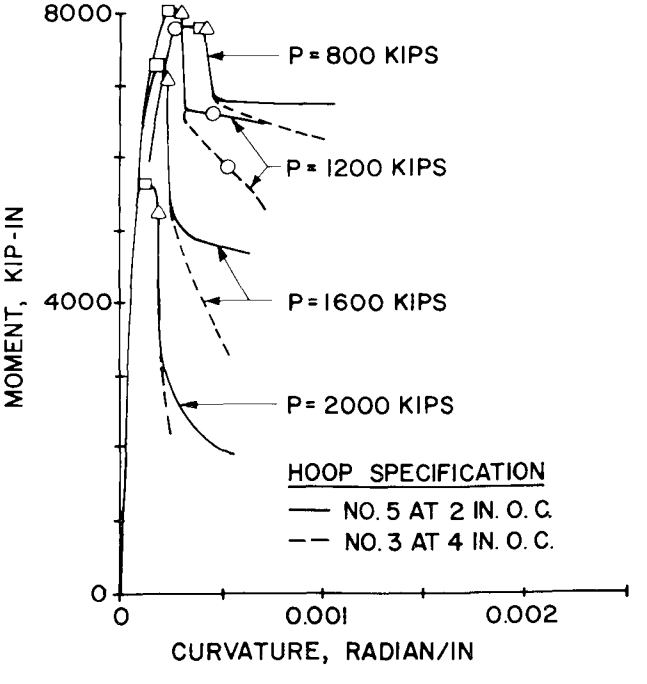

(b) FOR AXIAL LOADS $\geq$ 800 KIPS

FIG. C.1 MOMENT-CURVATURE RELATIONSHIPS FOR DIFFERENT AMOUNTS OF TRANSVERSE REINFORCEMENT-TIED COLUMN EXAMPLE

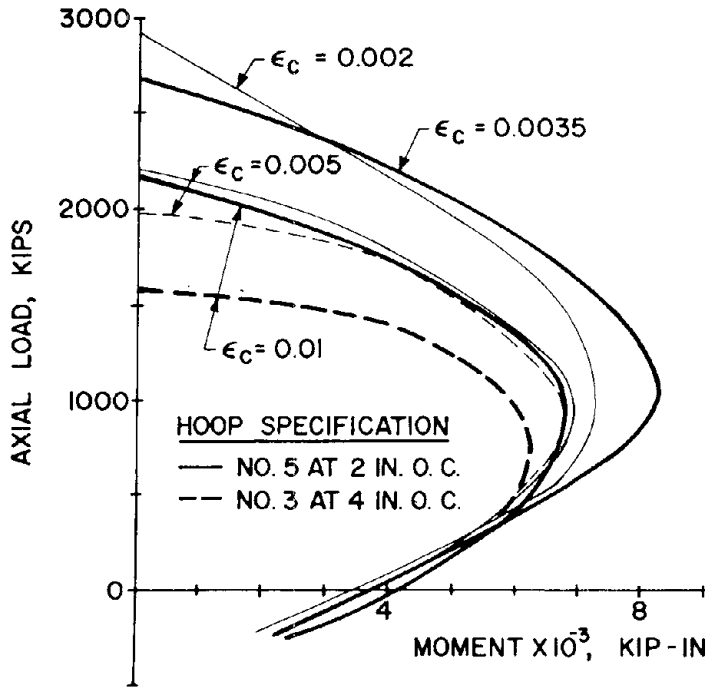

FIG. C.2 COMPARISON OF INTERACTION CURVES AT VARIOUS ULTIMATE CONCRETE COMPRESSIVE STRAINS FOR DIFFERENT AMOUNTS OF TRANSVERSE REINFORCEMENT-TIED COLUMN EXAMPLE

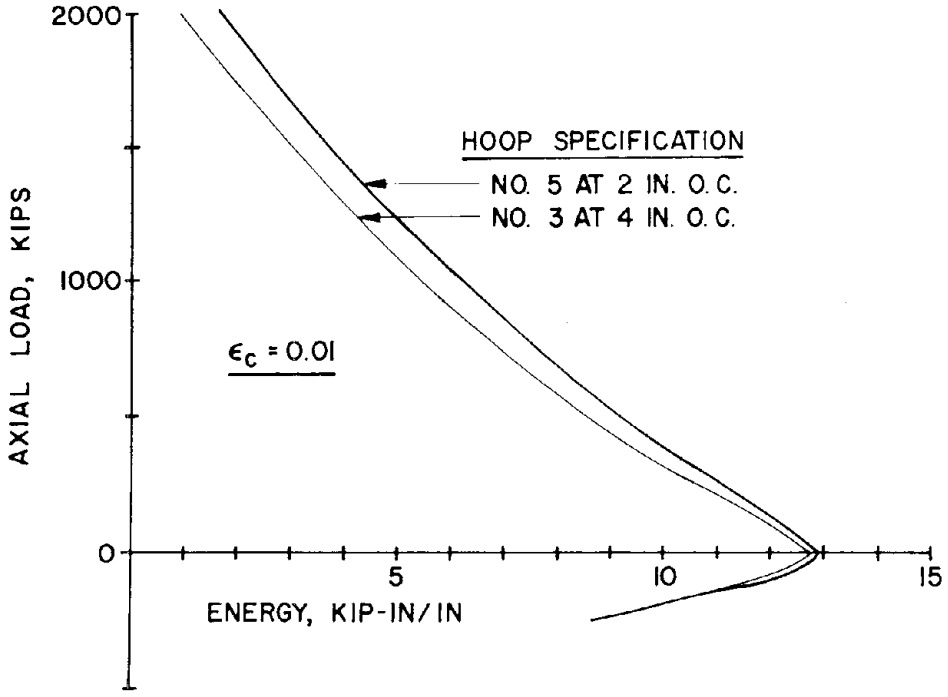

FIG. C.3 ENERGY ABSORPTION CAPACITY FOR DIFFERENT AMOUNTS OF TRANSVERSE REINFORCEMENT-TIED COLUMN EXAMPLE.

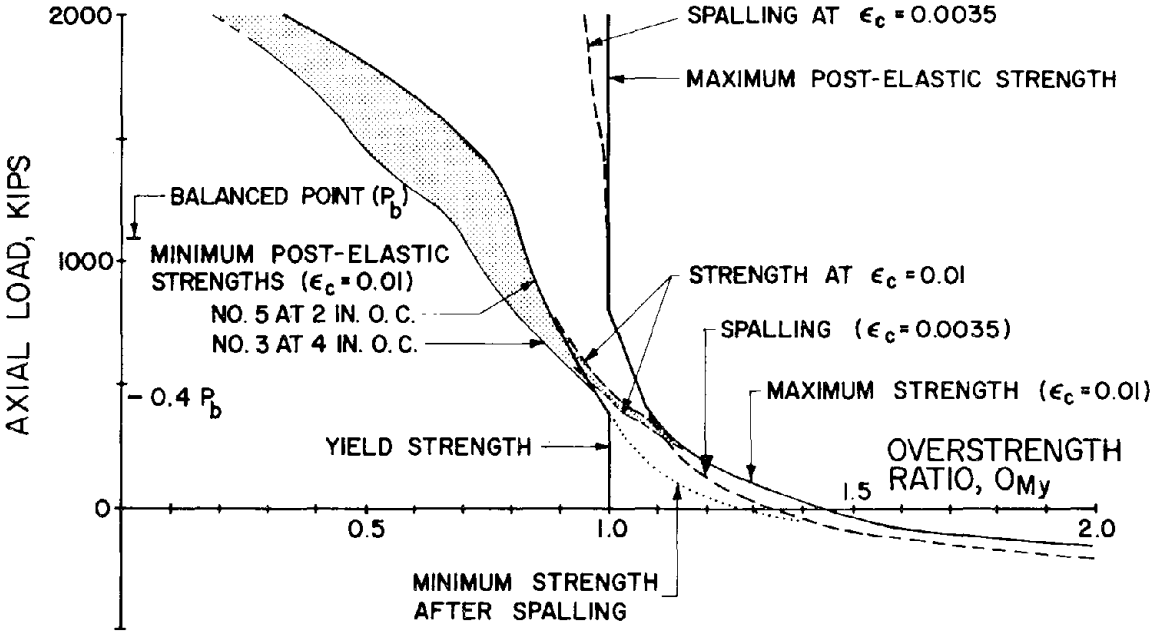

FIG. C.4 OVER-STRENGTH RATIOS FOR CONFINED SECTION-TIED COLUMN EXAMPLE

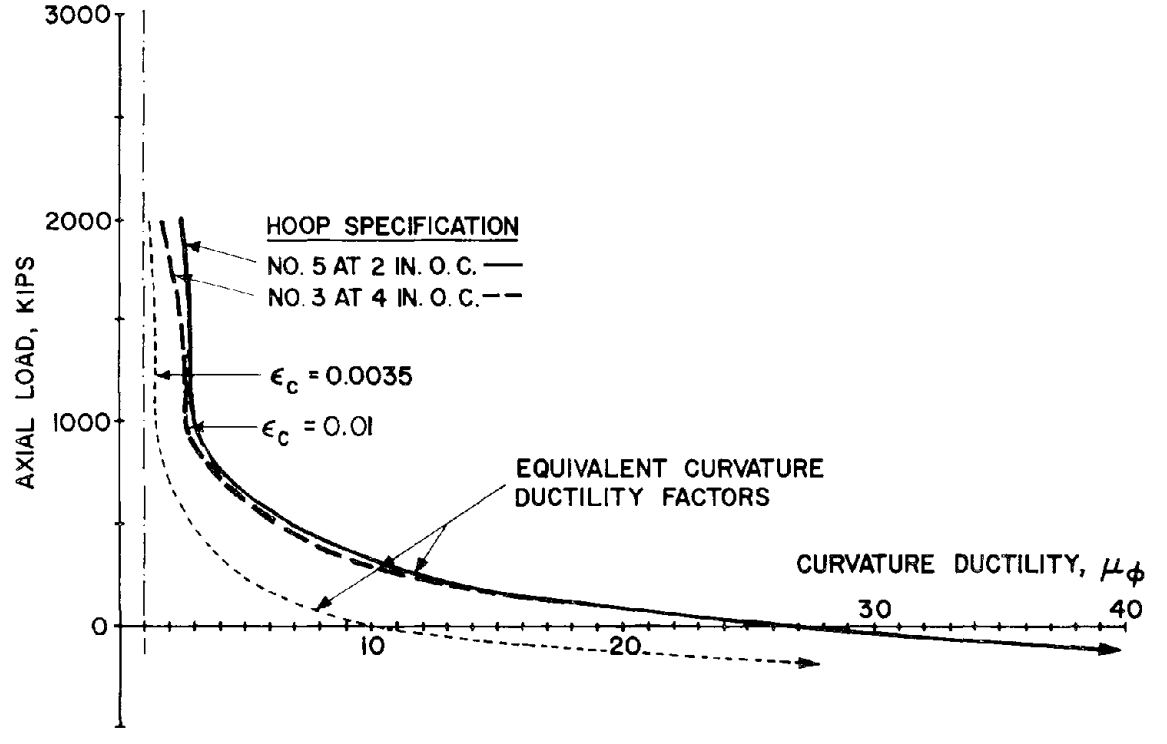

FIG. C.5 CURVATURE DUCTILITY FACTORS FOR DIFFERENT AMOUNTS OF TRANSVERSE REINFORCEMENT—TIED COLUMN EXAMPLE

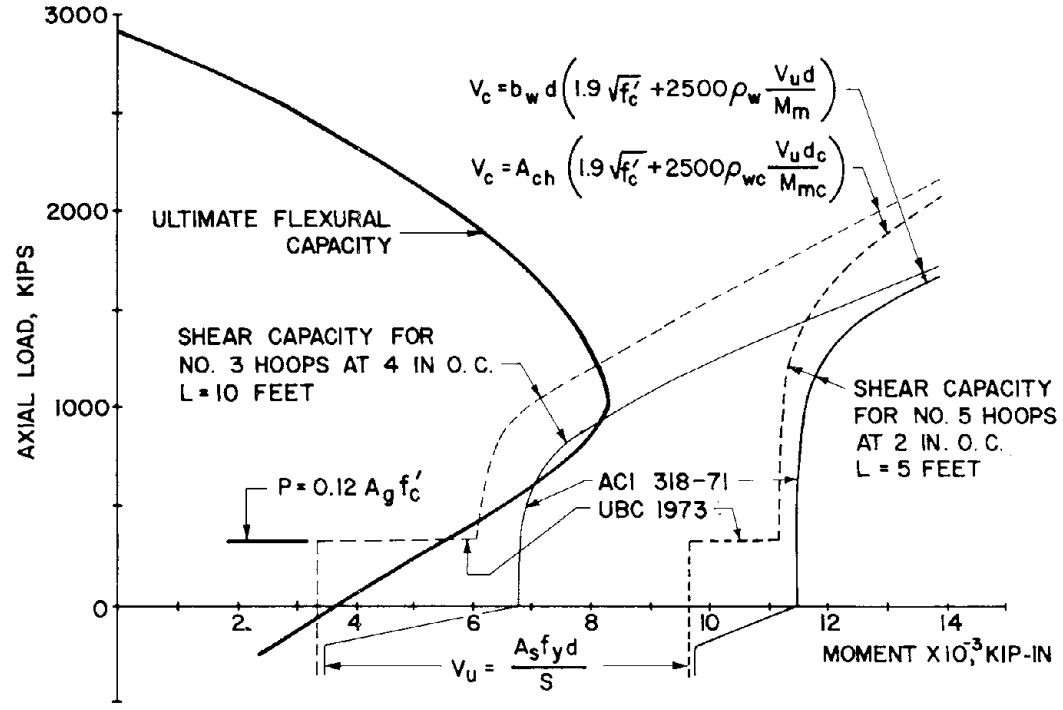

FIG. C.6 COMPARISON OF SHEAR AND FLEXURAL CAPACITIES FOR DIFFERENT AMOUNTS OF TRANSVERSE REINFORCEMENT-TIED COLUMN EXAMPLE

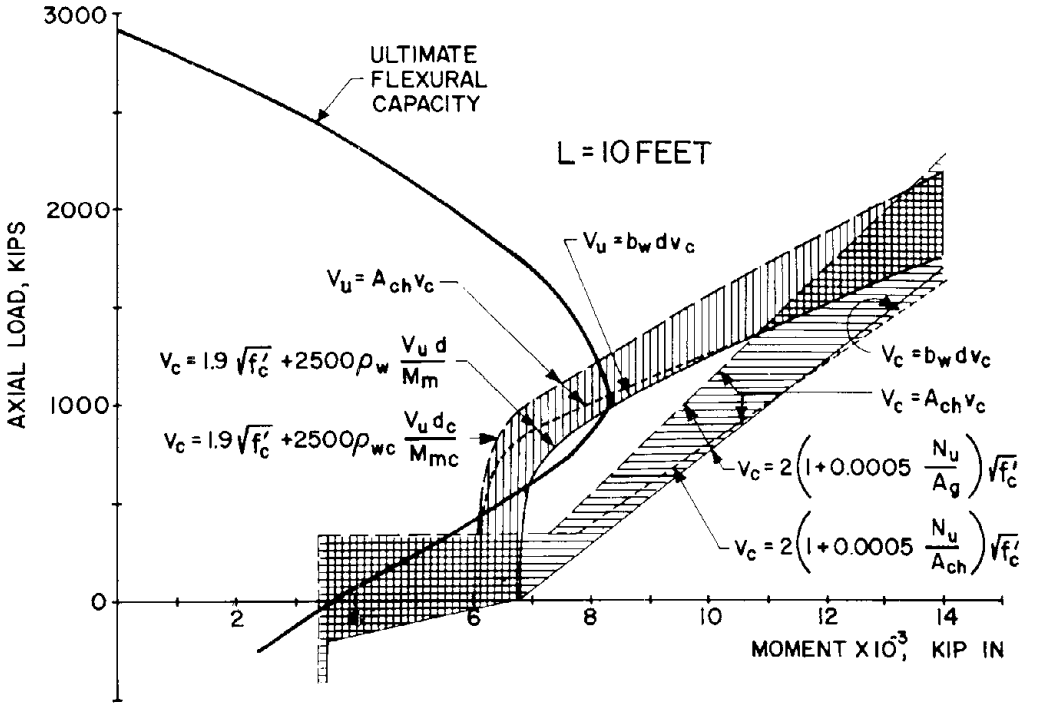

FIG. C.7 COMPARISON OF SHEAR AND FLEXURAL CAPACITIES USING DIFFERENT METHODS FOR COMPUTING SHEAR STRENGTH-TIED COLUMN EXAMPLE

APPENDIX D - DESCRIPTION OF NONLINEAR ANALYSES

D.1 INTRODUCTION

In addition to the nonlinear dynamic analyses described in Chapter 6, several other nonlinear analyses were performed to assess the sensitivity of the building's seismic response to different modeling assumptions and ground motion records. In Chapter 6, a standard nonlinear model and a failure model of Wing D were described and results obtained with these models were discussed. Additional analyses that have been performed using analytical idealizations based on the standard nonlinear model are listed in Table D.1. Other analyses of Wing D, which include the possibility of spalling, member failure, and hammering are described in Table D.2. Some of the results of these supplemental nonlinear analyses are briefly described below.

D.2 EFFECT OF DIFFERENT STRUCTURAL MODELS ON RESPONSE

Envelopes of maximum and minimum floor level displacements obtained for different structural models in which the effects of spalling, member failure, and hammering of the building were disregarded are presented in Fig. D.1. All of these models were subjected to the simulated ground motion record number 6. For these structural models, the displacements predicted using the simulated record were substantially smaller than the permanent deflections observed in the actual building. While most of the structural models considered resulted in displacements (or displacement patterns) that were similar to those obtained in the standard nonlinear model (case J) as discussed in Chapter 6, some significant differences can be observed in Fig. D.1.

For example, replacing the flexible first floor slabs with girders with much larger stiffnesses, but with the same strength (case M), substantially lowered the overall displacements and reduced the drifts in the bottom two stories. On the other hand, the effect of assuming that the columns were pinned, rather than fixed, at their base (case I) was to substantially increase the ground story drifts.

Inclusion of the lateral stiffness of the terrace canopy in the structural model (case B) tended to decrease displacements. In this case, computed drifts in the first story are much larger than those in the ground story. This is more in agreement with the pattern of permanent drifts observed in the actual building than are the results obtained with the standard nonlinear model.

It appears that the tied columns in the first story supporting the structural walls in the upper four stories of frame 29 have a large effect on the roof displacement and the drifts in the upper floors. When these tied columns (which would be expected to fail early in the building's response) were deleted entirely from the structural model (case F), the walls in frame 29 tended to overturn and the lateral dispalcements in the upper stories increased substantially.

D.3 EFFECT OF DIFFERENT GROUND MOTIONS ON RESPONSE

As illustrated in Fig. D.2, the ground motion records used in the analyses have a considerable effect on the maximum and minimum displacements computed. In this figure, cases A, D, E, H, and J correspond to models subjected to simulated ground motions. The ground motion in case A is identical to that considered in case D, except that the accelerations in case D are twice those in case A. Although the displacements are increased by slightly more than a factor of two when the accelerations are doubled, they are still not close to those developed in the actual building.

Cases G, U and V in Fig. D.2 correspond to structural models subjected to the derived Pacoima Dam base rock record (S-16°-E) for 0.40 g, 0,65 g and 0.80 g peak ground accelerations, respectively, and case O corresponds to the response resulting from this record filtered to account for local soil effects (which results in a peak acceleration of 0.66 g). The maximum and minimum displacements computed for these ground motions were generally much higher than those computed for the simulated records. Each of these records results in the formation of a collapse (panel) mechanism in the bottom two stories as described in Chapter 6. For cases G, V and O, the maximum northward deflections

exceeded 4 in. and would result in contact with the warehouse. These models, however, do not account for this event.

It is significant to note that cases O and V develop about the same magnitude of displacement. However, the peak displacements for each record occur in opposite directions. This indicates that the response of a structure (as indicated by the direction of the maximum displacement) is very sensitive to the to the details of the ground motion record (see Figs. 4.10 and 4.12) when a collapse mechanism forms.

D.4 EFFECT OF MEMBER FAILURE ON RESPONSE

Three different ground motion records were used in analyzing the failure model of Wing D. The maximum and minimum displacements obtained with these records are plotted in Fig. D.3. For the simulated ground motion record number 6, the displacements are slightly larger for the failure model than for the standard nonlinear model in which spalling, failure, and hammering were disregarded. The drifts in the first story were larger than those in the ground story in this case, which is in better agreement with the observed damages. However, the displacements are substantially less than the permanent displacements and would not be sufficient to produce contact with the retaining wall or warehouse.

The displacements obtained for the derived Pacoima Dam base rock record (0.5 g) were substantially larger than for the simulated record. The filtered Pacoima Dam record (0.66 g) resulted in even larger displacements which would produce hammering against the warehouse as discussed in Chapter 6. It is interesting to note that for the filtered record, the failure model displaces farther to the south than the standard nonlinear model; however, for displacements towards the north (compare cases O and R) the maximum displacement occurs for the standard model.

The response of yielding structures is apparently very sensitive to the ground motion characteristics, especially the sequence of acceleration pulses once a collapse mechanism has formed. The modification of member properties due to spalling or failure, or the impact

of buildings against adjacent structures can have significant effect on the structural response. This makes it very difficult to predict exactly the response of a structure subjected to severe ground motions unless the details of the accelerogram and the member properties are known.

TABLE D.1 DESIGNATION AND DESCRIPTION OF NONLINEAR ANALYSES OF WING D - MEMBER FAILURE NOT CONSIDERED

STRUCTURAL MODEL	SIMULATED RECORDS				DERIVED PACOIMA DAM BASE ROCK RECORDS (S·16°·E)				
	2	5	6		Unfiltered				Filtered
Peak Acceleration, g	0.5	0.5	0.5	1.0	0.4	0.5	0.65	0.8	0.66
1. Standard Nonlinear Wing D Model - Moments of Inertia Uncorrected for Joint Rigidity	H	E	A	D			G		
2. Same as 1 but with Nonlinear Lateral Spring to Represent Canopy			B						
3. Same as 1 but with First Story Tied Columns in Frame 29 Deleted			F						
4. Standard Nonlinear Wing D Model - Moments of Inertia Corrected to Account for Rigidity of Beam-Column Joints			J	W	U			V	O
5. Same as 4 but with Columns Pinned at Bases			I						
6. Same as 4 but Column Strength and Stiffnesses Reduced to Correspond to Confined Section Properties			K						
7. Same as 4 but Slabs assumed to have Very High Moment of Inertia - Moment Capacity Unchanged			M						
8. Same as 4 but Slabs Assumed to Remain Elastic			N						
9. Same as 4 but Strain Hardening Modulus Reduced to Nearly Zero			T						

TABLE D.2 DESIGNATION AND DESCRIPTION OF NONLINEAR ANALYSIS OF WING D - MEMBER FAILURE INCLUDED

STRUCTURAL MODEL	Simulated Records				Derived Pacoima Dam Base Rock Record (S-16°-E)				
	2	5	6		Unfiltered				Filtered
Peak Acceleration, G	0.5	0.5	0.5	1.0	0.4	0.5	0.65	0.8	0.66
Standard Nonlinear Model but Including;									
a. Failure of Terrace Canopy									
b. Failure of First Floor Tied Columns;			P			S			R
c. Spalling of Spiral Columns at Ductility of 2; and									
d. Hammering Against Warehouse (Gap = 4 in.)									

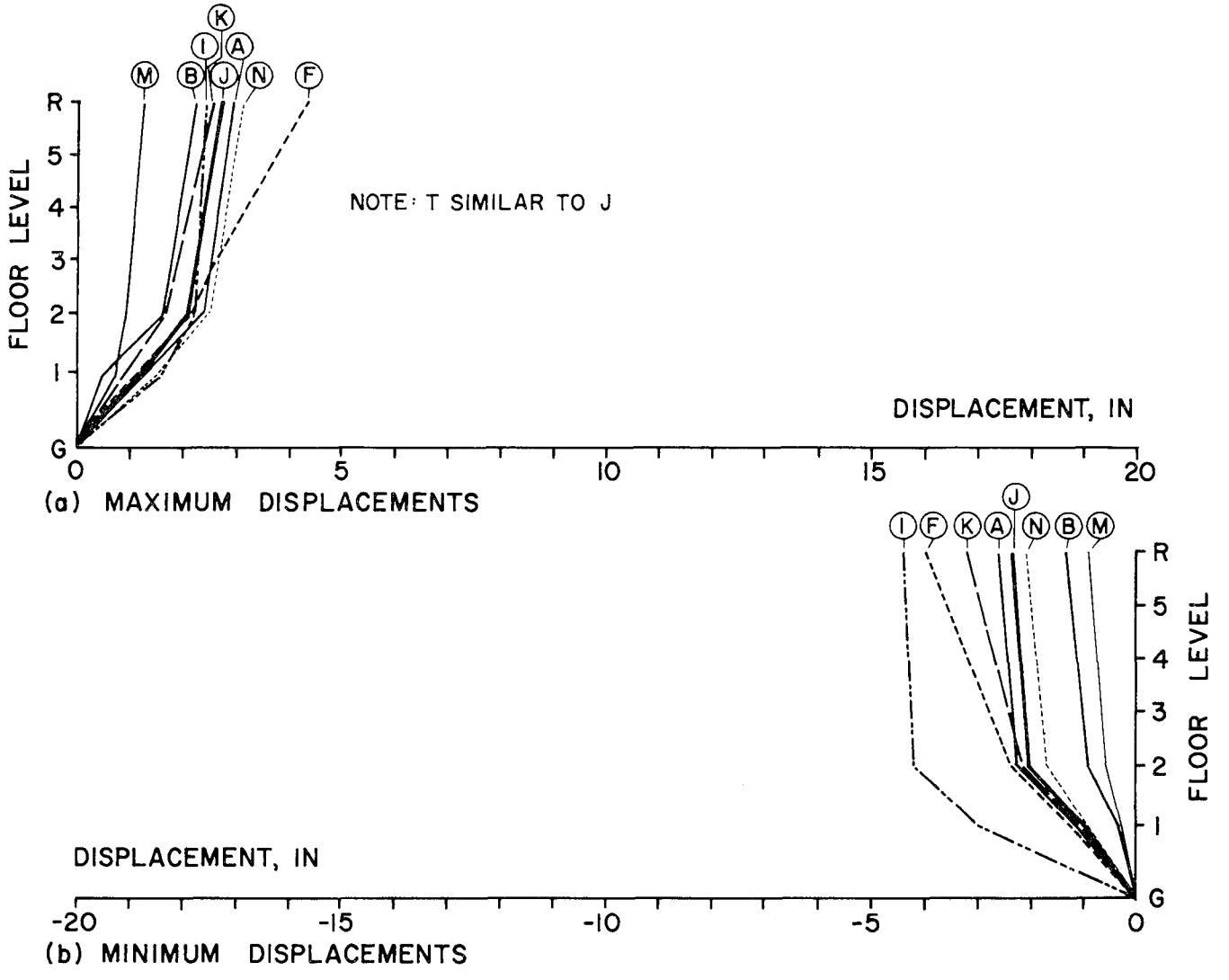

FIG. D.1 ENVELOPES OF MAXIMUM AND MINIMUM DISPLACEMENTS FOR DIFFERENT STRUCTURAL MODELS SUBJECTED TO SIMULATED RECORD 6

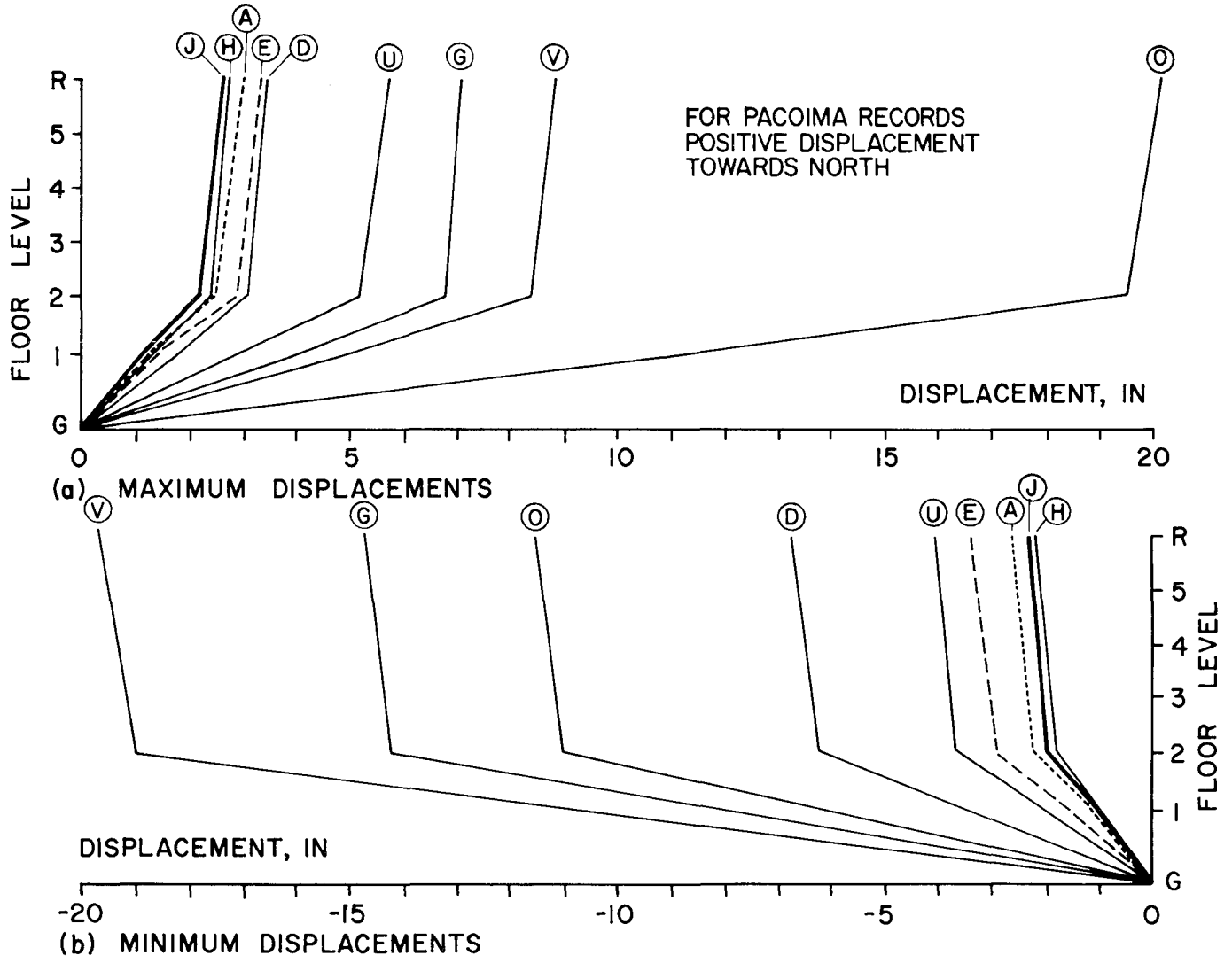

FIG. D.2 ENVELOPES OF MAXIMUM AND MINIMUM DISPLACEMENTS FOR NONLINEAR MODEL SUBJECTED TO DIFFERENT GROUND MOTIONS

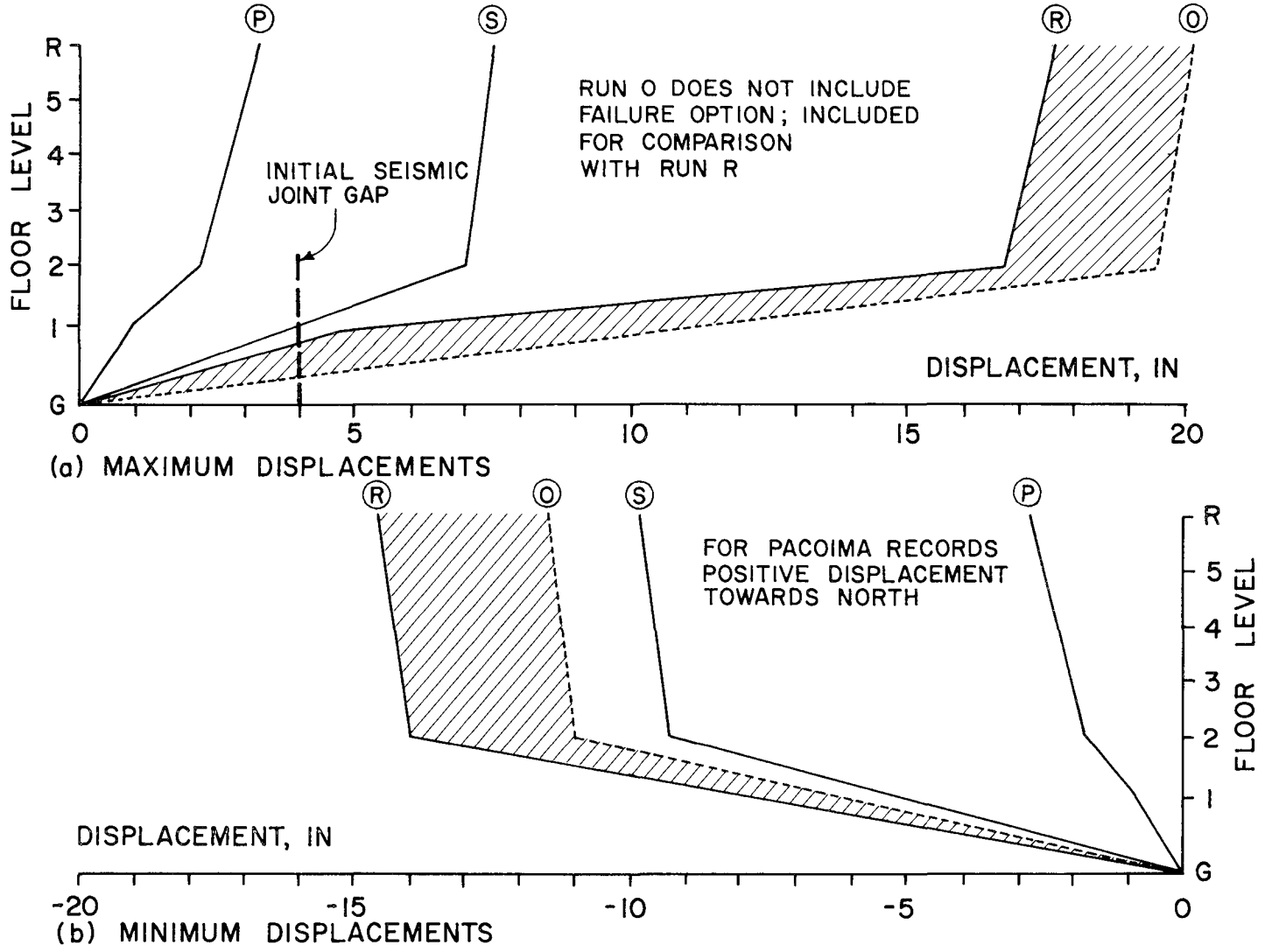

FIG. D.3 ENVELOPES OF MAXIMUM AND MINIMUM DISPLACEMENTS FOR NONLINEAR ANALYSES INCLUDING MEMBER FAILURE

EARTHQUAKE ENGINEERING RESEARCH CENTER REPORTS

EERC 67-1 "Feasibility Study Large-Scale Earthquake Simulator Facility," by J. Penzien, J. G. Bouwkamp, R. W. Clough and D. Rea - 1967 (PB 187 905)

EERC 68-1 Unassigned

EERC 68-2 "Inelastic Behavior of Beam-to-Column Subassemblages Under Repeated Loading," by V. V. Bertero - 1968 (PB 184 888)

EERC 68-3 "A Graphical Method for Solving the Wave Reflection-Refraction Problem," by H. D. McNiven and Y. Mengi 1968 (PB 187 943)

EERC 68-4 "Dynamic Properties of McKinley School Buildings," by D. Rea, J. G. Bouwkamp and R. W. Clough - 1968 (PB 187 902)

EERC 68-5 "Characteristics of Rock Motions During Earthquakes," by H. B. Seed, I. M. Idriss and F. W. Kiefer - 1968 (PB 188 338)

EERC 69-1 "Earthquake Engineering Research at Berkeley," - 1969 (PB 187 906)

EERC 69-2 "Nonlinear Seismic Response of Earth Structures," by M. Dibaj and J. Penzien - 1969 (PB 187 904)

EERC 69-3 "Probabilistic Study of the Behavior of Structures During Earthquakes," by P. Ruiz and J. Penzien - 1969 (PB 187 886)

EERC 69-4 "Numerical Solution of Boundary Value Problems in Structural Mechanics by Reduction to an Initial Value Formulation," by N. Distefano and J. Schujman - 1969 (PB 187 942)

EERC 69-5 "Dynamic Programming and the Solution of the Biharmonic Equation," by N. Distefano - 1969 (PB 187 941)

Note: Numbers in parenthesis are Accession Numbers assigned by the National Technical Information Service. Copies of these reports may be ordered from the National Technical Information Service, 5285 Port Royal Road, Springfield, Virginia, 22161. Accession Numbers should be quoted on orders for the reports (PB --- ---) and remittance must accompany each order. (Foreign orders, add $2.50 extra for mailing charges.) Those reports without this information listed are not yet available from NTIS. Upon request, EERC will mail inquirers this information when it becomes available to us.

EERC 69-6 "Stochastic Analysis of Offshore Tower Structures," by A. K. Malhotra and J. Penzien - 1969 (PB 187 903)

EERC 69-7 "Rock Motion Accelerograms for High Magnitude Earthquakes," by H. B. Seed and I. M. Idriss - 1969 (PB 187 940)

EERC 69-8 "Structural Dynamics Testing Facilities at the University of California, Berkeley," by R. M. Stephen, J. G. Bouwkamp, R. W. Clough and J. Penzien - 1969 (PB 189 111)

EERC 69-9 "Seismic Response of Soil Deposits Underlain by Sloping Rock Boundaries," by H. Dezfulian and H. B. Seed - 1969 (PB 189 114)

EERC 69-10 "Dynamic Stress Analysis of Axisymmetric Structures under Arbitrary Loading," by S. Ghosh and E. L. Wilson - 1969 (PB 189 026)

EERC 69-11 "Seismic Behavior of Multistory Frames Designed by Different Philosophies," by J. C. Anderson and V. V. Bertero - 1969 (PB 190 662)

EERC 69-12 "Stiffness Degradation of Reinforcing Concrete Structures Subjected to Reversed Actions," by V. V. Bertero, B. Bresler and H. Ming Liao - 1969 (PB 202 942)

EERC 69-13 "Response of Non-Uniform Soil Deposits to Travel Seismic Waves," by H. Dezfulian and H. B. Seed - 1969 (PB 191 023)

EERC 69-14 "Damping Capacity of a Model Steel Structure," by D. Rea, R. W. Clough and J. G. Bouwkamp - 1969 (PB 190 663)

EERC 69-15 "Influence of Local Soil Conditions on Building Damage Potential during Earthquakes," by H. B. Seed and I. M. Idriss - 1969 (PB 191 036)

EERC 69-16 "The Behavior of Sands under Seismic Loading Conditions," by M. L. Silver and H. B. Seed - 1969 (AD 714 982)

EERC 70-1 "Earthquake Response of Concrete Gravity Dams," by A. K. Chopra - 1970 (AD 709 640)

EERC 70-2 "Relationships between Soil Conditions and Building Damage in the Caracas Earthquake of July 29, 1967," by H. B. Seed, I. M. Idriss and H. Dezfulian - 1970 (PB 195 762)

EERC 70-3 "Cyclic Loading of Full Size Steel Connections," by E. P. Popov and R. M. Stephen - 1970 (PB 213 545)

EERC 70-4 "Seismic Analysis of the Charaima Building, Caraballeda, Venezuela," by Subcommittee of the SEAONC Research Committee: V. V. Bertero, P. F. Fratessa, S. A. Mahin, J. H. Sexton, A. C. Scordelis, E. L. Wilson, L. A. Wyllie, H. B. Seed and J. Penzien, Chairman - 1970 (PB 201 455)

EERC 70-5 "A Computer Program for Earthquake Analysis of Dams," by A. K. Chopra and P. Chakrabarti - 1970 (AD 723 994)

EERC 70-6 "The Propagation of Love Waves across Non-Horizontally Layered Structures," by J. Lysmer and L. A. Drake - 1970 (PB 197 896)

EERC 70-7 "Influence of Base Rock Characteristics on Ground Response," by J. Lysmer, H. B. Seed and P. B. Schnabel - 1970 (PB 197 897)

EERC 70-8 "Applicability of Laboratory Test Procedures for Measuring Soil Liquefaction Characteristics under Cyclic Loading," by H. B. Seed and W. H. Peacock - 1970 (PB 198 016)

EERC 70-9 "A Simplified Procedure for Evaluating Soil Liquefaction Potential," by H. B. Seed and I. M. Idriss - 1970 (PB 198 009)

EERC 70-10 "Soil Moduli and Damping Factors for Dynamic Response Analysis," by H. B. Seed and I. M. Idriss - 1970 (PB 197 869)

EERC 71-1 "Koyna Earthquake and the Performance of Koyna Dam," by A. K. Chopra and P. Chakrabarti - 1971 (AD 731 496)

EERC 71-2 "Preliminary In-Situ Measurements of Anelastic Absorption in Soils Using a Prototype Earthquake Simulator," by R. D. Borcherdt and P. W. Rodgers - 1971 (PB 201 454)

EERC 71-3 "Static and Dynamic Analysis of Inelastic Frame Structures," by F. L. Porter and G. H. Powell - 1971 (PB 210 135)

EERC 71-4 "Research Needs in Limit Design of Reinforced Concrete Structures," by V. V. Bertero - 1971 (PB 202 943)

EERC 71-5 "Dynamic Behavior of a High-Rise Diagonally Braced Steel Building," by D. Rea, A. A. Shah and J. G. Bouwkamp - 1971 (PB 203 584)

EERC 71-6 "Dynamic Stress Analysis of Porous Elastic Solids Saturated with Compressible Fluids," by J. Ghaboussi and E. L. Wilson - 1971 (PB 211 396)

EERC 71-7 "Inelastic Behavior of Steel Beam-to-Column Subassemblages," by H. Krawinkler, V. V. Bertero and E. P. Popov - 1971 (PB 211 335)

EERC 71-8 "Modification of Seismograph Records for Effects of Local Soil Conditions," by P. Schnabel, H. B. Seed and J. Lysmer - 1971 (PB 214 450)

EERC 72-1 "Static and Earthquake Analysis of Three Dimensional Frame and Shear Wall Buildings," by E. L. Wilson and H. H. Dovey - 1972 (PB 212 904)

EERC 72-2 "Accelerations in Rock for Earthquakes in the Western United States," by P. B. Schnabel and H. B. Seed - 1972 (PB 213 100)

EERC 72-3 "Elastic-Plastic Earthquake Response of Soil-Building Systems," by T. Minami - 1972 (PB 214 868)

EERC 72-4 "Stochastic Inelastic Response of Offshore Towers to Strong Motion Earthquakes," by M. K. Kaul - 1972 (PB 215 713)

EERC 72-5 "Cyclic Behavior of Three Reinforced Concrete Flexural Members with High Shear," by E. P. Popov, V. V. Bertero and H. Krawinkler - 1972 (PB 214 555)

EERC 72-6 "Earthquake Response of Gravity Dams Including Reservoir Interaction Effects," by P. Chakrabarti and A. K. Chopra - 1972 (AD 762 330)

EERC 72-7 "Dynamic Properties on Pine Flat Dam," by D. Rea, C. Y. Liaw and A. K. Chopra - 1972 (AD 763 928)

EERC 72-8 "Three Dimensional Analysis of Building Systems," by E. L. Wilson and H. H. Dovey - 1972 (PB 222 438)

EERC 72-9 "Rate of Loading Effects on Uncracked and Repaired Reinforced Concrete Members," by S. Mahin, V. V. Bertero, D. Rea and M. Atalay - 1972 (PB 224 520)

EERC 72-10 "Computer Program for Static and Dynamic Analysis of Linear Structural Systems," by E. L. Wilson, K.-J. Bathe, J. E. Peterson and H. H. Dovey - 1972 (PB 220 437)

EERC 72-11 "Literature Survey - Seismic Effects on Highway Bridges," by T. Iwasaki, J. Penzien and R. W. Clough - 1972 (PB 215 613)

EERC 72-12 "SHAKE-A Computer Program for Earthquake Response Analysis of Horizontally Layered Sites," by P. B. Schnabel and J. Lysmer - 1972 (PB 220 207)

EERC 73-1 "Optimal Seismic Design of Multistory Frames," by V. V. Bertero and H. Kamil - 1973

EERC 73-2 "Analysis of the Slides in the San Fernando Dams during the Earthquake of February 9, 1971," by H. B. Seed, K. L. Lee, I. M. Idriss and F. Makdisi - 1973 (PB 223 402)

EERC 73-3 "Computer Aided Ultimate Load Design of Unbraced Multistory Steel Frames," by M. B. El-Hafez and G. H. Powell - 1973

EERC 73-4 "Experimental Investigation into the Seismic Behavior of Critical Regions of Reinforced Concrete Components as Influenced by Moment and Shear," by M. Celebi and J. Penzien - 1973 (PB 215 884)

EERC 73-5 "Hysteretic Behavior of Epoxy-Repaired Reinforced Concrete Beams," by M. Celebi and J. Penzien - 1973

EERC 73-6 "General Purpose Computer Program for Inelastic Dynamic Response of Plane Structures," by A. Kanaan and G. H. Powell - 1973 (PB 221 260)

EERC 73-7 "A Computer Program for Earthquake Analysis of Gravity Dams Including Reservoir Interaction," by P. Chakrabarti and A. K. Chopra - 1973 (AD 766 271)

EERC 73-8 "Behavior of Reinforced Concrete Deep Beam-Column Subassemblages under Cyclic Loads," by O. Kustu and J. G. Bouwkamp - 1973

EERC 73-9 "Earthquake Analysis of Structure-Foundation Systems," by A. K. Vaish and A. K. Chopra - 1973 (AD 766 272)

EERC 73-10 "Deconvolution of Seismic Response for Linear Systems," by R. B. Reimer - 1973 (PB 227 179)

EERC 73-11 "SAP IV: A Structural Analysis Program for Static and Dynamic Response of Linear Systems," by K.-J. Bathe, E. L. Wilson and F. E. Peterson - 1973 (PB 221 967)

EERC 73-12 "Analytical Investigations of the Seismic Response of Long, Multiple Span Highway Bridges," by W. S. Tseng and J. Penzien - 1973 (PB 227 816)

EERC 73-13 "Earthquake Analysis of Multi-Story Buildings Including Foundation Interaction," by A. K. Chopra and J. A. Gutierrez - 1973 (PB 222 970)

EERC 73-14 "ADAP: A Computer Program for Static and Dynamic Analysis of Arch Dams," by R. W. Clough, J. M. Raphael and S. Majtahedi - 1973 (PB 223 763)

EERC 73-15 "Cyclic Plastic Analysis of Structural Steel Joints," by R. B. Pinkney and R. W. Clough - 1973 (PB 226 843)

EERC 73-16 "QUAD-4: A Computer Program for Evaluating the Seismic Response of Soil Structures by Variable Damping Finite Element Procedures," by I. M. Idriss, J. Lysmer, R. Hwang and H. B. Seed - 1973 (PB 229 424)

EERC 73-17 "Dynamic Behavior of a Multi-Story Pyramid Shaped Building," by R. M. Stephen and J. G. Bouwkamp - 1973

EERC 73-18 "Effect of Different Types of Reinforcing on Seismic Behavior of Short Concrete Columns," by V. V. Bertero, J. Hollings, O. Kustu, R. M. Stephen and J. G. Bouwkamp - 1973

EERC 73-19 "Olive View Medical Center Material Studies, Phase I," by B. Bresler and V. V. Bertero - 1973 (PB 235 986)

EERC 73-20 "Linear and Nonlinear Seismic Analysis Computer Programs for Long Multiple-Span Highway Bridges," by W. S. Tseng and J. Penzien - 1973

EERC 73-21 "Constitutive Models for Cyclic Plastic Deformation of Engineering Materials," by J. M. Kelly and P. P. Gillis - 1973 (PB 226 024)

EERC 73-22 "DRAIN - 2D User's Guide," by G. H. Powell - 1973 (PB 227 016)

EERC 73-23 "Earthquake Engineering at Berkeley - 1973" - 1973 (PB 226 033)

EERC 73-24 Unassigned

EERC 73-25 "Earthquake Response of Axisymmetric Tower Structures Surrounded by Water," by C. Y. Liaw and A. K. Chopra - 1973 (AD 773 052)

EERC 73-26 "Investigation of the Failures of the Olive View Stairtowers during the San Fernando Earthquake and Their Implications in Seismic Design," by V. V. Bertero and R. G. Collins - 1973 (PB 235 106)

EERC 73-27 "Further Studies on Seismic Behavior of Steel Beam-Column Subassemblages," by V. V. Bertero, H. Krawinkler and E. P. Popov - 1973 (PB 234 172)

EERC 74-1 "Seismic Risk Analysis," by C. S. Oliveira - 1974 (PB 235 920)

EERC 74-2 "Settlement and Liquefaction of Sands under Multi-Directional Shaking," by R. Pyke, C. K. Chan and H. B. Seed - 1974

EERC 74-3 "Optimum Design of Earthquake Resistant Shear Buildings," by D. Ray, K. S. Pister and A. K. Chopra - 1974 (PB 231 172)

EERC 74-4 "LUSH - A Computer Program for Complex Response Analysis of Soil-Structure Systems," by J. Lysmer, T. Udaka, H. B. Seed and R. Hwang - 1974 (PB 236 796)

EERC 74-5 "Sensitivity Analysis for Hysteretic Dynamic Systems: Applications to Earthquake Engineering," by D. Ray - 1974 (PB 233 213)

EERC 74-6 "Soil-Structure Interaction Analyses for Evaluating Seismic Response," by H. B. Seed, J. Lysmer and R. Hwang - 1974 (PB 236 519)

EERC 74-7 Unassigned

EERC 74-8 "Shaking Table Tests of a Steel Frame - A Progress Report," by R. W. Clough and D. Tang - 1974

EERC 74-9 "Hysteretic Behavior of Reinforced Concrete Flexural Members with Special Web Reinforcement," by V. V. Bertero, E. P. Popov and T. Y. Wang - 1974 (PB 236 797)

EERC 74-10 "Applications of Reliability-Based, Global Cost Optimization to Design of Earthquake Resistant Structures," by E. Vitiello and K. S. Pister - 1974 (PB 237 231)

EERC 74-11 "Liquefaction of Gravelly Soils under Cyclic Loading Conditions," by R. T. Wong, H. B. Seed and C. K. Chan - 1974

EERC 74-12 "Site-Dependent Spectra for Earthquake-Resistant Design," by H. B. Seed, C. Ugas and J. Lysmer - 1974

EERC 74-13 "Earthquake Simulator Study of a Reinforced Concrete Frame," by P. Hidalgo and R. W. Clough - 1974 (PB 241 944)

EERC 74-14 "Nonlinear Earthquake Response of Concrete Gravity Dams," by N. Pal - 1974 (AD/A006583)

EERC 74-15 "Modeling and Identification in Nonlinear Structural Dynamics, I - One Degree of Freedom Models," by N. Distefano and A. Rath - 1974 (PB 241 548)

EERC 75-1 "Determination of Seismic Design Criteria for the Dumbarton Bridge Replacement Structure, Vol. I: Description, Theory and Analytical Modeling of Bridge and Parameters," by F. Baron and S.-H. Pang - 1975

EERC 75-2 "Determination of Seismic Design Criteria for the Dumbarton Bridge Replacement Structure, Vol. 2: Numerical Studies and Establishment of Seismic Design Criteria," by F. Baron and S.-H. Pang - 1975

EERC 75-3 "Seismic Risk Analysis for a Site and a Metropolitan Area," by C. S. Oliveira - 1975

EERC 75-4 "Analytical Investigations of Seismic Response of Short, Single or Multiple-Span Highway Bridges," by Ma-chi Chen and J. Penzien - 1975 (PB 241 454)

EERC 75-5 "An Evaluation of Some Methods for Predicting Seismic Behavior of Reinforced Concrete Buildings," by Stephen A. Mahin and V. V. Bertero - 1975

EERC 75-6 "Earthquake Simulator Study of a Steel Frame Structure, Vol. I: Experimental Results," by R. W. Clough and David T. Tang - 1975 (PB 243 981)

EERC 75-7 "Dynamic Properties of San Bernardino Intake Tower," by Dixon Rea, C.-Y. Liaw, and Anil K. Chopra - 1975 (AD/A008406)

EERC 75-8 "Seismic Studies of the Articulation for the Dumbarton Bridge Replacement Structure, Vol. I: Description, Theory and Analytical Modeling of Bridge Components," by F. Baron and R. E. Hamati - 1975

EERC 75-9 "Seismic Studies of the Articulation for the Dumbarton Bridge Replacement Structure, Vol. 2: Numerical Studies of Steel and Concrete Girder Alternates," by F. Baron and R. E. Hamati - 1975

EERC 75-10 "Static and Dynamic Analysis of Nonlinear Structures," by Digambar P. Mondkar and Graham H. Powell - 1975 (PB 242 434)

EERC 75-11 "Hysteretic Behavior of Steel Columns," by E. P. Popov, V. V. Bertero and S. Chandramouli - 1975

EERC 75-12 "Earthquake Engineering Research Center Library Printed Catalog" - 1975 (PB 243 711)

EERC 75-13 "Three Dimensional Analysis of Building Systems," Extended Version, by E. L. Wilson, J. P. Hollings and H. H. Dovey - 1975 (PB 243 989)

EERC 75-14 "Determination of Soil Liquefaction Characteristics by Large-Scale Laboratory Tests," by Pedro De Alba, Clarence K. Chan and H. Bolton Seed - 1975

EERC 75-15 "A Literature Survey - Compressive, Tensile, Bond and Shear Strength of Masonry," by Ronald L. Mayes and Ray W. Clough - 1975

EERC 75-16 "Hysteretic Behavior of Ductile Moment Resisting Reinforced Concrete Frame Components," by V. V. Bertero and E. P. Popov - 1975

EERC 75-17 "Relationships Between Maximum Acceleration, Maximum Velocity, Distance from Source, Local Site Conditions for Moderately Strong Earthquakes," by H. Bolton Seed, Ramesh Murarka, John Lysmer and I. M. Idriss - 1975

EERC 75-18 "The Effects of Method of Sample Preparation on the Cyclic Stress-Strain Behavior of Sands," by J. Paul Mulilis, Clarence K. Chan and H. Bolton Seed - 1975

EERC 75-19 "The Seismic Behavior of Critical Regions of Reinforced Concrete Components as Influenced by Moment, Shear and Axial Force," by B. Atalay and J. Penzien - 1975

EERC 75-20 "Dynamic Properties of an Eleven Story Masonry Building," by R. M. Stephen, J. P. Hollings, J. G. Bouwkamp and D. Jurukovski - 1975

EERC 75-21 "State-of-the-Art in Seismic Shear Strength of Masonry - An Evaluation and Review," by Ronald L. Mayes and Ray W. Clough - 1975

EERC 75-22 "Frequency Dependencies Stiffness Matrices for Viscoelastic Half-Plane Foundations," by Anil K. Chopra, P. Chakrabarti and Gautam Dasgupta - 1975

EERC 75-23 "Hysteretic Behavior of Reinforced Concrete Framed Walls," by T. Y. Wong, V. V. Bertero and E. P. Popov - 1975

EERC 75-24 "Testing Facility for Subassemblages of Frame-Wall Structural Systems," by V. V. Bertero, E. P. Popov and T. Endo - 1975

EERC 75-25 "Influence of Seismic History of the Liquefaction Characteristics of Sands," by H. Bolton Seed, Kenji Mori and Clarence K. Chan - 1975

EERC 75-26 "The Generation and Dissipation of Pore Water Pressures during Soil Liquefaction," by H. Bolton Seed, Phillippe P. Martin and John Lysmer - 1975

EERC 75-27 "Identification of Research Needs for Improving a Seismic Design of Building Structures," by V. V. Bertero - 1975

EERC 75-28 "Evaluation of Soil Liquefaction Potential during Earthquakes," by H. Bolton Seed, I. Arango and Clarence K. Chan 1975

EERC 75-29 "Representation of Irregular Stress Time Histories by Equivalent Uniform Stress Series in Liquefaction Analyses," by H. Bolton Seed, I. M. Idriss, F. Makdisi and N. Banerjee 1975

EERC 75-30 "FLUSH - A Computer Program for Approximate 3-D Analysis of Soil-Structure Interaction Problems," by J. Lysmer, T. Udaka, C.-F. Tsai and H. B. Seed - 1975

EERC 75-31 "ALUSH - A Computer Program for Seismic Response Analysis of Axisymmetric Soil-Structure Systems," by E. Berger, J. Lysmer and H. B. Seed - 1975

EERC 75-32 "TRIP and TRAVEL - Computer Programs for Soil-Structure Interaction Analysis with Horizontally Travelling Waves," by T. Udaka, J. Lysmer and H. B. Seed - 1975

EERC 75-33 "Predicting the Performance of Structures in Regions of High Seismicity," by Joseph Penzien - 1975

EERC 75-34 "Efficient Finite Element Analysis of Seismic Structure - Soil - Direction," by J. Lysmer, H. Bolton Seed, T. Udaka, R. N. Hwang and C.-F. Tsai - 1975

EERC 75-35 "The Dynamic Behavior of a First Story Girder of a Three-Story Steel Frame Subjected to Earthquake Loading," by Ray W. Clough and Lap-Yan Li - 1975

EERC 75-36 "Earthquake Simulator Study of a Steel Frame Structure, Volume II - Analytical Results," by David T. Tang - 1975

EERC 75-37 "ANSR-I General Purpose Computer Program for Analysis of Non-Linear Structure Response," by Digambar P. Mondkar and Graham H. Powell - 1975

EERC 75-38 "Nonlinear Response Spectra for Probabilistic Seismic Design and Damage Assessment of Reinforced Concrete Structures," by Masaya Murakami and Joseph Penzien - 1975

EERC 75-39 "Study of a Method of Feasible Directions for Optimal Elastic Design of Framed Structures Subjected to Earthquake Loading," by N. D. Walker and K. S. Pister - 1975

EERC 75-40 "An Alternative Representation of the Elastic-Viscoelastic Analogy," by Gautam Dasgupta and Jerome L. Sackman - 1975

EERC 75-41 "Effect of Multi-Directional Shaking on Liquefaction of Sands," by H. Bolton Seed, Robert Pyke and Geoffrey R. Martin - 1975

EERC 76-1 "Strength and Ductility Evaluation of Existing Low-Rise Reinforced Concrete Buildings - Screening Method," by Tsuneo Okada and Boris Bresler - 1976

EERC 76-2 "Experimental and Analytical Studies on the Hysteretic Behavior of Reinforced Concrete Rectangular and T-Beams," by Shao-Yeh Marshall Ma, Egor P. Popov and Vitelmo V. Bertero - 1976

EERC 76-3 "Dynamic Behavior of a Multistory Triangular-Shaped Building," by J. Petrovski, R. M. Stephen, E. Gartenbaum and J. G. Bouwkamp - 1976

EERC 76-4 "Earthquake Induced Deformations of Earth Dams," by Norman Serff and H. Bolton Seed - 1976

EERC 76-5 "Analysis and Design of Tube-Type Tall Building Structures," by H. de Clercq and G. H. Powell - 1976

EERC 76-6 "Time and Frequency Domain Analysis of Three-Dimensional Ground Motions, San Fernando Earthquake," by Tetsuo Kubo and Joseph Penzien - 1976

EERC 76-7 "Expected Performance of Uniform Building Code Design Masonry Structures," by R. L. Mayes, Y. Omote, S. W. Chen and R. W. Clough - 1976

EERC 76-8 "Cyclic Shear Tests on Concrete Masonry Piers, Part I - Test Results," by R. L. Mayes, Y. Omote and R. W. Clough 1976

EERC 76-9 "A Substructure Method for Earthquake Analysis of Structure - Soil Interaction," by Jorge Alberto Gutierrez and Anil K. Chopra - 1976

EERC 76-10 "Stabilization of Potentially Liquefiable Sand Deposits using Gravel Drain Systems," by H. Bolton Seed and John R. Booker - 1976

EERC 76-11 "Influence of Design and Analysis Assumptions on Computed Inelastic Response of Moderately Tall Frames," by G. H. Powell and D. G. Row - 1976

EERC 76-12 "Sensitivity Analysis for Hysteretic Dynamic Systems: Theory and Applications," by D. Ray, K. S. Pister and E. Polak - 1976

EERC 76-13 "Coupled Lateral Torsional Response of Buildings to Ground Shaking," by Christopher L. Kan and Anil K. Chopra - 1976

EERC 76-14 "Seismic Analyses of the Banco de America," by V. V. Bertero, S. A. Mahin, and J. A. Hollings - 1976

EERC 76-15 "Reinforced Concrete Frame 2: Seismic Testing and Analytical Correlation," by Ray W. Clough and Jawahar Gidwani - 1976

EERC 76-16 "Cyclic Shear Tests on Masonry Piers, Part II - Analysis of Test Results," by R. L. Mayes, Y. Omote and R. W. Clough - 1976

EERC 76-17 "Structural Steel Bracing Systems: Behavior under Cyclic Loading," by E. P. Popov, K. Takanashi and C. W. Roeder - 1976

EERC 76-18 "Experimental Model Studies on Seismic Response of High Curved Overcrossings," by David Williams and William G. Godden - 1976

EERC 76-19 "Effects of Non-Uniform Seismic Disturbances on the Dumbarton Bridge Replacement Structure," by Frank Baron and Raymond E. Hamati - 1976

EERC 76-20 "Investigation of the Inelastic Characteristics of a Single Story Steel Structure using System Identification and Shaking Table Experiments," by Vernon C. Matzen and Hugh D. McNiven - 1976

EERC 76-21 "Capacity of Columns with Splice Imperfections," by E. P. Popov, R. M. Stephen, and R. Philbrick - 1976

EERC 76-22 "Response of the Olive View Hospital Main Building during the San Fernando Earthquake," by Stephen A. Mahin, Vitelmo V. Bertero, Anil K. Chopra, and Robert G. Collins - 1976